UNIVERSIDADE DE LISBOA
FACULDADE DE CIÊNCIAS
DEPARTAMENTO DE FÍSICA

Development and Optimization of a Low-Cost Myoelectric Upper Limb Prosthesis

Ema de Matos Castanheira e Lopes

Mestrado Integrado em Engenharia Biomédica e Biofísica
Engenharia Clínica e Instrumentação Médica

Dissertação orientada por:
Prof. Dr. Nuno Miguel de Pinto Lobo Matela
Prof. Dr. Bruno Alexandre Rodrigues Simões Soares

2022

Acknowledgements

2021 was not an easy year, but working on this dissertation was an exciting and exceptional experience. It was a remarkable journey full of setbacks, mistakes, acknowledgements and limitations imposed by the pandemic crisis. However, knowing that this dissertation can help many people, especially people with economic and health difficulties, whether they are children or adults, kept me motivated and focused on this work as well as on giving my best.

This work would not be possible without the support of my supervisors, Prof. Dr Nuno Matela and Prof. Dr Bruno Soares. I would like to express my gratitude for their professionalism, understanding, guidance and assistance during this journey.

Secondly, I would like to thank Prof. Dr.ª Cláudia Quaresma for her incredible support, kindness, professionalism and guidance. This dissertation cooperation between two colleges and professors would not be possible without her.

Thirdly, I would like to thank to all my professors, especially Prof. Drª. Raquel Conceição for helping me with my doubts.

At last, I would like to thank my family, especially my parents, for their emotional support during this journey. Thank you for giving me the encouragement I needed throughout these five years, especially during this last chapter of my academic life.

Thank you!

Abstract

In recent years, the increase in the number of accidents, chronic diseases, such as diabetes, and the impoverishment of certain developing countries have contributed to a significant increase in prostheses users. The loss of a particular limb entails numerous changes in the daily life of each user, which are amplified when the user loses their hand. Therefore, replacing the hand is an urgent necessity. Developing upper limb prostheses will allow the re-establishment of the physical and motor functions of the upper limb as well as reduction of the rates of depression. Therefore, the prosthetic industry has been reinventing itself and evolving. It is already possible to control a prosthesis through the user's myoelectric signals, control known as pattern recognition control. In addition, additive manufacturing technologies such as 3D printing have gained strength in prosthetics. The use of this type of technology allows the product to reach the user much faster and reduces the weight of the devices, making them lighter. Despite these advances, the rejection rate of this type of device is still high since most prostheses available on the market are slow, expensive and heavy. Because of that, academia and institutions have been investigating ways to overcome these limitations. Nevertheless, the dependence on the number of acquisition channels is still limiting since most users do not have a large available forearm surface area to acquire the user's myoelectric signals.

This work intends to solve some of these problems and answer the questions imposed by the industry and researchers. The main objective is to test if developing a subject independent, fast and simple microcontroller is possible. Subsequently, we recorded data from forty volunteers through the BIOPAC acquisition system. After that, the signals were filtered through two different processes. The first was digital filtering and the application of wavelet threshold noise reduction. Later, the signal was divided into smaller windows (100 and 250 milliseconds) and thirteen features were extracted in the temporal domain. During all these steps, the MatLab® software was used. After extraction, three feature selection methods were used to optimize the classification process, where machine learning algorithms are implemented. The classification was divided into different parts. First, the classifier had to distinguish whether the volunteer was making some movement or was at rest. In the case of detected movement, the classifier would have to, on a second level, try to understand if they were moving only one finger or performing a movement that involved the flexion of more than one finger (grip). If the volunteer was performing a grip on the third level, the classifier would have to identify whether the volunteer was performing a spherical or triad grip. Finally, to understand the influence of the database on the classification, two methods were used: cross-validation and split validation.

After analysing the results, the e-NABLE Unlimbited arm was printed on The Original Prusa i3 MK3, where polylactic acid (PLA) was used.

This dissertation showed that the results obtained in the 250-millisecond window were better than the obtained ones in a 100-millisecond window. In general, the best classifier was the K-Nearest Neighbours (KNN) with k=2, except for the first level that was LDA. The best results were obtained for the first classification level, with an accuracy greater than 90%. Although the results obtained for the second and third levels were close to 80%, it was concluded that it was impossible to develop a microcontroller dependent only on one acquisition channel. These results agree with the anatomical characteristics since they are originated from the same muscle group. The cross-validation results were lower than those obtained in the training-test methodology, which allowed us to conclude that the inter-variability that exists between the subjects significantly affects the classification performance. Furthermore, both the dominant and non-dominant arms were used in this work, which also increased the discrepancy between signals. Indeed, the results showed that it is impossible to develop a microcontroller adaptable to all users. Therefore, in the future, the best path will be to opt for the customization of the prototype. In order to test the implementation of a microcontroller in the printed

model, it was necessary to design a support structure in Solidworks that would support the motors used to flex the fingers and Arduino to control the motors. Consequently, the e-NABLE model was re-adapted, making it possible to develop a clinical training prototype. Even though it is a training prototype, it is lighter than those on the market and cheaper.

The objectives of this work have been fulfilled and many answers have been given. However, there is always space for improvement. Although, this dissertation has some limitations, it certainly contributed to clarify many of the doubts that still exist in the scientific community. Hopefully, it will help to further develop the prosthetic industry.

Key-words: Myoelectric signals, Upper Limb Prostheses, Pattern Recognition Control, 3D Printing, Machine Learning Algorithms

Resumo

Nos últimos anos, o aumento do número de acidentes por doenças crónicas, como, por exemplo, a diabetes, e o empobrecimento de determinados países em desenvolvimento têm contribuído para um aumento significativo no número de utilizadores de próteses. A perda de um determinado membro acarreta inúmeras mudanças no dia-a-dia de cada utilizador. Estas são amplificadas quando a perda é referente à mão ou parte do antebraço. A mão é uma ferramenta essencial no dia-a-dia de cada ser humano, uma vez que é através dela que são realizadas as atividades básicas, como, por exemplo, tomar banho, lavar os dentes, comer, preparar refeições, etc. A substituição desta ferramenta é, portanto, uma necessidade, não só porque permitirá restabelecer as funções físicas e motoras do membro superior, como, também, reduzirá o nível de dependência destes utilizadores de outrem e, consequentemente, das taxas de depressão. Para colmatar as necessidades dos utilizadores, a indústria prostética tem-se reinventado e evoluído, desenvolvendo próteses para o membro superior cada vez mais sofisticadas. Com efeito, já é possível controlar uma prótese através da leitura e análise dos sinais mioelétricos do próprio utilizador, o que é denominado por muitos investigadores de controlo por reconhecimento de padrões. Este tipo de controlo é personalizável e permite adaptar a prótese a cada utilizador. Para além do uso de sinais elétricos provenientes do musculo do utilizador, a impressão 3D, uma técnica de manufatura aditiva, têm ganho força no campo da prostética. Por conseguinte, nos últimos anos os investigadores têm impresso inúmeros modelos com diferentes materiais que vão desde o uso de termoplásticos, ao uso de materiais flexíveis. A utilização deste tipo de tecnologia permite, para além de uma rápida entrega do produto ao utilizador, uma diminuição no tempo de construção de uma prótese tornando-a mais leve e barata. Além do mais, a impressão 3D permite criar protótipos mais sustentáveis, uma vez que existe uma redução na quantidade de material desperdiçado. Embora já existam inúmeras soluções, a taxa de rejeição deste tipo de dispositivos é ainda bastante elevada, uma vez que a maioria das próteses disponíveis no mercado, nomeadamente as mioelétricas, são lentas, caras e pesadas. Ainda que existam alguns estudos que se debrucem neste tipo de tecnologias, bem como na sua evolução científica, o número de elétrodos utilizados é ainda significativo. Desta forma, e, tendo em conta que a maioria dos utilizadores não possuí uma área de superfície do antebraço suficiente para ser feita a aquisição dos sinais mioelétricos, o trabalho feito pela academia não se revelou tão contributivo para a indústria prostética como este prometia inicialmente.

Este trabalho pretende resolver alguns desses problemas e responder às questões mais impostas pela indústria e investigadores, para que, no futuro, o número de utilizadores possa aumentar, assim como o seu índice de satisfação relativamente ao produto. Para tal, recolheram-se os sinais mioelétricos de quarenta voluntários, através do sistema de aquisição BIOPAC. Após a recolha, filtraram-se os sinais de seis voluntários através de dois processos diferentes. No primeiro, utilizaram-se filtros digitais e no segundo aplicou-se a transformada de onda para a redução do ruído. De seguida, o sinal foi segmentado em janelas mais pequenas de 100 e 250 milissegundos e extraíram-se treze features no domínio temporal. Para que o processo de classificação fosse otimizado, foram aplicados três métodos de seleção de features. A classificação foi dividida em três níveis diferentes nos quais dois algoritmos de aprendizagem automática foram implementados, individualmente. No primeiro nível, o objetivo foi a distinção entre os momentos em que o voluntário fazia movimento ou que estava em repouso. Caso o *output* do classificador fosse a classe movimento, este teria de, num segundo nível, tentar perceber se o voluntário estaria a mexer apenas um dedo ou a realizar um movimento que envolvesse a flexão de mais de que um dedo (preensão). No caso de uma preensão, passava-se ao terceiro nível onde o classificador teria de identificar se o voluntário estaria a realizar a preensão esférica ou em tríade. Para todos os níveis de classificação, obtiveram-se resultados para o método de validação cruzada e o método de teste e treino, sendo que neste, 70% dos dados foram utilizados como conjunto de treino e 30% como teste.

Efetuada a análise dos resultados, escolheu-se um dos modelos da comunidade e-NABLE. O modelo foi impresso na impressora The Original Prusa i3 MK3S e o material escolhido foi o ácido poliláctico (PLA). Para que fosse possível testar a implementação de um microcontrolador num modelo que originalmente depende da flexão do cotovelo realizada pelo utilizador, foi necessário desenhar uma estrutura de suporte que suportasse, não só os motores utilizados para flexionar os dedos, como, também, o Arduíno. O suporte desenhado foi impresso com o mesmo material e com a mesma impressora.

Os resultados obtidos mostraram que a janela de 250 milissegundo foi a melhor e que, regra geral, o melhor classificador é o K-Nearest Neighbors (KNN) com k=2, com exceção do primeiro nível, em que o melhor classificador foi o Linear Discriminant Analysis (LDA). Os melhores resultados obtiveram-se no primeiro nível de classificação onde a accuracy foi superior a 90%. Embora os resultados obtidos para o segundo e terceiro nível tenham sido próximos de 80%, concluiu-se que não era possível desenvolver um microcontrolador dependente apenas de um canal de aquisição. Tal era expectável, uma vez que os movimentos estudados são originados pelo mesmo grupo muscular e a intervariabilidade dos sujeitos um fator significativo. Os resultados da validação cruzada foram menos precisos do que os obtidos para a metodologia de treino-teste, o que permitiu concluir que a intervariabilidade existente entre os voluntários afeta significativamente o processo de classificação. Para além disso, os voluntários utilizaram o braço dominante e o braço não dominante, o que acabou por aumentar a discrepância entre os sinais recolhidos. Com efeito, os resultados mostraram que não é possível desenvolver um microcontrolador que seja adaptável a todos os utilizadores e, portanto, no futuro, o melhor caminho será optar pela personalização do protótipo. Tendo o conhecimento prévio desta evidência, o protótipo desenvolvido neste trabalho apenas servirá como protótipo de treino para o utilizador. Ainda assim, este é bem mais leve que os existentes no mercado e muito mais barato. Nele é ainda possível testar e controlar alguns dos componentes que no futuro irão fazer parte da prótese completa, prevenindo acidentes.

Não obstante o cumprimento dos objetivos deste trabalho e das muitas respostas que por ele foram dadas, existe sempre espaço para melhorias. Dado à limitação de tempo, não foi possível testar o microcontrolador em tempo-real nem efetuar testes mecânicos de flexibilidade e resistência dos materiais da prótese. Deste modo, seria interessante no futuro fazer testes de performance em tempo real e submeter a prótese a condições extremas, para que a tensão elástica e a tensão dos pins sejam testadas. Para além disso, testar os mecanismos de segurança da prótese quando o utilizador tem de fazer muita força é fundamental. O teste destes parâmetros evitará a ocorrência de falhas que poderão magoar o utilizador, bem como estragar os objetos com os quais a prótese poderá interagir. Por fim, é necessário melhorar o aspeto cosmético das próteses. Para que isso aconteça, poderão ser utilizados polímeros com uma coloração próxima do tom da pele do utilizador. Uma outra forma de melhorar este aspeto, seria fazer o scanning do braço saudável do utilizador e usar materiais flexíveis para as articulações e dedos que, juntamente com uma palma de termoplásticos resistentes e um microcontrolador, permitissem um movimento bastante natural próximo do biológico.

Em suma, apesar de algumas limitações, este trabalho contribuiu para o esclarecimento de muitas das dúvidas que ainda existiam na comunidade científica e ajudará a desenvolver a indústria prostética.

Palavras-chave: Sinais Mioelétricos, Próteses do Membro Superior, Controlo por Reconhecimento de Padrões, Impressão 3D, Algoritmos de Aprendizagem Automática

Contents

List of Figures

List of Tables

List of Abbreviations

AAC	Average Amplitude Changes
AAV	Average Absolute Value
ABS	Acrylonitrile butadiene styrene
ANN	Artificial Neural Networks
CSP	Common Spatial Patterns
coif	Coiflets Wavelets
CWT	Continuous Wavelet Transforms
db	Daubechies Wavelets
dB	Decibel
DOF	Degree of Freedom
DT	Decision Trees
DWT	Discrete Wavelet Transform
EMD	Empirical Mode Decomposition
EMG	Electromyography
FDA	Food Drug Administration
FCR	Flexor Carpi Radialis
FDS	Flexor Digitorum Superficialis
FIR	Finite Impulse Response
FL	Fuzzy Logic
FSM	Finite State Machine
g	Gram
GMM	Gaussian Mixture Models
HAD	Hard Threshold Function
Hz	Hertz
IAV	Integral Absolute Value
IIR	Infinte Impulse Response
KNN	K-Nearest Neighbour
LDA	Linear Discriminant Analysis
MAV	Mean Absolute Value
MAX	Maximum Value
MFL	Maximum Fractal Length
MIN	Minimum Value
ML	Machine Learning

mm	Millimetres
MMAV I	Modified Mean Absolute Value Type 1
MMAV II	Modified Mean Absolute Value Type 2
ms	Milliseconds
MSE	Mean Square Error
MUAP	Motor Unit Action Potential
mV	Millivolt
MVC	Maximal Voluntary Contraction
NB	Naive Bayes
NPR	Non-Pattern Recognition
PCA	Principal Component Analysis
PET-G	Polyethylene terephthalate glycol
PID	Proportional–Integral–Derivative
PLA	Polylactic Acid
PR	Pattern Recognition
RMS	Root Mean Square
s	Seconds
sEMG	Surface Electromyographic Signal
SD	Standard Deviation
SNR	Signal-to-Noise Ratio
SOFT	Soft Threshold Function
SSC	Slope Sign Changes
SSI	Simple Square Integral
SVM	Support Vector Machines
sym	Symelets Wavelets
TMR	Target Muscle Re-Innervation
VAR	Variance
WA	Wilson Amplitude
WL	Waveform Length
WT	Wavelet Transform
ZC	Zero Crossings

1. Introduction

1.1. Motivation

One of the most crucial structures of the human body is the hand since it plays a fundamental role in perceiving tactile sensations and performing basic daily activities. The human hand is also an indispensable tool in the establishment of interpersonal communication [1][2]. The loss of a total or part of the upper limb causes personal difficulties that result in an emotional detriment of the affected ones [3]. Besides that, researchers found that the rates of clinical depression range from 21 to 35% [4]. Unfortunately, many people suffer from upper limb deficiencies that might be either due to congenital malformations or from limb amputations.

In 2019, 2 million people lived without a body member. Thirty-five percent of those lived without an upper limb [5]. In the United States of America (USA), the prevalence of amputations was 1.6 million in 2005, which might duplicate until 2050 [6]. In 2019, The American Academy of Physical Medicine and Rehabilitation estimated that approximately 30000 to 40000 amputations were performed in the USA [7]. In Europe, Italy performs 3500 upper limb amputations per year [2], and the United Kingdom alone has more than three hundred people that suffer from upper limb amputation every year [8]. In Portugal, between 2000 and 2015, 11786 amputations of the upper limb were performed [9]. For the paediatric population, the occurrence of congenital malformations is the principal reason for the loss or non-formation of the upper limb. Globally, the number of newborns babies with congenital malformations is 7.9 per 10000 live births [10]. Epidemiologic studies from Finland, Canada, and Australia have estimated an overall incidence of upper limb anomalies between 3.4 and 5.3 per 10000 live births [11]. In Sweden, the prevalence for upper limb anomalies was 21.5 out of 10000 and in the USA it was 13.7 per 10000 live births [12].

The loss of the total or part of the upper limb has numerous consequences, mainly at young ages. Besides the damages to mental health, the negative impact on muscle development and bilateral coordination is significant. The use of prosthetic devices at an early age is truly beneficial for children. Subsequently, there is an improvement in muscular performance, bimanual activity, symmetrical growth, and manual dexterity development [13][14]. As the estimation by the World Health Organization for individuals with physical disabilities who require prosthetic treatment is about 0.5% of the world population, the prosthetic industry has been growing and innovating in the development of new prosthetic solutions [15]. Among all the available commercial options, cosmetic prostheses are the most used. Nevertheless, when it comes to functionality, body-powered and electrical prostheses are better classified.

Despite the efforts made by the industries, the prostheses that are currently available in the market still need improvement. Due to the fact that this market is relatively small, the development is still slow and expensive. Academic institutions have been developing new techniques to promote precise control. Nevertheless, the advances in the educational environment do not reach the industry due to the lack of robustness and usability [16]. Nowadays, there is a gap between prostheses' functionality and natural body functionality [17]. Besides the lack of robustness and functionality, the current prostheses are heavy and expensive. These features are responsible for the rejection rates, which are still significant. Biddiss *et al* [18] found that the rejection rate in children is about 38% for passive prostheses, 45% for body-powered prostheses and 32% for electric prostheses. In adults, the rejection rate is 39% for passive

prostheses, 26% for body-powered prostheses and 23% for electric prostheses. In general, myoelectric prostheses, an electrical prosthesis type, have a limited clinical and commercial impact which justifies the abandonment average rate of 25% among users [19].

Solving these limitations and needs might change the prosthetic industry and the lives of thousands of amputees and children. Creating more advanced customized solutions is the key to balancing the users' needs and industries' products.

1.2. Objectives

The aim of this dissertation is to investigate if it is possible to develop a low-cost and simple model suitable for every customer. This model incorporates a myoelectric controller in a low-cost 3D printable model. Therefore, we will have a hybrid functional upper limb prototype with a 3D printable design, controlled by the patient through myoelectric signals. To accomplish the objective, this work was divided into two parts. In the first part, we studied the different methodologies and signal processing techniques to develop a reliable and simple machine learning controller algorithm. In the second part, we optimised an online 3D printable model.

The field of prosthetics has been growing. More recently, many prostheses use machine learning algorithms that analyse features extracted from myoelectric signals for further gesture recognition. Because of that, academic researchers have been giving more and more attention to the methodology that can be followed to improve the results. Although there are many previous studies regarding real-time gesture recognition models, there are no standardised concepts. Furthermore, there is a gap when it comes to the recognition of a dataset with grasps and fingers movements with a low number of acquisition channels. Therefore, the first part of this work is focused on finding if the use of a single channel acquisition is enough to build a machine learning controller algorithm that identifies different hand gestures for a large population.

The second part focuses on re-designing and customising the 3D-printed prosthetic model originally designed by the e-NABLE community. Since this prototype will replace the user's forearm and its functions, we must ensure that we combine the degree of freedom of the integrant parts of the prosthesis with the studied myoelectric controller.

1.3. Structure

This dissertation is structured in six chapters:

Chapter 1 includes the motivation and objectives of this work.

Chapter 2 presents a basic description of upper limb anatomy and disabilities, the current commercial solutions, and the user needs. This chapter also describes the role of additive manufacturing in prosthetic design and some concepts of electromyography since it is the basis of myoelectric control.

Chapter 3 describes the different types of myoelectric controllers and the drawbacks that still exist in the prosthetic control.

Chapter 4 focuses on the signal pre and processing techniques as well as the followed methodology and describes design specifications for the optimized structures.

Chapter 5 discusses the results obtained during the classification process and the features of the produced prototype.

Chapter 6 presents the conclusion of this dissertation that includes some future perspectives for further developments and future studies in this scientific area.

2. Background Research

This chapter describes some of the fundamental concepts about the upper limb anatomy and the associated pathologies related to the theme of this dissertation. These concepts are fundamental to developing a functional and useful prosthetic device. Furthermore, the current prostheses and the more advanced and recent technologies involved in their production are also discussed.

2.1. Upper Limb Anatomy

The upper limb is divided into four regions. The first part is the arm, which extends from the shoulder to the elbow, the second part is the forearm, which goes from the elbow to the wrist. The third one goes from the wrist to the hand. The bones of the upper limb are divided along these four structures: the humerus, radius, ulna, eight carpal bones (small bones divided into two rows), five metacarpal bones (distributed by the palm) and fourteen phalanges (Figure 2.1) [20][21][22].

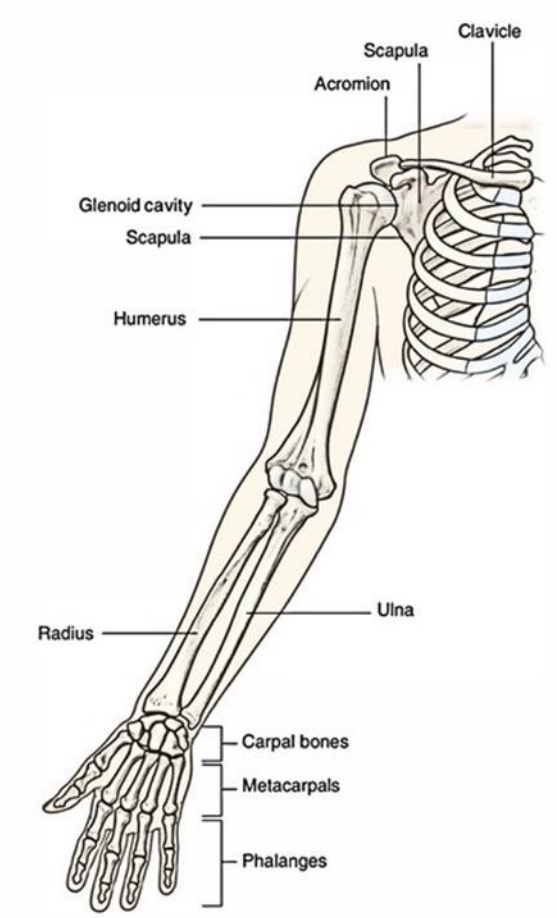

Figure 2.1: Upper Limb bones structure (extracted from [20]).

The loss of the hand has a massive impact on users' lives since it limits their lives in the most basic daily activities. Only the use of a prosthesis could replace some of the loss functions. Therefore, it is crucial to develop a prosthesis capable of performing the same movements as the missing limp part. There are six fundamental movements that need to be analysed: flexion, extension, abduction, adduction,

supination, and pronation. Flexion is a movement of an anterior body part to the coronal plane (Figure 2.2-A). Conversely, the extension is the movement of a part of the body posterior to the coronal plane (Figure 2.2-A). Abduction is the movement away from the midline of the body. In this movement, an upper limb part goes from the frontal plane to the opposite direction of the body midline (moving away). In turn, adduction is the movement towards the midline (approaching) - Figure 2.2-A. Rotation is the movement of the bone along the longitudinal axis. Pronation is a rotation of the palm (Figure 2.2-C). Conversely, supination is the movement of the palm previously to the anatomical position (Figure 2.2-C). These movements are performed by flexors, extensors and abductors muscles of the upper limb (Figure 2.2-A) [20][21][23][24].

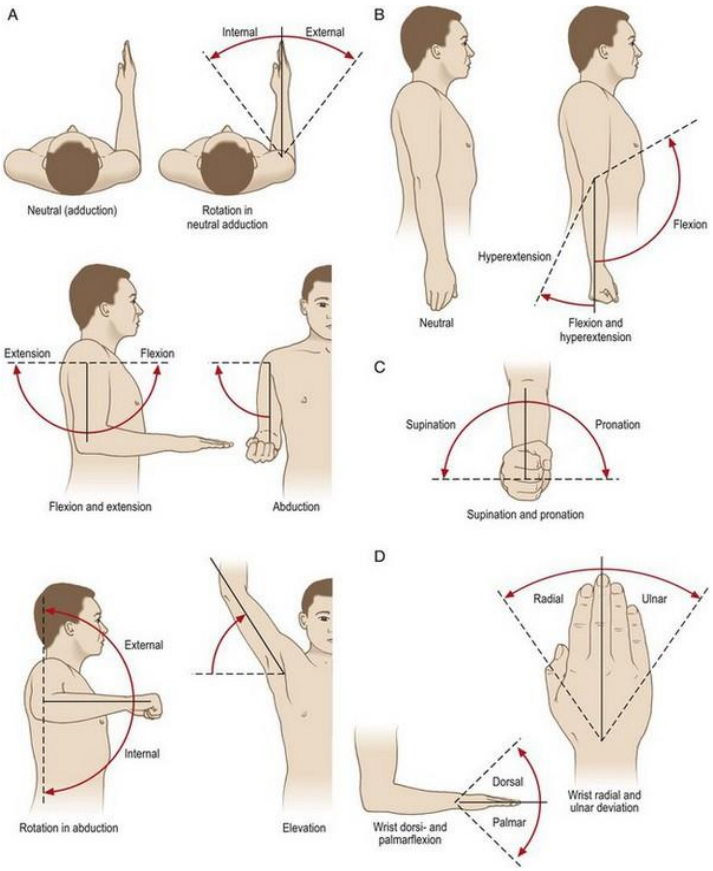

Figure 2.2: Upper Limb Movements: A- Internal and external rotation of the arm; Extension and Flexion of the forearm and elevation. B- Flexion of the Forearm, C- Supination and Pronation of the forearm, D- Ulnar and Radial Deviation (extracted from [24]).

Thumb flexion is the separation of the thumb from the second finger. Thumb abduction and adduction occur in the carpometacarpal joint (Figures 2.3- 5 and 6). The anteposition is the movement of the thumb and the fifth finger when one moves towards the other [20][21][23][25][26].

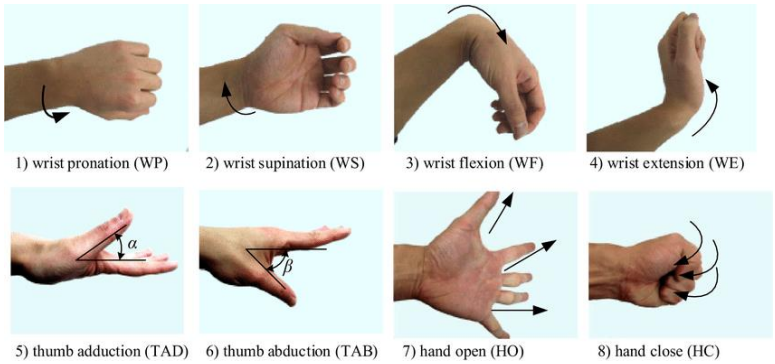

Figure 2.3: Wrist movements (1-4), thumb movements (5-6), hand basic movements (7-8) – extracted from [26].

The rest of the hand movements are performed on the wrist joint. This joint can be flexed and extended along the perpendicular plane to the palm up to about an 80 to 70 degree angle, respectively- see figure 2.3 - 3 and 4. Hand flexion allows the closing of the digital chain, which promotes hand closing. The extension, on the other side, induces the opening of the hand. Phalanges flexion and extension take place around a transverse axis, which passes at the level of the proximal and distal interphalangeal joints. The proximal interphalangeal joint does not perform flexion and extension at all. The adduction and abduction movements are performed on the axis of the hand. While the abduction movement makes the fingers move away from the hand axis, the adduction one brings the fingers closer to the hand axis. These movements are performed during the digital extension movement [20][21][23][25].

Digital grips use two or more fingers to hold an object without the aid of the palm [27]. Grasping movements are the most precise ones (Figure 2.4). The hand starts opening with the fingers' extension and abduction to capture the object. Then, the hand closes through the action of the fingers' flexor muscles and the thumb adductor muscle. The digital grip is a precise movement. The fingers' position is achieved by fixing the wrist, the metacarpophalangeal and interphalangeal joints. Finally, the object is fixed with the thumb opposition and the second and third fingers flexion [23][28].

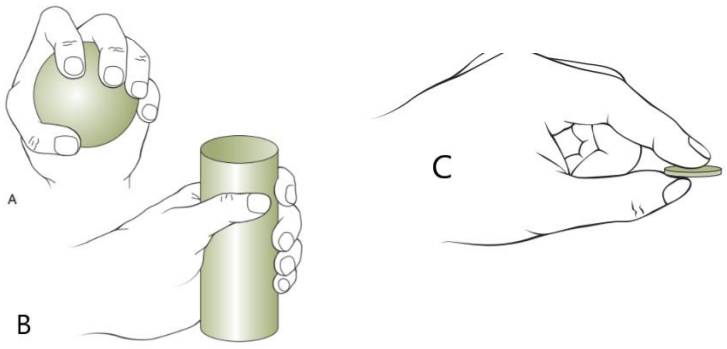

Figure 2.4: Grasp Movements: A- Spherical Grip, B- Cylindrical Grip, C- Tripod Grip (extracted from [28]).

The muscles that originate the hand movements are located in the forearm and in the hand. Because of that, it is essential to study the hand muscles as well (Figure 2.5).

In this dissertation, studying the muscles responsible for the grasp movements is crucial since they originate the myoelectric signals that will be used to control the developed prototype. Due to the limitations of the prosthesis user, only the signals that are generated at the forearm level will be recorded.

Because of that, in the following table, it is possible to observe the principal muscles involved in the forearm and hand movements (Table 2.1, 2.2 and 2.3) [20][21][23][29][30][31].

Table 2.1: Arm muscles and its functions (based on the information from [20][21][23][29][30]).

Arm Muscles	Localization (Figure 2.6)	Affected Structures
Deltoide	Lateral third of the clavicle	Flexion and Extension of the arm; Abduction of the shoulder and of the arm and Stabilization of the shoulder joint
Brachialis	Distal half of the anterior side of the humerus	Flexion of the forearm
Biceps brachii	Supraglenoid tubercle of the scapula and apex of the coracoid process of the scapula	Flexion of the forearm at the elbow joint, supination of the forearm
CoracoBrachialis	Coracoid process of the scapula	Adduction and flexion of the Arm
Triceps brachii	Posterior surface of the humerus and infraglenoide tubercle of the scapula	Extension of the forearm

Table 2.2: Forearm muscles and its functions (based on the information from [20][21][23][29][30]).

Forearm Muscles	Localization (Figure 2.6)	Affected Structures
Abductor Pollicis Longus	Posterior surface of the radius	Abduction of the thumb and the wrist
Extensor Pollicis Longus	Lateral Surface of the Ulna	Extension of the thumb and wrist abduction
Extensor Pollicis Brevis	Dorsal surface of the radius	Extension of the metacarpal joint of the thumb
Extensor Digitorum	Lateral epicondyle of the humerus	Extension of the wrist and extension of the phalanges of the finger
Flexor Pollicis Longus	Anterior surface of the radius and interosseous membrane (forearm)	Flexion of the interphalangeal and the metacarpophalangeal joint of the thumb
Flexor Digitorum Superficialis	Medial epicondyle of the humerus, coronoid process of the ulna and superior half of anterior border	Flexion of the proximal interphalangeal and the metacarpophalangeal joints

Flexor Digitorum Profundus	Proximal parts of the anterior and lateral surfaces of the Ulna and interosseous membrane	Flexion of the distal interphalangeal joints
Pronator Teres	Humeral head and ulnar head	Pronation of the forearm and flexion of the elbow
Pronator Quadratus	Anterior surface of the Ulna	Pronation of the forearm and binding of the radius and ulna
Palmaris Longus	Medial epicondyle of the humerus	Flexion of the hand at the wrist joint
Flexor Carpi Ulnaris and Radialis	Medial Epicondyle of the humerus and humeral head and posterior border of the ulna respectively	Flexion of the wrist and ulnar deviation
Supinator	Lateral epicondyle of the humerus	Supination of the forearm
Extensor Carpi Ulnaris and Radialis	Lateral epicondyle of the humerus and posterior border of the ulna and Lateral supra-epicondylar bridge of the humerus	Extension, adduction (Extensor Carpi Ulnaris) of the wrist joint and abduction of the hand at the wrist joint (Extensor Carpi Radialis)
Extensor Indicis Proprius	Posterior side of the distal third of the ulnar shaft	Extension of the second finger
Extensor Digiti Minimi	Lateral epicondyle of the humerus	Extension of the little finger
Brachioradialis	Proximal two-thirds of the supra epicondylar ridge of the humerus	Flexion of the Forearm

Table 2.3: Hand muscles and its functions (based on the information from [20][21][23][29][30]).

Hand Muscles	**Localization (Figure 2.5)**	**Affected Structures**
Thenar Eminence: Flexor Pollicis Brevis, Abductor Pollicis Brevis, Opponens Pollicis)	**Flexor Pollicis Brevis and Abductor Pollicis Brevis**: Flexor retinaculum and tubercles of trapezium and scaphoind carpal bones **Opponens Pollicis:** Flexor retinaculum and tubercle of the trapezium and scaphoid carpal bones	**Flexor Pollicis Brevis**: Thumb Flexion **Abductor Pollicis Brevis**: Thumb abduction **Opponens Pollicis:** Thumb Flexion, abduction and medial rotation

Hypothenar eminence: Flexor Digiti Minimi Brevis, Abductor Digiti Minimi Brevis, Opponens Digiti Minimi	**Flexor Digiti Minimi** Brevis: retinaculum (carpal Bone) **Abductor Digiti Minimi**: Pisiform (carpal Bone) **Opponens Digiti Minimi:** hamate and retinaculum (carpal bones)	**Flexor Digiti Minimi Brevis:** Flexion of the thumb **Abductor Digiti Minimi**: Abduction of the thumb **Opponens Digiti Minimi**: Opposition of the thumb
Interossei	Sides of two adjacent metacarpais and palmar surfaces of the metacarpals (hand)	Abduction of the fingers, adduction of the fingers and thumb
Lumbricallis	Tendons of the Flexor Digitorum Profundus (hand)	Flexion of the metacarpophalangeal joints and extension of the interphalangeal joints

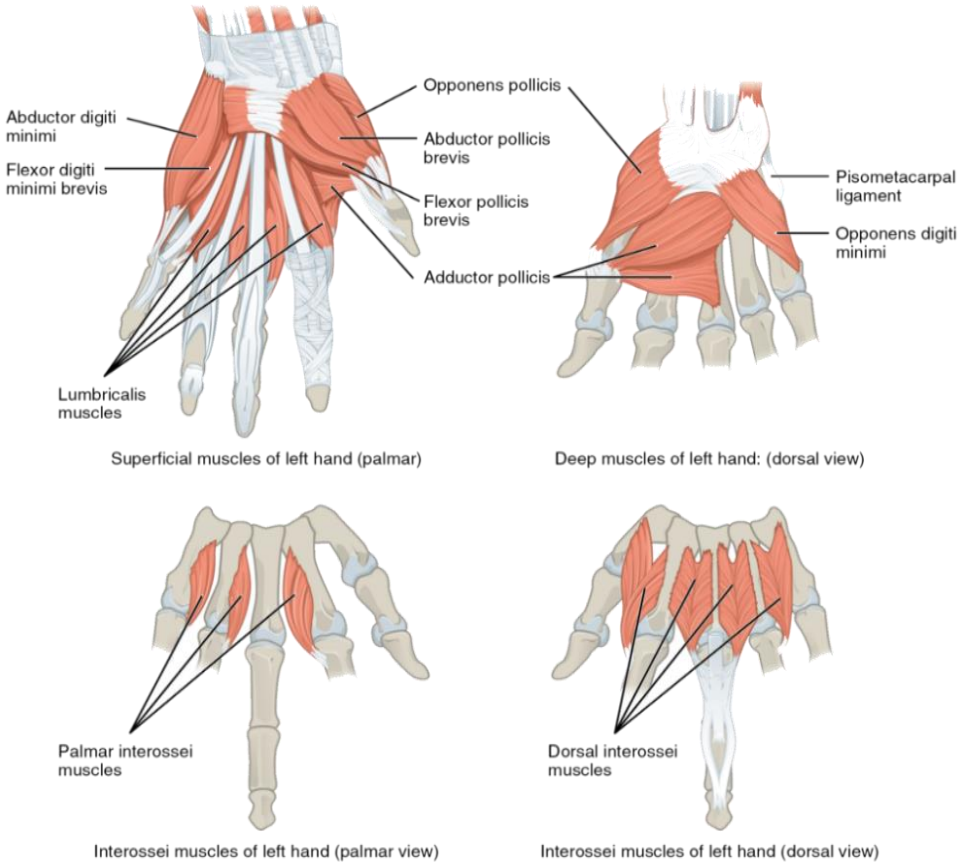

Figure 2.5: Superficial and Deep Muscles of the Hand (extracted from [31]).

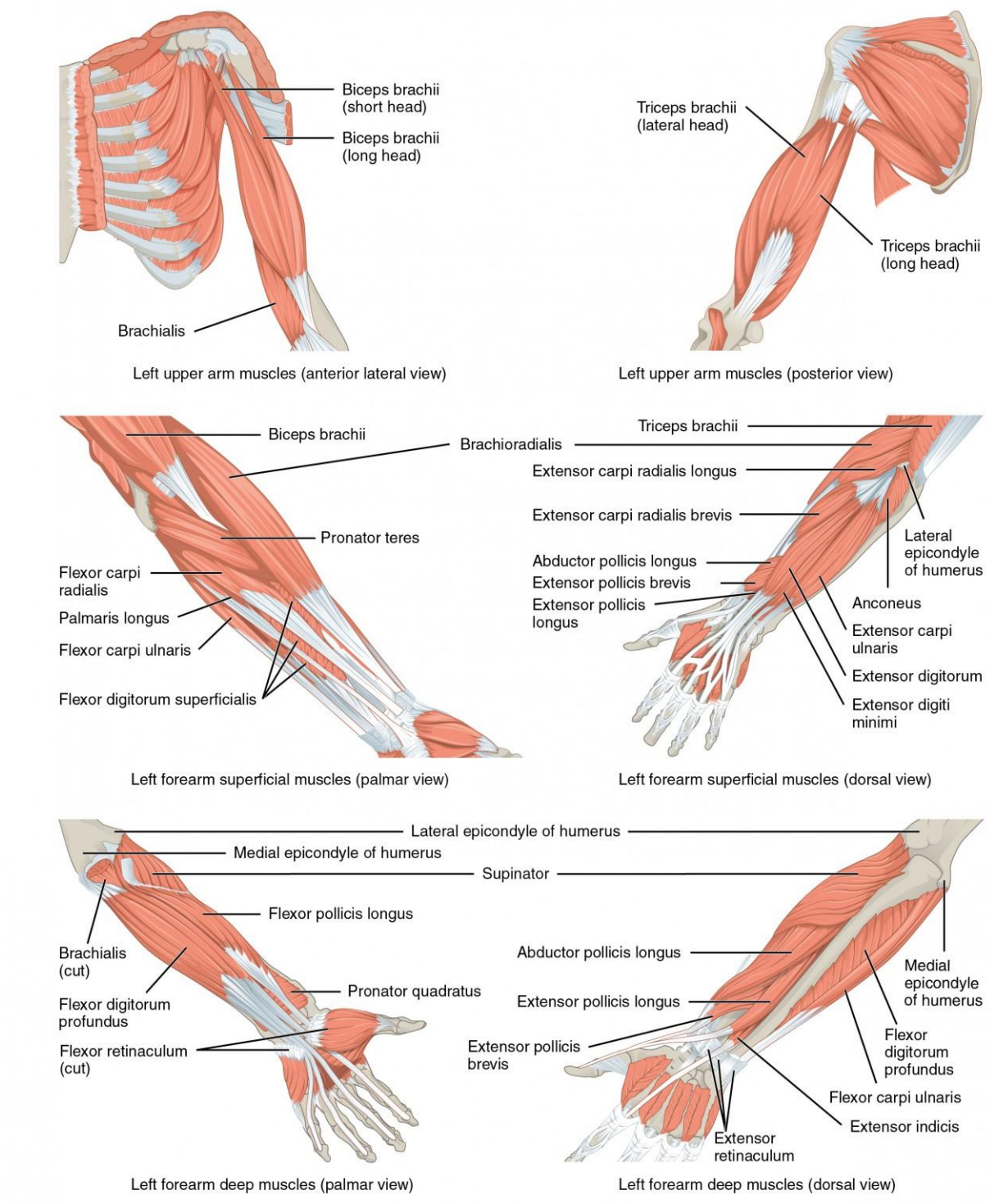

Figure 2.6: Upper Limb Muscles (Superficial and deep muscles illustration)- (extracted from [31]).

2.2. Upper Limb Pathologies

2.2.1. Congenital Malformations

The formation of the upper limb occurs between the fourth and eighth weeks after fertilization. The upper limb embryogenesis starts with the lateral migration of two mesoderm layers and it ends with

the plaque, which is responsible for muscle formation [32][33][34]. Structural congenital malformations are responsible for physical anomalies in limbs. The majority of the structural defects occur in the earliest weeks of pregnancy [35].

Although 50% of congenital anomalies are not associated with a specific cause, it is possible to identify genetic, social, environmental and behavioural risk factors. The genetic pool of some ethnic communities gives precedence to the appearance of rare mutations worldwide. Mother's age, the presence of diabetes, alcohol and drugs consumption, intake of medication with vasoconstriction effects and radiation exposure are some examples that contribute to increasing chromosomal abnormalities occurrence. It is thought that the prevalence of structural anomalies is higher in developing countries. This might be related to the lack of access to primary health care and family planning appointments. Ninety-four per cent of congenital anomalies are observed in populations with a low financial income and poor health care systems [11][36]. Another frequent cause is the existence of amniotic bands in the uterine cavity.(Figure 2.7) [36][32]. During its development, the embryo is surrounded by a thin membrane (amnion). In rare cases, this band can run through the uterine cavity. Since in the urinary cavity, the membrane can bind around the upper or lower limbs. There is a blockage in blood flow when this happens, which leads to tissue necrosis of the affected limb or part of it. This condition is called amniotic band syndrome. There are two treatments, but their application depends on the early detection of this condition. The success of the uterus fetal surgery treatment depends on the degree of the damage. Postnatal treatment is the reconstructive surgery of the limb. After this, prosthetic treatment is highly recommended [36][37].

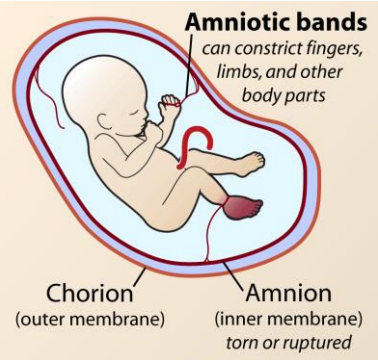

Figure 2.7: Amniotic Band Syndrome Illustration (extracted from [37]).

There are two main types of congenital anomalies: longitudinal ones and transverse ones that are illustrated in Figure 2.8. The longitudinal congenital anomalies are the partial or total loss of a limb part, known as dysmelia. Of all malformations of the upper appendicular skeletal bones, the radial ray deficiency is the most common one, which happens with an average incidence of 1.01 per 10,000 live births [11]. In comparison to the radial deficiency, ulnar longitudinal deficiencies are four times less common, with an incidence of 0.44 per 10,000 live births [11]. In this case, the most affected structures are the hand and the wrist [11][38][32] In transverse anomalies, the limb resembles an amputation stump [10]. The congenital transverse deficiencies incidence is 1 per 20,000 live births [38]. Adams-Oliver syndrome, Holt-Oram syndrome, absent radius syndrome-thrombocytopenia are some of the best examples [38][32]. This dissertation does not detail these syndromes because they are associated with other severe diseases such as heart failure and neurological concerns. Syndromes like these are rare and

the principal concerns are not the missing of a body limb. Because of that, this dissertation will focus on finding a solution for subjects with longitudinal congenital malformations [39].

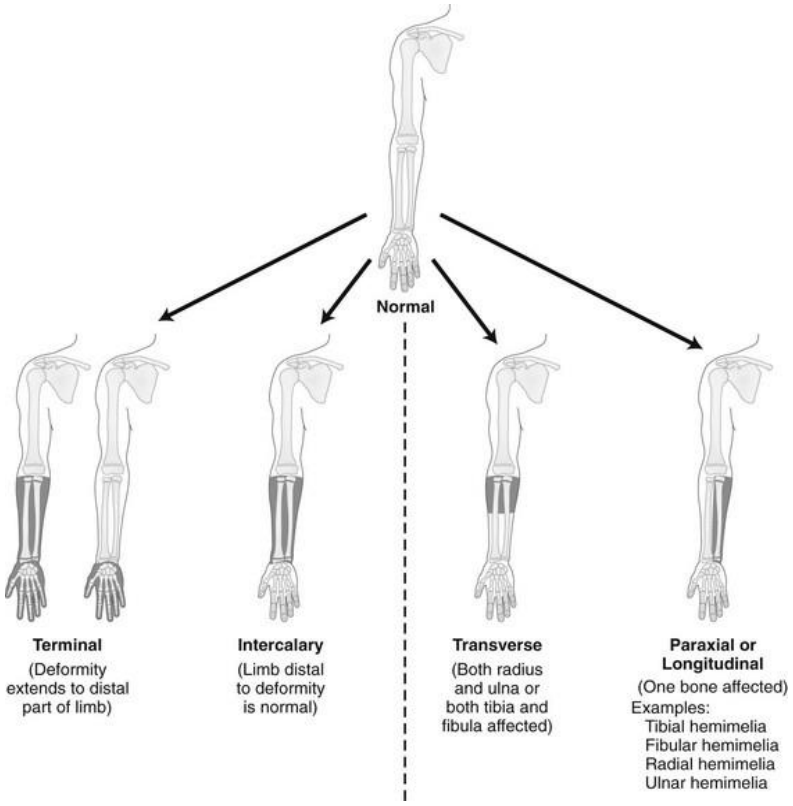

Figure 2.8: Upper Limb Anomalies: Terminal and Intercalary at left and transverse and longitudinal at right (extracted from [39]).

2.2.2. Traumas and amputations

Traumatic events or severe diseases can lead to the loss of the upper limb part. In the last few years, wars in African and Middle East countries have caused a million injuries, of which 8% need prostheses [20]. Conversely, in developed countries, the leading cause of amputations are vascular disorders, Strokes, Transient Ischemic Attacks, Subarachnoid and Subdural Haemorrhages are a few examples of such vascular pathologies. In second place are traumas, and in third, a list of other risk factors. Untreated infections such as meningitis, encephalitis, polio and epidural abscess, sepsis, and diseases such as diabetes, cancerous tumours, neuromuscular diseases, and degenerative diseases (Huntington's Disease, Parkinson's Disease) are risk factors as well [40][41]. Depending on the amputation level, upper limb amputations can be classified into partial hand amputation, wrist disarticulation, transcarpal, transradial or transhumeral amputation and shoulder disarticulation illustrated in Figure 2.9 [42][43][44]. In Figure 2.9, the black lines represent the end of the upper limb for each amputation case.

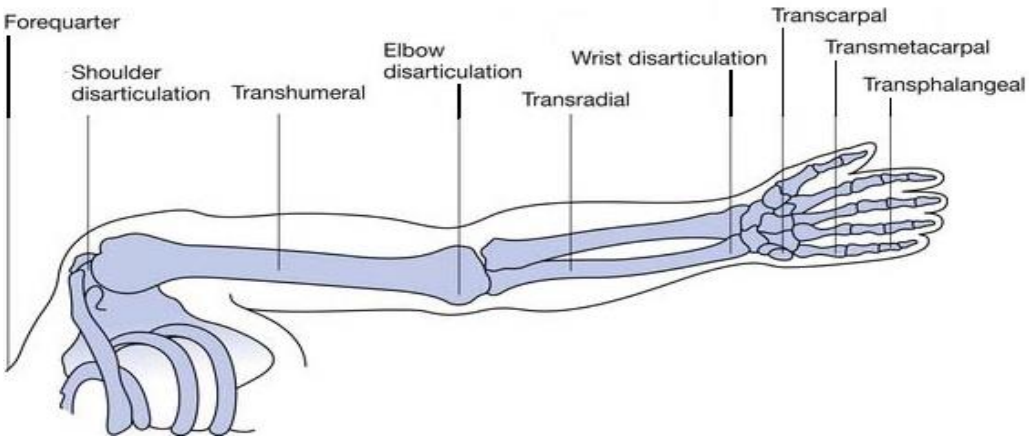

Figure 2.9: Upper Limb Amputation's Levels (adapted from [44]).

2.3. Additive Manufacturing in Prosthetic Development

In the last years, additive manufacturing techniques have grown due to their extensive applications in solving health problems. With these techniques, the production of structures with a high degree of complexity in a short time is a reality. At the same time, it is possible to save material and financial resources [45][46]. The interest of the industries in 3D printing arose in 2013. According to experts' expectations, 3D print technology grew from 6 billion to 21 billion from 2016 to 2021. The main advantage is the possibility of printing a single part instead of a unique prosthetic model which ends up being more economical. Furthermore, the time to market is short when compared to current prosthetic production techniques. The personalization and customization levels provided by 3D print technology are the most central factors to raise the users' awareness [13][47].

However, since this technology has not been regulated by the Food and Drug Administration (FDA) standards, some tests need to be done to verify its effectiveness and security. [48] In the academic world, some studies are exploring new solutions and materials to improve this technology. Most of the current 3D printable prostheses are electric and body-powered ones. The best examples of it are the online models that are available to the community, such as Cyborg Beast, the Raptor Hand and Limbitess Arm body-powered models from the e-NABLE community and Handiii Coyote, an externally powered prosthesis [45][46][47].

2.4. Current Prosthetic Solutions

The upper limb prostheses can be categorized into passive prostheses and active prostheses [49][50][51]. Passive prostheses are divided into two groups: static and dynamic prostheses. While the fixed prostheses only serve for aesthetic purposes, the dynamic ones allow the patient to grab some objects since they are controlled by internal mechanisms [51][52]. Active prostheses perform grasping movements because they are controlled by internal mechanisms. Those mechanisms can be electric actuators or corporal cables. Body-powered prostheses depend a lot on the user, which means that the user has to perform auxiliary movements to promote prostheses movement. Conversely, electrical prostheses do not require any movements from the patient [13][47][51][52].

2.4.1. Passive Prostheses

Passive prostheses are the most competitive prostheses in the market due to their low price. For this reason, these prostheses are sought by one-third of the users [42][52]. These prosthetic devices have some postural benefits since they restore the body's symmetry, particularly when the user has proximal amputations. These prostheses are usually made of flexible latex, rigid plastic materials or silicone [44]. Some academic studies present, as an alternative to silicone, the use of 3D printed Filaflex® structures [47][53][49]. However, this type of prosthesis is manufactured for cosmetic purposes and therefore does not meet the functional needs of the users. One of the most well-known prostheses is the LIVINGSKIN ™ arm, illustrated in Figure 2.10 [54].The WILMER Passive Hand Prosthesis (Figure 2.11) enables the user to perform some movements because it includes a functional hook [55].

Figure 2.10: LIVINGSKIN ™ arm by Össur Company (extracted from [54]).

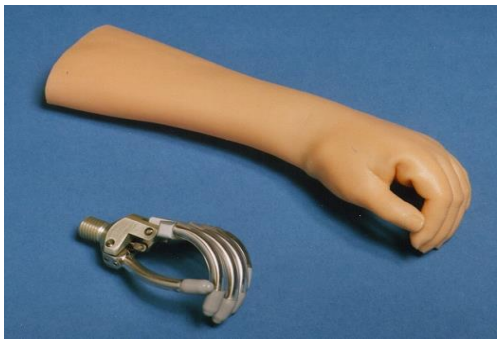

Figure 2.11: WILMER Passive Hand Prosthesis by TU Delft (extracted from [55]).

2.4.2. Body-Powered Prostheses

Body-powered prostheses operate through active hands and operational cables, which move through body movement [13][42][56]. Some of these prostheses, mainly the recent ones, are produced using 3D printing technology. As already mentioned, body-powered prostheses are devices dependent on their user. Therefore, non-elastic cables, which have the same function as the flexors, are connected to a healthy part of the residual limb (elbow or hand). As a result, the movement of the prosthesis structure will depend on the flexion of the healthy structures. Elastic cords and a combination of materials that provide phalanges resistance are used to perform the extensors functions [47]. Body-powered prostheses are reliable devices that can be used in work and dusty environments. For this reason, they are often preferable for workers with outdoor jobs. However, these devices are mechanically inefficient. In most cases, users cannot perform muscular prehensile strength with body-powered prostheses. The extreme user's effort is often painful and causes discomfort in the residual limb

[51]. In economic terms, these prostheses can cost between $4000 and $10000 [49][45][47]. This price is lower when body-powered prostheses are made of 3D printable materials.

Many institutions and communities use this type of prostheses since they are the most cost-effective ones. The best example is the "Enabling the Future" project from the e-NABLE community. This online community has models of low-cost e-NABLES prostheses available as well as their design features [57]. The most popular and successful e-NABLE models are the Raptor Hand (Figure 2.12) and Cyborg beast (Figure 2.13). The first design of this community was the Limbitless Arm (Figure 2.14), an open-source design featuring an Arduino Micro microcontroller, a single servo capable of producing torque, muscle sensors, and a Kevlar survival cord to move the fingers. The downside of this design is that the hand can only open and close because there is only a single servo motor in the design. Conversely, the Limbitless arm is very inexpensive and comfortable for the user [14].

Raptor Hand (Figure 2.12) is a 3D prosthesis composed of a modular tension system that contains elastic and nylon wires. The flexion movement is accompanied by the wrist flexion and the closing movement of the fingers. The cost of this prototype is 35€ [58].

Figure 2.12: Raptor Hand (extracted from [58]).

The Cyborg Beast has1.5 *mm* elastic Velcro strings on the dorsal surface of the fingers that allow the passive extension of the finger. Conversely, the flexion movement is performed by 1*mm* non-elastic nylon strands. These strings are placed along the palmar surface of each finger. The materials used were Polylactic Acid (PLA) and Acrylonitrile Butadiene Styrene (ABS). The Cyborg beast (Figure 2.14) weighs 184.2g and costs 42.48 €. The total printing and assembly time is about 2.5 hours [59].

Figure 2.13: Cyborg Beast (Extracted from [59])

Figure 2.14: Limbitless Arm (extracted from [14])

In Portugal, Patient Innovation, a non-profit association, is categorized as a platform that allows patients, collaborators and caregivers to share their solutions with others. As a rule, the available solutions focus on solving medical problems and can be found in the following categories: conditions, symptoms, location, activities, devices or therapies. Since 2018, Patient Innovation has developed low-cost body-powered prostheses to offer Portuguese children with upper limb disabilities [60]. To help this initiative, Professor Dr Bruno Soares and Professor Dr. ª Cláudia Quaresma from the Nova School of Science and Technology of the Nova University of Lisbon created a laboratory with 3D printers where mechanical engineers' students and biomedical engineers' students can develop and optimize prosthetic solutions for the users.

2.4.3. Electrical Prostheses

Since 1990, NASA and other technological institutions have been developing robotic hands with no more than two degrees of freedom. Despite the high technology, those hands are not suitable for daily use due to different physical restrictions. However, some of the prototypes are good examples of actual robotic hands [61].

Electrical prostheses are composed by servomotors, batteries, microcontrollers and electromyography sensors. The force distribution is mainly done equally by all fingers through a single servo motor. However, the most advanced ones distribute the force individually for each finger from different servomotors [45]. Noise and slow movements are the limitations imposed by conventional direct current (DC) electric motors. These prostheses have advantages such as comfort, cosmetic acceptance and superior compressive force. Regarding the disadvantages, it is possible to identify the noise, slow movements and strength limitations [62].

2.4.4. Myoelectric Prostheses

Myoelectric prostheses belong to electrical prostheses, which means that they have motors and microcontrollers as well. The received input is the amplitude of the myoelectric signals, which results from muscle activation. Once detected by the surface electrodes, the signals need to be amplified and filtered. The resulting output activates the prosthesis, exercising an autonomous and robust control [42][45][63][64]. Besides that, these prostheses have more than two degrees of freedom, which is why they are preferable for daily activities.

Nevertheless, the market price of the myoelectric prostheses is too high, between 21000 € and 64000 €. Most commercial models are too heavy to be used by children [65]. These devices are also noisy due to external factors like fatigue, sweat and external pressures. The residual tissue of the stump and the environment during EMG acquisition increase the noise as well. These types of parameters will increase the response time of the prosthesis and make it move slower [66]. At a mechanical level, the existence of frictional forces on the control cable is decisive for the relationship between the control movement and the movement of the final effector [67].

Despite the overall limitation, there are many industries producing myoelectric prosthetic devices. However, the most well-known are the OttoBock Co in Germany, the Utah Arm Company in the USA, the Ossur and the OpenBionic™. These prostheses typically perform hand and grip positions and, in most cases, are capable of controlling each finger independently [8]. The most popular non-pattern myoelectric control prostheses on the market are BeBionic Hand, Michelangelo Hand and i-Limb Hand

[47][68][69][70]. Besides these known commercial prostheses, there are still ongoing prostheses such as the Modular Prosthetic Limb system sponsored by the Defence Advanced Research Projects Agency, the Smart Hand, and the UNB hand [8].

The BeBionic hand (Figure 2.15) is a top product by Ottobock. It is a comfortable, intuitive and precise hand with fourteen different grip patterns and hand movements. The performance of the individual motors of each finger allows a natural and coordinated movement. This prosthesis has a proportional control that regulates the speed through the strength of the muscles. This prosthesis was designed with engines that optimize the weight distribution, which gives some comfort to the user. An integrated sensor is attached to the hand since it allows varied movements and different thumb positions. The BeBionic includes software and wireless technology that allows the user to customize the available functions according to their lifestyle. The materials chosen for its construction are strong enough to support up to 45kg. The innovative palm design protects the prosthesis from impacts and physical damage and helps to reduce noise [68].

Figure 2.15: Be-Bionic Arm by Ottobock (extracted from [68]).

The i-Limb® (Figure 2.16), produced by Össur, is a multi-articulated prosthesis. Thumb control is manual but automatically switches between the lateral and reference positions. The i-Limb offers eighteen automated options [69].

Figure 2.16: i-Limb by ossur (extracted from [69]).

Michelangelo's hand (Figure 2.17) is an Ottobock product. This hand has specific characteristics when it comes to finger's control. While a servomotor controls the thumb, the first and the second fingers, the third and fourth fingers move passively. Multiaxial movement patterns minimize unilateral

Figure 2.17: Michelangelo's hand by Ottobock UK (extracted from [70]).

compensation movements performed by the patient maintaining the body's natural posture. When the prosthesis is activated, it is possible to choose three positioning modes that allow seven different grips. However, as soon as the prosthesis is no longer in use, it returns to its resting position. The material that makes up the fingers is lightweight but resistant, which confers a high precision during the grasping process to the prosthesis. The patient can also choose to use a silicone glove that gives it a more natural look [47][70].

The DEKA arm, an advanced prosthetic arm recently approved by the FDA, has a fully powered three degree-of-freedom (DOF) shoulder, an elbow, a two DOF wrist, and six hand gripping patterns [71][72].

Figure 2.18: DEKA arm (extracted from [72]).

Another very effective solution that has currently been developed is the OpenBionics™ upper limb prosthetic device that uses 3D printed parts to lower production costs and allows customization of each commercialized prosthesis. The device produced by OpenBionics™ is the Hero Arm. This prosthesis uses proportional control to control the speed of the movement. This device made with nylon 12 can lift up 8 Kg and weights 340 g [73].

Myo Plus Prosthesis (Figure 2.19), is one of the most recent Ottobock products. It is a myoelectric prosthesis controlled by pattern recognition-based methods. This prosthesis has the extraordinary capacity to learn and interpret the individual movement patterns of the user, through the use of the MyoPlus App. This intuitive control enables the users to adapt their prostheses to their individual needs. However, this prosthesis is not ideal or recommended for daily activities. [74]

Figure 2.19: MyoPlus Prosthesis by Ottobock UK (extracted from [74]).

These devices are controlled essentially by proportional control. This control uses the myoelectric signal of the user to control the speed of the prosthesis. Therefore, it is possible to conclude that the use of myoelectric signals as a natural control source has brought numerous advantages, mainly because it can be used in commercial devices [16]. Besides that, the use of myoelectric prostheses is becoming more natural. However, there is still a gap between the operational control and the natural appearance of the human hand. The operational control is still slow and, unfortunately, mobile apps control the more complex movements. Besides that, these prostheses are the most expensive prostheses on the market, which means that only some users have access to them. Therefore, it is essential to study the electrical signals for a better understanding of such controller mechanisms.

2.4.4.1. Electromyography as an input of Myoelectric Control

Muscles have specialized cells that are responsible for the movements of the upper limb and guarantee stabilization. In this way, it is vital to understand the functional unit of the neuromuscular systems. The muscle fibres are unnerved by a single motor neuron that excites the fibres through a semi-permeable membrane phenomenon. The space between the somatic motor neuron and muscle fibre, also called synapse, is a neuromuscular joint. This structure receives the impulse and opens calcium channels. Calcium diffuses into the cell triggering the release of a neurotransmitter, acetylcholine (ACh). This chemical substance is combined with neurotransmitter receptors on the skeletal muscle membrane. The binding of this neurotransmitter to the receptor opens the sodium channels and consequently leads to cell depolarisation. Cell Depolarization or skeletal action potentials are followed by fibre in a contraction- excitation-contraction coupling process. A single relaxation-contraction cycle is referred to as a muscle cramp. The resting potential of the skeletal membrane is, on average, -80 *mV*. This membrane potential goes up to 30 *mV* with the opening of sodium channels [21]. To sum up, this signal is the result of the sum of all the sarcomere actions [75]. Muscle fibres are not activated individually. Indeed, EMG is a combination of action potentials, called the Motor Unit Action Potential (MUAP) [21][76][77][78].

Electromyography (EMG) is a technique for monitoring the electrical activity of muscle motor units. There are two ways for measuring myoelectric signals: through needles (invasive process) or surface electrodes (non-invasive procedure) [5]. The raw myoelectric signal´s amplitude ranges from -5 to 5 *mV* with a 10-500 *Hz* frequency range [40].The electrical noise is outside the frequency range of 0 - 500 *Hz* [79].

The amplitude of the measured signal is influenced by a series of intrinsic and extrinsic factors. The first ones are those inbuilt into the user's physiological and anatomical characteristics. The most known intrinsic factors are the muscular fibre composition, the muscle fibre diameter, the distance between the active fibres and the amount of tissue between the muscle surface and the electrode [80][79][81]. Extrinsic factors are those that affect the moment of acquisition. One of the examples is the electrodes' configuration that can be transmitted by the distance between the electrodes and the respective area. Another example is the placement of the electrodes that can be outside of the motor points of the muscle or in the lateral border of the muscle. The sweating and temperature of the patient are essential as well [80][81]. The resultant noise of the electronic parts used in the measurement kit, the electromagnetic radiation of the room where the acquisition is being made, and patients´ movement during the entire acquisition are also extrinsic factors. This frequency of this type of noise is expected to be limited to an interval between 0 and 20 *Hz* [79].

Another common phenomenon that occurs during signal acquisition is crosstalk. Due to the fact that there are signal losses at the tendon level, the system parts that are not propagated originate the crosstalk. Besides that, the signal originated by the surrounded muscles can also affect the acquisition of the signal. The electrical activity of the heart is also a factor that influences the measurement of myoelectric signals. High-pass and bandpass filters are often used to remove the frequency of this interference [82].

2.5. Prostheses: User Needs

Given the high rejection rates of this medical device, it is important to consider the user's opinion. For that reason, a literature review was conducted on the articles that explore the user opinions about the existing models on the market and inquire what they would like to see in a prosthetic device.

Regardless of the user's age or abilities, the prosthesis should be practical and easy to use. Factors such as strength, functionality and appearance are the most basic requirements sought by patients. Also, the size, weight, shape and colour of the prosthesis are important characteristics [49][50][83]. Many prostheses on the market were created to improve the user's bimanual function and provide a better life to the users. However, all of them have advantages and disadvantages that the users identified based on the most critics and problems found by the users (Table 2.4) [84].

Table 2.4: Advantages and disadvantages of the existing prosthesis types.

Types of prostheses	Advantages	Disadvantages
Passive	Similar shape to the human hand; Skin colour products; Made with Flexible material and silicone; Low Price	Do not meet the users' functionality needs
Body-powered	Effective-cost; Permeability; Lighter; Fewer adjustments to the user	Low sensory feedback; Mechanically inefficient; Dependent on the user; No strength to perform daily activities
Electrical	Multiple degrees of freedom; More natural and intuitive response; Require less visual feedback; Faster than body-powered	Noisy; Slow control (below the time value required by the market); High prices; Heavy; sEMG signal dependence; Battery dependence

In general, the ability to simultaneously control the different parts and components is a functional limitation that generates mechanical and electronic noise. The grip strength, the speed of each movement, the sensory feedback, the execution of tasks in real-time and the bidirectional communication at the level of the peripheral nervous system are also some of the limitations of such medical devices [42]. The mechanical effort, tension forces, deformity and elasticity of the prosthesis are the most important properties to have in mind during its development [85][86]. Recovering sensorial feedback is also a deterministic part of successful rehabilitation. Developing bilateral sensory systems that establish an interaction between the user and the electronic components can be a solution [85][86].

Some users report problems with the position of the surface electrodes. As mentioned in section 2.4.4.1, myoelectric signals are affected by internal and external factors. For that reason, some transient changes occur, promoting the degradation of the environment, which limits the clinical validity of the prosthetic device [87]. With the natural movement of the limb, some electrodes might change their position, which affects the recording process [88]. Developing acquisition training sets that study and equate all these factors could be the solution to solve these control problems.

3. State of the art

The first goal of this dissertation work is to create a 3D printed body-powered myoelectric controlled model. Since the first part of this study focuses on developing a low-cost myoelectric controller, we need to investigate the best pre and processing EMG signal methods and what has been developed and how it has been developed. There are three types of control systems where one of them is used in commercial prostheses, and the other two which have been studied over these last years.

The existing control methods are based on pattern or non-pattern recognition methods [51]. The first clinically acceptable myoelectric control appeared in the 1960s. In the following two decades, the evolution of this type of control, created by the russians, stagnated. This stagnation was related to the lack of applicability at commercial level. However, over the past forty years, North American, Japanese and Italian universities have contributed to the evolution of myoelectric control [89]. The current commercial myoelectric control systems can be categorized as ON/OFF control, proportional control and classifier-based control [90].

In the following points, there is a detailed description of each type of control: Non-Pattern Recognition (NPR) and Pattern Recognition (PR). NPR control is one of the most used controllers since it is simple and is adaptable to all users. PR control has gained attention in the last years due to the number of grasps that it can bring to the prosthetic device.

3.1. Non-Pattern Recognition Based Methods for Myoelectric Control

Non-pattern recognition-based methods include ON-OFF control, proportional control, Proportional-Integral-Derivative (PID) control, onset analysis and finite state machines [51]. These types of control are focused on the determination of the motor action through the amplitude of the EMG signal [87].

Commercial systems usually receive sEMG signals from two channels. Two options make the switch between the control modes. In the first one, the user switches the function via a co-contraction. In the second one, the sEMG signal reaches a slope in each channel which determine the function to be used. All these types of control are separated into two groups [16][91].

The first control is based on threshold detection, where the on/off control, the finite state machine control and the onset control are included. Such control systems usually allow a slight contraction to close the hand, strong contractions to open the hand. As an alternative, the industries choose to proportional control. These controls promote the variation of the velocity and the force in a continuous way, where the user controls at least some of the inputs. Nevertheless, it is not possible to move each finger independently [91].

The current commercial prostheses use the difference in EMG signals from a single pair of the antagonist's muscles to control one DOF at a time, which electronically is the direct control. Therefore, the prostheses have two DOF in the bicep and triceps to move the elbow and the hand through switching mechanisms. In addition, some prostheses have a third additional mechanism that requires a switching mechanism and becomes cumbersome. Nevertheless, these mechanisms are slow and expensive. So the need to investigate new control systems made academia study pattern recognition control and regression control [92].

In commercial and academic prosthetic hands, the Finite State Machine (FSM) control is widely used in prosthetic control and wheelchair control. This type of control has several sets of states that switch according to muscle contraction or prosthetic modes but require several intrinsic sequential control actions. The identification of different grasping movements makes this control one of the most advanced non-recognition tool methods [51][89].

ON-OFF and proportional control models are also used. However, they only offer two DOF. Proportional control uses force, speed, or position in a continuous range, which means the user input is the muscle contraction. ON-OFF binary control system gives only a single speed or rate of actuation to the prosthesis. Conversely, Onset analysis is where muscle activation and deactivation are done according to the temporal characteristics. In this type of control, the rectified signals are compared with thresholds obtained with the background noise [89].

Nowadays, more than 90% of the industrial controls are still based on PID control method. A PID controller can be considered a phase-sweep compensator with one pole at the origin and another at infinity.[93] This algorithm is an excellent option to calculate the difference between several inputs. PID control adjusts the different parameters of the prosthesis, such as speed, position and control [94].

Direct control is also a chosen method for prosthetic market products. This method interprets each input signal as an indicative function. This type of control is sufficient for sudden movements. Direct control does the correspondence between independent muscle contraction and the on/off of one DOF actuation [95]. The limitations of non-pattern recognition-based control methods are related to the functions that they perform [90][96].

In most cases, non-pattern-controlled prostheses can perform a single movement like opening and closing the hand or the wrist flexion. This type of control is slow because it involves more than one switching system [87].

3.2. Pattern Recognition Based Methods for Myoelectric control

Pattern recognition control is a better alternative for the limitations caused by direct control. This control is divided into five parts: acquisition of EMG signal, signal pre-processing, data windowing and feature extraction, gesture recognition and finally, control motors programming. Since mathematical models are out of use when designing real-time prototypes due to their complexity, the application of machine learning algorithms for gesture recognition seems to be the perfect solution. Therefore, the pattern recognition (PR) based methods include Artificial Neural Networks (ANN), Linear Discriminant Analysis (LDA), Fuzzy Logic (FL), Gaussian Mixture Models (GMM), Naive Bayes (NB), K-Nearest Neighbour (KNN), Decision Trees (DT) and Support Vector Machines (SVM) due to their high accuracies (>95%) [51][90][97].

The use of this type of control gives users more DOF and promotes muscle tone. However, these prostheses are not available in the market due to the complex learning and training methods. At the same time, in real life, it is complicated to control muscle fatigue and arm movement [91]. In pattern recognition control, there will always be delays of 250 milliseconds. However, in theory, the clinical delay should be between 100 and 125 milliseconds since human eyes do not perceive these values [98]. As stated by Farrell *et al* [99] the real-time prosthetic device maximum delay for the response of the prosthetic device should be 300 milliseconds.

Several studies search the best methodology to produce an effective and fast PR myoelectric control from those that already exist in the market. In 1978, Writa *et al* [100] created the first system to control myoelectric signals using LDA.

Twenty-seven years later, in 2005, Chan and Englehart [101] proposed a Widen Markov Model classifier. With a four-channel-six-function design, the accuracy was 94.67%. In 2009, Tenore *et al* [102] acquired EMG signals from five healthy subjects with thirty-two channels and one amputee with nineteen channels. Since the objective was to distinguish flexion and extension finger movements, the authors extracted time-domain (TD) features analysed by a Multi-Layer Perceptron (MLP) classifier. They obtained accuracies of 90%. Besides that, the authors proved that there is no statistical difference between healthy subjects and amputees.

In 2011, due to the lack of investigation related with the use of a single channel, Timeny *et al* [103] proposed a different classification method with a single electrode channel placed on the extensor and flexor muscles. Since the use of a single channel saves a lot of computational time, through the application of Empirical Mode Decomposition (EMD), a method that is based on the local time-scale characteristics of the signal, the authors increased the accuracy by 10.3%. Later in 2013, another survey from the same authors [8], after reducing the set features, compared LDA and SVM and concluded that LDA showed the highest accuracy (98%) In 2014, F. Riillo *et al* [104] showed that it is possible to identify five different movements from twenty healthy subjects with the combination of Principal Component Analysis (PCA) and Common Spatial Patterns (CSP) with LDA. The results showed an accuracy between 84% and 87%. In 2015, Stango *et al* [105] developed an interesting SVM classifier to identify gestures in EMG signals followed by spatial correlation obtaining reasonable accuracy measures. In the following year, Curline-wandl and Ali [106] developed a 3D printed transradial prosthesis with a single channel controller. The author showed that the accuracy is good in producing a low-cost and lightweight device, but the prototype has only a single DOF. Later in 2017, Gnazali *et al* [107] created a microcontroller with a Fuzzy-PID control. The author obtained an excellent accurate force control but with a unique DOF. Trognum *et al* [108], also in 2017, discussed a methodology to classify patterns in sEMG signals. With a short set of subjects, the author obtained an accuracy of 83% with the ANN classifier. In the same year, Mayor *et al* [109] developed a method capable of discriminate dexterous hand movements through a reduced number of electrodes. The authors extracted features from ten amputees and then classified the movements with SVM, LDA and KNN. The results showed an accuracy of 99.2 % for SVM and an accuracy of 98.94% for KNN with a lower computational time. In the same year, Raurale *et al* [110] used eight channels to identify wrist and hand gestures. The authors obtained an average accuracy of 95%. They only took 500 milliseconds.

Finally, in 2020, Zhou *et al* [95] propose the development of a compact and cost-effective PR control myoelectric system. The authors tested three classifiers and their performances with offline tests. The classifiers were LDA, SVM and RF. During the same year, Li C *et al* [111]., identified nine different movements, such as wrist movements, forearm supination/pronation, and hand grasps processing the EMG signal. To classify each movement, the authors used SVM and GNRR and obtained 98.64% and 96.27 % accuracy, respectively.

Despite the variety of classifiers considered, given the stochastic and non-stationary sEMG signals nature, the best classifiers are LDA and KNN due to their easiest implementation and SVM due to it kernel-based characteristics [88][112]. The use of neural networks is also quite advantageous. ANN uses artificial intelligence to implement tasks through learning. This classifier represents both linear and non-linear relationships and can be used in real-time acquisitions. Classification using the FL algorithm tolerates contradictions in the data since it analyses it even when class separation may be difficult [89].

The biggest disadvantage of PR control is that the patient must undergo Target Muscle Re-Innervation (TMR) surgery in most cases. TMR is a procedure that reduces phantom limb pain and allows the patient to produce meaningful inputs for myoelectric control. This process requires the transference of selective nerves from the brachial plexus to the patient's new muscle sites. The decision to relocate the nerves depends on the type of amputation. For patients with transhumeral enlargement and shoulder dislocations, it is the most recommended procedure [66][113]. Fortunately, the PR-based control scheme has been proved clinically on patients who undergo this surgery which is a new start for commercial PR systems [114][115].

3.2.1. Surface EMG Signal Processing Methods

Now that the classification methods are presented, it is essential to understand how it is possible to have accurate classifications.

In myoelectric prostheses, the EMG signals are used to generate the output for prostheses control. Besides that, signal processing methods are fundamental to ensure that the signal is clean and ready to be analysed and classified. Therefore, proceedings such as filtration, rectification, normalization and windowing are essential for reasonable myoelectric control [80].

As mentioned in section 2.4.4.1, there are a lot of internal and external factors that affect the signal. It is imperative to eliminate this noise. Filtering the signal is the most direct way to increase the sEMG signal's fidelity, maintaining the principal spectrum frequencies and removing the noise [116][117]. Consequently, filtering the signal at this stage can make a difference in producing an accurate control system. There are four types of filters: high-pass filters, low-pass filters, band-pass filters and notch filters [79]. For this kind of filters, the most recommended low cut-off frequencies are between 5 *Hz* and 28 *Hz*, and the high frequencies are between 450 e 450 *Hz* [79]. In previous academic research, the most used filters are Butterworth, Chebyshev, Hamming and Kaiser Windows [118]. Besides digital filtering, some authors consider the application of wavelet transform to reduce the noise, since it can remove the high frequency noisy contents.

As previously discussed, to produce real-time devices it is necessary to have a maximum time response of 300 milliseconds [126]. To reach this goal and to promote a fast, accurate control is crucial to window the signal. This process is more useful for EMG acquisitions since this signal is non-stationary, which means that the features of the total time would not be representative. Thus, it is important to divide the signal into several time segments in a process known as windowing. There are two types of windowing: overlap and non-overlap or adjacent windowing. Since the processor has a high speed (less than 50 milliseconds), the processing time is inferior to the segment length, making the processor idle for a while. For that reason, overlapping is preferable for real-time control [89][119]. In the adjacent window (Figure 3.1 (a)), the adjacent segments are used for posterior feature extraction and classification. Despite this method occupying less memory and considering that processing time is part of the segment length, the processor is idle during the remaining time. For that reason, the overlap classification merges in myoelectric control systems since during that idle time more outputs are produced. Nevertheless, increments like this produce a denser and redundant stream of class [89]. As an alternative to solve the problems caused by the previous processes, continuous segmentation can be used. In this type of segmentation, the signal is divided into overlap segments (Figure 3.1 (b)) of both transient and steady-state signals. This approach reduces the maximum delay and increases the classification performance [120]. In theory, choosing a segment with a length inferior to 200 milliseconds is enough to estimate movements since this value is the minimum interval between distinct

contractions [121]. The accuracy of the classifier decreases with the decrease of the segment length. The choice of the segment has to consider two aspects: the first one is promoting good accuracy, the second one is occupying the shortest storage space.

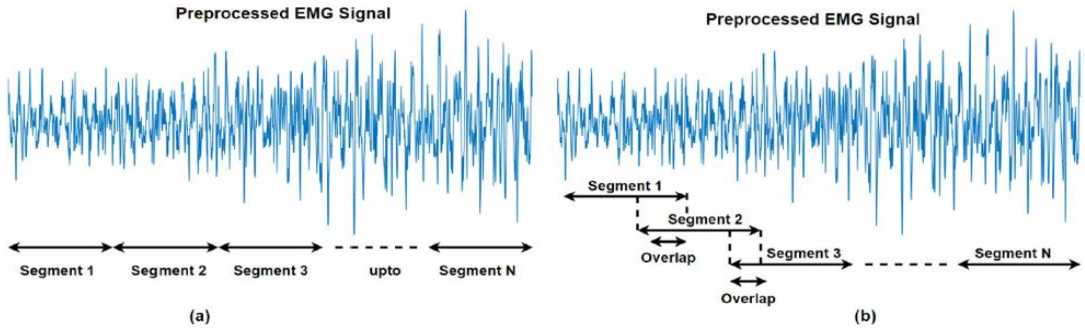

Figure 3-1: Segmentation processes (a- disjoint segmentation; b- overlapping segmentation) (extracted from [89]).

The optimal value depends on the selected features, which means that the set of features should be the most representative of the movement. Within the different types of features are the time-domain one, the frequency domain and the time-frequency domain. Some studies found out that time-domain features perform better with LDA [122]. Due to their computational simplicity, time-domain features are the most used features in myoelectric control. While frequency features are focused on spectrum characteristics, time-domain extract information from the signal amplitude. This amplitude can be defined as the time-varying standard deviation of the signal, which measures the activation of the motor units. At the clinical level, frequency domain features are used to study muscle fatigue and provide information regarding neural and muscular pathological changes [123]. Finally, time-frequency domain features are the most complex ones since they are represented by a matrix. Although, with a good classifier and after dimensionality reduction being applied, time-frequency domain features give robustness to the system.

In time domain it is possible to calculate the average absolute value, the slope of the average absolute value, the root mean square, the variance, maximum value, minimum value, standard deviation, simple square integral, waveform length and zero crossings.

In the frequency domain, it is possible to calculate the median frequency, the average peak frequency and the average power [82]. The features selection should be a thorough process because a good classification reflects a good performance. The most convenient features for the LDA algorithm have been extensively investigated by Hudgins *et al* [124] and Ortiz-Catalan *et al* [125]. The most used features are the average absolute value, the waveform length, zero crossings and cardinality [112]. For the classifiers used in the Zhou *et al* [95] survey, the authors used fifteen features among the following: variance, integral absolute value, average amplitude change, difference absolute standard deviation value, kurtosis, LOG detector, modified mean absolute value type 1 and type 2, mean absolute value, root mean square, waveform length, mean frequency, variance of central frequency and power spectrum deformation. This work will mainly use time-domain features because of their low computational processing time and their accurate results.

The features that are used have an important role in classification performance. Having features that are not correlated or have a low variance for each class can increase the classification performance because each gives different information to the classifier, which is helpful for instances that are within

the boundaries of each class. However, when the set has many features, the computational time increases, which needs to be avoided. Moreover, correlated features can give redundant information, so using them will decrease the accuracy and increase the processing time. Because of that, reducing the set of features to the ones that had the principal information can decrease the processing time and increase the accuracy. Therefore, it is a good practice to remove some of them to increase the classification and reduce the computational cost. The most used feature selection methods are filter and wrapper methods. Filter methods study the feature itself, and does not use classification systems or predictive models. One of the most applied filter methods is mutual information since it is used when the features are numeric, which is the case for myoelectric signals. However, in certain sets it is vital to find out how each feature affects the whole set. The wrapper methods used predictive models such as LDA or KNN or regression models to select the best features. Some examples are genetic algorithms, swarm particle optimization, CSP, and backward or forward feature selection. Reducing features can significantly increase the accuracy and reduce the processing time, contributing to maximum class separability, robustness minimizing the misclassification rate [127][128].

But, in some cases, the entire feature set is still relevant, mainly if the feature matrix has more than one column or come from different levels of wavelet coefficients. For those cases, some authors suggest applying dimensionality reduction techniques such as PCA, Uncorrelated Linear Discriminant Analysis, Orthogonal Fuzzy Neighbourhood Discriminative [126]. Such processes remove the number of arbitrary variables and put the features in another space dimension.

3.3. Current Problems and Future Perspectives

In the last decade, the scientific community has been suggesting some innovative methods for myoelectric control. However, at the commercial level, the current prostheses are underdeveloped and far from those advanced technologies in an intriguing way [16]. Although there are different PR controlled prostheses, the number of limitations need to be analysed. In the majority of the surveys, the signal used for classification is the steady-state signal. In real-time performance, steady-state and isolated isometric contractions do not happen. Because of that, it is expected a decrease in the offline average accuracy. Despite the high classification performance during online tests (average accuracy > 90%), the implementation of the classifier in the real set is much lower. Because of that, it is necessary to include transient contractions in the training data since they can increase real performance [88][129]. Besides using steady-state signals, the classification of long-term myoelectric signals has numerous problems. The main reason is the quantity of external and internal factors that affect those signals decreasing the performance of the classifier. The existence of classification errors due to the difference between training and test sets is also common. In the He *et al* [115] survey, the authors tested the behaviour of the classification error curve with data acquired during eleven days. The authors demonstrate that the difference in classification and error rates were smaller as the acquisition days increased. This study reveals that measuring transient signals over a long period of time might improve the accuracy and promote the robustness to control systems. Furthermore, the current studies involve a small number of subjects (usually less than ten), limiting the study to a non-representative population. The number of channels that is used it still high when compared to the available user's surface area.

Moreover, producing simple prostheses is essential since they are configured by orthopaedic technicians and are used by recent users that are using a prostheses for the first time [16].

If these problems were not considered, the developed prototype would be produced with limitations in classification accuracy and control.

To sum up, it is essential to:

- Develop a prototype with multiple degrees of freedom, with a natural and intuitive control [130] [131];
- Develop a platform or systems that correlate and connect the EEG signal with EMG signals [130] [131];
- Create a fast learning process to identify and classify the EMG signals [130][131];
- Create a protocol for a significant number of participants;
- Build a prototype with low-cost materials to make it affordable to all users [88];
- Finding the best filtering methodology to eliminate the noise from EMG signals [88];
- Investigate the importance of trying deep learning algorithms to classify the signal [87];
- Develop models of EMG and ML capable of recognizing short and long time duration [132];
- Introducing the transient signals in the training set [132];
- Develop a general controller capable of recognizing the signals from different amputees [132].

In this master dissertation, it is intended to test if it is possible to develop a prototype with multiple degrees of freedom with a fast and simple learner. This learner will identify and classify the myoelectric signals that will contain both transient and steady states. Furthermore, the possibility of having a prototype that fits everybody will be tested. Adding the intuitive controller to a prototype made with low-cost materials, affordable to all the users will also increase the percentage of customers who will use the prosthesis. Besides that, including a larger population of users/customers will help the children and adults with low income. Therefore, some of these current problems will be investigated with this project.

4. Methodology

4.1. EMG signal processing and classification for Pattern Recognition myoelectric control

The main goal of this dissertation is to develop a low-cost and simple myoelectric controller in which the input is the volunteer's intention. The idea is to promote a functional device similar to the biological hand. There is no consensus in the current surveys and available literature about filtering the signal and how the channel needed to be used at a minimum. Therefore, this dissertation intends to investigate if reducing the number of electrodes decreases the prosthetic device's functionality as well as the influence of increasing the number of volunteers and the complexity of the acquired movements in the classification performance. In this section, the different combinations of signal processing techniques and pattern recognition algorithms for a single channel acquisition are described. The main purpose of such combination is to evaluate which of them could be the best solution for the recognition of four different hand gestures - Rest Position, Spherical Grip, Tripod Grip and Index Finger Flexion. Considering what is being said, this section intends to answer the next questions:

1) How accurate is the classification of hand gestures based on surface signals with one single channel acquisition?
2) Is a single-channel acquisition enough to develop a volunteer-independent prosthesis controller?

2) Is there an optimal processing signal technique that achieves the best classification rates in the shortest time possible?

4.1.1. Materials

To develop a good control system, it is essential to study the best signal processing methods. Therefore, we needed to follow a rigorous and controlled acquisition protocol. The Ethical Committee of the Faculty of Science of the University of Lisbon approved our acquisition protocol and experiment in June 2021.

Forty-five volunteers (aged 18-24 years, 15 males and 25 females) participated in this study (Table A.1 in Appendix A). Each participant received a thorough description of the experiment in oral and written form. All volunteers signed a consent form, available in appendix A, where they provided permission to publish their data for scientific and educational purposes.

Unfortunately, it was impossible to acquire data from amputees due to pandemic conditions, so all the selected volunteers were healthy individuals without any known neurological or physical pathological conditions. This means that this work will serve as a control methodology for later to be tested on amputees.

4.1.2. Experimental setup and protocol

The acquisition setup included electrodes designed to record muscle activity and an acquisition system connected to a laptop. The myoelectric signals were recorded with BIOPAC (Model MP-36, Biopac Inc, Goleta, CA) acquisition unit (Figure A.1-Appendix A) with built-in universal amplifiers that record a wide range of physiological signals. The BIOPAC data acquisition system recorded raw EMG signals and saved data in .txt format for later offline analysis [133].

The information is received in one of the four channels and connected through a USB cable to the app BIOPAC Lessons Student installed in a laptop. To record myoelectric signals, three Ag/AgCl electrodes were used (EL502, Biopac Inc.), which were placed on the surface of the skin of Flexor Digitorum Superficialis (red electrode) and Flexor Carpi Radiallis (white electrode) with a reference electrode (black electrode) on the wrist. For accurate records, the electrodes incorporate liquid electrolyte gel and moderately-high chloride salt concentration. These disposable electrodes have a circular contact and are suitable for short-term recordings, including surface EMG.

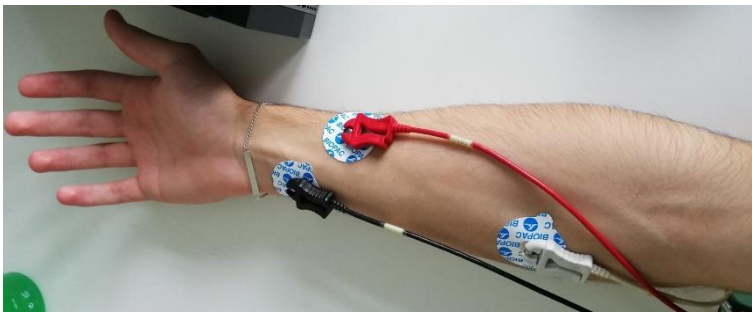

Figure 4.1: Acquisition Electrodes Position.

One of the aims of this dissertation work is to decrease the number of acquisition channels to reduce computational cost. Therefore, to test how accurate this will be, we used three electrodes and one acquisition channel. The gain of the system was x1000. The sampling rate was 500 *Hz*.

This experiment was divided into one training part and one real-time acquisition. The volunteers performed three gestures that were followed up by resting time to avoid muscular fatigue. Since the focus of this work is the recognition of three specific hand and finger movements, the volunteers were asked to avoid exerting high forces and contraction in fatiguing positions. During the train session, it was necessary to initiate a calibration phase to establish the rest and maximal voluntary contraction (MVC) for all exercises. This calibration stage was useful to see the force that each volunteer was putting on the object and if the different records were similar or if it was necessary to repeat the acquisition.

Recognizing these hand gestures will improve the quality of the user's life since it can substantially impact the basic life diary activities in the simplest and fastest way possible. The number of repetitions and the exercise order were not randomised to trigger an unconscious reaction on the part of the volunteer.

- In the first exercise (spherical grip), the volunteers were asked to perform the movement by holding a spherical tennis ball (Figure A.2 in Appendix A).
- In exercise 2 (tripod grip), the volunteers had to perform the movement by pressing the thumb to the first and second finger digit (Figure A.3 a) in Appendix A).

- Finally, for the third exercise/hand gesture (index finger flexion), the volunteers were asked to perform the movement of the flexion of the finger. During the resting phase, the volunteer's forearm was laid down on the table with the back of the hand (Figure A.3 b) in Appendix A).

Right before the acquisition started, and as recommended in Jamal *et al* [134] search, we cleaned the sweat of the volunteer's skin with alcohol, which is a crucial step to improve the quality of the acquisition and the reduction of possible artefacts.

The used protocol during the acquisitions was:

- Before starting the records, to each volunteer was given a written consent form that included the associated risks and the explanation of the experiment itself.
- After signing the consent form, the volunteers received instructions to complete the training session.
- Each volunteer was asked to sit down in a chair in a comfortable position. Each volunteer has to maintain an upright body posture with an angle of 90 degrees between the elbow and the table.
- During the training stage, we tested the right place to put the electrodes through the display of the signal. Right after, we marked the electrode place for the testing stage. These registrations ensure that the electrodes were in the same position in case one of them moved.
- The acquisition started.
- The volunteer performed the pick ball movement (spherical grip), where the volunteer reached the red ball, which had been placed on the table, held the ball for 2 seconds and then dropped it.
- The second movement was the tripod grip. During these hand gestures, the volunteer pulls the three fingers (index, thumb and middle finger) together.
- On the third-hand gesture, finger flexion, the volunteer flexed the finger on the surface of the palm.
- Each exercise was repeated ten times in a total time of 40 seconds.
- Every volunteer repeated each gesture with both arms (dominant and non-dominant).
- The data was saved, and the acquisition ended.

During the training phase and the test acquisition, it was necessary to pay attention to the placement of the electrodes. As mentioned in section 2.4.4.1, controlling these processes is very important to ensure excellent and accurate results. The space between the muscles and the volume conductor of adipose tissue acts like a low pass filter. This filter decreases the amplitude and frequency of the EMG signal. In this way, the configuration of the electrodes should be bipolar, and they should be placed parallel to the muscle fibre [127].

The signal was stored in a matrix $[N \times 1]$, in which N is the number of samples stored by the amplitude values of the signal. The data was subsequently analysed in MATLAB Software.

4.1.3. Frequency Analysis

Before choosing which filter that will be used, it is necessary to understand which frequency components are related to the energy of the sEMG signal and which ones are significant for movement classification. Besides that, it is also important to identify the noisy frequency contents. Choosing a cut-off value lower than half of the frequency sampling rate avoids aliasing the signal [135]. In this work, the sampling rate was 500 *Hz*. Because of that, the maximum higher cut-off frequency should be 250 *Hz* to avoid aliasing.

To remove the noisy frequency content, it was needed to study the signal in the frequency domain. Therefore, we used Fast Fourier Transform (FFT) instead of Fourier Transform (FT) to reduce computational time. Thus, it was used the pwelch function available on MATLAB software.

First the power spectrum was calculated for six volunteers to identify the frequency content of the raw signal. However, with power spectrum (Figure 4.2) it was not possible having the information about the equipment noise and the volunteer's skin impedance. Since removing the baseline noise is a crucial step, the signals were divided into the moment of contraction and the resting phase. Then, the pwelch function was applied, to find out the dominant frequencies of the noise and the dominant frequencies that represent the hand movement information.

In Figure 4.3, it is possible to distinguish two curves between 0 to 50 *Hz* and 50 *Hz* to 250 *Hz* since there is a drop of power spectral density at 50 *Hz*. The first conclusion that can be taken is that the BIOPAC system has an internal filter that eliminates the power grid interference with a typical frequency band between 50 and 60 *Hz*. The existence of that filter explains why there is a drop in the power density value in these frequency values. Secondly, it is possible to conclude that the signal has a maximum peak occurrence between 0 and 20 *Hz*, which might be justified by the external and internal noisy interferences. As mentioned before, the myoelectric signal is affected by numerous noise sources with frequency bands between 10 and 20 *Hz*. The increase of power density values in this band can be explained by the displacement of the electrodes or the cables related to volunteers' sweat or volunteers' involuntary movement. Although it might not be so evident, it is also possible to have interferences caused by the baseline cardiac noise.

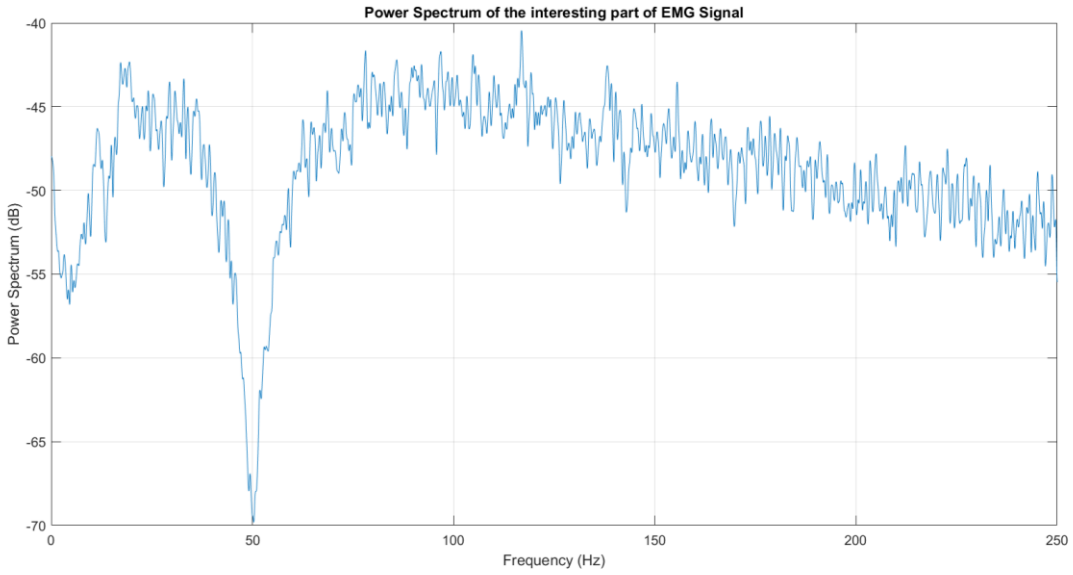

Figure 4.2: Power spectrum of the signal obtained in volunteer number 1.

Lastly, it is possible to observe that around 80 *Hz*, the power spectral density decreases. Around the frequency band between 150 and 200 *Hz* the spectral density reached values close to 0 V_2/Hz. Even though for most volunteers, the power spectral density is not significant around 150 *Hz*, for some of them, this reduction is around 200 *Hz*.

To identify the contents of the baseline noise and the relevant part of the signal, we plotted the pwelch function for each subject. The results obtained in volunteer number one are in Figure 4.3. As it can be seen, the power spectral density reaches its maximum for the baseline noise at a frequency value of 0 *Hz*. It is also visible that the power spectral density is greater for the first frequency curve (0-50 *Hz*) than for the second one (50-250 *Hz*). This might mean that the frequency content is in the range of 20 to 140 *Hz*, not the last frequencies (150 - 250 *Hz*). As it can be observed, the baseline noise (red line) has frequency contents in the frequency range between 0 and 20 *Hz*. Because of that, we considered that the noise content is in this frequency range. Besides that, it is also possible to conclude that the power spectral density decreases after 80 *Hz* for volunteer number one, reaching a minimum value in the frequency range between 150 and 200 *Hz*.

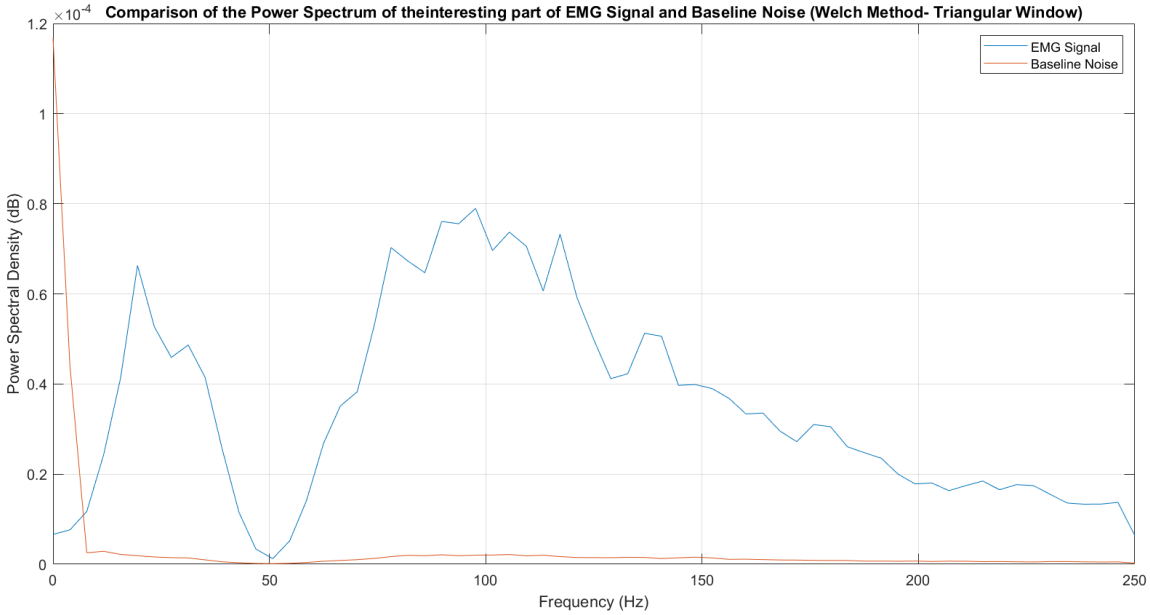

Figure 4.3: Pwelch plot of the baseline noise (red line) and the interesting part of the signal (blue line) for volunteer number 1.

The results obtained in volunteer four are different since the frequency content reaches its maximum after 200 *Hz* (Figure B.1 – Appendix B). However, the results obtained for other volunteers are similar to those obtained in volunteer number one (Figure B.1-B.11 – Appendix B). Considering that, we tested a few cut-off frequencies, where the low frequency values were set between 10 and 20 *Hz* and the high frequency values between 150 and 200 *Hz*. The results are within the cut-off frequencies suggested in the literature. Almost all authors widely use the first range of frequencies (10-20 *Hz*). However, the second range was adopted specifically for our dataset.

Processing the acquired data is a crucial process for the success of the built prosthetic device. The first step for obtaining a clean signal is filtering the signal.

4.1.4. Digital Filtering

Many filters can be used when it comes to the filtration process. There are two types of filters, the Finite Impulse Response filters (FIR) and Infinite Impulse Response filters (IIR).

IIR or recursive filters are designed to use previously calculated outputs. Therefore, they use delayed input signals and feedback of the output signal during the filtration process [136]. These filters are commonly used in linear time-variant systems or signals since their implementation reduces the computer memory and processing time [137][138]. Besides that, some authors prefer to use IIR filters since they can achieve a sharper transition region roll-off and produce linear phases [139]. Compared to FIR filters, IIR have a shorter time delay and require fewer arithmetic operations [136]. FIR filters have an impulse response with a finite duration because it settles to zero in finite time. Moreover, these filters can compensate the phase shifts of the signal [140]. However, these filters take too much processing time [141].

The most used and recommended filter for sEMG signals is the Butterworth since it has a flat passband response. This filter is defined only by two parameters (number of poles and cut off frequency). Furthermore, these filters have the best compromise between attenuation and phase response, implying a lower waveform distortion. These features make this ideal for situations where it is necessary to preserve the amplitude linearity in the passband region [136].

When it comes to windows filters, the history is different. Savitzky-Golay filters are polynomial filters used to smooth a noisy signal like sEMG. They performed much better than the rest of the FIR filter since they preserved high-frequency components [142].However, since Savitzky-Golay filters are moving average window filters, it was necessary apply to the signal a low-pass and a high-pass filters with the defined cut-off frequencies.

Considering that, the filter design app from MATLAB Software was used to design and construct a stable filter for sEMG signals. Then, it was implemented the butter function to design the Butterworth filter. First, we tested the application of only bandpass filters. Since there is no agreement in the order of Butterworth filters, we used six orders for each frequency band. Each filter was evaluated accordingly, with two metrics described in the following paragraphs. Besides the Butterworth filter, we also tested the Hamming window, the Kaiser window, and the Savitzky-Golay filter.

Of course, choosing the frequency is important, but it was necessary to ensure that the applied filter was a stable filter. Because of that, it was needed to consider the specific characteristics that make this filter stable. Therefore, the selected filters had all the poles within the unit circle and an infinite impulsive response that tended to zero (Figure B.11 and B.12 in Appendix B).

The signal-to-noise ratio (SNR) metric measures in decibels the quality of the EMG signal. This metric represents the raw and filtered signal ratio between the moment of muscle contraction and when the muscle is at rest, often called baseline noise [143][144]. In this dissertation, the baseline noise was considered the moment when the volunteers were performing the rest position since it is the moment that contains the equipment noise. Equation 4.1 presents the formula used to calculate the SNR, where A is the signal representing the contraction moments and rms is the root mean square.

$$\mathrm{SNR}=20\log\left(\frac{\text{rms (A)}}{\text{rms (Baseline Noise)}}\right) \quad (4.1)$$

To complete this evaluation, we added another metric, the Mean Square Error (MSE), which measures the average squared difference between the filtered signal and the original one [145]. In the following equation, x represents the amplitude of the original signal and $\bar{x}$ the filtered signal.

$$MSE = \frac{1}{N} \times \sum_{n=1}^{N} (x(n) - \bar{x}(n))^2 \quad (4.2)$$

4.1.5. Wavelet threshold noise reduction

Besides the mentioned external factors that can affect the EMG signal, signals are affected by electronic component noise that has an energy band that varies from 0 to several thousand *Hz*. Since this type of noise has random frequency components, it becomes difficult for digital filters to remove it. Therefore, some authors propose the use of the DWT algorithm as a filtering process to reduce or eliminate this type of noise [146]. Despite these advantages, there is no consensus about the proper filtration process or even a single methodology to develop control PR systems in current surveys and research, which is a problem for the industry [147][148].

To figure out which methodology is better, it was decided to test and compare how the quality of the signal improved using wavelet decomposition. Therefore, it is essential to study the theory behind this method.

As already explained in section 2.4.4.1, the EMG signal is multicomponent since it is originated from various MUAPs originated in different periods and with different frequencies [76]. Because of that, the signal can be decomposed into several scales by Wavelet Transform (WT) [147]. WT is a time-scale representation of the signals that provide a good frequency resolution at high frequencies. In this work, the DWT was used since it removes the redundancy of CWT. The DWT is the projection of the signal over a set of basis functions that are temporal shifts and dilatations of a protype function, known as mother wavelet. This basis function and its shifted versions belong to a space that is decomposed into a lower resolution approximation space and a detail space. Then, the signal is decomposed into wavelets, scaled, and shifted version of the chosen mother wavelet. These wavelets have properties such as symmetry and orthogonality that should be considered when the DWT technique is used [207]. In the wavelet noise threshold reduction method, the original signal passes through a combination of low pass and high pass filters, originating the approximation coefficient subsets (cA1) and detail coefficient subsets (cD1) until the desired level [149][150][146]. After that, the coefficients are modified according to a specific threshold. Lastly, the inverse wavelet transform is applied, and the original signal is reconstructed originating the filtered signal [151][152]. This process is illustrated in figure C-1 in Appendix C. To sum up, we have three essential steps:

- **Decomposing the raw signal into coefficients:** decomposing the signals into detail coefficients (cD) and approximation coefficients (cA) that contain high frequencies components originated by the application of high pass filters and low-frequency components originated by the low pass filter, respectively; [149] [150] [151] [152]
- **Estimate the threshold to get new coefficients:** the noise parts are in the detail coefficients, which means that the threshold value will be calculated considering the noise variance of these coefficients and then applied to them; [149] [150] [151] [152]
- **Reconstruct the signals with the new coefficients:** the filtered signal is constructed based on the modified cD coefficients and the cA coefficients. [149] [150] [151] [152]

It is essential to choose the right threshold and the mother wavelet to improve the classification performance. There are two types of wavelets, orthogonal waves and biorthogonal. There are six wavelet families that are widely used in sEMG signal filtration process. The first family is the Daubechies wavelets that have 10 sub-types. The second ones are the Symlets wavelets that are divided into 7 sub-types. The third one is the Coiflet wavelet family that has 5 sub-types. Finally, it is possible to identify the BiorSplines wavelets and the ReverseBior wavelets both with 15 sub-types and the Discrete Meyer wavelet [148].

Besides selecting the correct type of wavelet, it is crucial to choose the number of decomposition levels of the signal. This number goes from 1 to $\log_2 N$, where N is the length of raw signal [148].

After selecting the decomposition level, it is crucial to choose the threshold rule and function that will be applied. According to Donoho *et al* [153], the calculation of the threshold depends on two parameters: the standard noise energy of the signal σ and on the parameter that depends on the length of the data samples (N). There are four types of threshold rules, but three of them are widely used. The universal threshold rule uses a fixed threshold that depends on the two previous parameters. Conversely, the SURE threshold rule uses the Stein's Unbiased Estimate of Risk (SURE) rule. Finally, the Minimax Rule also uses a specific threshold proposed by Stein [148].

When it comes to threshold function, the most used are the hard (HAD) and the soft (SOFT) functions. In the HAD, the detail coefficients whose absolute values are lower than the threshold are set to be zero, while the other ones are kept. The SOF does the same that HAD one, but then the non-zero coefficients are shrunk towards zero [148][153].

Therefore, it was searched which wavelet types were used in previous academic investigation that could be used in this master dissertation. Guo *et al*. [154] used the sym5 wavelet with three decomposition levels for lower limb prosthesis control. The authors tested the Universal, SURE, Hybrid, Minimax threshold rules and HAD, SOF threshold functions. Zhang *et al* [155] used the wavelet family sym8 with four decomposition levels for upper-limb prosthesis control. Phinyomark *et al* [146] applied seven mother wavelets: the second and seventh order of the daubechies family (db2, db7), the fifth order of the symelets family (sym5) and the fourth and fifth-order of the coiflet wavelets (coif4, coif 5). They conclude that the best decomposition level was the fourth level.

Considering the applied state of the art wavelet families, we tested the third, fourth and fifth decomposition levels for the following wavelet families: db, syms and coif. The best wavelets described in literature db2, db6, db10, sym2, sym7, coif4 and coif5 were tested. In order to test each wavelet, the wdenoise MATLAB function was used. For the threshold rules, the Universal, the SURE and the Minimax rules with HAD and SOFT threshold functions were used. To evaluate each wavelet and threshold, the same two metrics were used - SNR and MSE. Then, the same six volunteers' signals were analysed.

4.1.6. Signal windowing and feature extraction

When the objective is to classify the sEMG signal, its original form becomes meaningless. For this reason, the recorded data was rectified. In this experiment, the RMS envelope was applied (Figure 4.4), which is a process that uses a moving window that calculates the square root of the data (filtered signal) that is inside the window [156]. The envelope was obtained using the following formula [157], where l is the length of the window and x the signal:

$$RMS_{envelope} = (\frac{1}{l}\sum_{1}^{l} x^2(l))^{\frac{1}{2}} \qquad (4.3)$$

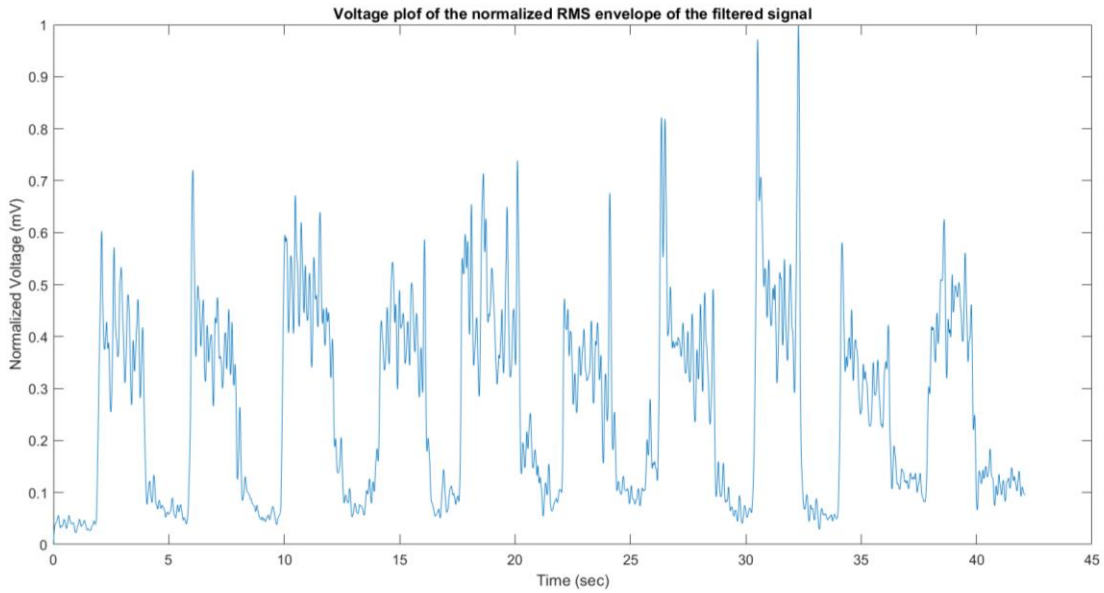

Figure 4.4: Illustration of the enveloped filtered signal.

To implement the formula, it was needed to choose the size of the window (l). The size of the window varies according to the velocity of the movement in the study. Using longer windows is better. Despite being recommended to use different window sizes, a length between 50 milliseconds and 100 milliseconds works for both cases [111][156][157]. For this dissertation, a window of 25 milliseconds it was used since the duration of the hand gestures was two seconds.

After selecting the best filtering process, it was applied the offset compensation by applying the detrend function. Since it will be compared the activity from the same muscles from different individuals, it was needed to normalize the data [158]. The normalisation process will convert the signals to a common scale to all recorded data. Therefore, to eliminate the intervariability, the maximum and minimum values of the collect signal (Equation 4.4) were used, in a procedure that transforms the original data into a real value between 0 and 1 [159][160]. In the following equation the x represents the filtered signal, x_{max} and x_{min} the maximum and minimum of the filtered signal, respectively.

$$x_{norm} = \frac{x - x_{min}}{x_{max} - x_{min}} \qquad (4.4)$$

Since the device must have a maximum response time of 300 milliseconds, the signals must be divided into several segments to perform meaningful classification in a record processing time. After removing the intervariability of the volunteer's data, the signal was divided into 100 milliseconds and 250 milliseconds time segments to extract time-domain features. The next step was to determine which window size would improve classification performance. Therefore, adjacent windows were used as well as the transient signal. As it can be seen in Figure 4.5, the continuous record of the EMG signals makes it possible to observe a significant peak related to the change of the hand gesture.

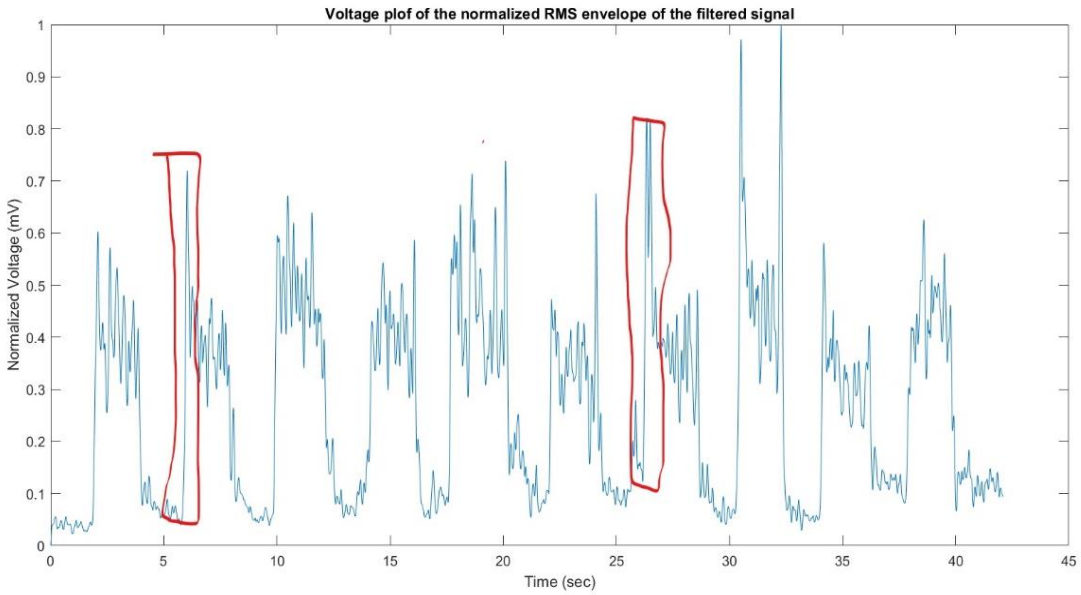

Figure 4.5: Representation of the huge peak related to the change of the hand gesture during a continuous record (red line).

The selection of the right set of features has an enormous influence on classification performance, as we demonstrated in section 3.2.2. A set of thirteen time-domain features was used [127][161][162][163]. In the following equations, N is the length of the EMG signal and x_i represents the EMG signal in a segment i.

Mean Absolute Value (MAV) is the average rectified value. This feature detects muscle contraction levels [127][164][165].

$$MAV = \frac{1}{N}\sum_{n=1}^{N}|X_i| \qquad (4.5)$$

To improve the weighting function's smoothness and add robustness to the built prosthetic, it is possible calculate the mean modified absolute value and mean modified absolute value type 2. [82]

$$MMAV = \frac{1}{N}\sum_{n=1}^{N} Wn|X_i| \qquad (4.6)$$

Where

$$W_n = \begin{cases} 1, & 0.25N \leq i \leq 0.75N \\ 0, & otherwise \end{cases} \qquad (4.7)$$

Conversely,

$$MMAV2 = \frac{1}{N}\sum_{n=1}^{N} W_n|X_i| \qquad (4.8)$$

Where,

$$W_i = \begin{cases} 1, & 0.25N \leq i \leq 0.75N \\ \frac{4i}{N}, & i < 0.25N \\ \frac{4(i-N)}{N}; & otherwise \end{cases} \quad 4.9$$

Waveform Length (WL) is a measure of the complexity of the signal since it is the cumulative length of the signal waveform over the selected window. This feature indicates the amplitude-frequency of the waveform and its duration [164].

$$\text{WL} = \sum_{i=1}^{N} |X_{i+1} - X_i| \quad (4.10)$$

Root Mean Square (RMS) represents the muscle's constant force and non-fatiguing contractions [164].

$$RMS = \sqrt{\frac{1}{N}\sum_{i=1}^{N} {X_i}^2} \quad (4.11)$$

Slope Sign Change (SSC) is a feature similar to zero crossing. The number of positive and negative slope changes among three consecutive segments, which is performed with the threshold function to avoid interference in the EMG signal [82][165].

$$SSC = \sum_{i=2}^{N-1} f[(X_i - X_{i-1}) \times (X_i - X_{i+1})] \quad (4.12)$$

Where

$$f(x) = \begin{cases} 1, & if\ x \geq threshold \\ 0, & otherwise \end{cases} \quad (4.13)$$

This means that in MatLab® code we needed to implement these conditions:

$$[(X_i > X_{i-1} \cap X_i > X_{n+1}) \cup (X_i < X_{i-1} \cap X_i < X_{i+1})] \cup [|X_i - X_{i+1}| \geq thershold \cup |X_i - X_{i-1}| \geq threshold] \quad (4.14)$$

Integrated absolute value (IAV) is used as a pre-activation index for muscle activity, because it measures the summation of the absolute amplitude values of the signal. In mathematical terms it is the area under the curve of the rectified EMG signal [164][166].

$$IAV = \sum_{i=1}^{N} |X_i| \quad (4.15)$$

Simple Square Integral (SSI) express the energy of the EMG signal [164].

$$SSI = \sum_{i=1}^{N} |X_i|^2 \quad (4.16)$$

Zero crossing (ZC) provides an approximate estimation of frequency domain properties [82][167].

$$ZC = \sum_{i=1}^{N-1} [sgn\ (X_i \times X_{i+1}) \cap |X_i - X_{i+1}| \geq threshold] \quad (4.17)$$

In the case of zero crossing, we need to define some boundaries as well,

$$(\{X_i > 0 \cap X_{i+1} < 0\} \cup \{X_i < 0 \cap X_{i+1} > 0\}) \cap |X_i - X_{i+1}| \geq threshold \quad (4.18)$$

Maximum Fractal Length (MFL) is one of the most recently studied features that measure the activation of low-level muscle contractions [168][169].

$$MFL = log_{10}(\sqrt{\sum_{i=1}^{N-1} (X_{i+1} - Z_i)^2}) \quad (4.19)$$

Variance (VAR) expresses the power of the EMG signals [164].

$$VAR = \frac{1}{N-1}\sum_{I=1}^{N}|x_I|^2 \quad (4.20)$$

Wilson Amplitude (WA) measures the frequency information of the myoelectric signal. This feature indicates how many times the difference in signal amplitude between two adjacent segments exceeds a predetermined threshold which is related to the motor unit action potential and subsequently to muscle contractility [82][165].

$$WA = \sum_{i=1}^{N-1} f(|X_i - X_{i+1}|) \quad (4.21)$$

Where,

$$f(x) = \begin{cases} 1, & x \geq thershold \\ 0, & otherwise \end{cases} \quad (4.22)$$

Average amplitude change (AAC) is the average length of the EMG waveform over the time segment [170].

$$AAC = \frac{1}{N}\sum_{i=1}^{N-1}|X_{i+1} - X_i| \quad (4.23)$$

Some features depend on a threshold value related to the equipment's gain. The suitable threshold value is used in ZC, SSC, and WA features, and it is in the amplitude range between 10 and 100 *mV* [171].

As explained in the state of the art (Chapter 3), feature selection methods help reduce the overfitting, improve the accuracy, and reduce the training and testing time. For this dissertation, three different feature selection methods were applied to the dataset. Then it was observed which of them improved the accuracy level through *Orange Software*. This software is an open source of machine learning and data visualization that was created in 1996 at the University of Ljubljana. The first feature selection filter method that was applied was the information gain, which calculates each feature's expected amount of information. The second one was the chi-squared test. From statistics, this test represents a way to prove if a variable is independent of another. When applied to machine learning, this test calculates whether the features are independent of the target. Finally, it was used the Relief-based feature selection method. This metric is used to evaluate the ability of each feature in distinguishing the classes. The increase of these values is related to how good the feature is. Based on that, the best five and ten features for each metric were chosen and the results for a KNN with k=5 analysed.

4.1.7. Classification

As it was seen before, there are a variety of classifiers that identify different motion patterns. Due to simplicity and fast computational response, LDA and KNN proved to be the best for real-time classifiers.

LDA estimates the probability of a new example belonging to a specific class based on each input value by using hyperplanes to separate data which contain different classes. This algorithm is widely used for binary and multi-class classification. LDA is a classifier with numerous advantages compared to others, since it needs a period of interactive training which avoids overfitting [172]. Moreover, for real-time devices, LDA has a low computational cost, one of the most critical requirements for this kind of applications. However, this classifier struggles in solving multiple motion problems since it yields poor results when applied to non-linear data, as the case of the EMG signals acquired during dynamic movements. Despite that fact, this classifier showed better results than others applied in the academic field [173]. The same way it happens for other classifiers, LDA considers that each feature follows a Gaussian distribution and has the same variance. In addition, this algorithm assumes that the features

are randomly sampled and presents a lack of multicollinearity [103][156]. KNN is also one of the most implemented classifiers for EMG classification in real-time. KNN is a non-parametric method that classifies the data based on the closest feature space since the training sets are mapped into multidimensional feature space. In this space, the value is classified according to the most frequent class among the k nearest data. To compute the distance between vectors, KNN uses the Euclidean distance [149][157][158].

SVM and ANN are widely used for sEMG classification since both can generate good classification results. Previous authors recommended the use of this classifier for specific hand gesture recognition. They concluded that using the Kernel function increases the classifier performance. SVM is usually preferred to high-dimensional feature space. Conversely, ANN has good resistance to noise. However, both classifiers take too much time during the training stage, require large storage space and have high computation complexity. For scenarios where it is wanted to build low-cost real-time devices, those are precisely the characteristics that are not needed. So it was decided to not use both [109]. More specifically, for cases where the aim was to recognize a set of dexterous movements, KNN was faster than SVM and did not show significant differences on applied statistics tests.

After knowing the assumptions of the classifiers, it was necessary to know which problems it will be faced. Having such knowledge will prevent misclassification problems and wrong interpretations of the results. In order to answer the existing problems and minimise possible degradations caused by the changes in electrode position, the influence of using a classifier divided into two or three levels was tested. In each level, different sets of the four performed hand gestures would be recognized.

Considering the assumptions of each classifier, the distribution of our database was tested. It is known that sEMG signals do not follow a normal distribution. Nevertheless, the normality of the features was tested. Therefore, it was implemented the Anderson Darling test to investigate if the resulting data matrix followed a normal distribution. With the test results it was possible reject the null hypothesis, which means that our data do not follow a Gaussian distribution. One of the LDA assumptions is that the data follow a normal distribution, which could explain why LDA should not use in this dissertation. In most multiclass classification cases, the normality of the feature set is often violated, but the results are still accurate [176]. Despite these disadvantages, LDA is still used in scientific academia since it demonstrated good classification results.

Then, the classification was divided into four stages to reduce the computation time and reduce the influence of the displacement of the electrodes. Thus, the problem was reduced to binary classification instead of analysing the four classes at once. Therefore, the classifier will recognise if the volunteer is performing any movement or at rest in the first classification level. Then, in the second level, it were tested two options (illustrated by steps 1 and 2 in Figure 4.6). First, it was tested if the classifier recognised all the gestures accurately (step 1 in Figure 4.6). Then, it was tested if it would be better to divide the classification into binary classifications. Therefore, in the second classification level, the classifier had to identify if the subject would perform, for example, movement A or the other movements (step 2 in figure 4.6). The A, B and C represent the hand gestures that volunteers performed in this dissertation (Spherical Grip, Tripod Grip and Index Finger Flexion). Finally, in the third classification level, the classifier had to identify if the volunteer was performing the B or the C movement. For each level, two classifiers, LDA and KNN, were tested. In order to optimise the KNN classifier, six different values of k (2, 5, 7, 9, 11 and 15) were used. For both of them, the cross-validation and split validation methods were applied to the database. It is also important to note that the chosen classifiers can differ between levels since what matters is having the most precision and accurate results in the shortest time possible. The final result will be a tree classifier with sub classification levels, where the input is the vector of features and the output is the performed movement (Figure 4.6).

To evaluate the selected machine learning algorithms, the accuracy, recall, precision and kappa coefficient were calculated. Besides these metrics, the confusion matrix was also plotted. This one display the true positive, true negative, false positive and false negative predictions for binary classification and the number of instances that were misclassified for multiclass problems.

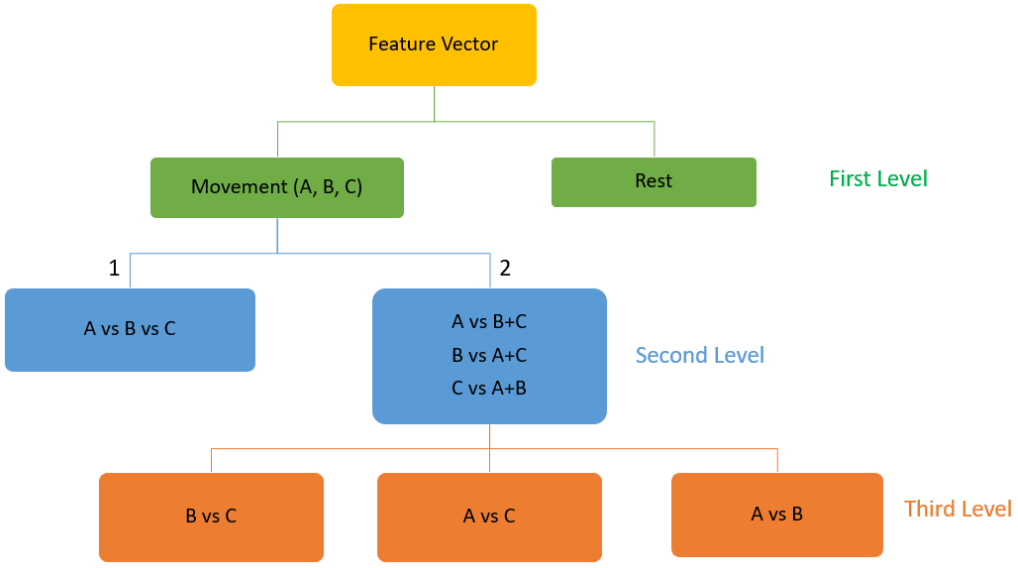

Figure 4.6: Scheme of the classification stages. First level: The classifier has to recognize if the volunteer is performing any movements or at rest. Second level: is divided into two options (1 and 2). If the results were better for option 2, the next step is recognising two gestures in a third level.

Finally, for similar results, the accuracy of the two implemented classifiers (LDA and KNN) was compared with a paired t-test to observe if there were significant differences between them.

4.1.8. Technical validation

To verify that the acquired data is similar to the produced in real-life, it was necessary to evaluate the effect of the experimental conditions. Therefore, the difference between movements and baseline noise was determined by applying two state-of-the-art classifiers (LDA and KNN) and comparing the obtained classification to those of the literature. It should be retained that if the results of the designed classifier were about 90%, it can be considered that the device is ready to go to the market, but if the results showed a level of accuracy lower than 90%, it is necessary to identify and investigate the reasons and the failures that are responsible for such low classification performance.

4.2. Design of the Prosthetic Hand

After studying the best signal processing methods and the best classifiers that in the future will be part of the myoelectric microcontroller, we chose a 3D printable model. Hence, the users' opinion is crucial for the success of the designed prototype. Therefore, their experience with previous models should be taken into consideration.

The UnLimbited Arm 2.1 model, an e-NABLE model, is widely used by amputees and children that have congenital disorders. This model is lighter when compared to the more advanced prosthesis available on the market. Besides that, the Unlimbited Arm is easy to build because all the parts can be printed by 3D printers, which makes the time to market short and users' customization possible. However, one of the aims of this work is to develop a myoelectric prototype. Thus, it was needed to change some parts and design new ones without compromising the prosthesis weight and the associative cost.

4.2.1. Materials

In additive manufacturing, there are a lot of 3D printers and techniques to produce a model. In this dissertation, the most widely available and the cheaper technique was used, Fused Deposition Modelling (FDM).

FDM is a fast, easy, versatile and low-cost manufacturing process. Firstly, the filament is melted and then deposited layer by layer. However, the parameters and printer settings must be defined before printing the desired part. Despite the advantages of such technology, in FDM the final structure has relatively low mechanical properties due to the inter-layer adhesion issues. In this sense, parameters such as the connection between the fibre and matrix (which for polymers is a reduced problem), fibre orientation, and voids formation should be considered [41][160][161][162]. FDM has numerous advantages that make the built prototype unique, such as using coloured filaments and low-cost raw materials. In addition to this, unlike what happens with other techniques, the vapours produced here are of low toxicity. Despite the advantages listed above, there is a need to use build supports [111].

In the FDM, mainly in the biomedical field, the most used materials are PLA, poly (e-caprolactone) (PCL), ABS, Polyethylene terephthalate glycol (PET-G), polyamides (commercially known as nylon). This type of material has some degree of rigidity, which is a key factor since we need to build a resistant prototype [45][177][178][179].

The UnLimbited Arm was already designed, so the .stl files were downloaded and rescaled. In this dissertation, it was not possible to work with amputees or with children with congenital malformation, so it was necessary to rescale the model to fit in a young adult. Because of that, the bicep perimeter, the length of the forearm, the length of the beginning of the palm to the fingertip and the wrist perimeter were measured - Table 4.1.

Table 4.1: Distance of the bicep perimeter, the length of the forearm, the length of the beginning of the palm to the fingertip and the wrist perimeter in millimetres.

Structure to measure	**Distance (*mm*)**
Hand Length (C- Figure D-1)	185
Forearm length (B- Figure D-1)	230
Bicep Circumference (A – Figure D-1)	275
Tension Pin Hole	65

Pin Hole	3

After measuring the distances, the .stl files were opened on Open Scad Software. Then, the code of each piece was changed to rescale and readapt the device to a young adult. All the files were rescaled except the pins of the device that were of the same size (3.00 *mm*). After modifying the model, we sent the .stl files to Prusa Slicer software. This software is used to define the printing parameters as well as filament settings. Besides, it can be tested the best printing position to ensure that the printed piece has the minimum amount of support material and can be printed in a faster printing time.

In this dissertation, we used the original Prusa i3 MK3S by Prusa Research, available on the laboratories of the Nova School of Science and Technology. The material that used was PLA. This material is thermoplastic, which means that it has the properties that we need to adapt the shape of the printed forearm part to the user. Since there are some printing parameters already defined by the e-NABLE community, the printing process was defined according to them. In one of the parts, it was necessary to change some parameters like the velocity and the speed to decrease the printing time (table D.1- Appendix D). In addition to the printing parameters described in table D.1, we used the 0.30 *mm* QUALITY print parameter. During the printing process, the visual features of the printed material were evaluated to ensure that the quality printing was maintained. It was essential to ensure that didn´t exist any defects between layers and bad adhesion between the plate and the printed material. The blue colour was used for PLA material and purple for pins and support material.

Before starting the assembly process, it was necessary to do a small cleaning of the printed material to remove the support structures and correct some defects present on the surface of the parts. During this process, the pliers and sandpaper were used. Since the parts of the prosthesis model were all separated (Figure 4.7). Therefore, the assembling process was divided into three parts:

- The prosthesis fingers were assembled by placing the pins corresponding to the interphalangeal joints forming the finger.
- The fingers were connected to the palm on the metacarpophalangeal region.
- The entire forearm-elbow frame was assembled after the hand was complete.

Before assembling the forearm-elbow part to the hand, it was necessary to mould both pieces with hot water. The water was boiled and the pieces were glued and moulded. We use a rolling pin to mould the forearm since it has a similar geometric shape. Next, the cuff was moulded with a specific piece, the jig (Figure D.2 in Appendix D). Then, the tension mechanism was set. Five tension wires were placed on the fingers and joined to the mechanisms of the cuff (Figure D.4). The extremities of the wires were tied to the tensioner pins. After that, the elastic wires were placed on each interphalangeal joint to give

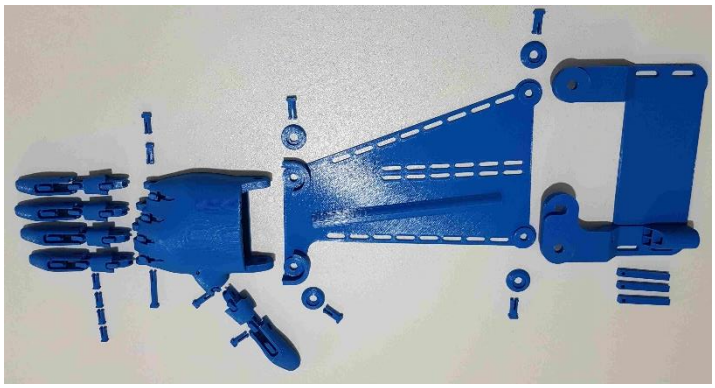

Figure 4.7: Prosthesis before the assembly.

some tension during the movement. To ensure that the wires were placed in the right place, we used a clamp to pull the strings while we were tying the knots. We removed the excess wire with scissors after tying the knots around the fingers and tension pins. Finally, we added rubber thimbles.

5. Results and Discussion

5.1. EMG signal processing and classification for Pattern Recognition myoelectric control

In this section, the results obtained during this study will be presented in the following order: firstly, a briefly describe of the pre-processing methods to select and clean our data; secondly, the analysis of the digital filtering and wavelet transformation of the signal; at last, the discussion of the different processing techniques and the outcome results.

5.1.1. Pre-Processing Data

Despite the efforts made to control our real-time acquisitions, sEMG records are susceptible to external factors that contaminate the signal. Therefore, the noise increases and the quality of the signal decreases, which is negative for further classification and hand gesture recognition. The occurrence of such factors causes fluctuations in the amplitude of the sEMG signal. Besides the signal amplitude changes, muscle fibre orientation changes and motor unit firing rates influenced phase response. In our case, the change in the electrodes' position, the flexibility of each patient's skin, and the sweat during the acquisition time were identified as possible noise sources. To mitigate such problems, the SNR of each signal and for each movement was calculated. The signals with an SNR lower than 2 *dB* were eliminated from our dataset to clean the possible outliers and avoid lower classification performances. Choosing only the best signals for the training and test sets will increase the classification results and reduce the computational time. Because of that, the signals from five volunteers were eliminated during these processes, which means that the set was reduced to forty volunteers.

After eliminating the signals, the data was labelled by choosing a threshold value. To ensure that the baseline was well identified, the signals were divided into different intervals and calculated the average of the baseline values according to a specific threshold defined for each movement and each volunteer.

Finally, it was necessary organize the dataset for posterior filtering and processing methods application.

5.1.2. Digital filtering

As mentioned in section 2.4.4.1, removing the signal's noise is crucial for promoting accurate control. In order to measure the quality of the filters, the SNR and MSE metrics were used. As explained before, the MSE measures the error by comparing the reconstructed signal to the raw signal. For constant or periodic signals, it is possible to use the SNR, which is a value that compares the desired signal level to the level of background noise. The quality of the signal is positively related to SNR and negatively associated with MSE. Therefore, in this section, the SNR and MSE values will be analysed.

Different filters were tested due to the high dependency between the filtering process and the dataset's characteristics. The results can be found in the graphics in Appendix E and the following figures. By observing the graphics in Appendix E, it is possible to conclude that the only FIR filter that showed better results was the Savitzky-Golay filter (sgolay in the graphic). As suggested in section 4.1.3, the Savitzky-Golay filter preserves the high-frequency components since they contain the energy corresponding to the muscle contractions (50-150 *Hz*). These filters have the lowest value of MSE when compared to Butterworth and Window filters (Figure E.2-E.22).

It was proved that Kaiser and Hamming windows filters add noise to the signal, decreasing SNR's value for all volunteers except for volunteers one, eight, nine and twenty-two. Nevertheless, these filters have the lowest values of MSE when compared to Butterworth filters. Due to the fact that the window filters decrease signal quality by adding noise, it was decided to analyse the obtained values for bandpass Butterworth.

Before analysing each volunteer in detail, three general conclusions can be taken. The first one is that the second and the fourth orders are the best filter orders. Moreover, in most cases, applying a bandpass filter is advantageous because it attenuates the noise, which increases the SNR. The sEMG signals are affected by numerous noise sources that increase the noise in a specific low-frequency band between 10 *Hz* and 20 *Hz*, which explains the obtained results. The final one is that using 20 *Hz* as the low cut-off frequency is better to remove and attenuate the baseline noise than using 10 *Hz*.

Regarding volunteer number one, the SNR reached its maximum value (31.37 *dB*) for a frequency band between 20 and 150 *Hz* (orange line – Figure 5.1). This value was obtained when applying the fourth-order bandpass that increased the SNR by 38.60 %. The minimum SNR obtained was 30.43 *dB* when the sixth-order bandpass filter was applied with a frequency band of 20-200 *Hz* (red line – Figure 5.1). There is no considerable difference between the MSE values (standard deviation= 2,07E-3), but it is possible to observe that the first-order filters have the minimum MSE values. As the order increases, the MSE increases as well (Figure E.1). Therefore, the fourth-order passband filter can be considered the best option since it increases SNR to its maximum value and does not have a relevant MSE value (6.50E-03).

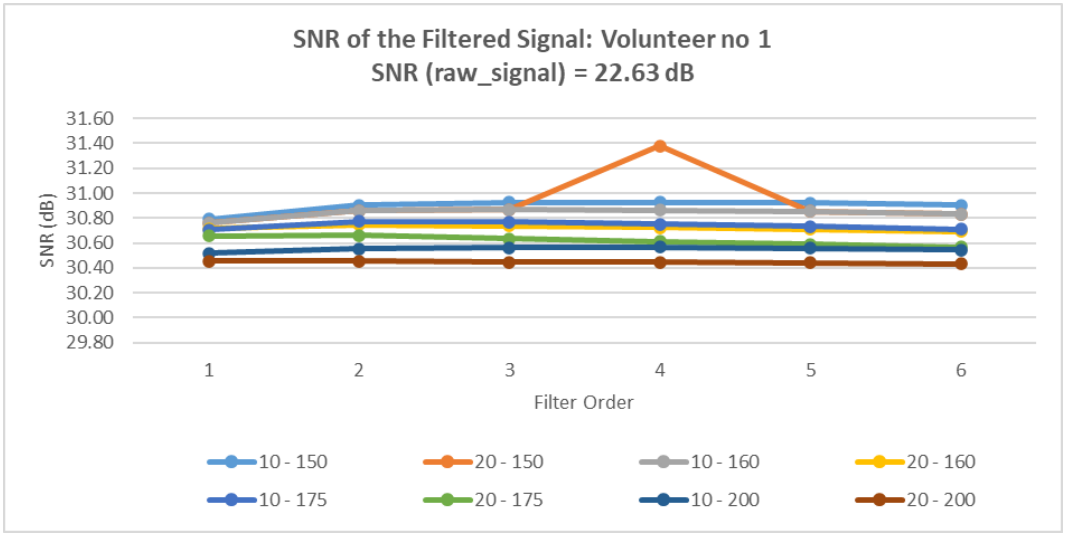

Figure 5.1: SNR values of the filtered signals when the bandpass Butterworth were applied – Volunteer number 1.

For volunteer four, the results are different. The maximum SNR value (54.16 *dB*) was obtained in the frequency range between 20 and 200 *Hz* (red line – Figure 5.2). This maximum value is translated into an increase of 14.57% when the second-order bandpass filter was applied. In general, as the superior limit of the frequency band increases, the SNR is higher. On the contrary, the minimum (50.48 *dB*) was obtained when the sixth-order filter was applied for a bandpass frequency of 10 to 150 *Hz*. The difference in the frequency range might be directly related to the original SNR. The acquisition of the sEMG signals for volunteer number four was made under perfect conditions (the SNR is already excellent). With this, it can be concluded that there is no contribution of certain noisy high-frequency contents during the acquisitions.

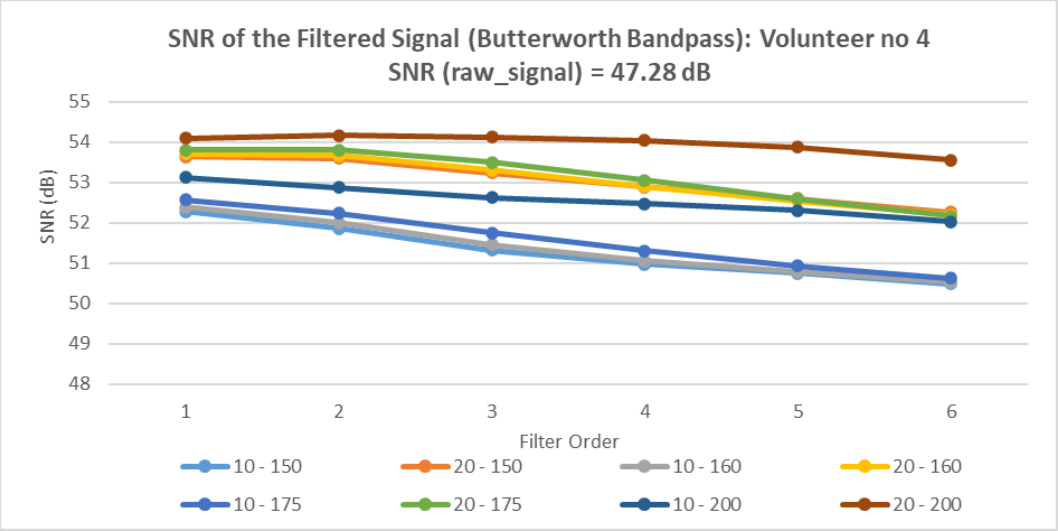

Figure 5.2: SNR values of the filtered signals when the bandpass Butterworth were applied – Volunteer number 4.

The overall results for volunteer number eight are similar to those previously obtained. As it can be seen in Figure 5.3, for a cut-off frequency of 20 *Hz*, the SNR always increases independently of the high cut-off frequency (150, 160, 175 or 200 *Hz*). It is also possible to observe that with the increase of the cut-off frequency from 10 *Hz* to 20 *Hz*, the SNR increases, which gives the idea that the noise content is located in higher frequencies. However, it was not tested the influence of the elimination of such higher frequency values because it would remove important sEMG information for posterior classification. Nevertheless, for a frequency of 20 *Hz* the SNR increases which also happens for the other volunteers, so it was decided to use this frequency despite the results. The SNR reaches its maximum value (34.26 *dB*) when it was applied a fourth-order bandpass filter (20 -150 *Hz*). The SNR increased 32.12 %. The minimum value (33.22) was obtained in a fifth-order bandpass filter (10-200 *Hz*). This minimum corresponded to an increase of 27.90% in the SNR. The MSE obtained values were low, which means that the signal was preserved (2.00E-03) – Figure E.7.

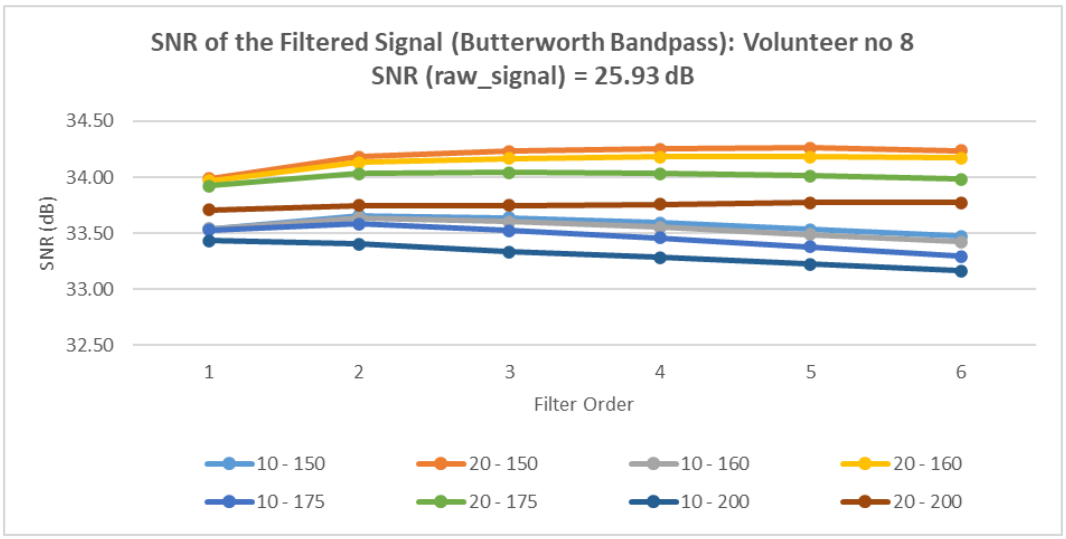

Figure 5.3: SNR values of the filtered signals when the bandpass Butterworth were applied – Volunteer number 8.

The results for volunteer nine are similar to the results obtained in the previous analysed volunteers, which means that the MSE and SNR increase with the filter order decrease and the increase of the high cut-off frequency. The maximum value (33.09 *dB*) was obtained when a fourth-order bandpass Butterworth (20-150 *Hz*) was applied (orange line – Figure 5.4). The minimum value (32.33 *dB*) was obtained when the sixth order filter was applied (10-200 *Hz*).

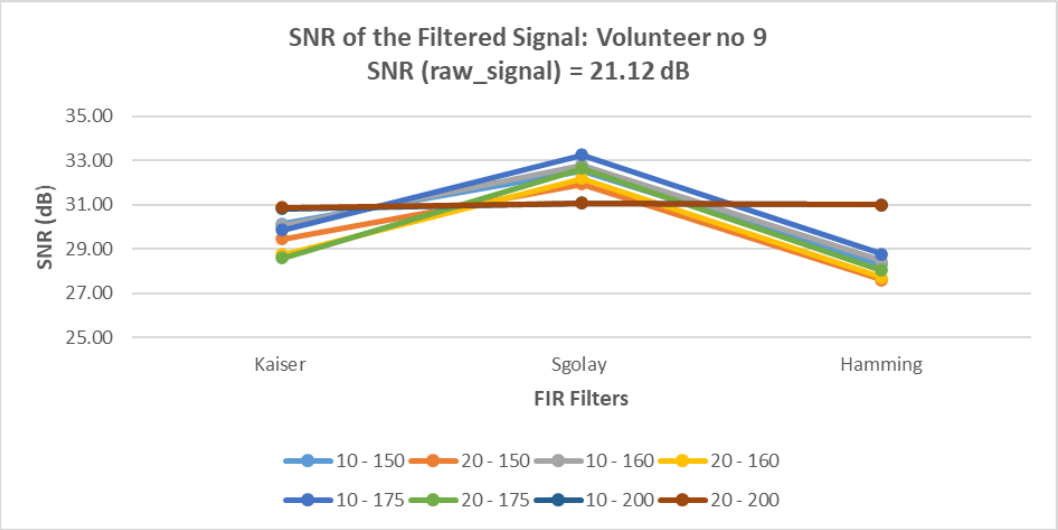

Figure 5.4: SNR values of the filtered signals when the bandpass Butterworth were applied – Volunteer number 9.

As for volunteer twenty-nine, the maximum value of SNR (35.40 *dB*) was obtained with the fourth-order bandpass filter. In figure 5.5, it is possible to observe that the SNR increases as the superior limit of the frequency band decreases, which means that the best frequency band is between 20 and 150 *Hz*. In this line of thought, the minimum SNR value (34.62 *dB*) was obtained in a first-order frequency passband filter between 20 and 200 *Hz*. It is possible to conclude that with the increase of the order of the filter, the MSE increases, which makes the fourth order an eligible filter.

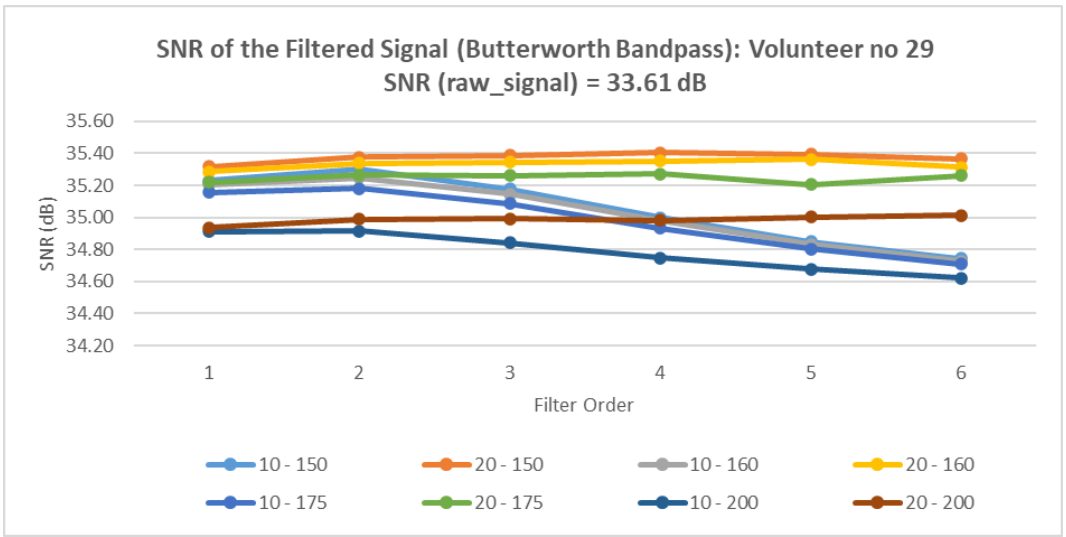

Figure 5.5: SNR values of the filtered signals when the bandpass Butterworth were applied – Volunteer number 29.

The results obtained in volunteer forty-one are interesting because they differ from the others. Contrary to what happens for most volunteers, there is no difference between the frequency bands (Figure 5.6). The SNR values are similar, which means that there is no significant difference between

them (standard deviation= 0.049). This means that having a high low cut-off frequency does not contribute to a better attenuation of the noise. These results demonstrate that the principal noise frequency contents are above 10 *Hz*. The MSE values are the lowest values of all the volunteers. The highest SNR values vary between 160 and 175 *Hz*. Therefore, it is expected that the noisy data has a frequency value very close to 175 *Hz*. In this case, the maximum SNR value (29.66 *dB*) was obtained when a sixth-order Butterworth filter was applied with corner frequencies of 20 *Hz* and 175 *Hz* (green line – Figure 5.6). The minimum SNR value (29.44 *dB*) was obtained when applying a second-order Butterworth filter with a passband between 20 and 200 *Hz*. The MSE values were also low (3.00E-03)- Figure E.15.

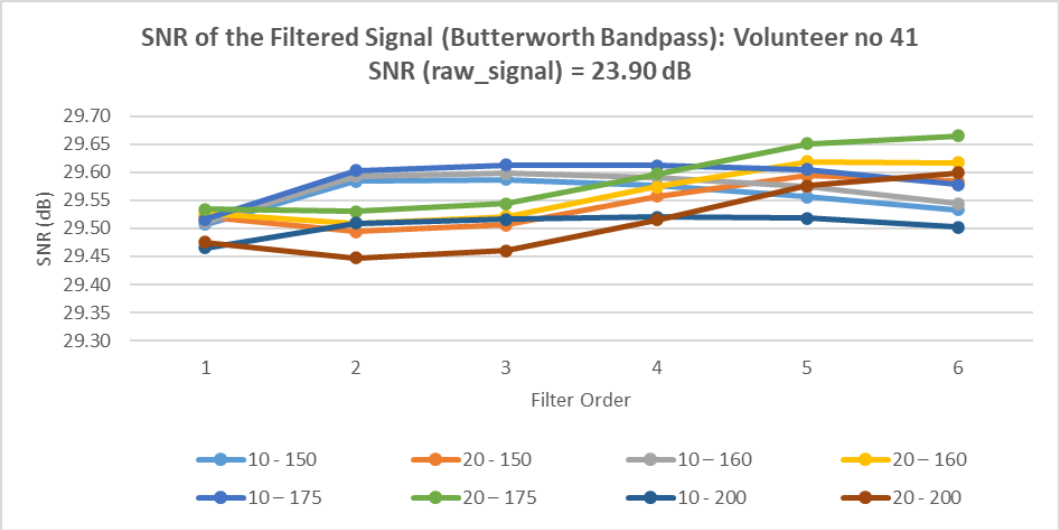

Figure 5.6: SNR values of the filtered signals when the bandpass Butterworth were applied – Volunteer number 41.

Besides these five volunteers, we also analyse the SNR and MSE values for volunteer twenty-two. The best SNR was obtained when a fourth-order Butterworth bandpass was applied (35.18 *dB* – Figure E.18- Appendix E). For all analysed volunteers' signals, except for two, the results show that the best frequency band is between 20 *Hz* and 150 *Hz*. Regarding the filter order and type, it is possible to conclude that the fourth-order Butterworth is the most effective filter since it increases the SNR of all filtered signals. The analysis of the power spectrum of the filtered signal shows that the power of the signal was preserved, reinforcing the idea that this is the best filter to attenuate noisy data. As we already explained before, EMG phase information is not considered. Therefore, the amplitude response characteristics are the ones that matter, which implies the use of a filter capable of preserving the amplitude linearity of the characteristics of the passband region [136]. Fortunately, the fourth-order bandpass Butterworth filter has these ideal characteristics, which makes it an acceptable filter.

To verify if the obtained cut-off frequencies were within the frequency band defined by the academic community, a comparison to the existing literature was made. As it is known, the amplitude of the sEMG signal is affected by different noise sources that can be either external or intrinsic factors. The intrinsic factors are inherent to the patient's physiological and anatomical characteristics. Examples of it include the distance between the active fibres and the amount of tissue between the muscle surface and the electrode [80][81][180]. During our acquisition, it was possible that some of these factors contributed to increasing the noise, since the recruited volunteers had different body shapes and characteristics. However, it is possible that the contribution of these factors is not the most significant one. Besides, the position of the red electrode could contribute for some of the noisy content, since it can be reading information from other muscles or reflected signals. Conversely, external factors like

electromagnetic radiation, the users' movement, and cable movement are the noisy sources that most affect the acquisition [180]. It is thought that the noise generated by motion artefacts is below 20 *Hz*, which suggests the use of a frequency corner equal to 20 *Hz*, the ideal one. Unshielded cables are considered noise sources since they have an intrinsic capacitance capable of generating current when moved in a magnetic ambient or an electric field. This current has a voltage that is similar to the magnitude of the detected EMG. The noise associated with this process has a frequency range of 1 to 10 Hz [181] [182]. In this dissertation, it was considered that the best low cut-off frequency was 20 *Hz*, which ensures that noise frequency contents like these ones can be smoothed. EMG amplitude is quasi-random since it depends on the motor firing rates, on the activation of motor units, and on the mechanical interaction between muscle fibres. Because of that, the first 20 *Hz* are unstable frequency components that can be considered noise. Therefore, they can be removed from the signal, which is possible with a fourth-order filter with a bandpass frequency between 20 *Hz* and 150 *Hz* [183]. Another common phenomenon that occurs during signal acquisition is crosstalk and the influence of the heart's electrical activity. To remove these interferences, the literature recommends the use of a high-pass filter with a cut-off frequency of 20 *Hz* [82]. In addition, the low cut-off frequency recommended by the international society of electrophysiology and kinetics is 20 *Hz* and by the EMG for non-invasive assessment of muscles between 10 and 20 *Hz*. By comparing the values suggested in the literature with the frequency obtained in this dissertation it is possible to conclude that almost all noise types can be smoothed and at the same time preserved the important signal information.

While the low cut-off frequency is within the literature frequency band, the obtained high cut-off frequency value is not. Most of the authors suggested values between 400 *Hz* and 500 *Hz*. Using these corner frequencies is very common since most authors use sampling rates of 1000 *Hz* or more. However, in our acquisition, it was used a sampling frequency of 500 *Hz*. With this in mind, it was investigated if using this value influences the classification rates. It was found out that Li *et al* [135] discovered that sampling data at 500 *Hz* could be computationally more adequate than typical 1000 *Hz* since it only affects the classification rates by 0.8 % for healthy subjects. In theory, Hakonen *et al* [127] proved that lower frequency components of myoelectric signals contain information about the activation rates of the active motor units, which is not significant for movement classification. In fact, the optimal cut-off frequencies vary depending on muscle and recorded data, which means that the selection of the best value is highly dependent on the metric chosen to analyse the best filter. Therefore, according to the used evaluation metrics, having a corner frequency of 150 *Hz* is essential to remove the noise present in the high-frequency interval. Besides that, the obtained frequency band contains the principal energy of the sEMG signal that is between 50 *Hz* and 150 *Hz*.

MSE values were low values which means that the useful information in the sEMG signal has remained and that the undesirable parts were removed.

Despite the good SNR values, some authors found out that using digital filters to remove the noise is not as effective as it was thought. Hargrove et al. show that time-domain features can achieve higher classification performances than the frequency domain or time-frequency domain features [107]. Due to this, we decided to reconstruct the signal with the approximation and transformed detail coefficients instead of using the wavelet coefficients on its original form, to investigate if using the wavelet transform algorithm is better than using traditional filters.

5.1.3. Wavelet threshold noise reduction

After analysing the results obtained in the digital filtering the results obtained in wavelet threshold noise reduction were analysed. The third, the fourth and the fifth levels of decomposition were tested since they are the most popular among the academic community. Observing the graphics in Appendix

F is possible to conclude that the SNR and MSE values increased from decomposition level three to decomposition level five. However, the difference between the MSE values from one decomposition level to the other is insignificant compared to the increase in SNR. So, the coefficients were plotted in MATLAB. Before applying a set of wavelets to the signals, nine decomposition levels were tested with the wavelet denoiser toolbox. It was possible to conclude that the coefficients after level six were not significant, which means that only the third, fourth and fifth levels were used. For each level, we tested the seven most used wavelet types used for filtering myoelectric signals. Consequently, for each wavelet, we tested three different threshold rules (SURE, Minimax and Universal Threshold) and for each of them the HAD and SOFT threshold functions. The results for each wavelet mother, level and threshold function are in the following figures.

In Figure 5.7, it is possible to observe the results obtained when the wavelet denoising method was applied for the fifth decomposition level. For volunteer number one, the SNR values increased with the increase of the decomposition level, reaching its maximum (29.70 *dB*) for the universal threshold rule with the HAD function for sym7 (snr_ut_hard in ocean blue bar – Figure 5.7). The lowest values of SNR were obtained when the SURE threshold rule and the universal threshold rule with soft function were applied. The minimum was obtained for the SURE threshold rule (26.33 *dB*). The best wavelet families were sym7, sym2 (orange bar), db6 (yellow bar) and db10. The same happened for the third and fourth levels (Figures F.1-F.4 in Appendix F). Regarding MSE values, the lowest ones were obtained when the SURE threshold rule was applied. The highest values were obtained for the universal threshold with soft function (Figure F.5). Comparing these results to those obtained in digital filtering, it is possible to conclude that Butterworth effectively eliminated the noise (29.70 < 31.37 *dB*). However, the MSE values were lower for wavelet threshold noise reduction method (2.52E-03 < 6.50E-03).

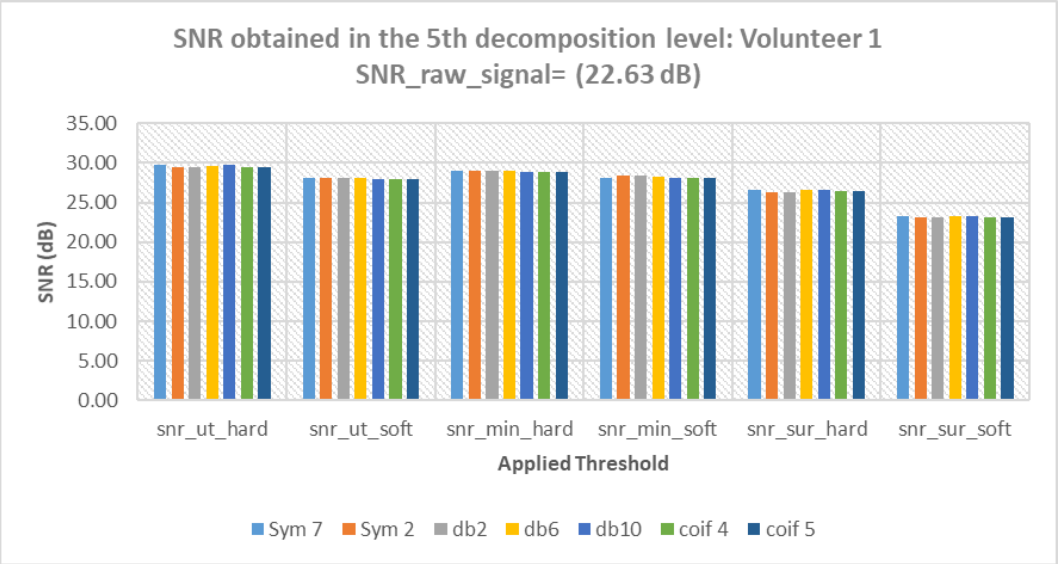

Figure 5.7: SNR values of the filtered signals when the wavelet transform noise reduction method was applied – Volunteer number 1.

For volunteer number four, the SNR also increases with the increase of the decomposition level. The maximum SNR was reached when the universal threshold rule with HAD function (snr_ut_hard in Figure 5.8) was applied. The minimum values were obtained for the SURE threshold rule (snr_sur_hard and soft in Figure 5.8). As it can be observed, the best wavelet families were sym2, sym7, db6 and coif 5. Regarding MSE values (Figure F.10), the variation between the decomposition levels was not significant, which means that the values were similar. Comparing the results obtained for the wavelet threshold noise reduction method with those obtained in digital filtering, it is possible to conclude that

Butterworth removed different noisy contents (49.91 < 54.16 *dB*). Regarding the MSE values, they are lower for wavelet threshold noise reduction method than those obtained in digital filtering (4.51E-03 < 3.22E-02)

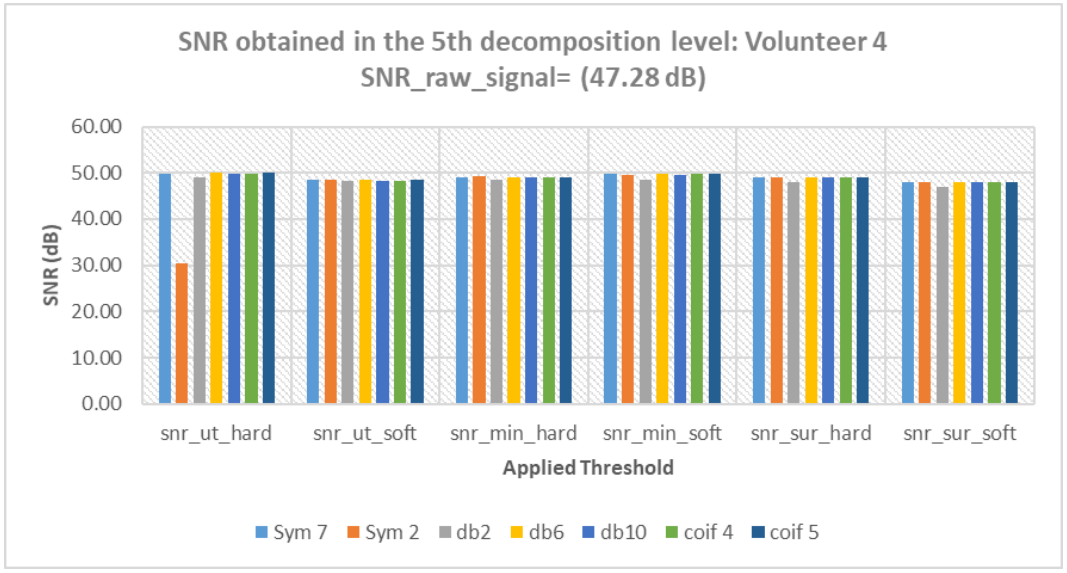

Figure 5.8: SNR values of the filtered signals when the wavelet transform noise reduction method was applied – Volunteer number 4.

For volunteer number eight, the obtained SNR values were also better for the fifth level than for the fourth and third levels (Figures F.11- F.14). Therefore, in Figure 5.9, it is possible to observe the SNR values obtained in the fifth level of decomposition. The maximum value (32.83 *dB*) was reached when the universal threshold rule was applied with the HAD threshold function for sym7 wavelet (illustrated by snr_ut_hard in Figure 5.9). Conversely, the minimum SNR value (28.70 *dB*) was obtained when the SURE threshold rule was applied. For all the levels, the SNR increase when compared to the raw SNR value, which means that wavelet threshold noise reduction improved the quality of the signal. Regarding MSE values (Figure F.15), they reached their minimum for the SURE threshold rule. Conversely, the universal threshold rule had the highest MSE values (2.36E-04). Once again, these values were low, which means that the interesting signal was preserved. Comparing these values to those obtained in the digital filtering section, it is possible to conclude that the bandpass Butterworth outperformed the wavelet noise reduction method. However, the MSE values for digital filtering were

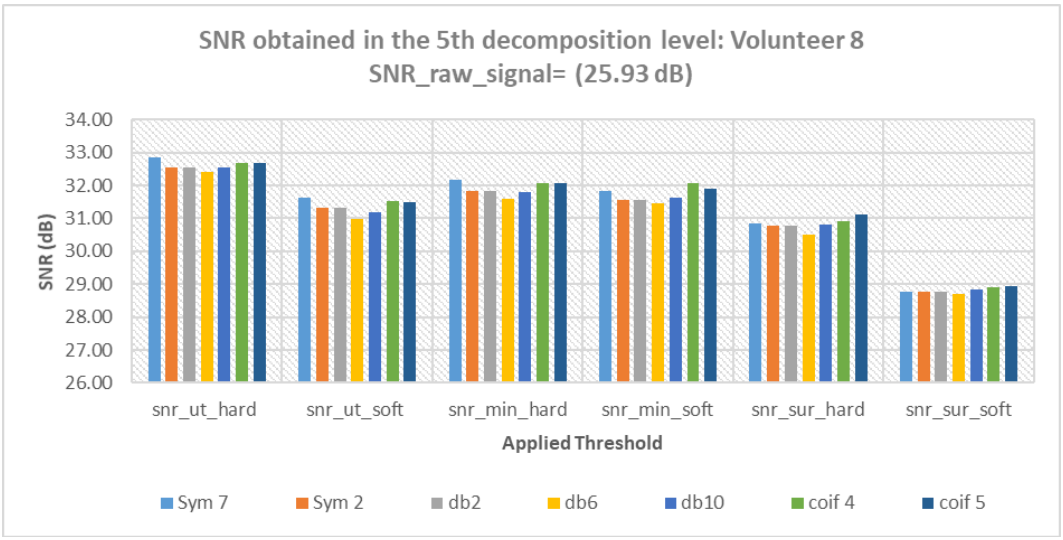

Figure 5.9: SNR values of the filtered signals when the wavelet transform noise reduction method was applied – Volunteer number 8.

lower, which might be related to the elimination of important peak information during the application of the IIR filter.

The SNR values increased for volunteer number nine, with the decomposition level reaching its maximum for the fifth level (29.14 *dB*) – Figure 5.10. The results obtained for the third and fourth levels were similar when it comes to wavelet families and threshold rules (Figures F.16 – F.19). In Figure 5.10, it is possible to observe the results obtained for each threshold and for each wavelet family. The best from all the threshold rules was the universal threshold rule with the HAD (illustrated as snr_ut_hard in Figure 5.10) and the minimax threshold rule with the soft function (snr_min_soft in Figure 5.10). The best wavelet family was db6, followed up by coif5. Regarding MSE values, it is possible to conclude that they were similar between levels. The lowest values were obtained when the SURE threshold rule was applied. Comparing these values to those obtained in digital filtering, it is possible to conclude that the maximum SNR was lower for wavelet noise reduction (29.14 < 33.09 *dB*). The MSE values obtained in this section were lower than those obtained in digital filtering (4.43E-03 < 4.00E-02), which means that during the application of Butterworth some relevant signal information was lost.

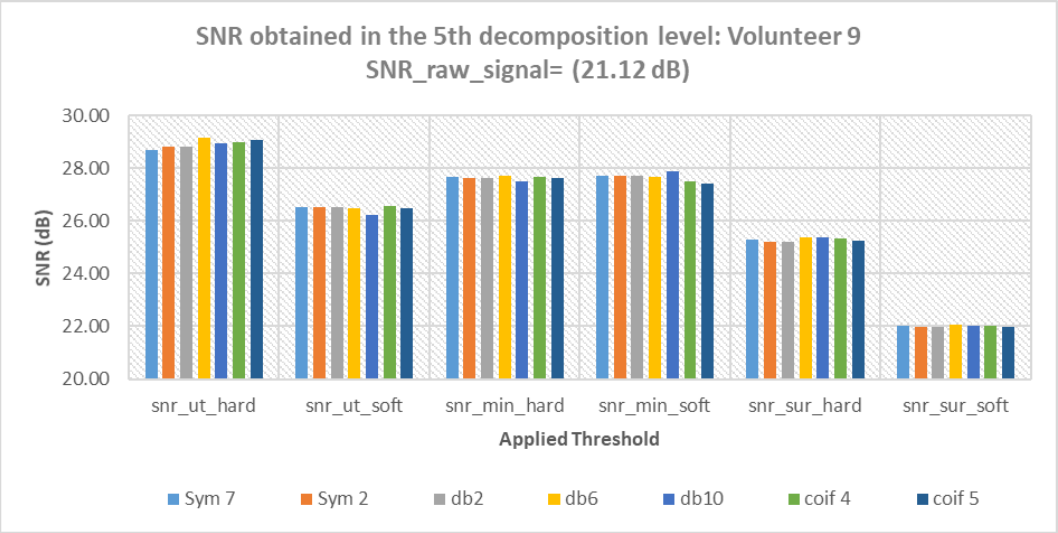

Figure 5.10: SNR values of the filtered signals when the wavelet transform noise reduction method was applied – Volunteer number 9.

The most interesting values were obtained for volunteer number twenty-nine. As already expected, the SNR values increased with the increase of the level of decomposition, reaching their maximum for the fifth level (Figure 5.11). For the third (Figure F.21), fourth (Figure F.23) and fifth levels, the universal threshold and the minimax threshold are the ones that had the highest SNR values. For the fifth level, the maximum SNR value (38.40 *dB*) was reached for the coif5. However, sym2, sym7 and db2 also show good results (38.24, 38.30, 38.30 *dB*). As it can be seen in Figure 5.11, the universal threshold rule with the HAD function was the best thresholding method. Regarding fifth level decomposition MSE values (Figure F.25), it is possible to conclude that the lower values were obtained in the SURE threshold rule and the higher ones in the Universal threshold rule. However, for all levels, the MSE results were low, which means that the interesting part of the signal was preserved. Comparing these values to those obtained in digital filtering, it is possible to conclude that the results obtained in the fourth and the fifth levels outperformed the bandpass Butterworth results (38.40 > 35.40 *dB*), which did not happen for the other volunteers. The MSE values are lower than those obtained in digital filtering (1.50E-03 < 3.30E-03), which means that some signal peaks might be removed during the implementation of the Butterworth filter.

Regarding volunteer number forty-one, it is possible to conclude that the SNR increased with the increase of the level of decomposition. Therefore, the fifth decomposition level obtained the best SNR values (Figure 5.12). In this master dissertation, the third, fourth and filth levels were tested, but since the fifth level was the best, it is represented in Figure 5.12. The values obtained in the other two levels are in Appendix F. In Figure 5.12, it is also possible to study the influence of each threshold rule and the influence of the threshold function when combined with a specific threshold rule. The lowest results were obtained for the third and fourth levels when the SURE threshold rule was applied (snr_sur_hard and soft illustrated in Figure F.26 to Figure F.29. However, the SNR value reached its maximum (29.47 *dB*) for the SURE threshold rule using the soft threshold function for the fifth level. Regarding the wavelet type, it is possible to conclude that the best wavelets were the sym7 and the db10. Between both, sym7 outperformed for almost all threshold rules. On average, the best threshold function was the HAD except when the minimax threshold rule was applied. The lowest SNR value (25.88 *dB*) was obtained in the SURE threshold rule used with the HAD function. The MSE values increased with the increase of the decomposition level. However, the difference between each level was low. The highest values of MSE were obtained in the universal threshold rule. In general, the SNR improved for all the levels and for all the threshold applied rules, which means that part of the noisy data was smoothed. Conversely, the MSE values were lower, which suggests that the signals were preserved. Comparing the results obtained for this volunteer to those obtained in digital filtering, it is possible to conclude that Bandpass Butterworth increased the SNR in the highest percentage than the wavelet method (29.66 > 29.47 *dB*). The MSE values are higher for digital filtering, which means that some essential parts of the signal might be eliminated.

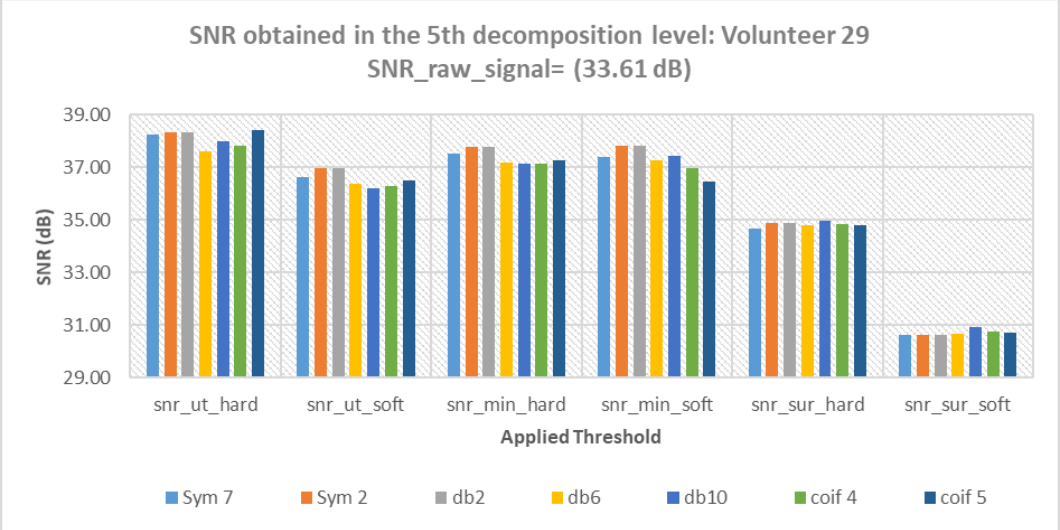

Figure 5.11: SNR values of the filtered signals when the wavelet transform noise reduction method was applied – Volunteer number 29.

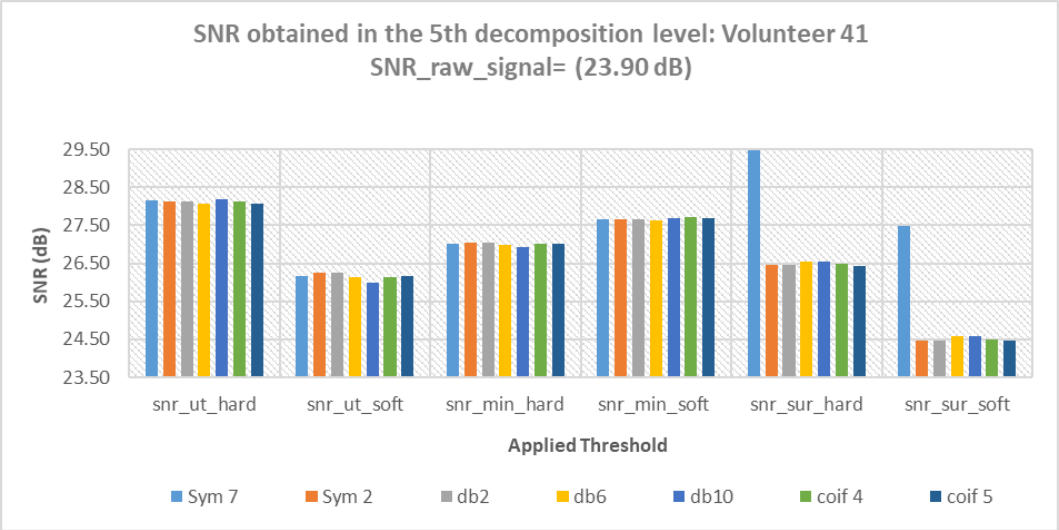

Figure 5.12: SNR values of the filtered signals when the wavelet transform noise reduction method was applied – Volunteer number 41.

Phynyomark *et al* [185] proved that the Daubechies wavelets and the fourth level of decomposition provide the minimum mean square error. The results obtained in this master dissertation are according to the principle proved by these authors since for almost all volunteers, the db was one of the best wavelets. Moreover, with the increase of the decomposition level, the SNR also increased, which is also concluded by the scientific paper authors. They compared three different threshold rules in other surveys: the SURE, the universal and the minimax [148]. As it happens in this dissertation, the authors also conclude that the universal threshold rule was better than the other ones. Besides that, Hussain *et al* [186] proved that universal threshold was the best. Moreover, these authors proved that the classification performance improved by using this rule with the HAD function [187]. According to Sohabi *et al* [188], the wavelets that are widely used for denoising biological signals are db2, db6 and db8 since they have a similar shape to MUAP. In this dissertation, db2 and db6 proved to be one of top three wavelets.

Phinyomark *et al.* [152] proved that the HAD threshold function is better than SOF, which agree with the results obtained in this dissertation. Regarding the decomposition levels, it was possible to conclude that the fifth level was the best level which is also proved by Englehart *et al.*[189]. The authors demonstrated that higher levels of decomposition improved the classification performance.

Despite the SNR values being more significant than the SNR value of the raw signal, the increase on the SNR when the bandpass Butterworth was applied, was higher than the obtained one for the wavelet. However, because the FFT transform cannot differentiate the noise that is in the high-frequency values from the useful part of the signal, the MSE values are higher for wavelet threshold noise reduction [151]. Preserving the critical signals is the most essential thing for gesture recognition. Despite the higher results, some information might get lost, which is not intended. For this reason, the wavelet transforms was applied to filter and reconstruct the signal. In this dissertation, as it happens in previous investigations, the universal threshold with HAD function was applied for all the volunteers' signals [190][191]. Regarding the wavelet family, the sym7 wavelet sub-type was used since it was one of the best wavelets. These results are according to what was expected since in most of the literature some authors suggested this method as an alternative to digital filters with the main purpose of increasing the classification rates. However, in the future it might be important considering the loss of frequency resolution in higher frequencies to avoid aliasing in high frequency ranges. Since we are optimising a real-time prototype, it was fundamental to consider if it makes sense to use this methodology for devices

like ours. Therefore, it was found out that DWT uses FIR filters that can easily be implemented on py-sharp and Arduino platforms.

For future work, it is important considering some aspects. Despite the promising results obtained in this dissertation, it is essential to note that there is a difference between the methodology followed by the authors and the followed in this work. In most surveys, the authors apply the wavelet threshold noise reduction after filtering the signal with digital filters. In this study, we tried to understand which method was better. As it was sawn, for digital filtering and wavelet denoise the SNR increased. However, some relevant information might be lost during the digital filtering process, even if very little. These results might indicate that using the two filtering processes can be advantageous since the noise at low and high frequencies is eliminated.

5.1.4. Classification performance

The uncertainty associated with the possibility of developing a low-cost model subject-independent microcontroller led us to test if using a single channel of acquisition would be enough to have accurate results.

As already stated in the previous chapters, the surface myoelectric signal is a signal affected by numerous external factors, mainly the changes in the positions of the electrodes and the equipment noise. These external noise sources and the nature of the signal degrade the classifier's performance because they create different features values. However, using specific pre and processing techniques can increase the accuracy. In order to answer the questions made at the beginning of chapter four and considering that long computational response times should be avoided, the influence of the window lengths (100 and 250 *ms*) and the number of features in the classification performance were tested. To recognize the performed hand gestures, LDA and KNN were used. To improve the classification performance, the classification was divided into binary classification problems, or levels, where in each of them two movements were recognized. Therefore, a tree-level classifier with two or three levels was defined according to the obtained results. In each level, the classifiers that were implemented were different (LDA and KNN). The KNN with five neighbours (k=5) was used to test how discriminative were the movements (explained in Figure 4.6). Before making that division, it was necessary to study which movements were more distinguishable from others. Therefore, the movements were divided into six sets.

The results of the first three sets (spherical grip and rest position, tripod grip and rest position, finger flexion and rest position) were similar for both windows. The results of the KNN of the window of 100 milliseconds are in Figure G.1. In Figure 5.13, it is possible to observe the obtained results for a window of 250 milliseconds. It can be concluded that the three movements were perfectly distinguishable from the rest position (average accuracy >90%), being the spherical grip the most distinguishable movement (average accuracy = 98.69%). Since the precision and the recall values were good, it is possible to suggest that more classes were classified as the right class. Based on these results, the first level of the classifier was defined to help the microcontroller detect if the volunteers were performing any movement or if they were at rest.

Conversely, the sets number four, five and six have the lowest scores (between 49 and 61%). Despite the similarity between the average accuracy, precision, and recall, it is possible to observe that the obtained accuracy and precision scores for the tripod grip and finger flexion (set number four) and spherical grip with finger flexion (set number five) were higher than those obtained in set number six. Therefore, it was tested if it would be advantageous having a second level that identified all the three movements at once or if it would be better to divide the results and have three levels of classification.

Before testing the different levels, it was tested which feature-set provided better results to optimize the classification process.

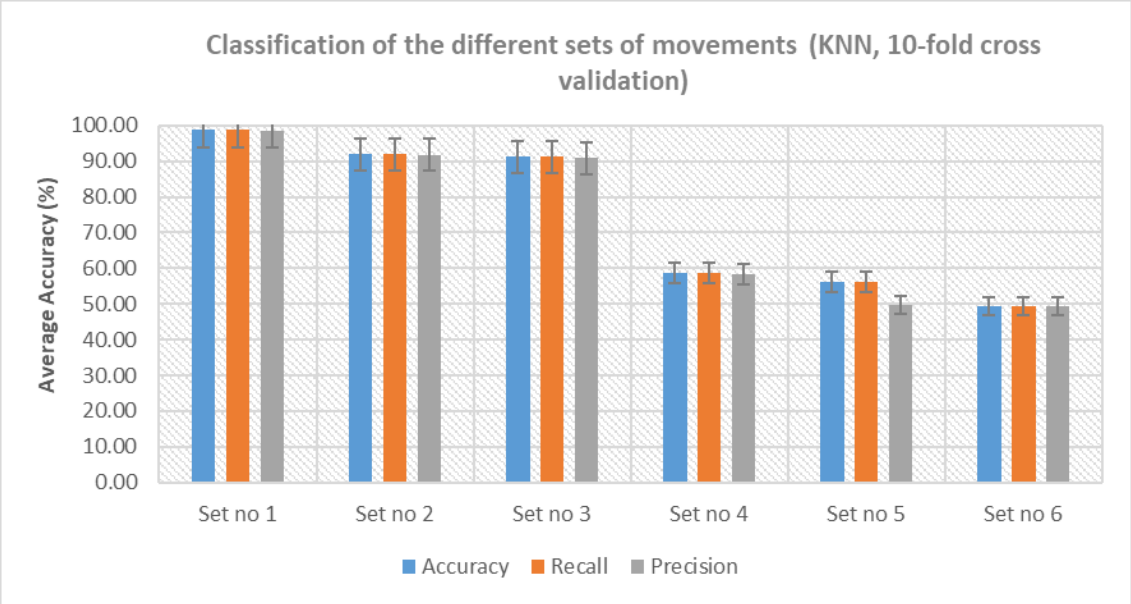

Figure 5.13: Accuracy, precision and recall average obtained values values for a window of 250 ms when the objective was to study the different sets – Setting 1 (spherical grip vs rest position):98.69%, Setting 2 (tripod grip vs rest position): 91.81%; Setting 3 (finger flexion vs rest position): 91.16%; Setting 4 (tripod grip vs finger flexion): 58.64%; Setting 5 (spherical grip vs finger flexion): 56.27% and Setting 6 (spherical grip vs tripod grip): 59.27%.

5.1.4.1. Feature selection

As mentioned before, not all the features contribute to the final result, which means that some of them are redundant. Because of that, it was necessary to apply different feature selection methods.

In this section, all the results obtained by each different feature selection method are presented. The results are discussed according to the accuracy and kappa coefficient evaluation metrics. The features methods will be implemented for all the classifier levels. Because of that, the results are discussed by level order. The results for a window length of 100 milliseconds and 250 milliseconds were similar. Due to that fact, only the graphics for one of them are showed.

For a window length of 100 milliseconds, the best set of features was obtained when the best five mutual information values were selected, which improved the accuracy to a maximum of 94.58%. The kappa coefficient was 0.87, which means that there were almost no misclassified classes. Regarding the window of 250 milliseconds, the best feature set was obtained when the best ten information gain values were selected (Figure G.2). For this window, the best feature set includes ten features: RMS, VAR, SSI, IAV, MAV, MMAV, WL, AAC, ZC and MFL. The kappa coefficient was 0.88, which means that almost all classes were classified correctly. Therefore, in this classification level (rest position vs movement), for a window length of 100 milliseconds five features were selected (RMS, VAR, SSI, WL, MAV). The reduction of the feature-set will reduce the processing time.

When the objective was to discriminate all the movements, the results showed that the relief f filter method had the highest accuracy average values. Since in this classification level (spherical grip vs tripod grip vs finger flexion), three classes were being analysed, the number of misclassified classes was compared. For both windows, the ten features with the highest relief f score were selected (MMAV 2, WA, MFL, ZC, SSC, AAC, WL, MMAV, RMS and MAV).

For the second level of the classifier (finger flexion vs grasp movements), as expected, the results are lower in both windows. Regarding the window of 100 milliseconds, the best accuracy (77.09%) was obtained in the best ten information gain values. The kappa coefficient reaches its maximum for the same feature set (0.55). Therefore, the selected features in this window were WA, ZC, MMAV2, MAD, AAC, WL, VAR, SSI, RMS and MFL. Regarding the windows of 250 milliseconds, the maximum accuracy (77.09%) was obtained in the best ten feature relief f scores (Figure G.4). However, the kappa coefficient for the best five feature relief f scores (0.20) is lower than the ten features obtained when the relief algorithm (0.21) was implemented. Conversely, the accuracy is lower than the previously obtained (77.01%). Since the differences between them are not significant, the next classification the best five features were used: IAV, MAV, MMAV, RMS, VAR.

For the third classification level (spherical grip vs tripod grip), the results are lower than for the first level of the tree classifier. For a window length of 100 milliseconds, the maximum accuracy (68.26%) was reached for the best ten features obtained when the relief f algorithm was applied. However, the best five features were obtained when the chi-squared test was applied. For this filter method, the maximum accuracy was 67.57% and the kappa coefficient 0.31. The differences between these two metrics are not significant, so in order to save time, the five features with the highest accuracy score were selected: IAV, MAV, RMS, VAR, SSI. In a window of 250 milliseconds (Figure G.7), the accuracy reached its maximum when selecting the ten features with the best information gain values (78.39%). The kappa coefficient was 0.56 (Figure G.8). In this way, the selected features were RMS, VAR, SSI, MFL, IAV. Despite an accuracy of 70% for the second and third levels, the recall and precision of each class are expected to be lower. Besides that, the kappa coefficients reveal that the probability of having misclassified classes is higher. It is expected that the tripod grip and index finger flexion are misclassified as spherical grip.

The results obtained in this section defined the features that were used in the posterior classification tests.

5.1.4.2. 10-fold cross-validation method

The results obtained from cross-validation will be discussed in this section. The kappa coefficient, the average accuracy and the elapsed time (time that the classifier take to train and classify the data used as test) will be analysed, as well as, the confusion matrices. The results obtained for each level are in the Table G1 and G2 in Anexo G. In this section, to simplify the analysis, the results will be discussed for levels.

Since the data is split into nine training sets and one testing set in this method, an increase in computational time and a decrease in classification rates are expected. In the first level of the tree level classifier, the results obtained in both classifiers (KNN and LDA) are higher than 88%. In Figure 5.14 it is possible to observe that the accuracy increased with the increase of the k-value. The precision and recall values reach their maximum for k=15 (94.102 ± 2.40%), which means that this classifier is probably the best KNN classifiers (Figure G.9). The lower results were obtained in a k=2 (92.54 ± 3.30%). It is interesting to observe that the results obtained in LDA and KNN do not differ at all, since accuracy was 94.18 ± 2.60% for LDA as well and recall and precision values. Regarding kappa coefficient, the maximum value was obtained when LDA was applied (0.83). To compare these results and to prove that they can be obtained using different classifiers, a paired t-test was applied. Therefore, it was possible to conclude that there is no significant difference between them because the p-value was 0.312. When comparing both classifiers in terms of processing time it is possible to conclude that LDA is the best classifier in a window of 250 milliseconds since the elapsed time was lower than the obtained for KNN (4.39 < 9.86 *s*). These results indicate the importance of the filtering process. As already

mentioned, removing noisy components can improve the SNR of the signal, making the movements perfectly distinguishable from the rest, even a single and isolated finger movement.

The results that can be taken for a window of 100 milliseconds are the same, but the obtained average accuracy values were lower (Figure G.10). The average accuracy increased with the increase of the k value, reaching its maximum for k=15 (91.67 ± 3.60%). Consequently, the minimum average accuracy was reached for k=2 (89.26 ± 4.44%). The precision values and recall also increased with the increase of the k value. The kappa coefficient reached its maximum for k=15 (0.83). Despite the high values obtained in KNN, LDA had a higher average accuracy. Therefore, the average accuracy was 91.81 ± 4.00%, and the kappa coefficient 0.83. Since the two obtained average accuracy values were similar, both classifiers were compared with a p-paired t test. The results showed that there was no statistical difference (p-value=0.151). Comparing both processing times, it is possible to conclude that LDA outperforms KNN (5.86 < 20.06 *s*). Comparing both windows, it is possible to conclude that the window length of 250 is better since the processing time is lower (4.39 < 5.86 *s*) and higher average accuracy (94.18 > 91.81 %).

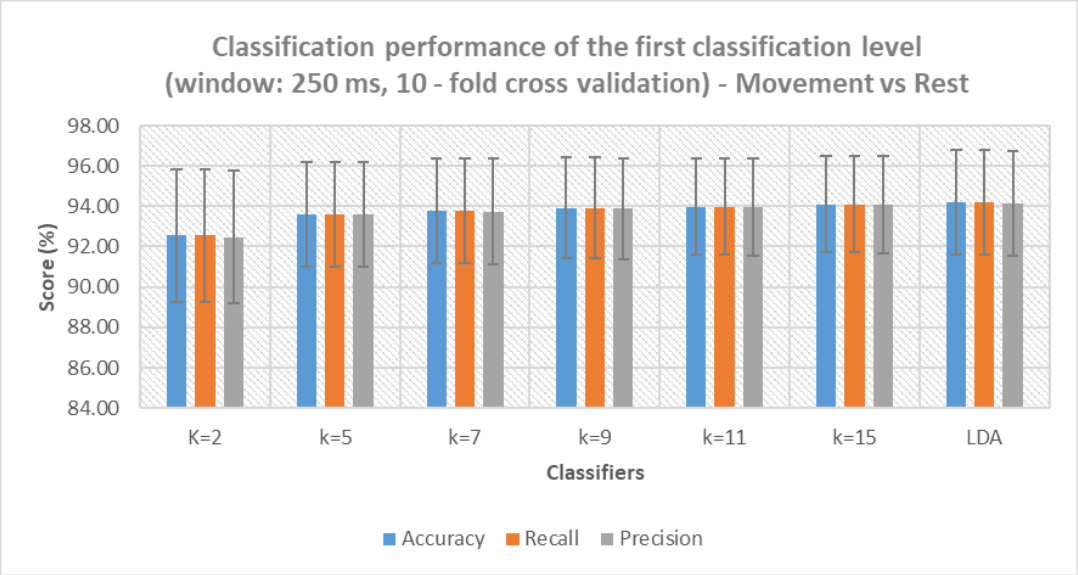

Figure 5.14: Results obtained in the first classification level (movement vs rest position) for a window of 250 *ms* when the 10-fold cross validation method was applied. The minimum accuracy was reached for KNN=2 (92.54 %) and the maximum for LDA (94.18 %).

.

After that, the set with three movements was analysed. In Figure 5.16, it is possible to observe the results obtained in a window of 250 milliseconds. The average accuracy of the KNN classifiers decreased with the increase of k-value until k=9, reaching a minimum of 43.59 ± 4.90 %. The kappa coefficient also decreases with the increase of the k-value until k=9, reaching a minimum of 0.15. The best KNN classifier is for k=2, where a maximum accuracy of 52.26 ± 16.8% was obtained. Despite the higher value (~50%), the associated error is greater than 10% (16.8%), which means that there are many different average accuracies obtained in all the training and test used samples. The classifier had an elapsed time of 6.72 seconds. The lower results were obtained in LDA, with an average accuracy of 45.19 ± 3.20%. Comparing both classifiers, it is possible to conclude that the kappa coefficient was lower for LDA than for KNN with k=2 (kappa= 0.17 < 0.29) and the elapsed time lower for LDA than for KNN (4.38 < 6.72 *s*).

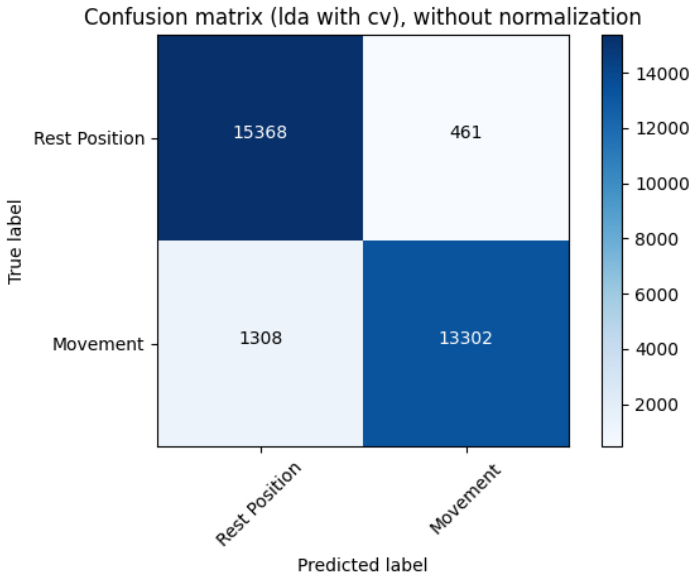

Figure 5.15: Confusion Matrix for the first level of the tree classifier when the 10-fold cross-validation method was applied to the window of 250 *ms*. Represents the number of instances that were classified correctly for both classes (15368 for rest position and 13302 for movement class) and the misclassified ones (461 for rest position and 1308 for movement class). – LDA.

Still in the second level, in Figure G.15, it is possible to observe the results obtained in a window of 100 milliseconds. LDA outperformed KNN classifiers, reaching a maximum accuracy of 47.56 ± 3.00%. The kappa coefficient was higher (0.15), and the elapsed time was 7.96 seconds. For the KNN classifier, the kappa coefficient and the average accuracy increased with the increase of the k-values, reaching a maximum of 0.12 and 45.09 ± 2.20% for KNN with k=5, respectively. When comparing both windows, it is possible to conclude that the elapsed time was greater for a window of 100 milliseconds. Conversely, the average accuracy percentages and the kappa coefficients were higher for a window of 250 milliseconds which lead us to conclude that this is a better window. Therefore, it is possible to conclude that the KNN with k=2 is the best classifier.

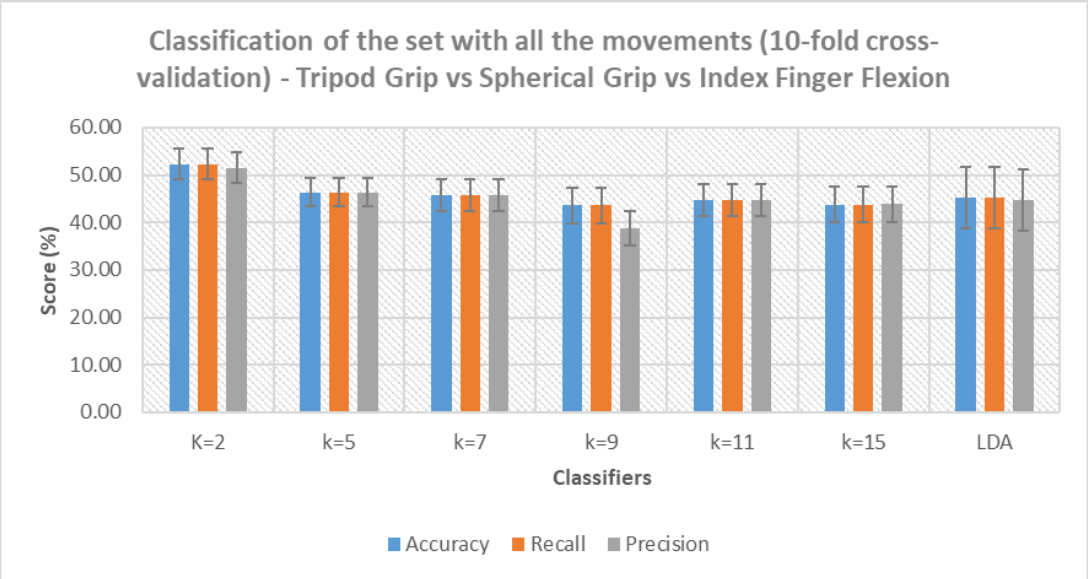

Figure 5.16: Results obtained when all the movements (spherical grip vs tripod grip vs finger flexion) were classified for a window of 250 *ms* when the 10-fold cross validation method was applied. The minimum accuracy was reached for KNN=9 (43.59 %) and the maximum for KNN=2 (52.26 %).

The low average accuracy and the low kappa coefficients were not satisfactory results. In order to identify the errors associated to the classification process, the confusion matrix for all the movements was plotted (Figure 5.17). As it can be seen, there are classes that were misclassified as it happens with tripod grip and finger flexion. These results indicate that spherical grip is probably the easiest to detect. Due to these uncertainties, a little research focused on the biomechanical features of the hand gestures performed here was done.

The capacity to grab or interact with objects depends on postural control, visual and tactile feedback. Besides that, it is crucial to consider the role that the biomechanical components, including joint movements and muscle activation have during the performance of such movements. As it is known, each volunteer's performance depends on the trajectory that each one took until reaching the object. Therefore, variations in orientation, neural processing time and speed of the hand path contribute to signal amplitude fluctuations. In addition, this type of movements are influenced by the use of the dominant or non-dominant arm since they involve different neural control mechanisms. These differences can influence the activation of the muscles and the time of response, which means that for each arm or volunteer, some differences can affect the myoelectric signal [28][192].

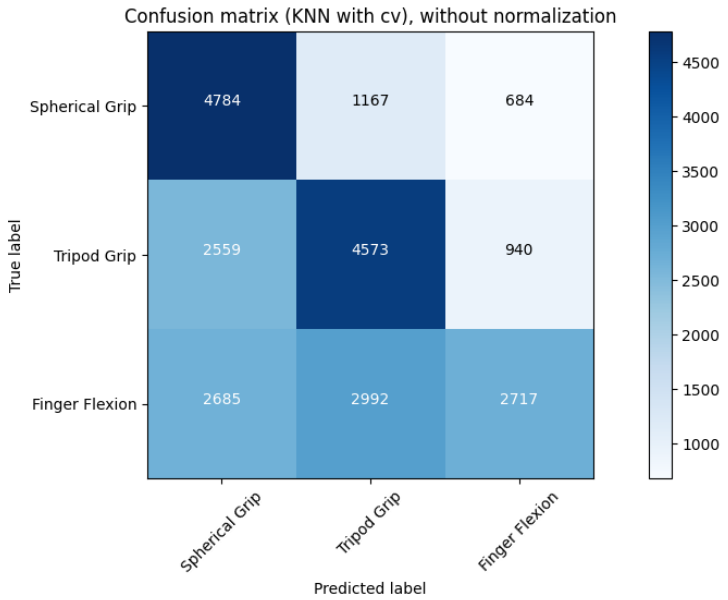

Figure 5.17: Confusion Matrix for all the movements when the 10-fold cross-validation method was applied for a window of 250 *ms*. Represents the number of instances that were classified correctly for all classes (4784 for spherical grip, 4573 for tripod grip and 2717 for finger flexion) and the misclassified ones (1851 for spherical grip, 3499 for tripod grip and 5677 for finger flexion)) – KNN, k=2.

During the grasping movements, the fingers and the thumb adjust their position. Considering the muscle tables in section 2.1 (Table 2.1, 2.2 and 2.3), the muscles involved in spherical grip are the flexor pollicis longus, the adductor pollicis, the flexor digitorum profundus and the flexor digitorum superficialis. Besides the actuation of these muscles, Betti *et al* [192] demonstrated the importance of the index finger for spherical grip. The authors concluded that the index finger has a specific activation pattern during grasping executions, with a different pattern for different grips, especially for the spherical grip. Conversely, tripod grip involves the thumb opposition and flexion against the thumb. Therefore, for precision grips such as the tripod grip, it is possible to observe the flexion of thumb joints, the flexion at metacarpophalangeal and proximal interphalangeal joints, the flexion and extension of distal interphalangeal joints, the activation of the flexor pollicis longus and the flexion originated by the flexor digitorum superficialis. As can be seen, the prehensions studied in this dissertation are originated

from the same muscles except the spherical one that has the contribution of the flexor pollicis longus and the adductor pollicis.

Keeping the anatomical and physiological features in mind, the first thought was that the amplitude values would influence the classification performance. As a matter of fact, the obtained results showed that the spherical grip was the gesture that was detected with more success when compared to the others. However, in this dissertation, the electrode was placed in the flexor digitorum superficialis, which means that the extra information about the flexor pollicis longus is not considered. Because of that, the obtained difference is not sufficient to conclude that spherical grip is the strongest grip and consequently the most detectable one. Conversely, the flexion of some joints generates the tripod grip. Since it was not used a glove or an angle measurement equipment during the acquisition, we only have the information given by the flexor digitorum superficialis muscle. Besides that, similar movements are more challenging to differentiate, making it easier to distinguish them from finger individual movements.

Because of that, the second level of the classifier would identify the finger flexion and both grasps movements. Since the precision, sensitivity and confusion matrix reveal that there are a lot of misclassified classes, lower results than those obtained in the first level are expected. Nevertheless, the number of misclassified classes is expected to be higher in the second level. Finally, the classifier will identify the tripod grip and the spherical grip classes in the third level. Thus, after identifying the occurrence of movement or not, the classifier will identify if the volunteer is using one finger only or moving more than one finger. With this division, we hope to improve the accuracy. Finally, in the third level, the classifier will discriminate the grasps from each other.

Consequently, the results obtained in the second level are now discussed. Regarding the window of 250 milliseconds, the average accuracies were around 65% (Figure 5.18). The higher values were obtained in a KNN with k=2, where the accuracy was 68.19 ± 8.80%. The average accuracy decreased with the increase of the k value, except for k=7 where an average accuracy of 64.06 ± 4.20% was obtained. The lower average results were obtained in k=15 (62.32 ± 2.70%). Despite the high average results for k=2, the classification of each class was low, which means that there were a lot of misclassified classes as can be seen in the confusion matrix (Figure 5.19). There were 5658 finger flexion instances that were classified as grasp movements and 1689 grasps movements classified as finger flexion movements. Despite the higher number of misclassified instances, the kappa coefficient reaches its maximum (0.23). The LDA had a lower average accuracy (64.06 ± 8.80%). As it can be observed in Figure G.18, the number of misclassified classes was higher than for KNN with k=2 (2508 misclassified grasp movements and 6195 misclassified finger flexion movements). Because of that the kappa coefficient decreased to 0.076. The LDA elapsed time was 4.21 seconds. In this dissertation, the performance of the classifier is more important than the elapsed time because the developed prototype should be robust and accurate. Therefore, the best classifier was KNN with k=2.

In Figure G.20, it is possible to observe the results obtained in the window of 100 milliseconds. It is possible to conclude that even though the higher accuracy was obtained in LDA (69.87 ± 0.60%), the kappa coefficient was the lowest one. Despite the low number of false positives (218), false negatives were 7257. For that reason, the best classifier was KNN with k=2 (Figure G.22). The number of grasps movements that were misclassified (1692) was one of the lowest for all k values and the kappa coefficient (0.062) was the higher one (Figure G.21). Comparing both windows, it is possible to conclude that the elapsed time was greater for a window of 100 milliseconds, which added to the lowest

kappa values and average accuracy, suggests that this window was the worst. So for the second level, the best window was 250 milliseconds.

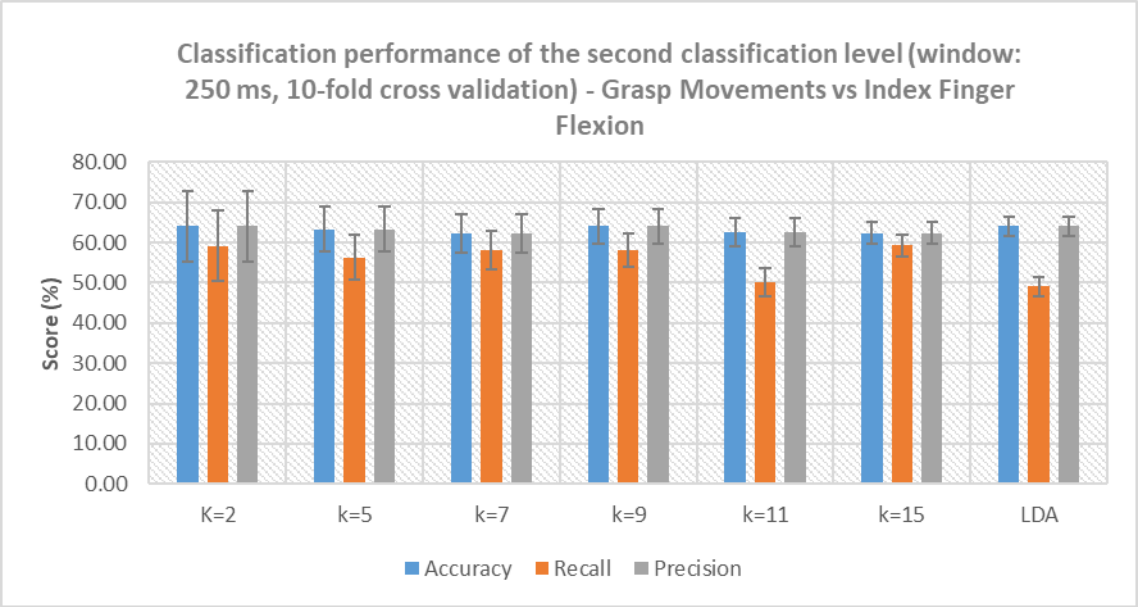

Figure 5.18: Results obtained in the second classification level (Grasp Movements vs Finger Flexion) for a window of 250 *ms* when the 10-fold cross validation method was applied. The minimum accuracy was reached for KNN=15 (62.32 %) and the maximum for KNN=2 (68.19 %).

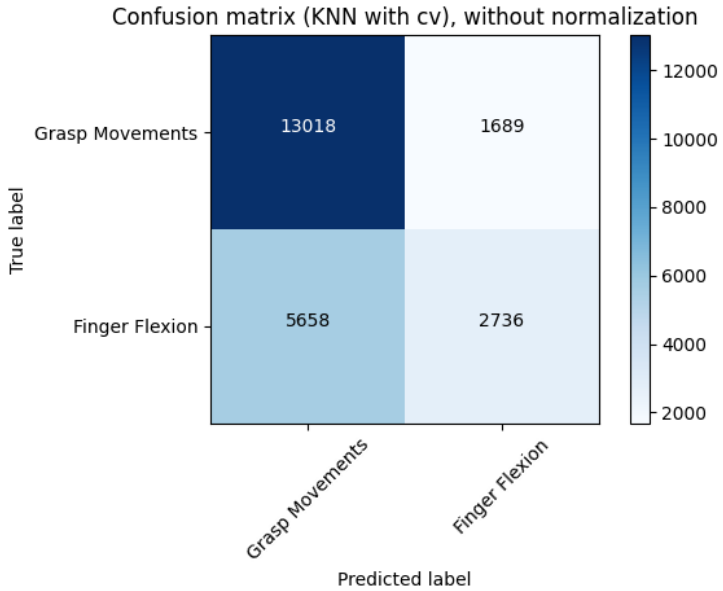

Figure 5.19: Confusion Matrix for the second classification level when the 10-fold cross-validation method was applied for a window of 250 *ms*. Represents the number of instances that were classified correctly for both classes (13018 for grasp movements and 2736 for finger flexion) and the misclassified ones (1689 for grasp movements and 5658 for finger flexion). –KNN (k=2).

For the third level, the average results were still lower. In Figure 5.21, it is possible to observe the results obtained with a window of 250 milliseconds. The results show that average accuracy and the kappa coefficient decreased with the k value increase. The minimum accuracy (63.57 ± 3.20%) was obtained in KNN with k= 15. Besides that, it is visible that the number of misclassified tripod classes was higher than the number of misclassified spherical grip instances, which supports the previously discussed anatomical differences. The maximum accuracy was 67.13 ± 11.7% and the kappa coefficient was 0.35 for k=2. However, the associated error was over 10%, which indicates a large variability of

average accuracy obtained values. The elapsed time rounds a total of 4 seconds, being the minimum 4.16 s (k=2). The LDA outperforms the KNN with k > 5 since the average accuracy was 64.77 ± 6.40% and the kappa coefficient was 0.28. Considering these classification results, it is possible to conclude that KNN with k=2 was the best classifier.

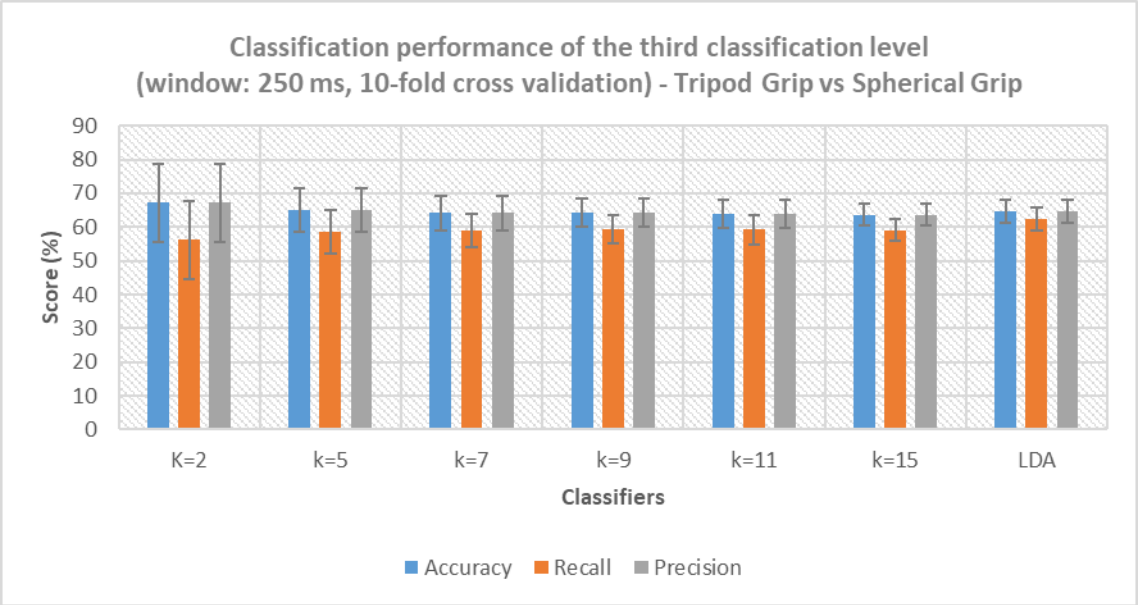

Figure 5.21: Results obtained in the third classification level (Tripod grip vs spherical grip) for a window of 250 *ms* when the 10-fold cross validation method was applied. The minimum accuracy was reached for KNN=15 (63.57 %) and the maximum for KNN =2 (67.13 %).

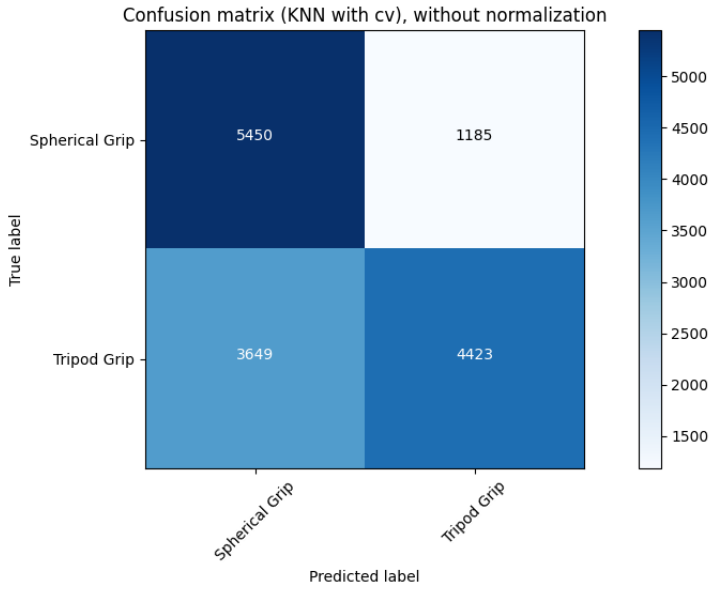

Figure 5.20: Confusion Matrix for the third level of the tree classifier when the 10-fold cross-validation method was applied for a window of 250 *ms*. Represents the number of instances that were classified correctly for both classes (5450 for Spherical Grip and 4423 for tripod grip) and the misclassify ones (1185 for Spherical Grip and 3649 for tripod grip). - KNN (k=2).

The results obtained in the window of 100 milliseconds suggested that the tripod grip and the spherical grip are similar movements due to their number of misclassified instances. In this case, LDA

outperformed the KNN reaching a maximum average accuracy of 66.64 ± 6.40%. This classifier's time to train and test was lower than the elapsed time obtained in KNN. Besides that, the kappa coefficient was the highest kappa coefficient value (0.26). The number of misclassified instances was lower for a window of 250 *ms* and the average accuracy higher, which indicates that this was the best window. Therefore, the best classifier was KNN with k=2.

5.1.4.3. Split validation method

The results obtained from the application of the split validation method to our data will be discussed in the same way that the cross-validation ones, which means that the results obtained in a window of 100 milliseconds are in Appendix H. The discussion will be focused on the precision, recall and accuracy average values. Besides that, the confusion matrices will also be analysed. Before starting the discussion it is important to note that the 70% of the data that was used as training set had at least one repetition of the movement for all volunteers. The results obtained for each level are in the following table.

In Figure 5.22, it is possible to observe the results obtained in the first level of the classifier for a window of 250 milliseconds. The average accuracy was greater than 88% for all the tested classifiers, which indicates that the probability of existing misclassified results was low. The minimum average accuracy was obtained in k=2 (91.53 ± 3.36%). The average accuracy increased with the increase of the k value reaching its maximum for a k=15 (93.07 ± 2.55%). Conversely, LDA outperforms the results obtained in k equals to two, five and seven. The average accuracy for LDA was 93.46 ± 2.56%. Since there are no significant differences between the results, a paired t-test was implemented. The obtained p-value (0.113) shows no significant difference between the two classifiers. Due to the fact that the device should respond in 300 milliseconds, the processing times of each classifier were analysed. While the elapsed time for LDA was 74.58 milliseconds, the elapsed time for KNN was 839.52 milliseconds. In conclusion, LDA seems to be the best classifier for the first classification level.

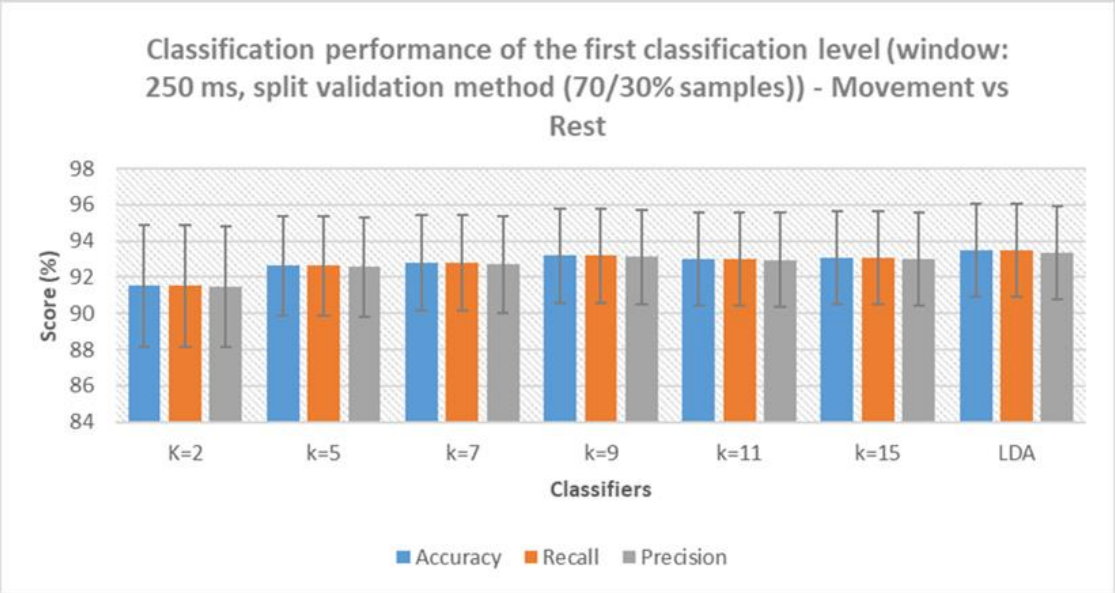

Figure 5.22: Results obtained in the first classification level (Movements vs Rest Position) for a window of 250 *ms* when the split validation method was applied. The minimum accuracy was reached for KNN=2 (91.53 %) and the maximum for LDA (93.46 %).

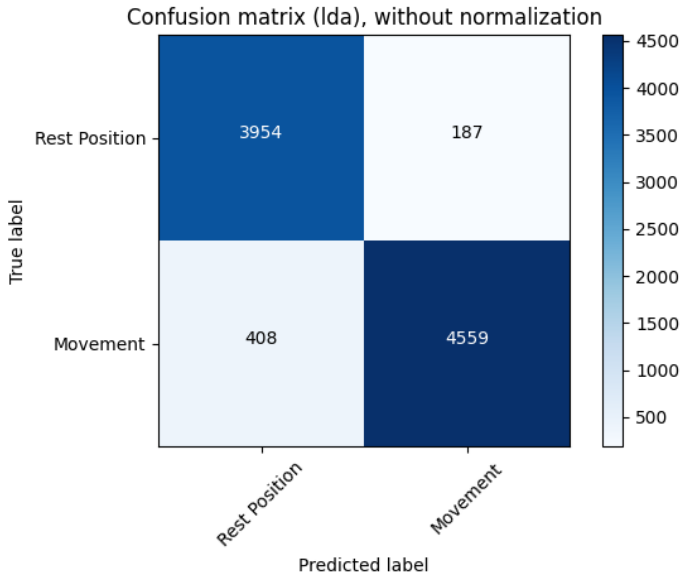

Figure 5.23: Confusion Matrix for the first classification level when split validation method was applied for a window of 250 *ms*. Represents the number of instances that were classified correctly for both classes (3954 for rest position and 4559 for movement class) and the misclassified ones (187 for rest position and 408 for movement class) – LDA.

Regarding the window of 100 milliseconds (Figure H.2), the results show the KNN (k=9) outperformed LDA (91.52 ± 3.71% (KNN) > 91.23± 4.02 % (LDA)). For KNN, the minimum was obtained with k=2 (88.34 ± 4.02%). Since the results were similar for LDA, we implemented a paired t-test. The obtained p-value was 0.308, which means that there were no statistical differences between the two classifiers. Therefore, the elapsed time and the kappa coefficient for both classifiers were calculated. LDA took 100.29 milliseconds, while KNN took 1.30 seconds. Because of that, it is possible to conclude that LDA was better than KNN, as suggested as well by the kappa coefficient (0.82 > 0.80). When comparing both windows, it is possible to conclude that the average accuracy obtained in LDA was greater for the window length of 250 milliseconds and the processing time lower (74.58 < 100.29 ms).

Similarly to the cross-validation method, the possibility of identify all movements at once was tested The results were better for the window of 250 milliseconds since it has the higher average accuracy percentages and kappa coefficient values (Figure 5.24). From all the tested k values, the best was k=2 since the average accuracy reaches its maximum (72.47 ± 0.71%). The processing time was only 366.84 milliseconds. This classifier had the lowest numbers of spherical misclassified instances (Figure 5.25). The minimum average accuracy was obtained when the LDA was implemented (44.83 ±

2.22%) – Figure H.6. Despite the classification results, the use of two levels to identify the three movements was tested.

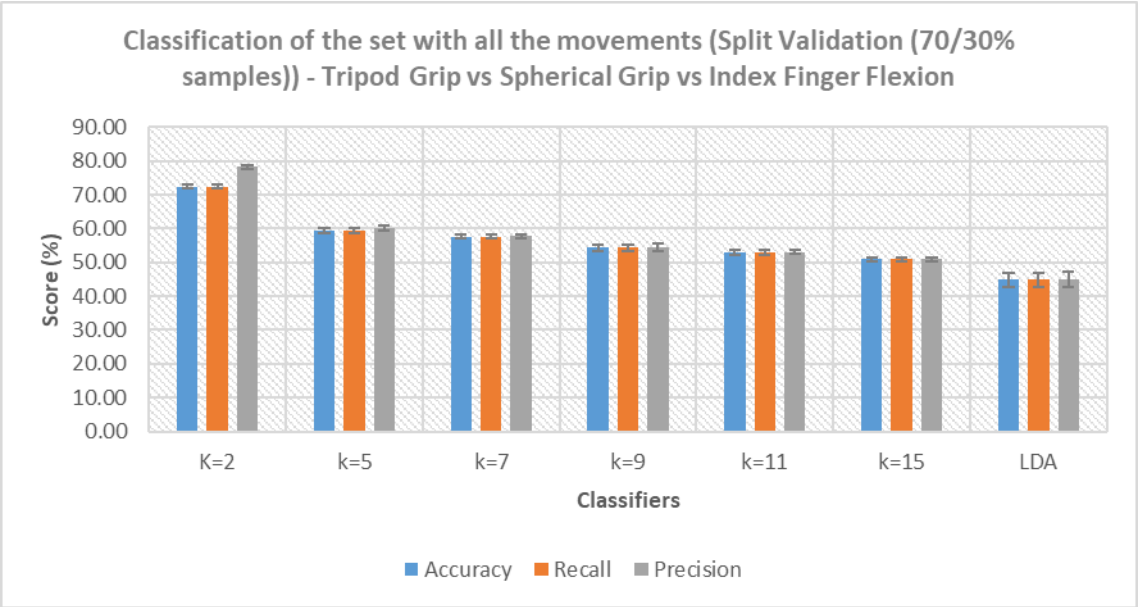

Figure 5.25: Results obtained when all the movements (Spherical Grip vs Tripod Grip vs Finger Flexion) were classified for a window of 250 *ms*: The minimum accuracy for KNN=15 was 50.89 % and the maximum for LDA was 72.47 %.

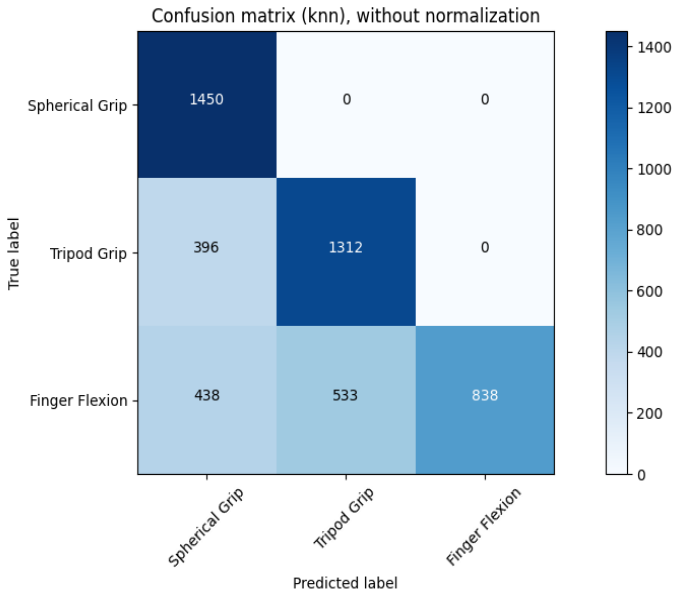

Figure 5.24: Confusion Matrix for all the movements when the split validation method was applied. Represents the number of instances that were classified correctly for all classes (1450 for spherical grip, 1312 for tripod grip and 838 for finger flexion) and the misclassified classes (0 for spherical grip, 396 for tripod grip and 971 for finger flexion)) - KNN (k=2).

For the window of 100 milliseconds, the results were lower (Figure H.7). The accuracy increased with the k value, reaching an average accuracy of 45.09 ±2.20% (KNN with k=15). The minimum accuracy was reached for KNN with k=5 (42.58 ±1.90%). For LDA, the average accuracy was 47.56 ±3.00%. Comparing both classifiers, it is possible to conclude that these results are not satisfactory which is related to the existing differences between the muscle pattern activation of each volunteer and with the electrode position. Despite these classification results, LDA was better than KNN since it had more accurate results and a lower processing time (7.96 < 9.63 *s*).

As for the second level, accuracy, precision and recall percentages were low. In Figure 5.26, it is possible to observe the accuracy level obtained in a window of 250 milliseconds on each of the used classifiers. The best results were obtained in KNN with k=2 (80.45 ±1.19%) with an elapsed time of 400.21 milliseconds. For the other k values, the classification results were similar, but the average accuracy decreased with the increase of the k value. The minimum accuracy was obtained when the LDA was implemented (63.61 ±2.71%). The results obtained in each class individually affect the average results, which means that the with this number, the misclassified classes might be read as good results. For that reason, and to avoid misinterpretations, the confusion matrices were plotted. As it can be observed, the index finger flexion was misclassified as grasp movements (Figure 5.26). According to the results in confusion matrices, it is possible to conclude that the best KNN classifier is with k=2 since all grasp movements instances were classified as grasp movements (Figure 5.27). However, 971 finger flexion instances were classified as grasp movements. It is possible to conclude that more grasps movements were misclassified with the increase of k. Conversely, the number of misclassified finger flexion instances decreases for k=5 but increases with the increase of k value.

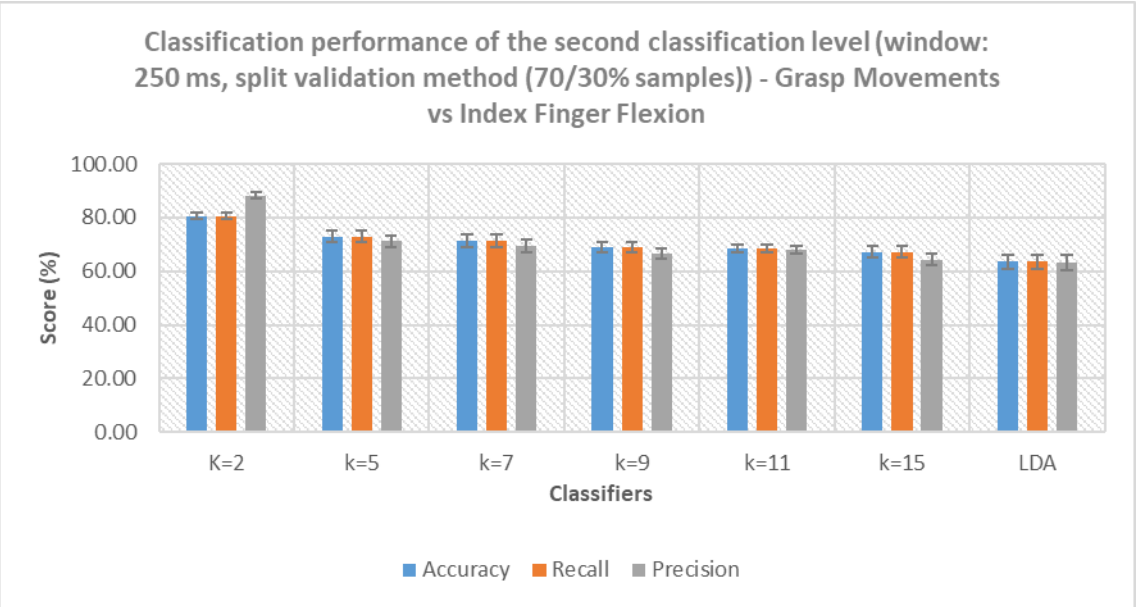

Figure 5.26: Results obtained in the second classification level (Grasp Movements vs Finger Flexion) for a window of 250 *ms*, when the split validation method was applied.The minimum accuracy was reached with KNN=15 (67.16 %) and the maximum for LDA and KNN (k=2) (80.45 %).

These results suggested that the choice of the k value is very important since it can promote either accurate or bad results. The main difference between these movements is probably the amplitude values. Using a low value of k neighbours increases the grasp class's precision. Nevertheless, when the k value increases, more outlier results and more factors affect the classification, decreasing the recall and precision obtained in each class. Besides the difference in anatomical characteristics of each movement, the fact that dominant and non-dominant information was extracted influences the result. In some volunteers, using both arms can degrade the performance of movements such as spherical grip and tripod grip, decreasing the signal amplitude. In addition, based on what has been discussed before, each volunteer's performance is smoothed with the increase of contraction time and it is affected by muscular fatigue that affects the amplitude of the signals. The fact that our feature dataset does not follow a normal distribution might be the reason for such poorer results obtained during the implementation of LDA. Furthermore, LDA was the worst classifier since 1549 finger flexion instances were classified as grasp movements (Figure H.11). Besides, the place where the electrode was placed could also influence the results since it can be measuring noise at tendon level or noise from the other forearm muscles.

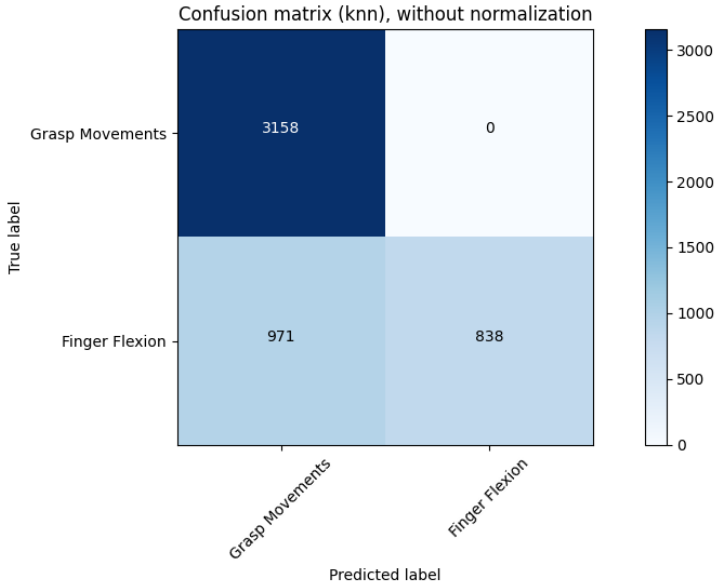

Figure 5.27: Confusion Matrix for the second level when the split validation method was applied for a window of 250 *ms*. Represents the number of instances that were classified correctly for the two classes (3158 for grasp movements and 838 for finger flexion) and the misclassified ones (0 for grasp movements and 971 for finger flexion) - KNN (k=2).

For a window of 100 milliseconds (Figure H.12), the KNN outperformed the LDA since the average accuracy was greater for KNN with k=2 (76.36 ± 2.36% (KNN) > 76.36 ± 2.71% (LDA)). Besides the higher average accuracy, the number of grasp instances that were misclassified was only 110. However, 1098 finger flexion instances were classified as grasps movements. For k=5 (average accuracy=67.60 ± 1.66%), the number of finger flexion instances that were misclassified decreased from 1098 to 974, but the grasp instances that were wrongly classified duplicated. It is also possible to conclude that with the increase of the k value, the number of misclassified finger flexion instances increased. However, the number of false positives - grasps instances classified as finger flexion movement- decreased. For a k=15, the number of false positives was lower than the obtained in k=2 (Figure H.13). Still, the number of false positives does not compensate for the rise of false negatives- finger flexion movements classified as grasp movements. Since the results of LDA and KNN with k=2 were equal, both of them were compared with a paired t-test. The p-values was 0.001 which means that both probably follow different distributions. Therefore, the elapsed time and the kappa coefficient of each classifier were compared. For LDA, the processing time was 55.81 milliseconds and the kappa coefficient was 0.02. For KNN, the elapsed time was 500.83 milliseconds and the kappa coefficient was 0.04. Since the results are similar, it is possible to conclude that LDA is the best option for the window of 100 milliseconds. To sum up, KNN with k= 2 is the best classifier.

Comparing both windows, it is possible to conclude that the window of 250 milliseconds is better than 100 *ms* since it has the maximum average accuracy (80.45 % (250 *ms*) > 76.37 % (100 *ms*) and a shorter processing time (400.21 *ms* (window of 250 *ms*) < 500.83 *ms* (window of 100 *ms*)).

In Figure 5.28, it is possible to observe the results obtained in the third classification level, more specifically for the window of 250 milliseconds. The average results decreased with the increase of the k-value, reaching an average minimum accuracy of 66.65 ± 1.41%. The best results were obtained in KNN with k=2 (average accuracy= 81.09 ± 0.52%). Conversely, the worst results were obtained with

LDA that reached an average accuracy of 63.61+1.73%. As previously mentioned, it is important to analyse the confusion matrix since these results might be affected by misclassified classes.

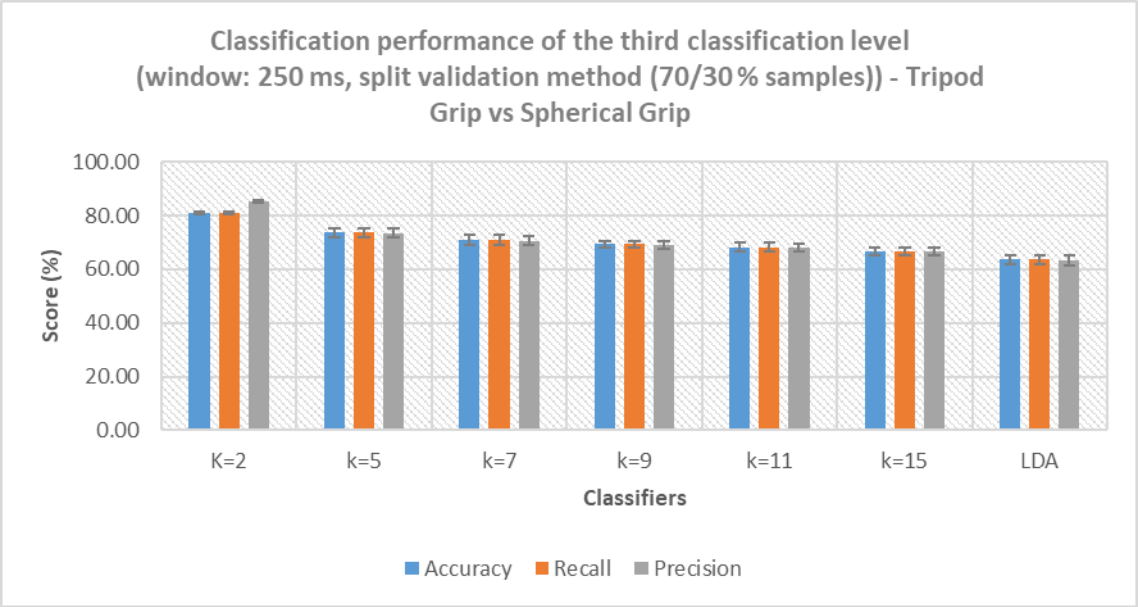

Figure 5.28: Results obtained in the third classification level (Tripod grip vs Spherical grip) when the split validation method was applied for a window of 250 *ms*. The minimum accuracy was reached for LDA=5 (63.61 %) and the maximum for KNN with k=2 (81.05 %).

For k=2, the number of false positives- the number of misclassified spherical grip instances- is zero and the number of false negatives is 597 (5.29). For k=5, the number of tripod grip misclassified results decreased from 597 to 377 and the number of false positives increased to 456. For the rest of the k-values, the number of the spherical grip instances that were classified as tripod grip movements increased up to 527 (k=15) and the number of false negatives to 526.

Despite the lower values of misclassified tripod grip instances, the increase in false positives is not accepted in real-time performances. Similarly to what happened in the second classification level (grasp movements vs finger flexion), these classification results suggested the influence of muscular fatigue and volunteer's variability during the performance of these hand gestures.

In this specific case, LDA was the worst classifier since false positives reached their maximum (624). The number of misclassified tripod instances was 525 (Figure H.15). These lower results might be explained by the fact that our dataset does not follow a normal distribution, and of course, by the previously discussed factors. Besides that, the difference between the precision and power grip can be due to the strong amplitude of the signals detected during the spherical volunteer's movement, which explains why higher values of tripod grip instances are misclassified. The amplitude can be a crucial factor because in this work, thirteen time-domain features are used. Therefore, considerable differences in the amplitude imply different features and consequently more accurate results, which is not the case. Besides that, it is known that power grips require more high force movements than precision grips. Because of that, in force grips the hand muscles are used to generate the force instead of using the strength of each finger. Unlike tripod grip, the spherical grip can be distinguished by dynamic and static phases. While in the dynamic phases, the hand and the thumb open until both reach a comfortable position to grasp the object, the static phase involves the fine adjustment of the finger to the object's shape (hold moment). Grips like spherical grip are related to the muscular antagonist activity between the upper limb digits and the hand, which involves the extrinsic and intrinsic muscles [193].

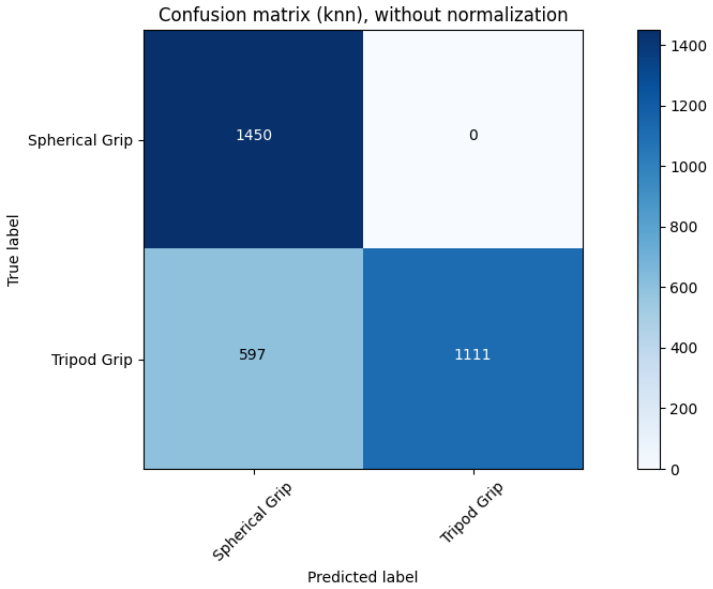

Figure 5.29:Confusion Matrix for the third classification level when the split validation method was applied for a window of 250 *ms*. Represents the number of instances that were classified correctly for both classes (1450 for spherical grip and 1111 for tripod grip) and the misclassify ones (0 for spherical grip and 597 for tripod grip) - KNN (k=2).

For a window of 100 milliseconds (Figure H.16), the maximum average accuracy was obtained in LDA (67.13 ± 4.37%)., where only 909 tripod instances were misclassified. For k=2, the average accuracy was 61.91±1.51%. Therefore, it is possible to observe that 479 false positives - the number of spherical grip instances that were misclassified - and 1199 false negatives were obtained during the classification. For k=5, the results were interesting since the number of false negatives decreased, but at the same time, the number of false positives duplicated. For the rest of the k-values testes, with the increase of parameter k, the average accuracy and the number of false positives decreased. Conversely, the number of false negatives increased. Therefore, it is possible to infer that the best k is k=2. Despite being the best KNN classifier, LDA is the best choice since it has a higher average accuracy percentage and a shorter elapsed time (52.86 *ms* (LDA) < 314.12 *ms* (KNN)). Comparing both windows, it is possible to conclude that the window of 250 milliseconds is better since it has a higher average accuracy percentage (81.09 % (250 *ms*) > 67.13 % (100 *ms*)) and lower values of false positives and false negatives. The only disadvantage is the processing time of 400.21 milliseconds that is higher than 52.86 milliseconds.

The movements that were under study were very similar. Subsequently, the signal that was being recorded was similar. Having similar signals is the same as having similar features and similar values which later are mirrored in the classification score. The similarity between the signal and the features is amplified when a single channel is used [109]. Besides that, the relationship between force and electric activity at low contraction levels might also decrease the accuracy rates, since it affects the amplitude of the signal [194]. To support these theories, previous research demonstrated a non-linear relationship between the strength of contraction and signal amplitude on dexterous movements. Subsequently, it is not easy to differentiate the muscular activities from each other [195]. These similarities between the three hand gestures added to the place where the electrode was placed contribute for lowest results.

5.1.4.4. Final evaluation and literature comparison

When the objective is to develop a real-time prosthetic device, each classifier's time used in training and testing processes should be considered. This is crucial to ensure that the maximum device response is 300 milliseconds. It is noticeable that there are some differences between the results obtained in cross-validation and train-test validation models. The most noticeable difference is in the second and third classification levels. The results obtained in cross-validation were lower than the obtained in train-test model due to the volunteers' intervariability. As previously explained, cross-validation randomly uses all the samples in training and testing sets, which means that the training set might not containing all volunteers. As it is known, as the time of acquisition increases, the performance of the volunteer decreases, affecting the acquired signal and, consequently, the quality of the extracted features. Furthermore, the anatomical differences between the performed hand movements and the way that each volunteer performs each gesture are also factors that increase the intervariability and consequently decrease the classification performance leading to misclassified classes. Using dominant and non-dominant arms could also be a factor that influences the differences between the volunteers' signals. Lastly, the position of the electrode used during the acquisitions might not be the best. Besides worse results, cross-validation takes too much time for training and testing both classifiers, which means that it cannot be considered for real-time applications, more specifically for training the users, but can be used to optimise the parameters of the microcontroller algorithm.

The classification results showed that it is more robust to use a three classification levels since it has fewer misclassified instances. Moreover, the kappa values for each level are superior to the kappa coefficient obtained using all the movements in the second level. Besides that, the average accuracies are also greater than the obtained when recognizing the three movements. Regarding the classifiers, it is possible to conclude that the first level will be constructed with LDA and the other two with KNN with k=2. The only disadvantage is the processing time, which with three levels is 789.59 milliseconds and for just two levels 506.29 milliseconds. In the future, it will be interesting to test if the increase of the channels will decrease the time that the classifier takes to recognize the different instances. Furthermore, it will be interesting test if a low window length, for example, 200 milliseconds, will improve the accuracy. Regarding to the acquisition process it will be interesting vary the position of the electrode and compare the classification results.

To the best of our knowledge, there are no studies that classify grasps and finger movements with the BIOPAC single-channel acquisition system. However, we compared our results to some studies whose conditions of acquisition, feature selection, or classification methods were similar.

As explained in chapter 3, myoelectric control has been used in recent years. Most studies analyse wrist and arm movements like forearm supination and pronation, wrist flexion and extension, radial and ulnar deviation [196][197][198]. In those studies, the authors obtained accurate results for these cases where the average accuracy was over 80%. Despite such good results, these movements are not complex and are not the most required ones by the users. Contrasting to other studies, this dissertation did not acquire forearm and wrist movements, which might be the first reason to explain the lower results obtained in this dissertation. The difference between the high accuracy percentages obtained in those studies and the results obtained in this dissertation is mainly related to the anatomical and physiological characteristics of the movements. The wrist extension, for example, has the contribution of almost all extensor forearm muscles (extensor digitorum, extensor indicis, extensor carpi radialis longus, extensor carpi radialis brevis and extensor carpi ulnaris). Since the surface of the electrodes is placed along the forearm, it is natural that the signal has a strong amplitude for movements that are originated by forearm muscles. Higher values of amplitude signals promote higher SNR, which originates differentiated features for each class, which does not happen for similar movements such as finger movements and

grasp movements. In the tripod grip, the thumb is brought into opposition with an index and middle finger, a movement originated by the joints (metacarpophalangeal joint and proximal interphalangeal joint). Conversely, finger flexion is controlled by flexor digitorum superficialis.

Besides that, as discussed in the state of the art, most of the available literature uses multi-channel acquisitions to recognize different hand gestures. However, using multi-channel to acquire the myoelectric signals systems is not recommended since amputees do not have a large surface area available. In addition, there is an increase in the training time, which drives the users to prefer less complex devices with only two or three degrees of freedom [199].

Al-Timemy *et al* [8] suggested a different classification method with a single electrode channel placed in the extensor (channel 10) and flexor muscles (Channel 1) separately. In their study, six subjects performed forearm pronation, forearm supination, wrist flexion, wrist extension, radial deviation, ulnar deviation, key grip, chuck grip, hand open, and rest state. The authors calculated the auto regression coefficients, root mean square value, zero crossings, integral absolute value and slope sign changes. The authors obtained an accuracy of 83.7 % for channel 1 and 80.16% for channel 10. Al-Timemy *et al* did not use the same classifiers, but it is still possible to compare the results since they used a single channel acquisition. The average accuracy percentages obtained in this master dissertation are lower than ones obtained by those authors. The difference in the performed movement might be the reason why this happens. The authors identify hand movements and forearm movements that, as already explained, are easier to differentiate than grasps and finger movements, which justifies the lower accuracies obtained in this dissertation work. Furthermore, the authors studied only six volunteers, which reduces the inter variability between the recorded myoelectric signals. Consequently, the average accuracy values are higher than those obtained in this work.

In the same work, Al-Timemy *et al* [8] recruited ten healthy subjects and two amputees to perform fifteen and twelve individual finger movements, respectively. Since the volunteers that participated in this dissertation experience were healthy, only the results obtained in the healthy subjects were considered. Each of their recruited volunteers performed flexion and extension of all the fingers; thumb abduction; little and ring fingers flexion; flexion of the ring, middle and index fingers; and finally, the flexion of the little, ring, middle and index fingers. The authors tested the influence of the number of channels in the accuracy result and the number of movements considered in all experiments. They concluded that the error rates increase with the addition of movements to the training and test sets. While the addition of movements decreases the accuracy values, the authors proved that using multi-channels increases the results. They concluded that the average accuracy sharply increased with the number of used channels reaching its maximum at six channels (98%). These findings support the conclusions that were previously reached. Considering what has been said, using a single channel of acquisition cannot be enough to study such complex movements due to the lower detected forearm surface area. Even though only three hand gestures were analysed in this dissertation, their complexity affects the results. As the authors proved, adding more complex movements to the set decreased the model's accuracy. Furthermore, the authors remove the transition regions of the signal, which might also contribute to accurate results. To sum up, it is possible to conclude that using a single channel for sEMG acquisition is not enough to produce a commercial prototype.

Chen *et al* [200] studied twenty-five hand gestures that include wrist motions, extensions of a single finger, extensions motions of multiple fingers. The sensors were placed to cover all the main muscles involved in those actions. They recruited four healthy subjects and each one repeated the gestures more than one hundred times. The authors reached an average accuracy between 78.80 and 90.30% when they used a set with finger movements, another with multi-finger flexion and finally a set with wrist motions. The difference between this academic study and our experiment is that the authors

analysed each subject separately, eliminating subjects' intervariability. Thus, they increase the classification score. Despite the good results, the accuracy value dropped when they tried to classify hand gestures that involved similar finger activities. Therefore, it is possible to conclude that movements like hook grip or lateral grip tend to confuse the classifier leading to bad performances. Once again, it was demonstrated that the movements that were used in this master dissertation are complex, which explains the lower classification performance.

Mayor *et al* [109] suggested a methodology that uses four channels to acquire dexterous gestures in amputees. The authors studied thirteen movements, including index flexion, hand close, and tripod grip. However, before analysing and implementing the classifier, the authors tested the influence of the window size on classification performance. They conclude that the accuracy increases until it reaches a maximum for a window of 300 *ms*. The authors divide the movements into three groups. The first one considered all the individual finger movements, the second considered gestures like hand open and hand close and the last one grasp gestures. In this work, the authors tested LDA, SVM and KNN. The LDA was the worst classifier. The SVM proved to be the best, followed by KNN. Despite the better results, SVM took too much time, making the KNN a better algorithm for real-time applications. The accuracy obtained by the authors was 99% for finger movements recognition, 97% for hand gesture recognition and grasp gestures. The results obtained in this master dissertation are lower than the results obtained by Mayor et al. The differences between this dissertation results and the authors are related to the number of channels used and how they separate the set of movements per classification. As suggested in the literature, the number of channels strongly influences classification performance since it increases the accuracy of the classifiers. Besides that, it was proven that dexterous movements, like isolated finger movements, are distinguishable between them but not when compared to grasps movements and hand gestures. Contrary to what happens in this dissertation, the authors analysed each classifier for each volunteer individually. By separating the volunteers, the inter variability on the training and testing samples will be eliminated, which explains the higher results obtained by the authors.

Shi *et al* [201] constructed a myoelectric prototype system to control a homemade prosthetic hand. Thirteen volunteers extended the index finger, the thumb, and four fingers. They placed electrodes on the flexor digitorum superficialis and extensor digitorum muscles to record the EMG activity and then extracted MAV, ZC, SSC, WL. To classify the performed movements, the authors used KNN. The authors studied the influence of using feature selection methods and varying the number of channels. The authors concluded that using a higher number of features increased the average accuracy value. However, the results did not fulfil the expectations (65 % < 80 %). The results obtained by the authors support the results obtained in this dissertation. It was possible to conclude that the average accuracy increased when almost all features were in the set. In our specific case, the classification was higher when five or ten features were selected. The accuracy values with more features are higher when compared to those that only have a part of the initial feature set with both windows. Regarding the number of channels, the authors concluded that adding more channels would increase the accuracy value. The authors studied the k value as well. They conclude that the accuracy increased to k=9 but decreased when k =11. These results are similar to the results obtained during this dissertation work. It was proved that for high values of k the average accuracy increases but the accuracy for each class and the precision and sensitivity of the classifier decrease.

Despite the lower results obtained in this dissertation, Kim *et al*.[202] proved that it is possible to recognize hand gestures with an accuracy of over 90%. The only difference between this dissertation and the authors' study is that they study wrist movements. These movements are originated by almost all the flexor and extensor muscles of the forearm, which means that using a single channel is enough to acquire the signal. Another advantage that the authors implemented was using a combination of two classifiers. The same way as in this dissertation, the authors implemented a tree classifier. However,

there is a difference. Instead of separating the movements, the authors decided to construct each tree level based on the percentage that each of the used classifiers can achieve. Using more than one classifier or choosing which the best for each situation is, can improve the performance of the systems, which improves the overall performance. Another interesting conclusion that can be taken is that in cases where the signal is that they test a set of twenty volunteers and they obtained good results as well. But the authors adopted the system for each user defining the threshold values of each of them. Thus, the variability between the subject does not affect the classification performance.

Wan *et al* [203] used a window of 250 *ms* with an overlap of 125 *ms*. They extracted four time-domain features ZC, SSL, WL, AR coefficients and MAV. The authors used eight channels and extracted data from eight surface electrodes and five force sensors. They recorded signals from thirteen volunteers and divided them into three groups to test which methodology would increase the classification performance. Since in this dissertation the use of sEMG electrodes is studied, only the results obtained in the experiment where the authors used the sEMG sensor will be analysed. The first difference that can be found is related to the movements that were performed in both experiments, the authors analysed wrist movements, grasps and finger movements. They concluded that the accuracy was lower when they tried to recognize finger movements and a combination of finger movements. They obtained the worst results for these movements that were misclassified by others similar to them. The main explanation is that these movements are complex and require more than one finger, which originates from slight signals. The accuracies vary from 68% to 83%.

Georgi *et al* [204] proved that the accuracy drops when the training samples contain all the subjects to percentages under 80%. These findings, added to the ones that were concluded during this discussion, can explain the lower results that were obtained in this dissertation. Conversely to what happened in other experiments, in this dissertation, all the subjects were analysed at once. This little difference causes a drop in the accuracy results.

In another study, Whadi *et al* [175] recognized three different hand gestures with a subject-independent trained classifier. The authors obtained a mean accuracy of 96.4%. Although the overall accuracy, the results dropped when the authors recognized the first gesture. This dropp is associated with the complex activity of several intrinsic muscles that actuate during the performed gesture. These results are far from the ones obtained in this dissertation. The main reason is that the authors study wrist movements, which are more distinguishable than complex movements like tripod grip and finger flexion. These results proved that, for simple movements, the inter variability that exists between the subjects is not significant. However, when the aim is to study a larger set of movements where finger movements are included, that intervariability influences the classification results [205].

From the comparison with the previous works, it is possible to conclude that using a single acquisition channel is sufficient to identify when the volunteer is performing a gesture or is at rest. Besides that, the results showed that each gesture is distinguishable from the rest position using a single channel, even if the gesture is a finger movement or a grasp. However, using a single acquisition system is not enough to promote an accurate and robustness control (accuracy < 90%) when the objective is to recognize dexterous movements from each other. Therefore, it is essential to investigate what could be done to improve these results (Chapter 6).

Despite these results, the objective of this work was accomplished since all questions made at the beginning of chapter 4 were answered.

5.2.Design of the Prosthetic Hand

This study aimed to build a prototype that was safe, ecological, ergonomic, and cheap. Besides that, the device should be more functional than the actual UnLimbited model and more independent of the movements of the healthy body parts of the volunteer.

This prosthesis is adapted to be a body-powered prosthesis. Because of that, it was needed to do some design modifications and create new systems to transform this body-powered prototype into a myoelectric prosthesis. Therefore, it was created a support system to hold the Arduino controller and the servomotors.

Since part of the prosthesis will be electronic, the tension system inherent to the cuff was removed. However, the tension wires systems remained connected to the fingers and forearm because they were linked to the servomotors, later added to the support. After reading a specific input, the motors will rotate and pull the fingers creating the flexion movement. Therefore, it was decided to create a new support system on which the prosthesis will be based instead of modifying the cuff part. The constructed system consists of a flat platform that will support the servomotors and support the Arduino. The support system's design (Figure 5.30) also includes a gutter system that is adaptable to the full size of the prosthesis.

In the previous section, it was possible to conclude that using a single channel acquisition system is enough to control a mechanism capable of activating and deactivating the prosthesis. However, the same does not happen for the other movements. Due to that fact, this prosthesis will be activated or deactivated according to the user signal. Conversely, the spherical grip and the tripod grip will be performed by proportional control. Therefore, in the case of the output will be tripod grip and based on an addition information given by the user the two motors will rotate with different velocities. In this way, the first and second fingers and the thumb can move quickly compared to the third and fourth fingers.

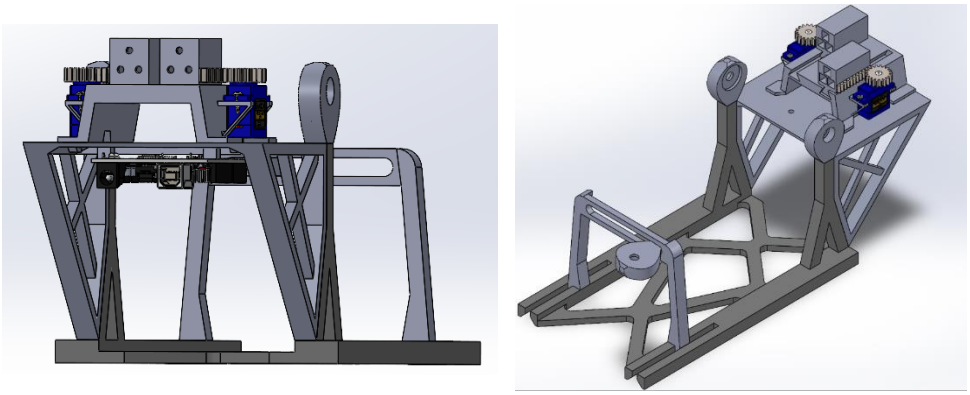

Figure 5.30: Posterior and Anterior view of the support system.

Since the prosthesis will perform two grips, it was decided to use only two motors. The motors were placed in the lateral side of the support system to give some stability to the support. Additionally, the chosen position allows the cables to be directly connected to the prosthesis without having to go through holes or be connected to another part of the prosthesis. This design alteration reduces the probability of wire tension failure. These two design specifications make the prosthesis much safer for the user. In addition, the fact that it does not depend on the user's strength makes the control much more accurate, giving more comfort to the user and increasing their safety.

In theory, the human hand weight is on average 0.585% of the total body weight, which means that the designed prosthesis needs to have less than 380.25 *g* (considering a user of 65 Kg) [206]. Therefore, the developed prototype should be lighter than that. In this dissertation, we used PLA which means that the created prototype weights less than 300 *g*.

Due to the low classification rates (< 80%) obtained on online tests, it is expected that the rates will be lower than 50% on offline tests. Having classification rates lower than 90% is a risk for the user's safety, which decreases the functionality and robustness of the prosthesis. Because of that, the built device will not be used as a daily use prosthesis but as a training device in clinical environments. However, the condition is that this device's condition is for training the activation prostheses and defining voltage-dependent security systems. In this dissertation, the adaptability of the designed system to any size does not restrain the training to a specific user, which is an advantage in clinical background.

Despite the combination of both controls (proportional control and pattern recognition control), it was possible to overcome some of the limitations inherent to the original model. The recognition of the rest position and the movement is already an improvement since the patient will no longer need to make much force or flex the elbow to grab some objects. Furthermore, the prosthesis now has two degrees of freedom instead of only one and increased the friction between the tips and the objects.

This prototype was produced within 24 hours, which proved that the 3D printing has a lower time-to-market. Besides that, the total material used in this prototype costs less than 50 €, which means that this prosthesis will cost less than 100 €.

Nevertheless, this prototype still has limitations. In this dissertation work, the risks associated with the failure of the prototype, such as tension pin failure, finger failure, elastic tension failure, locking mechanism failure and electronic failures were not considered. The risk associated with this prosthesis can be moderate or higher since it can put at risk the user's safety and can lead to the damaging of the object or making the finger useless. Besides that, the resistance of the material was not tested.

6. Conclusion and Future Work

Losing a hand or even part of the upper limb has a relevant influence on a patient's daily life and mental health. Furthermore, the increasing incidence of some diseases such as diabetes makes this problem more frequent. In addition, it is predicted that by 2050 the number of people who will need to use a prosthesis will have duplicated.

Several engineers created solutions to allow the user to live normally. Therefore, the prosthetic industry is growing today in its most significant period of development and growth. There are cosmetic prostheses, body-powered prostheses, and electrical prostheses within the different prostheses. The cosmetic prosthesis can be static or dynamic. The static ones are made of silicone and are similar to the arm. The dynamic cosmetic prostheses have hooks to grab the object. Despite the similarities in terms of colour and shape to the human arm, these prostheses do not have degrees of freedom or have just one. Therefore, the robustness of each one is limited. Secondly, there are body-powered prostheses. These are very competitive when it comes to their time to reach the market. Moreover, some of them are made of 3D printable materials, which allow each patient to customise their prototype. Besides that, these are lighter and cheaper prostheses. However, there is a huge dependence on the users' force during the flexion of a particular body part. Finally, the electrical prostheses give more natural and intuitive control and a high grip force. Additionally, this type of prosthesis is the only one that has multiple degrees of freedom and requires less visual attention. However, these prostheses are noisy, heavy and battery dependent.

According to the user, having a lighter, cost-effective, and high functionality level prosthesis is essential to daily activities. Because of that, during this dissertation, we tried to develop a hybrid system that combines the advantages of the 3D printable body-powered prosthesis and the myoelectric ones. Proportional control is widely used in the market since it is fast and requires low training times. However, only one or two degrees of freedom are available. To overcome this limitation, the industry and academia started to use artificial intelligence algorithms to identify different grip patterns. These algorithms introduced more degrees of freedom in prosthetic models, added more complex movements such as tripod grip, lateral grip, cylindrical grip, etc. This is possible because the authors used several multi-channel acquisitions, which in several scenarios is not possible. Furthermore, with this control it is not possible to identify dexterous movements.

In this dissertation, we explored the option of using a single channel to identify dexterous movements using two fast and straightforward classifiers. Besides that, we studied the possibility of developing a subject-independent microcontroller. Therefore, we filtered the signal, divided it into time segments and extracted features for further classification.

Filtering the signal is one of the most critical pre-processing signal techniques because it improves the overall accuracy and classification performance. In this work, two different filtering processes were tested. The first filter method, digital filtering, increased the SNR of the signal but it might remove some peak information. Wavelet threshold noise reduction suggested to be the best filtering method since the MSE values were lower.

Although the classification results obtained in this dissertation differ from those obtained in the literature, it can be concluded that the main limitations were in the methodology and the number of used channels. Nevertheless, this dissertation has overcome the drawbacks found in other articles and studies, mainly the use of many channels. Besides that, this dissertation studies dexterous movements in a unique dataset, which does not happen in other works. The authors usually separate hand movements and prehensions from finger isolated movements.

The overall results proved that using a single acquisition channel is sufficient to identify when the volunteer is performing a gesture or is at rest. Besides that, the results showed that each gesture is distinguishable from the rest position using a single channel, even if the gesture is a finger movement or a grasp. Despite the high offline accuracy percentages (> 90%), it is expected that the classification performance will decrease in the online tests. Conversely, the results of the second and third levels of the cascade classifier proved that single acquisitions are not enough to promote an accurate and robustness control (accuracy < 90%), which means that it is not recommended to use a single channel in real-time classifications. As it is known, the myoelectric signal is affected by numerous factors since it measures the activity of muscle groups that are close to each other. This phenomenon increases when the number of different movement types increases, making the estimation of each class's probability distributions even more difficult. Thus, it is possible to conclude that a single channel acquisition is not enough to produce a robust myoelectric controller. It would be interesting to test different electrode positions and increase the number of channels at a maximum of two channels soon. In addition, adding some features from the frequency domain could also be interesting.

Introducing amputated people in the volunteers' group would allow a precise evaluation of the real-time implementation of the myoelectric controller. It is known that following a specific methodology for amputees seems impossible due to the fact that there are too many different amputations and surgical procedures. Furthermore, some amputees might not have intact nervous structures. Therefore, it is fundamental to test this methodology in a group of amputees or children with congenital anomalies. As it was suggested in this work, it will not be easy to follow a specific methodology that fits every amputee, especially if the signal is recorded with a single acquisition system. So, the most probable scenario will be creating a personalised prosthetic device that fits each amputee and follows a specific signal processing methodology, which means that it is not possible to develop an independent subject controller as the prosthetic industry wanted.

Considering the obtained results, we printed a lighter and cheaper prototype than those available on the market. Since it was impossible to develop a microcontroller with the single use of pattern recognition control, we decided to use both types of control.

As with all studies and experiments, this dissertation has a few limitations that should be considered. The first limitation of this dissertation is that the studied volunteers are healthy, which is not enough to validate the development of a commercial prototype designed for amputees. The second one is that this study does not consider the movement of the arm in space and the load that the prosthesis will have to support. The third one is related to the impossibility of studying a few essential parameters for users as well as testing the mechanical success of the developed prosthesis. For example, covering the interior of the prosthesis with a breathable material would stabilise the reading of sEMG, reducing the amount of noisy external sources. Furthermore, it is also essential to study and improve the flexibility of the fingers, adapting them to the natural movement and degrees inherent to each joint.

Despite all the implemented methods, it is always space for improvement. Because of that, the following are suggested:

Improvement of the functionality of the myoelectric controller: this can be done through the reduction of the misclassified classes. To do that, it would be interesting to add one more acquisition channel to test how the accuracy of the classifier would increase. Furthermore, introducing wrist and arm movements can give robustness since in previous studies, the classification of such moments resulted in an average accuracy higher than 90%. Even though the index finger plays different activation roles in all grasp movements at the neuronal level, the signal recorded on the surface of the forearm skin is similar. Because of that, it would be crucial to place the electrodes in extensor muscles, or another group of muscles to increase the signal detection and consequently the classification performance.

Besides that, it will be interesting to use a motion capture glove and force sensors to identify individual finger movements as well as amplitude thresholds, which can be used as boundary limits to define security amplitude lock systems. Finally, testing other normalisation methods like peak to peak might increase the classification performance.

Improvement of the robustness of the prototype: in the future, it is important to test the microcontroller as well as the material used in the prototype. The robustness of a prototype is a measure of its security and functionality. Therefore, it will be interesting to test the flexibility and resistance of the material to compression and tension forces. In addition, testing the electronic components and the efficiency of the microcontroller would also increase the robustness of the prototype through target tests and majority voting. Besides that, testing more materials, mainly flexible, resistant and waterproof materials, would increase the functionality of the prosthesis and at the same time solve some of the limitations pointed out by users. Finally, testing the number of objects that the prosthesis can grab and how long it lasts prehension would also be essential to improve the robustness of the prosthesis. Therefore, it is important to test the prototype with box and block tests, target achievement control tests and Fit's Law tests. Besides these tests, it is fundamental to evaluate the motor's battery duration and their performance during daily use. A set of tension and compression forces should be applied to test the resistance of the prosthesis material. After that, the results should be produced and analysed. Moreover, the prototype should be tested underwater, under specific temperature conditions and in noisy environments.

Enhancement of the cosmetic appearance: The prototype produced in this dissertation is blue and has an artificial appearance. These prostheses are produced specially for children, which means that their appearance is very similar to a superhero hand. But limiting these types of prototypes to children is not a profitable solution. Therefore, the ideal would be to scan the healthy arm of the user and readapt the scan to a tension mechanism controlled by a microcontroller. After that, the next step would be redesigning some parts to promote an easy assembly and, finally, printing the parts with new and more sophisticated materials like FilaFlex®. Using this material would be a bonus point for users since it is available in skin colours. Besides that, this material is flexible, which could promote a more natural movement of the interphalangeal joints.

Despite the limitations and the overall results, this dissertation clarifies several questions and limits found in previous academic works and current commercial solutions. Besides that, in this work different methodologies were explored, which gives a great contribute to scientific community. This dissertation will contribute to advances in the prosthetic industry and in the implementation of new ideas and solutions to develop prosthetic solutions and to improve the state of the art as well.

7. References

[1] A. Kannenberg, 'Active Upper-Limb Prostheses: The International Perspective', *JPO J. Prosthetics Orthot.*, vol. 29, pp. 57–62.

[2] Z. L. Cordella Francesca, Ciancio Anna Lisa, Sacchetti Rinaldo, Davalli Angelo, Cutti Andrea Giovanni, Guglielmelli Eugenio, 'Literature Review on Needs of Upper Limb Prosthesis Users', *Front. Neurosci.*, vol. 10, p. 209, 2016.

[3] H. Mano, S. Fujiwara, and N. Haga, 'Adaptive behaviour and motor skills in children with upper limb deficiency', *Prosthet. Orthot. Int.*, vol. 42, no. 2, pp. 236–240, 2018.

[4] L. Resnik, H. H. Huang, A. Winslow, D. L. Crouch, F. Zhang, and N. Wolk, 'Evaluation of EMG pattern recognition for upper limb prosthesis control: A case study in comparison with direct myoelectric control', *J. Neuroeng. Rehabil.*, vol. 15, no. 1, pp. 1–13, 2018.

[5] A. B. Wanamaker, L. R. Whelan, J. Farley, and A. M. W. Chaudhari, 'Biomechanical analysis of users of multi-articulating externally powered prostheses with and without their device', *Prosthet. Orthot. Int.*, vol. 43, no. 6, pp. 618–628, 2019.

[6] K. Ziegler-Graham, E. J. MacKenzie, P. L. Ephraim, T. G. Travison, and R. Brookmeyer, 'Estimating the Prevalence of Limb Loss in the United States: 2005 to 2050', *Archives of Physical Medicine and Rehabilitation*, vol. 89, no. 3. pp. 422–429, 2008.

[7] L. Extremity (Upper, 'Robotic Prosthetic Market Size, Share & Trends Analysis Report By Extremity (Upper, Lower), By Technology (MPC, Myoelectric), By Region, And Segment Forecasts, 2020 - 2027', 2020.

[8] A. H. Al-Timemy, G. Bugmann, J. Escudero, and N. Outram, 'Classification of finger movements for the dexterous hand prosthesis control with surface electromyography', *IEEE J. Biomed. Heal. informatics*, vol. 17, no. 3, pp. 608–618, 2013.

[9] J. P. Matos, E. Carolino, and R. Ramos, 'Dados Epidemiológicos sobre amputações realizadas em Portugal entre 2000 e 2015'. Instituto Politécnico de Lisboa, Escola Superior de Tecnologia da Saúde de Lisboa, 2018.

[10] S. A. Boyadjiev Boyd, 'Congenital Limb Abnormalities'. [Online]. Available: https://www.merckmanuals.com/professional/pediatrics/congenital-craniofacial-and-musculoskeletal-abnormalities/congenital-limb-abnormalities.

[11] C. J. Dy, I. Swarup, and A. Daluiski, 'Embryology, diagnosis, and evaluation of congenital hand anomalies', *Curr. Rev. Musculoskelet. Med.*, vol. 7, no. 1, pp. 60–67, 2014.

[12] L. A. Goldfarb, Charles; Shaw, Neil; A.Steffen, Jennifer; B.Wall, 'The prevalence of Congenital Hand and Upper Extremity Anomalies based upon the New Yok Congenital Malformations Registry', *J. Pediatr. Orthop.*, vol. 37, no. 2, pp. 144–148.

[13] V. S. Nelson, K. M. Flood, P. R. Bryant, M. E. Huang, P. F. Pasquina, and T. L. Roberts, 'Limb deficiency and prosthetic management. 1. Decision making in prosthetic prescription and management', *Arch. Phys. Med. Rehabil.*, vol. 87, no. 3, pp. 3–9, 2006.

[14] J. M. Zuniga *et al.*, 'Functional changes through the usage of 3D-printed transitional prostheses in children', *Disabil. Rehabil. Assist. Technol.*, vol. 14, no. 1, pp. 68–74, 2019.

[15] I. Berre, M.; Casanova, H.; Chapal, K.; Despande, S. A.; Harte, C.; Heim, S.;Hughes, J.; Jacobs, N. A.; Jensen, J. S.; Khang, D. X.; McHugh, B.;Pupulin, E.; Sarhan, Y.; Sarwar, B.; Sermeno, E.; Singh, J. P.;Scott, M.; Sexton, S.; Shangali, H. G.; Stills, M., 'Guidelines for training personnel in developing countries for prosthetics and orthotics services', *WHO Libr. Cat. Data*, pp. 1–57, 2005.

[16] C. Igual, L. A. Pardo, J. M. Hahne, and J. Igual, 'Myoelectric control for upper limb prostheses', *Electronics (Switzerland)*, vol. 8, no. 11. 2019.

[17] R. M. Bongers, P. J. Kyberd, H. Bouwsema, L. P. J. Kenney, D. H. Plettenburg, and C. K. Van Der Sluis, 'Bernstein's levels of construction of movements applied to upper limb prosthetics', *J. Prosthetics Orthot.*, vol. 24, no. 2, pp. 67–76, 2012.

[18] E. Biddiss and T. Chau, 'Upper limb prosthesis use and abandonment: A survey of the last 25 years', *Prosthet. Orthot. Int.*, vol. 31, no. 3, pp. 236–257, 2007.

[19] D. Farina and O. Aszmann, 'Bionic limbs: Clinical reality and academic promises', *Science Translational Medicine*, vol. 6, no. 257. 2014.

[20] K. S. Saladin, *Human Anatomy 5th*, Second Edi. McGraw-Hill International, 2008.

[21] Rod R. Seeley; Trent D. Stephens ; Philip Tate, *Anatomia e fisiologia - Seeley*. 2005.
[22] B. K. Administration, 'Introduction to the Upper Limb', 2016. [Online]. Available: https://basicmedicalkey.com/introduction-to-the-upper-limb/. [Accessed: 10-Oct-2020].
[23] J. A. Esperança Pina, *Anatomia Humana e Locomoção*, 5th ed. 2017.
[24] M. K. Staff, 'Clinical History and Examination'. [Online]. Available: https://musculoskeletalkey.com/clinical-history-and-examination/. [Accessed: 08-Jan-2020].
[25] D. S. Pina, 'Biomecânica da articulação interfalângica proximal - nativa versus artroplástica', Universidade de Aveiro, 2015.
[26] D. Yang, Y. Gu, N. V. Thakor, and H. Liu, 'Improving the functionality, robustness, and adaptability of myoelectric control for dexterous motion restoration', *Experimental Brain Research*. 2019.
[27] K. Stollenwerk and R. Klein, 'GraspDB14 – Documentation on a database of grasp motions and its creation', Sankt Augustin, Germany January.
[28] D. J. Cech and S. "Tink" Martin, 'Prehension', in *Functional Movement Development*, 2012, pp. 309–334.
[29] S. S. MBBS, 'Upper limb muscles and movements'. [Online]. Available: https://www.kenhub.com/en/library/anatomy/upper-limb-muscles-and-movements. [Accessed: 05-Jan-2021].
[30] J. M. Biga, Lindsay; Dawson, Sierra; Harwell, Amy ; Hopkins, Robin; Kaufmann, Joel ; LeMaster, Mike; Matern, Philip ; Morrison-Graham, Katie; Quick, Devon; Runyeon, 'Anatomy & Physiology: Identify the skeletal muscles and give their origins, insertions, actions and innervations'. [Online]. Available: https://open.oregonstate.education/aandp/chapter/11-4-identify-the-skeletal-muscles-and-give-their-origins-insertions-actions-and-innervations/. [Accessed: 08-Jan-2020].
[31] J. G. Betts *et al.*, 'Anatomy and Physiology', 2013. [Online]. Available: https://openstax.org/books/anatomy-and-physiology/pages/1-introduction. [Accessed: 07-Jan-2021].
[32] B. Simeon and A. B. Boyd, 'Congenital Limb Abnormalities', *MSD Manual Professional Version*, 2020. [Online]. Available: https://www.msdmanuals.com/professional/pediatrics/congenital-craniofacial-and-musculoskeletal-abnormalities/congenital-limb-abnormalities#.
[33] M. A. Tonkin, 'Classification of congenital anomalies of the hand and upper limb', *J. Hand Surg. Eur. Vol.*, vol. 42, no. 5, pp. 448–456, 2017.
[34] World Health Organization Staff, 'Congenital Anomalies', 2010. [Online]. Available: https://www.who.int/news-room/fact-sheets/detail/congenital-anomalies. [Accessed: 20-Oct-2020].
[35] A. of B. D. Children, 'Structural and functional birth defects'. [Online]. Available: https://birthdefects.org/structural-and-functional-birth-defects/.
[36] J. H. Staff, 'Amniotic Band Syndrome'. [Online]. Available: https://www.hopkinsmedicine.org/health/conditions-and-diseases/amniotic-band-syndrome. [Accessed: 02-Dec-2020].
[37] S. UCSF benioff Children's Hospitals, 'Amniotic Band Syndrome'. [Online]. Available: https://fetus.ucsf.edu/amniotic-band-syndrome/. [Accessed: 15-Jan-2021].
[38] A. M. Travessa, P. Dias, A. Santos, S. Custódio, A. Sousa, and A. B. Sousa, 'Upper limb phocomelia: A prenatal case of thrombocytopenia-absent radius (TAR) syndrome illustrating the importance of chromosomal microarray in limb reduction defects', *Taiwan. J. Obstet. Gynecol.*, vol. 59, no. 2, pp. 318–322, 2020.
[39] T. Laor and J. H. Kan, 'Congenital Anomalies of Bone'. [Online]. Available: https://radiologykey.com/congenital-anomalies-of-bone/. [Accessed: 20-Jan-2021].
[40] C. Ibáñez, 'Real-time EMG Control for Hand Exoskeletons', 2018.
[41] C. DerSarkissian, 'Amputation overview'. [Online]. Available: https://www.webmd.com/a-to-z-guides/definition-amputation#1. [Accessed: 25-Oct-2020].
[42] F. Cordella *et al.*, 'Literature review on needs of upper limb prosthesis users', *Front. Neurosci.*, vol. 10, pp. 1–14, 2016.
[43] H. Maduri, P.; Akhondi, *Upper Limb amputation*. Treasure Island (FL): StatPearls Publishing,

2020.
[44] T. P. Sheehan, ‘Rehabilitation and Prosthetic Restoration in Upper Limb Amputation’, 2015. [Online]. Available: https://clinicalgate.com/rehabilitation-and-prosthetic-restoration-in-upper-limb-amputation/. [Accessed: 21-Jan-2021].
[45] J. ten Kate, G. Smit, and P. Breedveld, ‘3D-printed upper limb prostheses: a review’, *Disabil. Rehabil. Assist. Technol.*, vol. 12, no. 3, pp. 300–314, 2017.
[46] T. D. Ngo, A. Kashani, G. Imbalzano, K. T. Q. Nguyen, and D. Hui, ‘Additive manufacturing (3D printing): A review of materials, methods, applications and challenges’, *Compos. Part B Eng.*, vol. 143, pp. 172–196, 2018.
[47] Sayuk A, ‘Design and implementation of a low cost hand for prosthetic applications’, Faculdade de Ciências e Tecnologia da Universidade de Coimbra, 2015.
[48] L. E. Diment, M. S. Thompson, and J. H. M. Bergmann, ‘Three-dimensional printed upper-limb prostheses lack randomised controlled trials: A systematic review’, *Prosthet. Orthot. Int.*, vol. 42, no. 1, pp. 7–13, 2018.
[49] F. C. B. Dias Pinheiro, ‘Development of a Functional Upper Limb Prosthesis’, Instituto Superior Técnico.
[50] W. J. Gaine, C. Smart, and M. Bransby-Zachary, ‘Upper limb traumatic amputees: Review of prosthetic use’, *J. Hand Surg. Eur. Vol.*, 1997.
[51] C. Li, J. Ren, H. Huang, B. Wang, Y. Zhu, and H. Hu, ‘PCA and deep learning based myoelectric grasping control of a prosthetic hand’, *Biomed. Eng. Online*, vol. 17, no. 1, pp. 1–18, 2018.
[52] B. Maat, G. Smit, D. Plettenburg, and P. Breedveld, ‘Passive prosthetic hands and tools: A literature review’, *Prosthet. Orthot. Int.*, 2018.
[53] V. Lopes, ‘Design and Development of an Upper Limb Prosthesis’, Instituto Superior Técnico.
[54] Össur Staff, ‘Livingskin®’. [Online]. Available: https://www.ossur.com/en-us/prosthetics/arms/livingskin. [Accessed: 02-Feb-2021].
[55] D. of faculty 3mE S. TU Delft, ‘WILMER Passive Hand Prosthesis for Toddlers’. [Online]. Available: https://www.tudelft.nl/3me/over/afdelingen/biomechanical-engineering/research/biomechatronics-human-machine-control/delft-institute-of-prosthetics-and-orthotics/products/prostheses/wilmer-passive-hand-prosthesis-for-toddlers. [Accessed: 04-Mar-2021].
[56] S. Watve, G. Dodd, R. MacDonald, and E. R. Stoppard, ‘Upper limb prosthetic rehabilitation’, *Orthop. Trauma*, vol. 25, no. 2, pp. 135–142, 2011.
[57] E.-N. Staff, ‘Enabling the future’. [Online]. Available: https://enablingthefuture.org/. [Accessed: 14-Oct-2020].
[58] B. Phillips, G. Zingalis, S. Ritter, and K. Mehta, ‘A review of current upper-limb prostheses for resource constrained settings’, in *Proceedings of the 5th IEEE Global Humanitarian Technology Conference, GHTC 2015*, 2015.
[59] J. Zuniga *et al.*, ‘Cyborg beast: A low-cost 3d-printed prosthetic hand for children with upper-limb differences’, *BMC Res. Notes*, vol. 8, no. 1, pp. 1–9, 2015.
[60] P. I. Staff, ‘Patient Innovation’. [Online]. Available: https://patient-innovation.com/how-it-works?language=pt-pt. [Accessed: 20-Oct-2020].
[61] K. Andrianesis and A. Tzes, *Development and Control of a Multifunctional Prosthetic Hand with Shape Memory Alloy Actuators*, vol. 78, no. 2. 2015.
[62] S. G. Millstein, H. Heger, and G. A. Hunter, ‘Prosthetic use in adult upper limb amputees: A comparison of the body powered and electrically powered prostheses’, *Prosthet. Orthot. Int.*, vol. 10, no. 1, pp. 27–34, 1986.
[63] A. Manero *et al.*, ‘Implementation of 3D printing technology in the field of prosthetics: Past, present, and future’, *Int. J. Environ. Res. Public Health*, vol. 16, pp. 1–15, 2019.
[64] M. B. Burn, A. Ta, and G. R. Gogola, ‘Three-dimensional printing of prosthetic hands for children’, *J. Hand Surg. Am.*, vol. 41, no. 5, pp. 103–109, 2016.
[65] B. O’Keeffe, ‘Prosthetic rehabilitation of the upper limb amputee’, *Indian J. Plast. Surg.*, vol. 44, no. 2, pp. 246–252, 2011.
[66] K. Talbot, ‘Using Arduino to Design a Myoelectric Prosthetic’, Saint John´s University.
[67] A. Prakash, A. K. Sahi, N. Sharma, and S. Sharma, ‘Force myography controlled multifunctional hand prosthesis for upper-limb amputees’, *Biomed. Signal Process. Control*, vol. 62, p. 102122,

2020.
[68] ottobock company, ‘bebionic hand’. [Online]. Available: https://www.ottobockus.com/prosthetics/upper-limb-prosthetics/solution-overview/bebionic-hand/. [Accessed: 16-Sep-2020].
[69] Ö. Company, ‘i-limb Ultra’. [Online]. Available: https://www.ossur.com/en-us/prosthetics/arms/i-limb-ultra. [Accessed: 15-Sep-2020].
[70] O. Company, ‘Michelangelo Prosthetic Hand’. [Online]. Available: https://www.ottobockus.com/prosthetics/upper-limb-prosthetics/solution-overview/michelangelo-prosthetic-hand/. [Accessed: 17-Sep-2020].
[71] L. Resnik, S. L. Klinger, and K. Etter, ‘The DEKA Arm: Its features, functionality, and evolution during the veterans affairs study to optimize the DEKA Arm’, *Prosthetics and Orthotics International*, vol. 38, no. 6. pp. 492–504, 2014.
[72] W. Staff, ‘DEKA bionic arm’. [Online]. Available: http://www.dekaresearch.com/deka_arm.shtml. [Accessed: 04-Oct-2020].
[73] ‘Open Bionics’. [Online]. Available: https://openbionics.com/. [Accessed: 12-Dec-2020].
[74] O. Bock, ‘Myo Plus pattern recognition’, 2019. [Online]. Available: https://www.ottobock.com/en/apps/myoplusapp/myo-plus-app-da.html. [Accessed: 12-Dec-2020].
[75] B. Mokhlesabadifarahani and V. K. Gunjan, *EMG signals characterization in three states of contraction by fuzzy network and feature extraction*. SpringerBriefs, 2015.
[76] C. Ibáñez, ‘Real-time EMG Control for Hand Exoskeletons’, Universidad Carlos III de Madrid, 2018.
[77] S. Baccherini, ‘Pattern Recognition Methods for EMG Prosthetic Control’, Universita di Bologna, 2016.
[78] H. G. Lopes de Almeida, ‘Estudo e desenvolvimento de uma prótese de mão utilizando técnicas de soft robotics’, Instituto Superior De Engenharia de Lisboa, 2018.
[79] J. Wang and J. E. Bronlund, ‘Surface EMG Signal Amplification and Filtering’, *Int. J. Comput. Appl.*, vol. 82, no. 1, pp. 15–22.
[80] M. Halaki and K. Ginn, ‘Normalization of EMG Signals: To Normalize or Not to Normalize and What to Normalize to?, Computational Intelligence in Electromyography Analysis - A Perspective on Current Applications and Future Challenges’, *Comput. Intell. Electromyogr. Anal. - A Perspect. Curr. Appl. Futur. Challenges*, p. 448, 2012.
[81] C. J. De Luca, ‘The use of surface electromyography in biomechanics’, *J. Appl. Biomech.*, vol. 13, no. 2, pp. 135–163, 1997.
[82] R. H. Chowdhury, M. B. I. Reaz, M. A. Bin Mohd Ali, A. A. A. Bakar, K. Chellappan, and T. G. Chang, ‘Surface electromyography signal processing and classification techniques’, *Sensors (Switzerland)*, vol. 13, no. 9, pp. 12431–12466, 2013.
[83] D. Farina and S. Amsüss, ‘Reflections on the present and future of upper limb prostheses’, *Expert Rev. Med. Devices*, vol. 13, no. 4, pp. 321–324, 2016.
[84] S. L. Carey, D. J. Lura, and M. Jason Highsmith, ‘Differences in myoelectric and body-powered upper-limb prostheses: Systematic literature review’, *Journal of Rehabilitation Research and Development*, vol. 52, no. 3. pp. 247–262, 2015.
[85] J. S. Cuellar, G. Smit, P. Breedveld, A. A. Zadpoor, and D. Plettenburg, ‘Functional evaluation of a non-assembly 3D-printed hand prosthesis’, *Proc. Inst. Mech. Eng. Part H J. Eng. Med.*, vol. 233, no. 11, pp. 1122–1131, 2019.
[86] H. L. Benz *et al.*, ‘Upper extremity prosthesis user perspectives on unmet needs and innovative technology’, *Proc. Annu. Int. Conf. IEEE Eng. Med. Biol. Soc. EMBS*, vol. 38th Annua, pp. 287–290, 2016.
[87] O. W. Samuel *et al.*, ‘Intelligent EMG pattern recognition control method for upper-limb multifunctional prostheses: advances, current challenges, and future prospects’, *IEEE Access*, vol. 7, pp. 10150–10165, 2019.
[88] N. Parajuli *et al.*, ‘Real-time EMG based pattern recognition control for hand prostheses: a review on existing methods, challenges and future implementation’, *Sensors*, vol. 9, p. 4596, 2019.
[89] M. Asghari Oskoei and H. Hu, ‘Myoelectric control systems-A survey’, *Biomed. Signal Process.*

Control, vol. 2, no. 4, pp. 275–294, 2007.
[90] A. W. Shehata, S. Member, E. J. Scheme, S. Member, and J. W. Sensinger, 'Evaluating Internal Model Strength and Performance of Myoelectric Prosthesis Control Strategies', *IEEE Trans. Neural Syst. Rehabil. Eng.*, vol. 26, no. 5, pp. 1046–1055, 2018.
[91] A. D. Roche, H. Rehbaum, D. Farina, and O. C. Aszmann, 'Prosthetic Myoelectric Control Strategies: A Clinical Perspective', *Current Surgery Reports*, vol. 2, no. 3. 2014.
[92] L. J. Hargrove, L. A. Miller, K. Turner, and T. A. Kuiken, 'Myoelectric Pattern Recognition Outperforms Direct Control for Transhumeral Amputees with Targeted Muscle Reinnervation: A Randomized Clinical Trial', *Scientific Reports*, vol. 7, no. 1. 2017.
[93] K. H. Ang, G. Chong, and Y. Li, 'PID control system analysis, design, and technology', *IEEE Trans. Control Syst. Technol.*, vol. 13, no. 4, pp. 559–576, 2005.
[94] R. Ghazali, M. Z. Saad, S. Y. S. Hussien, M. H. Jali, F. N. Zohedi, and T. A. Izzuddin, 'Intelligent controller design for multifunctional prosthetics hand', *Int. J. Mech. Eng. Robot. Res.*, vol. 6, no. 6, pp. 495–501, 2017.
[95] H. Zhou and G. Alici, 'A compact and cost-effective pattern recognition based myoelectric control system for robotic prosthetic hands', in *IEEE/ASME International Conference on Advanced Intelligent Mechatronics, AIM*, 2020, pp. 270–275.
[96] A. D. Roche, H. Rehbaum, D. Farina, and O. C. Aszmann, 'Prosthetic Myoelectric Control Strategies: A Clinical Perspective', *Curr. Surg. Reports*, vol. 2, no. 3, p. 44, 2014.
[97] A. Waris, I. K. Niazi, M. Jamil, K. Englehart, W. Jensen, and E. N. Kamavuako, 'Multiday Evaluation of Techniques for EMG-Based Classification of Hand Motions', *IEEE J. Biomed. Heal. Informatics*, vol. 23, no. 4, pp. 1526–1534, 2018.
[98] Z. O. Khokhar, Z. G. Xiao, and C. Menon, 'Surface EMG pattern recognition for real-time control of a wrist exoskeleton', *Biomed. Eng. Online*, vol. 9, pp. 1–17, 2010.
[99] T. R. Farrell and R. F. Weir, 'The optimal controller delay for myoelectric prostheses', *IEEE Transactions on Neural Systems and Rehabilitation Engineering*, vol. 15, no. 1. pp. 111–118, 2007.
[100] R. W. Wirta, D. R. Taylor, and F. R. Finley, 'Pattern-recognition arm prosthesis: a historical perspective-a final report', *Bull. Prosthet. Res.*, vol. 10, no. 30, pp. 8–35, 1978.
[101] A. D. Chan and K. B. Englehart, 'Continuous myoelectric control for powered prostheses using hidden Markov models', *IEEE Trans. Biomed. Eng.*, vol. 52, no. 1, pp. 121–124, 2005.
[102] A. Tenore, Francesco V. G. Ramos, A. Soumyadipta, Acharya Fahmy, R. Etienne-Cummings, and T. Nitish V., 'Decoding of individuated finger movements using surface electromyography', *IEEE Trans. Biomed. Eng.*, vol. 56, no. 5, pp. 1427–1434, 2008.
[103] A. H. Al-Timemy, G. Bugmann, N. Outram, and J. Escudero, 'Single channel-based myoelectric control of hand movements with Empirical Mode Decomposition', in *2011 Annual International Conference of the IEEE Engineering in Medicine and Biology Society*, 2011, pp. 6059–6062.
[104] F. Riillo *et al.*, 'Optimization of EMG-based hand gesture recognition: Supervised vs. unsupervised data preprocessing on healthy subjects and transradial amputees', *Biomed. Signal Process. Control*, vol. 14, pp. 117–125, 2014.
[105] A. Stango, F. Negro, and D. Farina, 'Spatial correlation of high density EMG signals provides features robust to electrode number and shift in pattern recognition for myocontrol', *IEEE Trans. Neural Syst. Rehabil. Eng.*, vol. 23, no. 2, pp. 189–198, 2015.
[106] S. A. Curline-Wandl and M. Azam Ali, 'Single channel myoelectric control of a 3D printed transradial prosthesis', *Cogent Engineering*, vol. 3, no. 1. 2016.
[107] R. Ghazali, M. Z. Saad, S. Y. S. Hussien, M. H. Jali, F. N. Zohedi, and T. A. Izzuddin, 'Intelligent controller design for multifunctional prosthetics hand', *International Journal of Mechanical Engineering and Robotics Research*, vol. 6, no. 6. pp. 495–501, 2017.
[108] T. Jiralerspong, E. Nakanishi, C. Liu, and J. Ishikawa, 'Experimental study of real-time classification of 17 voluntary movements for multi-degree myoelectric prosthetic hand', *Applied Sciences (Switzerland)*, vol. 7, no. 11. 2017.
[109] J. J. V. Mayor, R. M. Costa, A. Frizera Neto, and T. F. Bastos, 'Dexterous hand gestures recognition based on low-density sEMG signals for upper-limb forearm amputees', *Research on Biomedical Engineering*, vol. 33, no. 3. pp. 202–217, 2017.
[110] S. Raurale, J. McAllister, and J. M. Del Rincon, 'EMG Wrist-hand Motion Recognition System

for Real-time Embedded Platform', *ICASSP, IEEE International Conference on Acoustics, Speech and Signal Processing - Proceedings*, vol. 2019-May. pp. 1523–1527, 2019.
[111] C. Li, G. Li, G. Jiang, D. Chen, and H. Liu, 'Surface EMG data aggregation processing for intelligent prosthetic action recognition', *Neural Computing and Applications*, vol. 32, no. 22. pp. 16795–16806, 2020.
[112] H. Ashraf *et al.*, 'Determination of Optimum Segmentation Schemes for Pattern Recognition-Based Myoelectric Control: A Multi-Dataset Investigation', *IEEE Access*, vol. 8, pp. 90862–90877, 2020.
[113] J. James Redett, Richard; Troyal Shores, 'Targeted Muscle Reinnervation'. [Online]. Available: https://www.hopkinsmedicine.org/plastic_reconstructive_surgery/services-appts/tmr.html. [Accessed: 24-Nov-2020].
[114] M. Asghari Oskoei and H. Hu, 'Myoelectric control systems-A survey', *Biomedical Signal Processing and Control*, vol. 2, no. 4. pp. 275–294, 2007.
[115] H. J., Z. D., J. N., S. X., F. D., and Z. X., 'User adaptation in long-term, open-loop myoelectric training: Implications for EMG pattern recognition in prosthesis control', *Journal of Neural Engineering*, vol. 12, no. 4. 2015.
[116] C. J. De Luca, L. Donald Gilmore, M. Kuznetsov, and S. H. Roy, 'Filtering the surface EMG signal: Movement artifact and baseline noise contamination', *J. Biomech.*, vol. 43, no. 8, pp. 1573–1579, 2010.
[117] Carlo J. De Luca, 'The Use of Surface Electromyography in Biomechanics', *J. Appl. Biomech.*, vol. 13, no. 2, pp. 135–163, 1997.
[118] U. Ozkaya, O. Coskun, and S. Comlekci, 'Frequency analysis of EMG signals with Matlab sptool', *9th WSEAS Int. Conf. Signal Process. SIP '10*, pp. 83–88, 2010.
[119] A. L. Fougner, Ø. Stavdahl, and P. J. Kyberd, 'System training and assessment in simultaneous proportional myoelectric prosthesis control', *J. Neuroeng. Rehabil.*, vol. 11, no. 1, pp. 1–13, 2014.
[120] K. Englehart and B. Hudgins, 'A Robust, Real-Time Control Scheme for Multifunction Myoelectric Control', *IEEE Transactions on Biomedical Engineering*, vol. 50, no. 7. pp. 848–854, 2003.
[121] M. A. Oskoei and H. Hu, 'Support vector machine-based classification scheme for myoelectric control applied to upper limb', *IEEE Transactions on Biomedical Engineering*, vol. 55, no. 8. pp. 1956–1965, 2008.
[122] T. Lorrain, N. Jiang, and D. Farina, 'Influence of the training set on the accuracy of surface EMG classification in dynamic contractions for the control of multifunction prostheses', *Journal of NeuroEngineering and Rehabilitation*, vol. 8, no. 1. 2011.
[123] N. Nazmi, M. A. A. Rahman, S. I. Yamamoto, S. A. Ahmad, H. Zamzuri, and S. A. Mazlan, 'A review of classification techniques of EMG signals during isotonic and isometric contractions', *Sensors (Switzerland)*, vol. 16, no. 8. 2016.
[124] M. Ortiz-Catalan, 'Cardinality as a highly descriptive feature in myoelectric pattern recognition for decoding motor volition', *Front. Neurosci.*, vol. 9, 2015.
[125] A. Phinyomark, A. Nuidod, P. Phukpattaranont, and C. Limsakul, 'Feature extraction and reduction of wavelet transform coefficients for EMG pattern classification', *Elektron. ir Elektrotechnika*, vol. 122, no. 6, pp. 27–32.
[126] N. Parajuli *et al.*, 'Real-time EMG based pattern recognition control for hand prostheses: A review on existing methods, challenges and future implementation', *Sensors (Switzerland)*, vol. 19, no. 20. 2019.
[127] M. Hakonen, H. Piitulainen, and A. Visala, 'Current state of digital signal processing in myoelectric interfaces and related applications', *Biomedical Signal Processing and Control*, vol. 18. pp. 334–359, 2015.
[128] R. Boostani and M. H. Moradi, 'Evaluation of the forearm EMG signal features for the control of a prosthetic hand', *Physiological Measurement*, vol. 24, no. 2. pp. 309–319, 2003.
[129] L. Hargrove, Y. Losier, B. Lock, K. Englehart, and B. Hudgins, 'A real-time pattern recognition based myoelectric control usability study implemented in a virtual environment', in *2007 29th Annual International Conference of the IEEE Engineering in Medicine and Biology Society*, 2007, pp. 4842–4845.

[130] M. B. I. Reaz, M. S. Hussain, and F. Mohd-Yasin, 'Techniques of EMG signal analysis: detection, processing, classification and applications', *Biol. Proced. Online*, vol. 8, no. 1, pp. 11–35, 2006.
[131] P.-G. Jung, G. Lim, S. Kim, and K. Kong, 'A wearable gesture recognition device for detecting muscular activities based on air-pressure sensors', *IEEE Trans. Ind. Informatics*, vol. 11, no. 2, pp. 485–494, 2015.
[132] A. Jaramillo-Yánez, M. E. Benalcázar, and E. Mena-Maldonado, 'Real-time hand gesture recognition using surface electromyography and machine learning: A systematic literature review', *Sensors*, vol. 20, p. 2467, 2020.
[133] S. BIOPAC Systems Inc, 'BIOPAC SITE'. [Online]. Available: https://www.biopac.com/. [Accessed: 15-Oct-2020].
[134] M. Z. Jamal, 'Signal Acquisition Using Surface EMG and Circuit Design Considerations for Robotic Prosthesis', *Comput. Intell. Electromyogr. Anal. Perspect. Curr. Appl. Futur. Challenges*, vol. 18, pp. 427–448, 2012.
[135] G. Li, Y. Li, L. Yu, and Y. Geng, 'Conditioning and sampling issues of EMG signals in motion recognition of multifunctional myoelectric prostheses', *Annals of Biomedical Engineering*, vol. 39, no. 6. pp. 1779–1787, 2011.
[136] G. De Luca, 'Fundamental Concepts in EMG Signal Acquisition', no. March. pp. 1–31, 2003.
[137] R. Oshana, 'DSP Software Development Techniques for Embedded and Real-Time Systems', *DSP Software Development Techniques for Embedded and Real-Time Systems*. 2006.
[138] V. R. Zschorlich, 'Digital filtering of EMG-SIGNALS', *Electromyography and Clinical Neurophysiology*, vol. 29, no. 2. pp. 81–86, 1989.
[139] P. Podder, M. Mehedi Hasan, M. Rafiqul Islam, and M. Sayeed, 'Design and Implementation of Butterworth, Chebyshev-I and Elliptic Filter for Speech Signal Analysis', *International Journal of Computer Applications*, vol. 98, no. 7. pp. 12–18, 2014.
[140] S. Mokhatab and W. A. Poe, 'Process Modeling in the Natural Gas Processing Industry', *Handbook of Natural Gas Transmission and Processing*. pp. 511–541, 2012.
[141] R. Oshana, 'Overview of DSP Algorithms', in *DSP for Embedded and Real-Time Systems*, 2012, pp. 113–131.
[142] M. Chakraborty and S. Das, 'Determination of Signal to Noise Ratio of Electrocardiograms Filtered by Band Pass and Savitzky-Golay Filters', *Procedia Technology*, vol. 4. pp. 830–833, 2012.
[143] S. Delsys, 'How to improve EMG signal quality', 2019. [Online]. Available: https://delsys.com/emgworks/signal-quality-monitor/improve/. [Accessed: 14-Feb-2021].
[144] S. Solnik, P. DeVita, P. Rider, B. Long, and T. Hortobágyi, 'Teager-Kaiser operator improves the accuracy of EMG onset detection independent of signal-to-noise ratio', *Acta of Bioengineering and Biomechanics*, vol. 10, no. 2. pp. 65–68, 2008.
[145] S. N. Kale and S. V. Dudul, 'Intelligent Noise Removal from EMG Signal Using Focused Time-Lagged Recurrent Neural Network', *Applied Computational Intelligence and Soft Computing*, vol. 2009. pp. 1–12, 2009.
[146] A. Phinyomark, C. Limsakul, and P. Phukpattaranont, 'Application of wavelet analysis in EMG feature extraction for pattern classification', *Measurement Science Review*, vol. 11, no. 2. pp. 45–52, 2011.
[147] R. L. Ortolan, R. N. Mori, R. R. Pereira, C. M. Cabral, J. C. Pereira, and A. Cliquet, 'Evaluation of adaptive nonadaptive filtering and wavelet transform techniques for noise reduction in EMG mobile acquisition equipment', *IEEE Trans. neural Syst. Rehabil. Eng.*, vol. 11, pp. 60–69, 2003.
[148] A. Phinyomark, P. Phukpattaranont, and C. Limsakul, 'The Usefulness of Wavelet Transform to Reduce Noise in the SEMG Signal', in *EMG Methods for Evaluating Muscle and Nerve Function*, M. Schwartz, Ed. InTech, 2012, pp. 107–132.
[149] J. Taelman, S. Van Huffel, and A. Spaepen, 'Wavelet-independent component analysis to remove electrocardiography contamination in surface electromyography', *Annual International Conference of the IEEE Engineering in Medicine and Biology - Proceedings*. pp. 682–685, 2007.
[150] J. Kilby and H. G. Hosseini, 'Wavelet analysis of Surface Electromyography signals', *Annual International Conference of the IEEE Engineering in Medicine and Biology - Proceedings*, vol. 26 I. pp. 384–387, 2004.

[151] X. Zhang, Y. Wang, and R. P. S. Han, 'Wavelet transform theory and its application in EMG signal processing', *Proceedings - 2010 7th International Conference on Fuzzy Systems and Knowledge Discovery, FSKD 2010*, vol. 5. pp. 2234–2238, 2010.
[152] A. Phinyomark, P. Phukpattaranont, and C. Limsakul, 'Wavelet-based denoising algorithm for robust EMG pattern recognition', *Fluctuation and Noise Letters*, vol. 10, no. 2. pp. 157–167, 2011.
[153] D. L. Donoho and J. M. Johnstone, 'Ideal spatial adaptation by wavelet shrinkage', *Biometrika*, vol. 81, no. 3. pp. 425–455, 1994.
[154] X. Guo, P. Yang, H. Liu, and W. Yan, 'Research and analysis on the effect of joint angle on EMG in thigh muscles', *2005 First International Conference on Neural Interface and Control, Proceedings*. pp. 139–142, 2005.
[155] Q. Zhang and Z. Luo, 'Wavelet de-noising of electromyography', *2006 IEEE International Conference on Mechatronics and Automation, ICMA 2006*, vol. 2006. pp. 1553–1558, 2006.
[156] P. A Konrad, 'The ABC of EMG', *A Pract. Introd. to Kinesiol. Electromyogr.*, vol. 1, pp. 30–5, 2005.
[157] Y. St-Amant, D. Rancourt, and E. A. Clancy, 'Effect of smoothing window length on RMS EMG amplitude estimates', in *Bioengineering, Proceedings of the Northeast Conference*, 1996, pp. 93–94.
[158] A. S. P. Sousa and J. M. R. S. Tavares, 'Surface electromyographic amplitude normalization methods: A review', *Electromyography: New Developments, Procedures and Applications*. pp. 85–102, 2012.
[159] Y. Lin, R. Palaniappan, P. De Wilde, and L. Li, 'A normalisation approach improves the performance of inter-subject sEMG-based hand gesture recognition with a ConvNet', *Proceedings of the Annual International Conference of the IEEE Engineering in Medicine and Biology Society, EMBS*, vol. 2020-July. pp. 649–652, 2020.
[160] K. S. Kim, H. H. Choi, C. S. Moon, and C. W. Mun, 'Comparison of k-nearest neighbor, quadratic discriminant and linear discriminant analysis in classification of electromyogram signals based on the wrist-motion directions', *Current Applied Physics*, vol. 11, no. 3. pp. 740–745, 2011.
[161] D. Tkach, H. Huang, and T. A. Kuiken, 'Study of stability of time-domain features for electromyographic pattern recognition', *Journal of NeuroEngineering and Rehabilitation*, vol. 7, no. 1. 2010.
[162] S. Negi, Y. Kumar, and V. M. Mishra, 'Feature extraction and classification for EMG signals using linear discriminant analysis', *Proceedings - 2016 International Conference on Advances in Computing, Communication and Automation (Fall), ICACCA 2016*. 2016.
[163] A. Phinyomark, S. Hirunviriya, C. Limsakul, and P. Phukpattaranont, 'Evaluation of EMG feature extraction for hand movement recognition based on euclidean distance and standard deviation', *ECTI-CON 2010 - The 2010 ECTI International Conference on Electrical Engineering/Electronics, Computer, Telecommunications and Information Technology*. pp. 856–860, 2010.
[164] C. Spiewak, 'A Comprehensive Study on EMG Feature Extraction and Classifiers', *Open Access Journal of Biomedical Engineering and Biosciences*, vol. 1, no. 1. 2018.
[165] A. Waris and E. N. Kamavuako, 'Effect of threshold values on the combination of EMG time domain features: Surface versus intramuscular EMG', *Biomedical Signal Processing and Control*, vol. 45. pp. 267–273, 2018.
[166] S. Abbaspour, M. Lindén, H. Gholamhosseini, A. Naber, and M. Ortiz-Catalan, 'Evaluation of surface EMG-based recognition algorithms for decoding hand movements', *Medical and Biological Engineering and Computing*, vol. 58, no. 1. pp. 83–100, 2020.
[167] D. C. Toledo-Perez, J. Rodriguez-Resendiz, and R. A. Gomez-Loenzo, 'A study of computing zero crossing methods and an improved proposal for EMG signals', *IEEE Access*, vol. 8. pp. 8783–8790, 2020.
[168] A. Phinyomark, P. Phukpattaranont, and C. Limsakul, 'Fractal analysis features for weak and single-channel upper-limb EMG signals', *Expert Systems with Applications*, vol. 39, no. 12. pp. 11156–11163, 2012.
[169] M. V. Markova, D. O. Shestopalov, and A. P. Nikolaev, 'Estimation of features informativeness

of the EMG signal in the problem of forearm prosthesis controlling', *Proceedings - 2018 Ural Symposium on Biomedical Engineering, Radioelectronics and Information Technology, USBEREIT 2018*. pp. 53–56, 2018.
[170] A. Phinyomark, P. Phukpattaranont, and C. Limsakul, 'Feature reduction and selection for EMG signal classification', *Expert Systems with Applications*, vol. 39, no. 8. pp. 7420–7431, 2012.
[171] K. Ernest Nlandu, S. Erik Justin, and E. Kevin Brian, 'Determination of optimum threshold values for EMG time domain features; a multi-dataset investigation', *Journal of Neural Engineering*, vol. 13, no. 4. p. 46011, 2016.
[172] F. Lotte, M. Congedo, A. Lécuyer, F. Lamarche, and B. Arnaldi, 'A review of classification algorithms for EEG-based brain-computer interfaces', *Journal of Neural Engineering*, vol. 4, no. 2. 2007.
[173] A. Phinyomark, F. Quaine, S. Charbonnier, C. Serviere, F. Tarpin-Bernard, and Y. Laurillau, 'EMG feature evaluation for improving myoelectric pattern recognition robustness', *Expert Systems with Applications*, vol. 40, no. 12. pp. 4832–4840, 2013.
[174] B. Saeed, S. O. Gilani, Z. U. Rehman, M. Jamil, A. Waris, and M. N. Khan, 'Comparative Analysis of Classifiers for EMG Signals', *2019 IEEE Canadian Conference of Electrical and Computer Engineering, CCECE 2019*. 2019.
[175] M. F. Wahid, R. Tafreshi, M. Al-Sowaidi, and R. Langari, 'Subject-independent hand gesture recognition using normalization and machine learning algorithms', *Journal of Computational Science*, vol. 27. pp. 69–76, 2018.
[176] T. Li, S. Zhu, and M. Ogihara, 'Using discriminant analysis for multi-class classification: An experimental investigation', *Knowledge and Information Systems*, vol. 10, no. 4. pp. 453–472, 2006.
[177] K. Tappa and U. Jammalamadaka, 'Novel biomaterials used in medical 3D printing techniques', *J. Funct. Biomater.*, vol. 9, no. 1, p. 17, 2018.
[178] H. Shin, S. Jo, and A. G. Mikos, 'Biomimetic materials for tissue engineering', *Biomaterials*, vol. 24, no. 24, pp. 4353–4364, 2003.
[179] S. H. Masood, 'Advances in Fused Deposition Modeling', in *Comprehensive Materials Processing*, 2014.
[180] J. Wang, L. Tang, and J. E Bronlund, 'Surface EMG Signal Amplification and Filtering', *Int. J. Comput. Appl.*, vol. 82, no. 1, pp. 15–22, 2013.
[181] E. A. Clancy, E. L. Morin, and R. Merletti, 'Sampling, noise-reduction and amplitude estimation issues in surface electromyography', *Journal of Electromyography and Kinesiology*, vol. 12, no. 1. pp. 1–16, 2002.
[182] R. H. Chowdhury, M. B. I. Reaz, M. A. Bin Mohd Ali, A. A. A. Bakar, K. Chellappan, and T. G. Chang, 'Surface electromyography signal processing and classification techniques', *Sensors (Switzerland)*, vol. 13, no. 9. pp. 12431–12466, 2013.
[183] M. B. I. Reaz, M. S. Hussain, and F. Mohd-Yasin, 'Techniques of EMG signal analysis: detection, processing, classification and applications', *Biol. Proced. Online*, vol. 8, pp. 11–35, 2006.
[184] E. A. Clancy, E. L. Morin, and R. Merletti, 'Sampling, noise-reduction and amplitude estimation issues in surface electromyography', *J. Electromyogr. Kinesiol.*, vol. 12, pp. 1–16, 2002.
[185] A. Phinyomark, C. Limsakul, and P. Phukpattaranont, 'A comparative study of wavelet denoising for multifunction myoelectric control', *Proceedings - 2009 International Conference on Computer and Automation Engineering, ICCAE 2009*. pp. 21–25, 2009.
[186] M. S. Hussain, M. B. I. Reaz, M. I. Ibrahimy, A. F. Ismail, and F. Mohd-Yasin, 'Wavelet based noise removal from EMG signals', *Informacije MIDEM*, vol. 37, no. 2. pp. 94–97, 2007.
[187] M. S. Hussain, M. B. I. Reaz, F. Mohd-Yasin, and M. I. Ibrahimy, 'Electromyography signal analysis using wavelet transform and higher order statistics to determine muscle contraction', *Expert Systems*, vol. 26, no. 1. pp. 35–48, 2009.
[188] N. M. Sobahi, 'Denoising of EMG Signals Based on Wavelet Transform', vol. 01, no. 05. pp. 17–23, 2011.
[189] E. K., H. B., and P. P.A., 'A wavelet-based continuous classification scheme for multifunction myoelectric control', *IEEE Transactions on Biomedical Engineering*, vol. 48, no. 3. pp. 302–311, 2001.

[190] A. Phinyomark, C. Limsakul, and P. Phukpattaranont, ‘EMG denoising estimation based on adaptive wavelet thresholding for multifunction myoelectric control’, *2009 Innovative Technologies in Intelligent Systems and Industrial Applications, CITISIA 2009*. pp. 171–176, 2009.
[191] T. Sharma and K. Veer, ‘Comparative study of wavelet denoising in myoelectric control applications’, *Journal of Medical Engineering and Technology*, vol. 40, no. 3. pp. 80–86, 2016.
[192] S. Betti, G. Zani, S. Guerra, U. Castiello, and L. Sartori, ‘Reach-to-grasp movements: A multimodal techniques study’, *Frontiers in Psychology*, vol. 9, no. JUN. 2018.
[193] J. M. LANDSMEER, ‘Power grip and precision handling.’, *Annals of the rheumatic diseases*, vol. 21. pp. 164–170, 1962.
[194] G. R. Naik, D. K. Kumar, and S. P. Arjunan, ‘Pattern classification of Myo-Electrical signal during different maximum voluntary contractions: A study using BSS techniques’, *Measurement Science Review*, vol. 10, no. 1. pp. 1–6, 2010.
[195] S. P. Arjunan and D. K. Kumar, ‘Decoding subtle forearm flexions using fractal features of surface electromyogram from single and multiple sensors’, *Journal of NeuroEngineering and Rehabilitation*, vol. 7, no. 1. 2010.
[196] R. N. Khushaba, M. Takruri, J. V. Miro, and S. Kodagoda, ‘Towards limb position invariant myoelectric pattern recognition using time-dependent spectral features’, *Neural Networks*, vol. 55. pp. 42–58, 2014.
[197] A. Alkan and M. Günay, ‘Identification of EMG signals using discriminant analysis and SVM classifier’, *Expert Systems with Applications*, vol. 39, no. 1. pp. 44–47, 2012.
[198] A. Phinyomark, P. Phukpattaranont, and C. Limsakul, ‘Feature reduction and selection for EMG signal classification’, *Expert Syst. Appl.*, vol. 39, no. 8, pp. 7420–7431, 2012.
[199] D. K. Kumar, S. P. Arjunan, and V. P. Singh, ‘Towards identification of finger flexions using single channel surface electromyography–able bodied and amputee subjects’, *J. Neuroeng. Rehabil.*, vol. 10, pp. 1–7, 2013.
[200] X. Chen, X. Zhang, Z. Y. Zhao, J. H. Yang, V. Lantz, and K. Q. Wang, ‘Multiple hand gesture recognition based on surface EMG signal’, *2007 1st International Conference on Bioinformatics and Biomedical Engineering, ICBBE*. pp. 506–509, 2007.
[201] S. W.-T., L. Z.-J., T. S.-T., C. T.-L., and Y. C.-Y., ‘A bionic hand controlled by hand gesture recognition based on surface EMG signals: A preliminary study’, *Biocybernetics and Biomedical Engineering*, vol. 38, no. 1. pp. 126–135, 2018.
[202] J. Kim, S. Mastnik, and E. André, ‘EMG-based hand gesture recognition for realtime biosignal interfacing’. p. 30, 2008.
[203] B. Wan, R. Wu, K. Zhang, and L. Liu, ‘A new subtle hand gestures recognition algorithm based on EMG and FSR’, *Proceedings of the 2017 IEEE 21st International Conference on Computer Supported Cooperative Work in Design, CSCWD 2017*. pp. 127–132, 2017.
[204] M. Georgi, C. Amma, and T. Schultz, ‘Recognizing hand and finger gestures with IMU based motion and EMG based muscle activity sensing’, *BIOSIGNALS 2015 - 8th International Conference on Bio-Inspired Systems and Signal Processing, Proceedings; Part of 8th International Joint Conference on Biomedical Engineering Systems and Technologies, BIOSTEC 2015*. pp. 99–108, 2015.
[205] A. A. Adewuyi, L. J. Hargrove, and T. A. Kuiken, ‘An Analysis of Intrinsic and Extrinsic Hand Muscle EMG for Improved Pattern Recognition Control’, *IEEE Transactions on Neural Systems and Rehabilitation Engineering*, vol. 24, no. 4. pp. 485–494, 2016.
[206] L. Paolo de, ‘Adjustments to zatsiorsky-seluyanov’s segment inertia parameters’, *Journal of Biomechanics*, vol. 29, no. 9. pp. 1223–1230, 1996.
[207] L. Brechet, M. Lucas, C. Doncarli and D. Farina, "Compression of Biomedical Signals With Mother Wavelet Optimization and Best-Basis Wavelet Packet Selection," in *IEEE Transactions on Biomedical Engineering*, vol. 54, no. 12, pp. 2186-2192, Dec. 2007, doi: 10.1109/TBME.2007.896596
[208] Hussain, M. S., Reaz, M. B. I., Mohd-Yasin, F., & Ibrahimy, M. I. (2009). Electromyography signal analysis using wavelet transform and higher order statistics to determine muscle contraction. Expert Systems, 26(1), 35-48

A. Materials used during data acquisition

Table A.1: Demographic table of the recruited volunteers

Participant Number	Age	Dominant Arm	Presence of motor issues or diseases?	Regular practice of physical exercise	Gender
1	22	Right	No	No	F
2	22	Right	No	Yes	F
3	18	Right	No	No	F
4	22	Right	No	No	F
5	22	Right	No	Yes	M
6	18	Right	No	No	M
7	22	Right	No	No	M
8	20	Left	No	Yes	M
9	20	Right	No	Yes	M
10	22	Right	No	No	F
11	19	Right	No	No	M
12	19	Right	No	No	M
13	20	Right	No	No	F
14	20	Right	No	Yes	M
15	22	Right	No	No	M
16	18	Right	No	No	F
17	21	Left	No	No	M
18	24	Left	No	Yes	M
19	19	Right	No	No	M
20	18	Right	No	No	M
21	18	Right	No	No	F
22	21	Right	No	No	F
23	20	Right	No	No	M
24	22	Right	No	No	F
25	20	Right	No	Yes	F
26	19	Left	No	Yes	F
27	22	Right	No	Yes	M
28	22	Right	No	No	M
29	22	Right	No	No	F
30	24	Right	No	No	M
31	23	Right	No	Yes	F
32	22	Right	No	No	F
33	18	Right	No	No	M
34	20	Left	No	No	F
35	20	Right	No	No	F
36	22	Right	No	No	F
37	21	Right	No	Yes	F
38	20	Right	No	Yes	F
39	19	Right	No	No	M

40	18	Right	No	No	F
41	18	Right	No	No	F
42	20	Right	No	Yes	F
43	18	Right	No	Yes	M
44	22	Right	No	No	F
45	20	Right	No	Yes	F

Consent form:

PROJECTO: Development and Optimization of a Low-Cost Upper Limb Prosthesis

INVESTIGADOR RESPONSÁVEL: Prof. Doutor Nuno Matela e Aluna Ema Lopes

Agradecemos o seu interesse e colaboração neste estudo.
Por favor, preencha o formulário que se segue. Receberá uma cópia quando sair.

1. Confirmo que li e compreendi o folheto informativo associado ao projeto. ☐
2. Foi-me dada a oportunidade de ler e considerar a informação apresentada, e fazer perguntas, as quais foram respondidas de forma satisfatória. ☐
3. Compreendo que a minha participação é voluntária e que sou livre de desistir do estudo em qualquer altura, sem ter que dar quaisquer explicações e sem quaisquer consequências. ☐
4. Compreendo que os dados recolhidos durante o estudo possam ser do conhecimento dos membros da equipa de investigação, sempre que necessário para o estudo. Autorizo que os membros da equipa tenham acesso a esses dados. ☐
5. Compreendo que, caso esta investigação venha a ser publicada, todos os dados serão mantidos anónimos e nenhuma informação será identificável como sendo minha. ☐
6. Gostaria que me fosse enviado o relatório final do estudo. ☐

   O meu endereço de e-mail é: _____
7. Gostaria de ser contactado para o endereço acima acerca de sessões ou estudos adicionais relacionados com este estudo. ☐
8. Declaro que não comuniquei nenhuma razão potencial de qualquer natureza que constitua um eventual facto de risco para a minha saúde ou integridade física. ☐
9. Declaro que participo neste estudo sem qualquer remuneração ou contrapartida, para além do ressarcimento das despesas em que tiver incorrido. ☐
10. **Declaro que tomo a minha decisão de forma inteiramente livre.** ☐
11. **Concordo em participar neste estudo.** ☐

Nome do Participante Assinatura Data

_____ ___/____/____

Sou da opinião que o participante compreendeu os aspetos relevantes da informação fornecida e está apto a tomar uma decisão informada.

Assinatura do Investigador Responsável Data

_____ ___/____/____

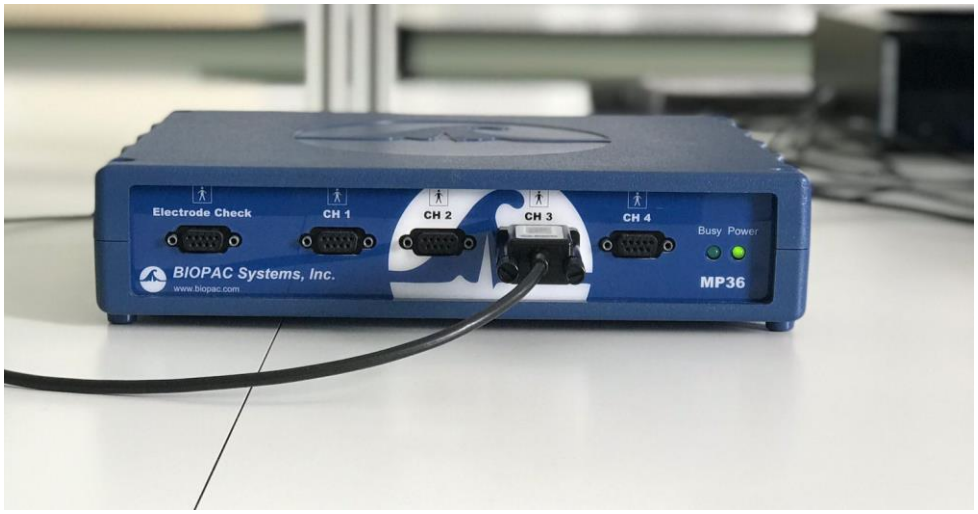

Figure A.1: BIOPAC acquisition system.


Figure A.2: Illustration of the acquired movement: Spherical Grip.

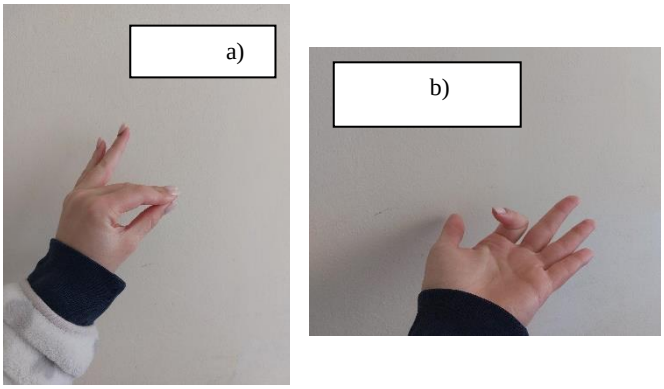

Figure A.3: Illustration of the acquired movements: a) Tripod Grip and b) Finger Flexion.

B. Power Spectrum of the signals

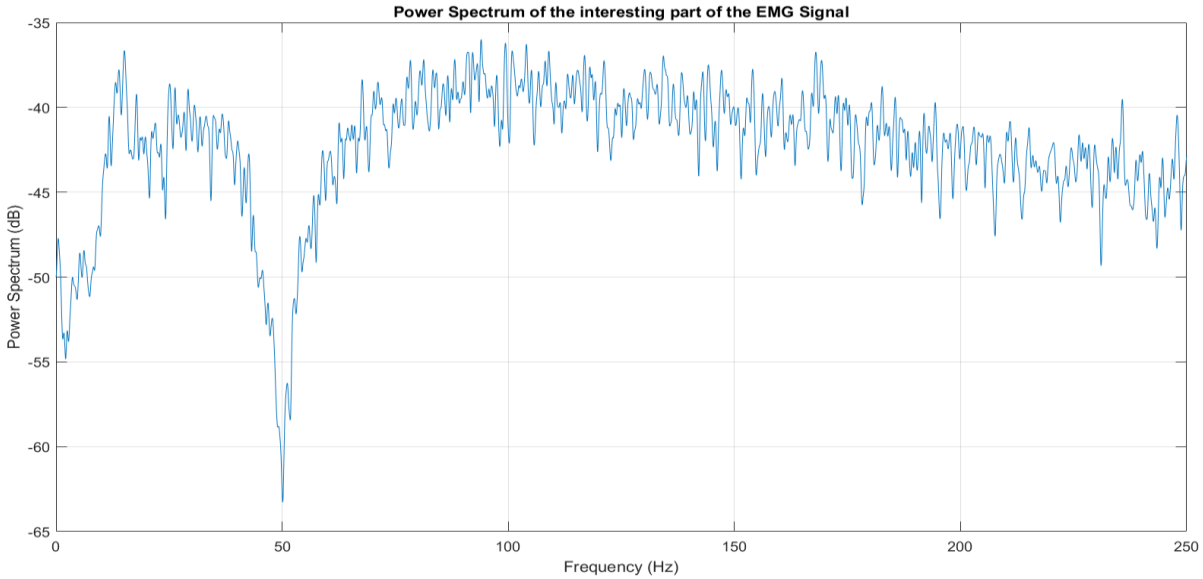

Figure B.1: Power spectrum of the signal for volunteer number 4.

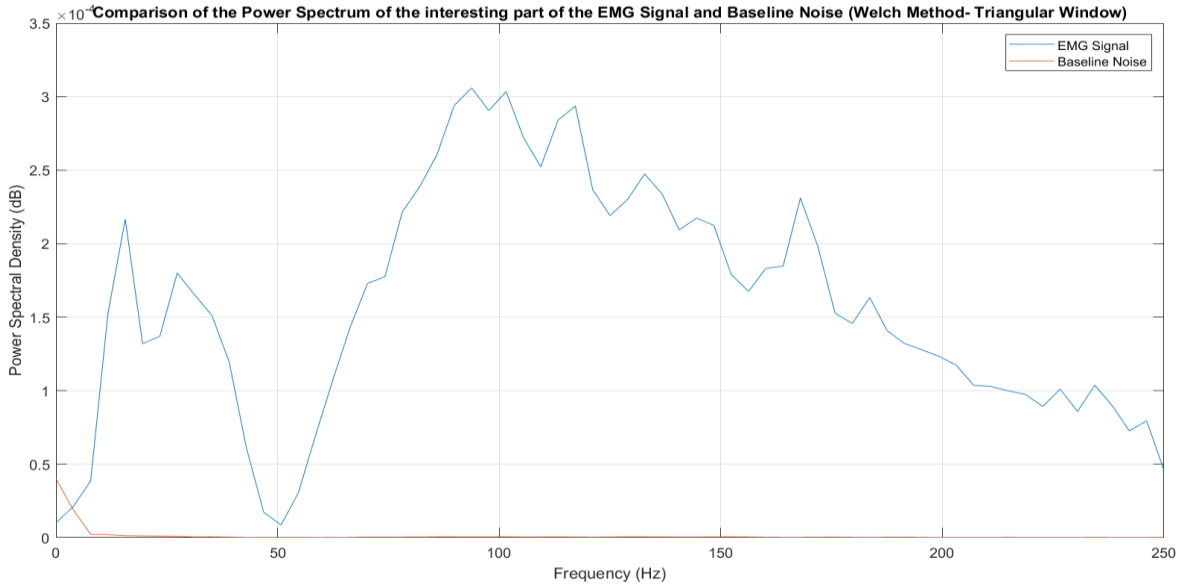

Figure B.2: Pwelch plot of the baseline noise (red line) and the interesting part of the signal (blue line) for volunteer number 4.

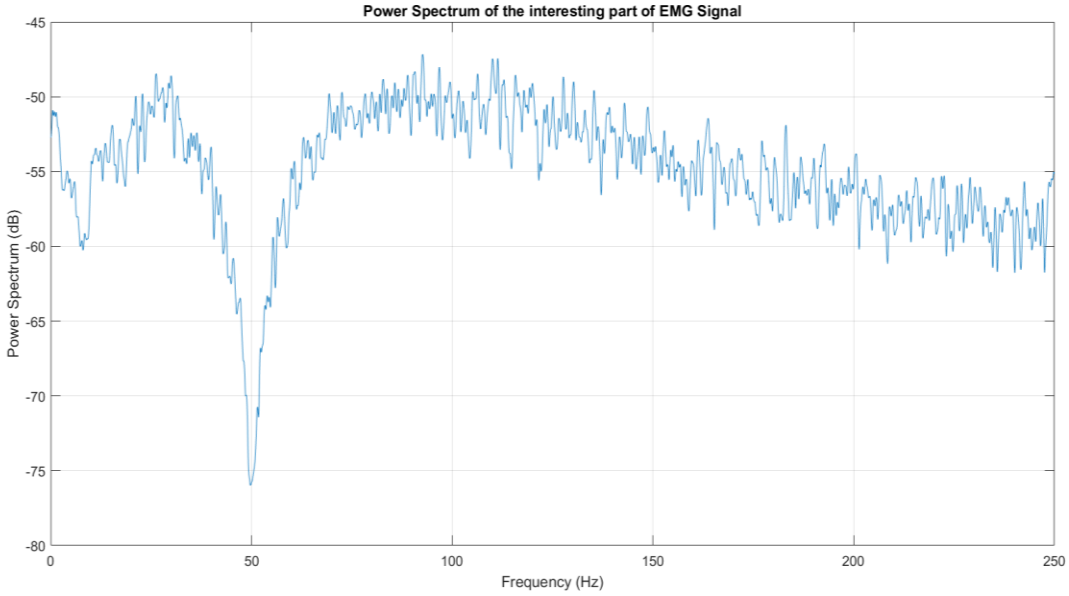

Figure B.3: Power spectrum of the signal for volunteer number 8.

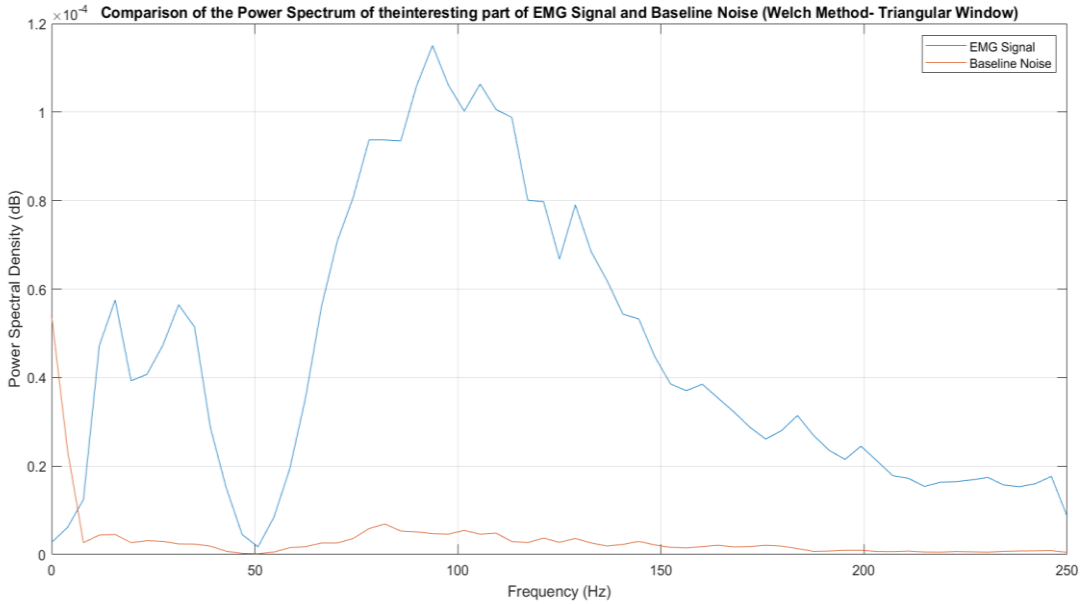

Figure B.4: Pwelch plot of the baseline noise (red line) and the interesting part of the signal (blue line) for volunteer number 8.

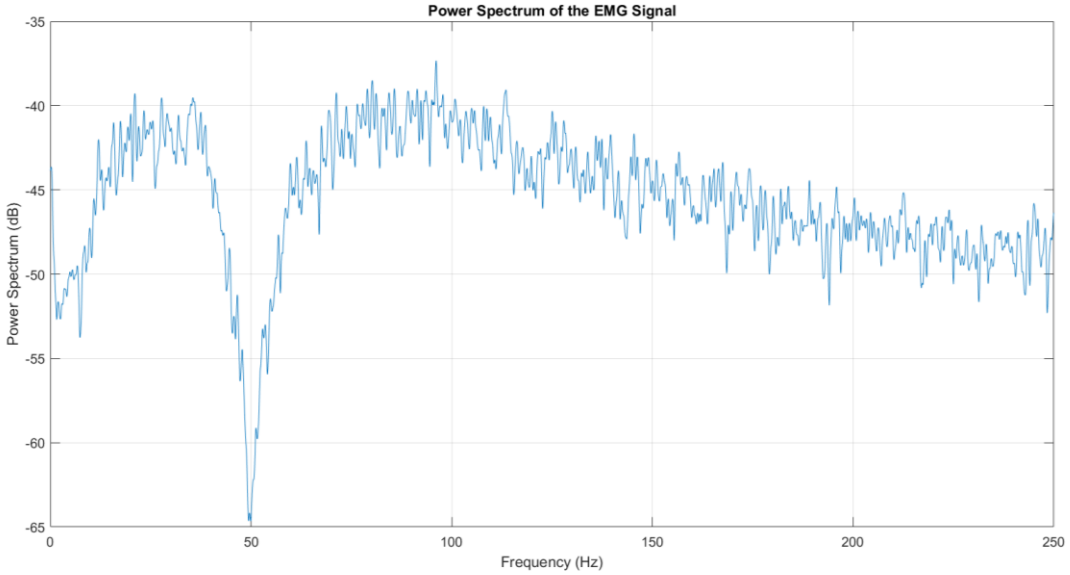

Figure B.5: Power spectrum of the signal for volunteer number 9.

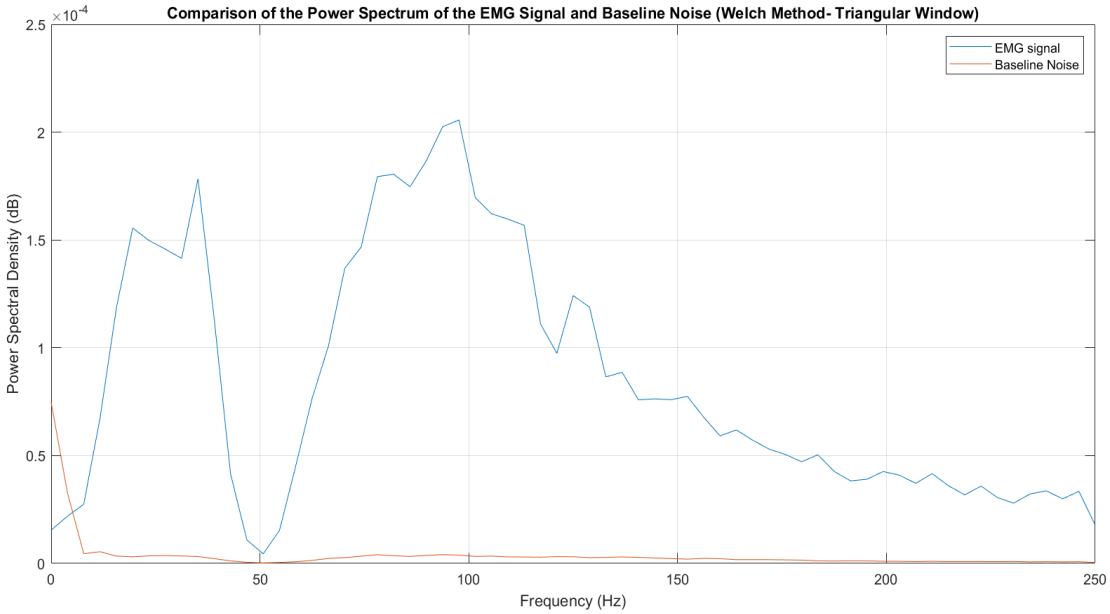

Figure B.6: Pwelch plot of the baseline noise (red line) and the interesting part of the signal (blue line) for volunteer number 9.

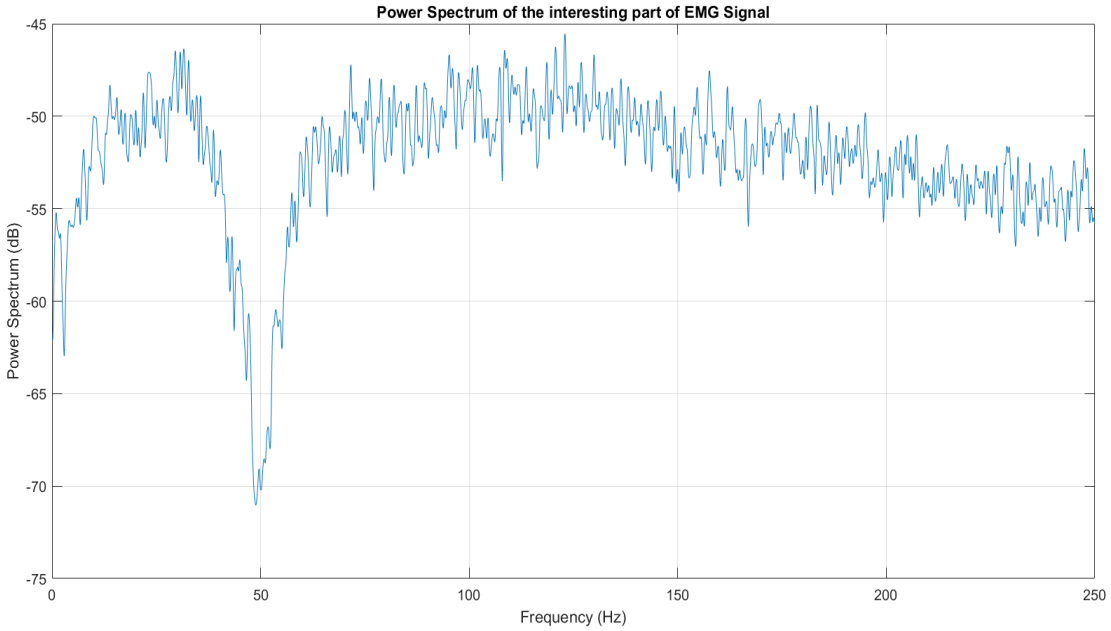

Figure B.7: Power spectrum of the signal for volunteer number 29.

Figure B.8: Pwelch plot of the baseline noise (red line) and the interesting part of the signal (blue line) for volunteer number 29.

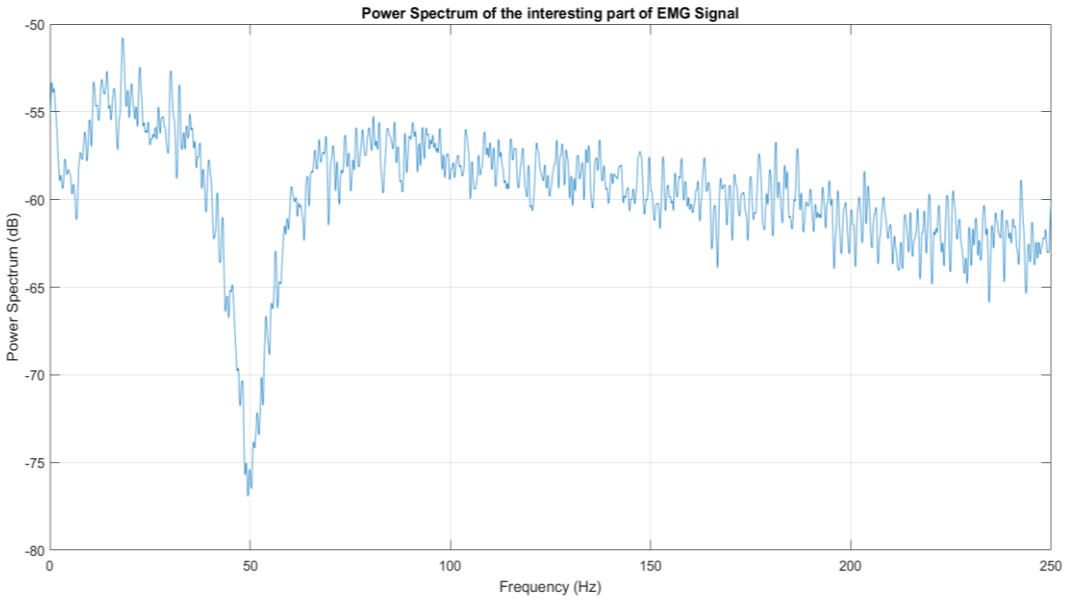

Figure B.9: Power spectrum of the signal for volunteer number 41.

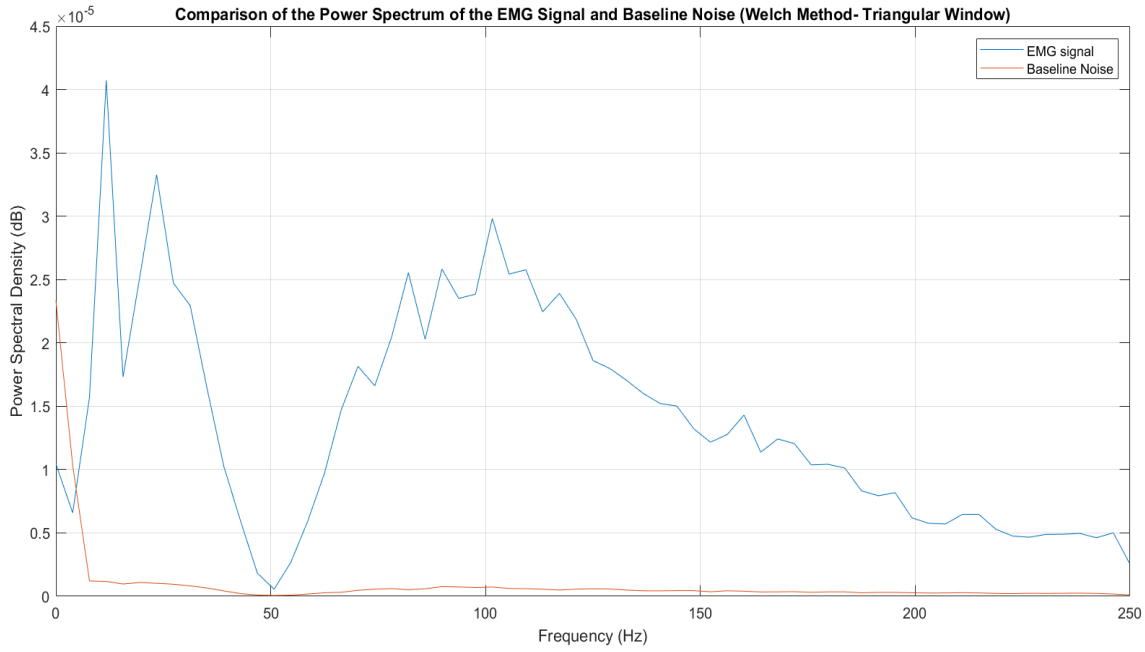

Figure B.10: Pwelch plot of the baseline noise (red line) and the interesting part of the signal (blue line) for volunteer number 41.

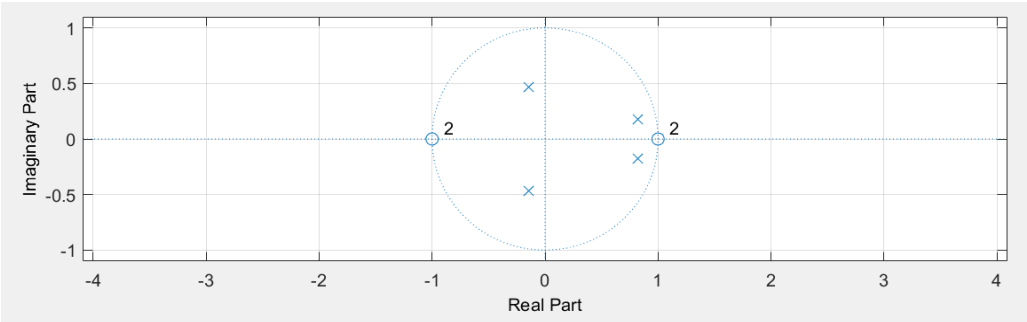

Figure B.11: Poles of the fourth-order Butterworth Bandpass for a frequency band between 20-150 *Hz*.

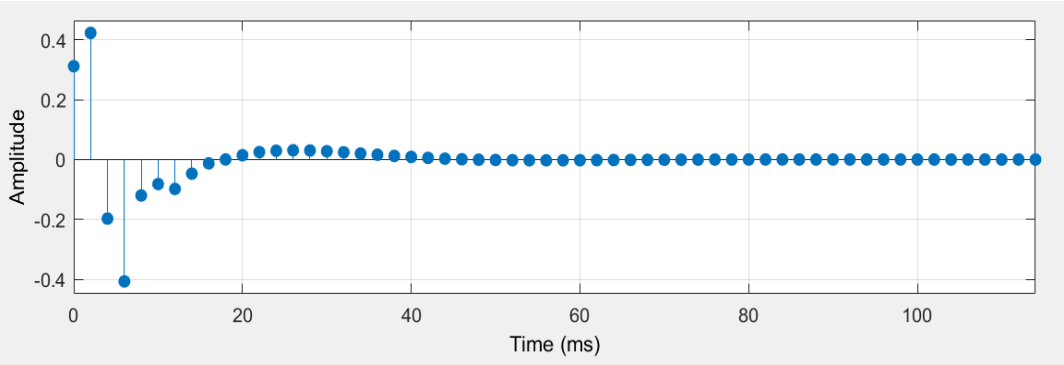

Figure B.12: Impulsive response of the fourth-order Butterworth Bandpass for a frequency band between 20-150 *Hz*.

C. Wavelet transform illustration

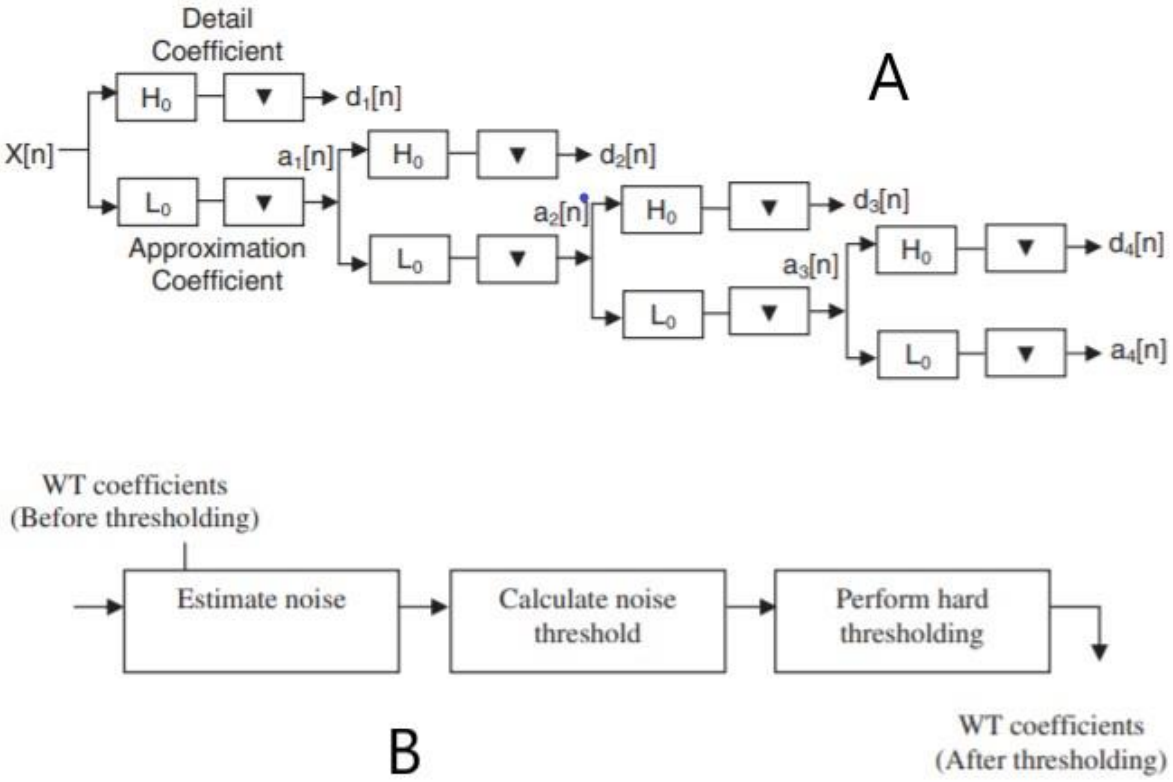

Figure C.1: Illustration of the Wavelet Transform Noise Reduction method. A- represents the application of discrete wavelet transform. First, the signal is passed through high and low pass filters (H and L, respectively). After that, in B, the detail coefficients (d[n]) are compared to a threshold. After that, the signal is reconstructed with the approximation coefficients and modified detail coefficients (extracted from: [208]).

D. Materials used in the design of the prosthetic model

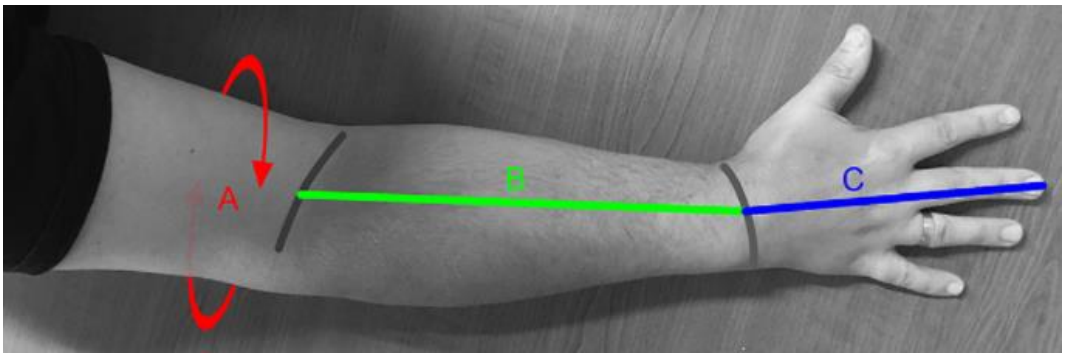

Figure D.1: Necessary measures for Assembly. A: Bicep perimeter; B: Forearm length; C: Hand Length .

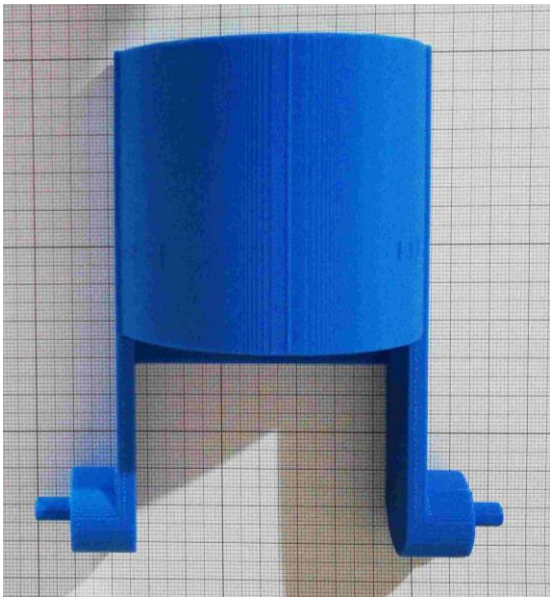

Figure D.2: Jig piece.

Figure D.3: Elastic Tension Mechanism of the fingers.

Figure D.4: Tension Mechanism of the fingers (its linked on the forearm and cuff.

Table D.2: Printing parameters.

Printer Parameters	Value
Quality	
Layer height	0.20 (*mm*)
Vertical Shells perimeter	3
Horizontal Shells – Solid Layer	3
Horizontal Shells – Bottom	3
Fill density (%)	Honeycomb
Printing temperature	220 (°C)
Bed temperature	60 (°C)
Support	
Support Type	On build plate only

E. Digital Filtering Results

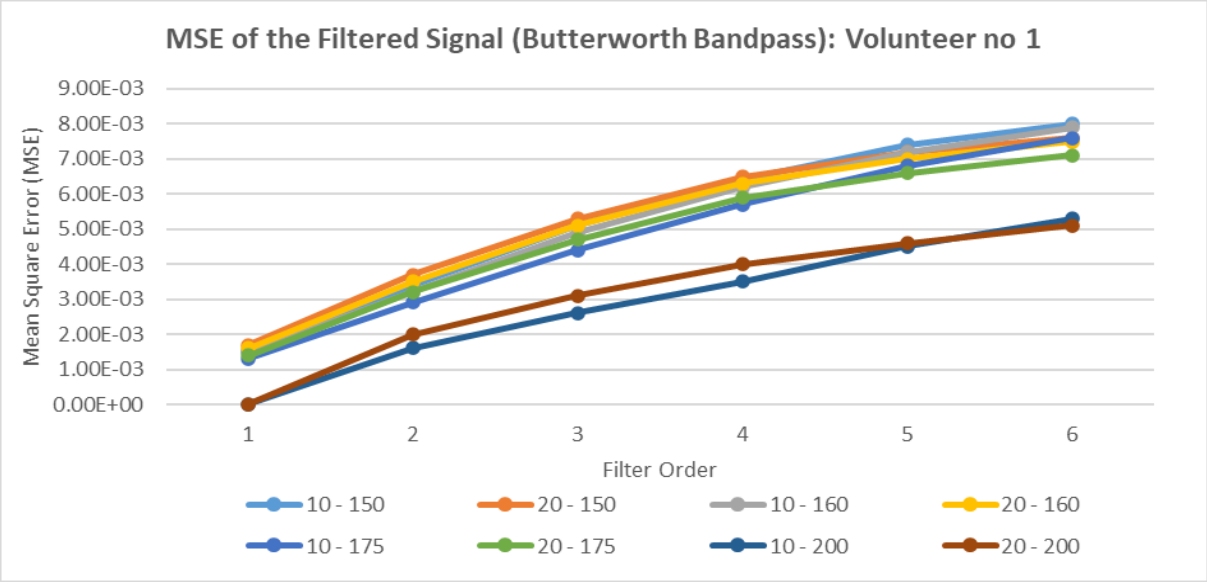

Figure E.1: MSE values of the filtered signal when six order different bandpass Butterworth filters were applied – Volunteer number 1.

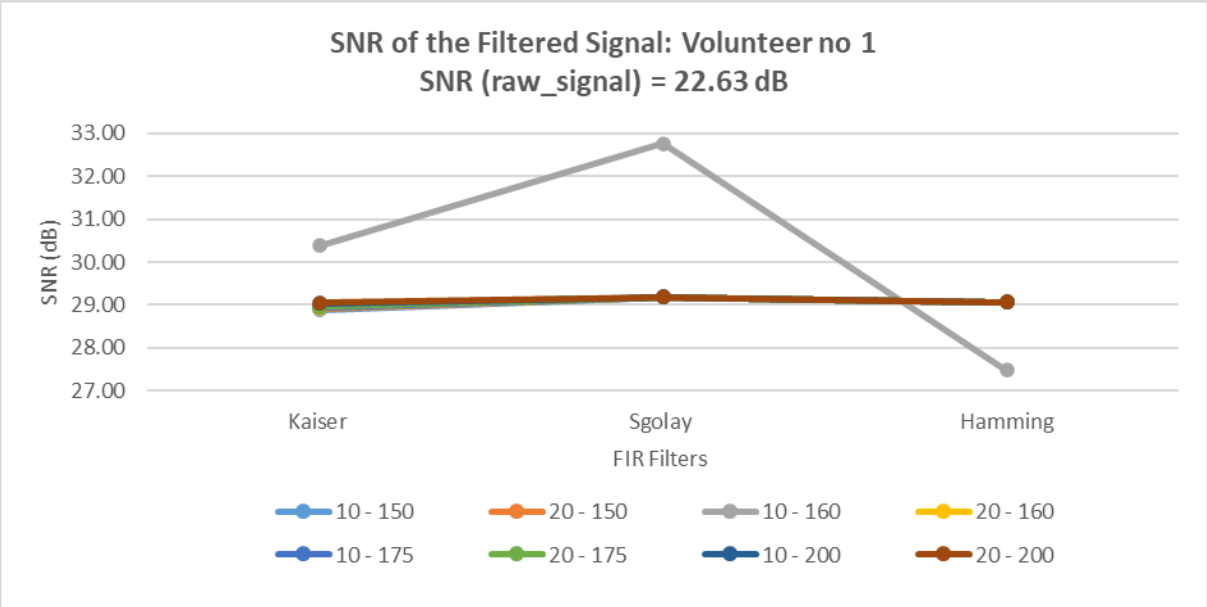

Figure E.2: SNR values of the filtered signal when the FIR filters were applied – Volunteer number 1.

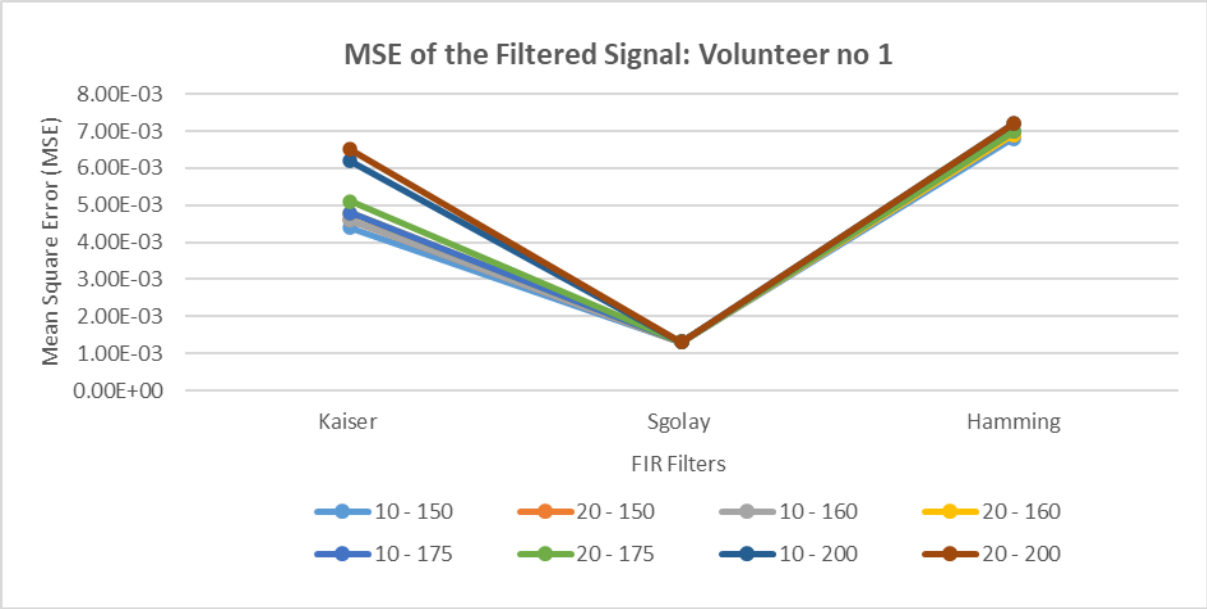

Figure E.3: MSE values of the filtered signal when six order different Bandpass Butterworth filters were applied – Volunteer number 1.

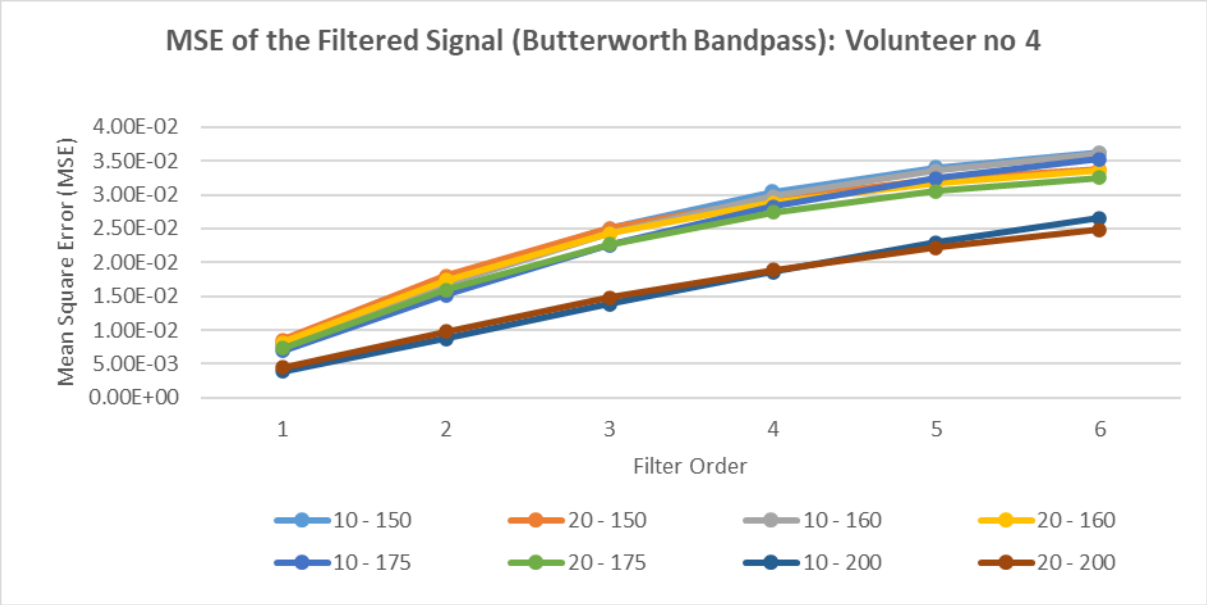

Figure E.4: MSE values of the filtered signal when six order different Bandpass Butterworth filters were applied – Volunteer number 4.

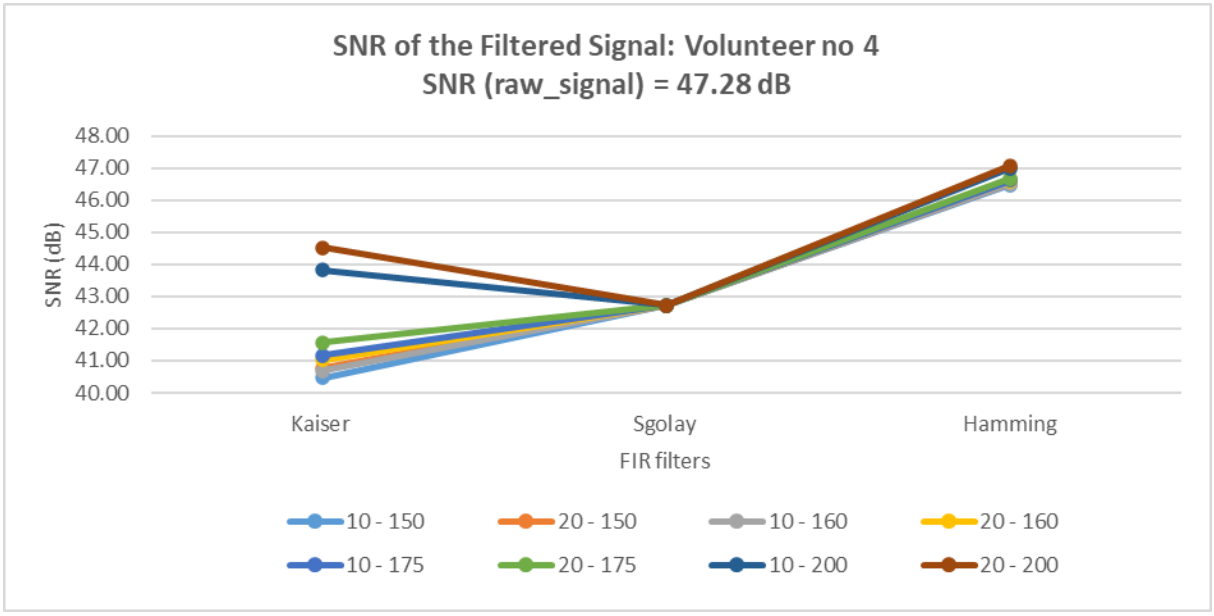

Figure E.5: SNR values of the filtered signal when the FIR filters were applied – Volunteer number 4.

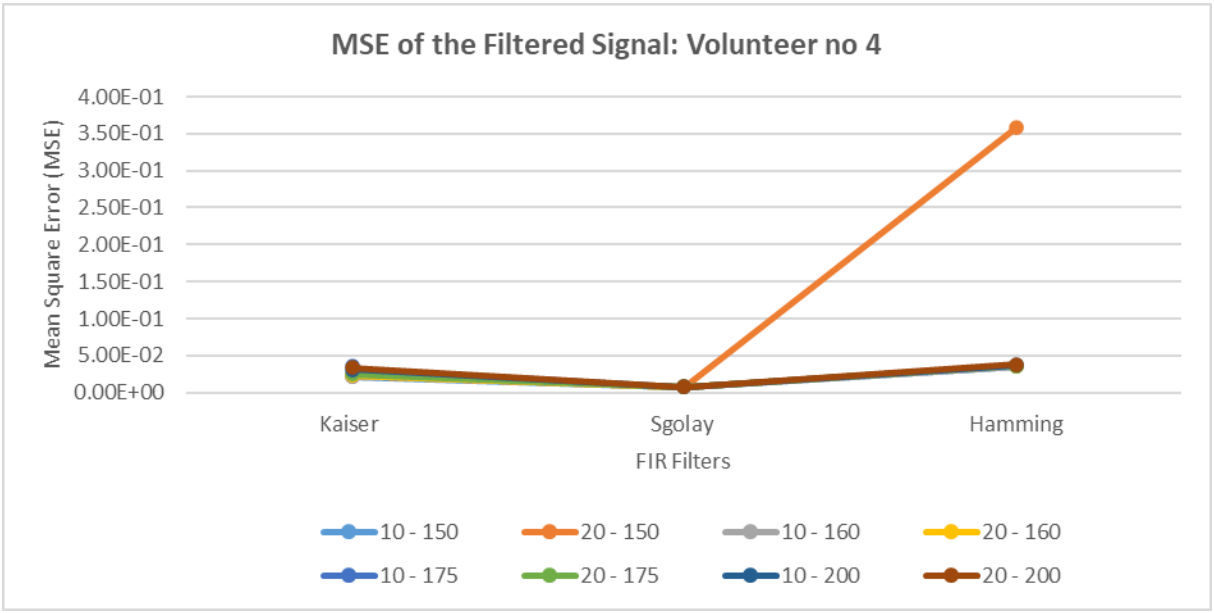

Figure E.6: MSE values of the filtered signal when the FIR filters were applied – Volunteer number 4.

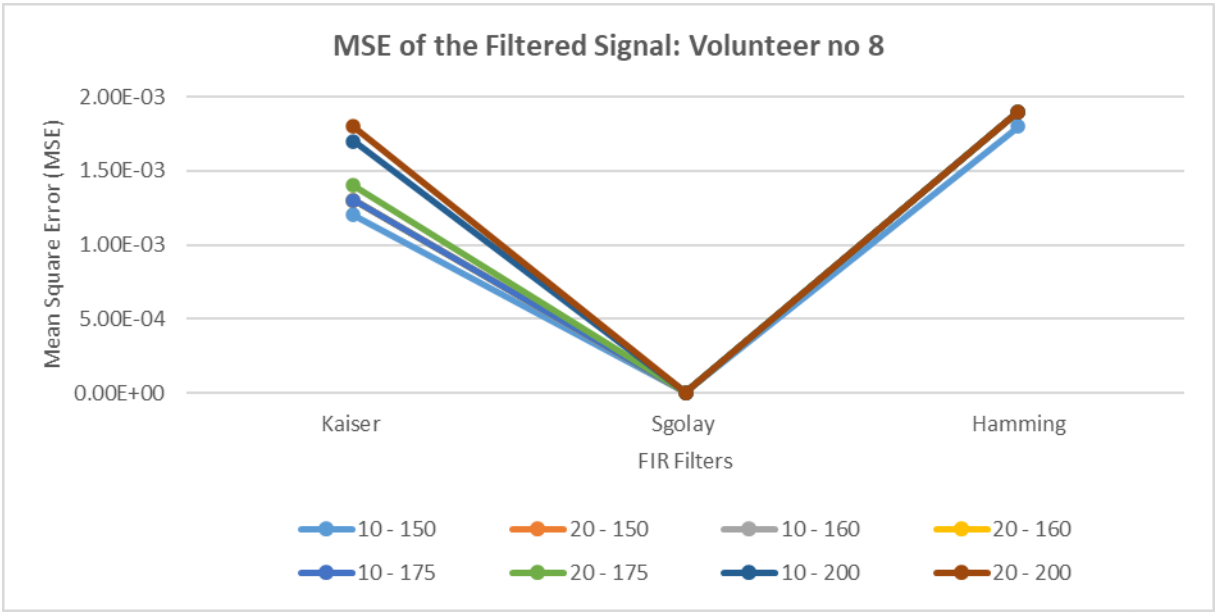

Figure E.7: MSE values of the filtered signal when six order different Bandpass Butterworth filters were applied – Volunteer number 8.

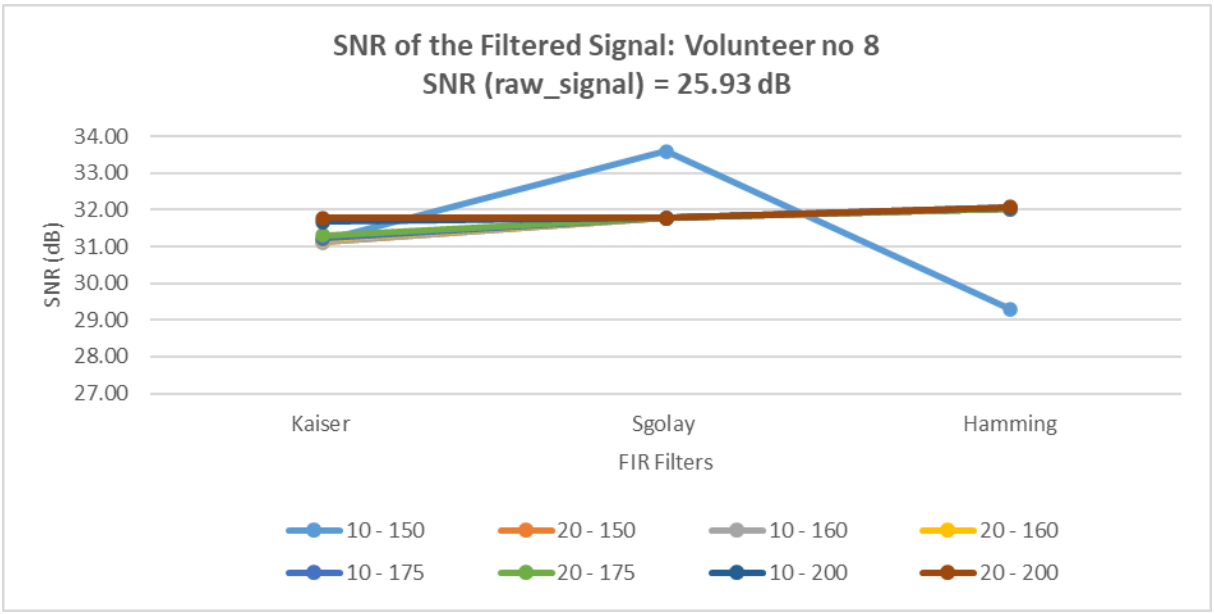

Figure E.9: MSE values of the filtered signal when the FIR filters were applied – Volunteer number 8.

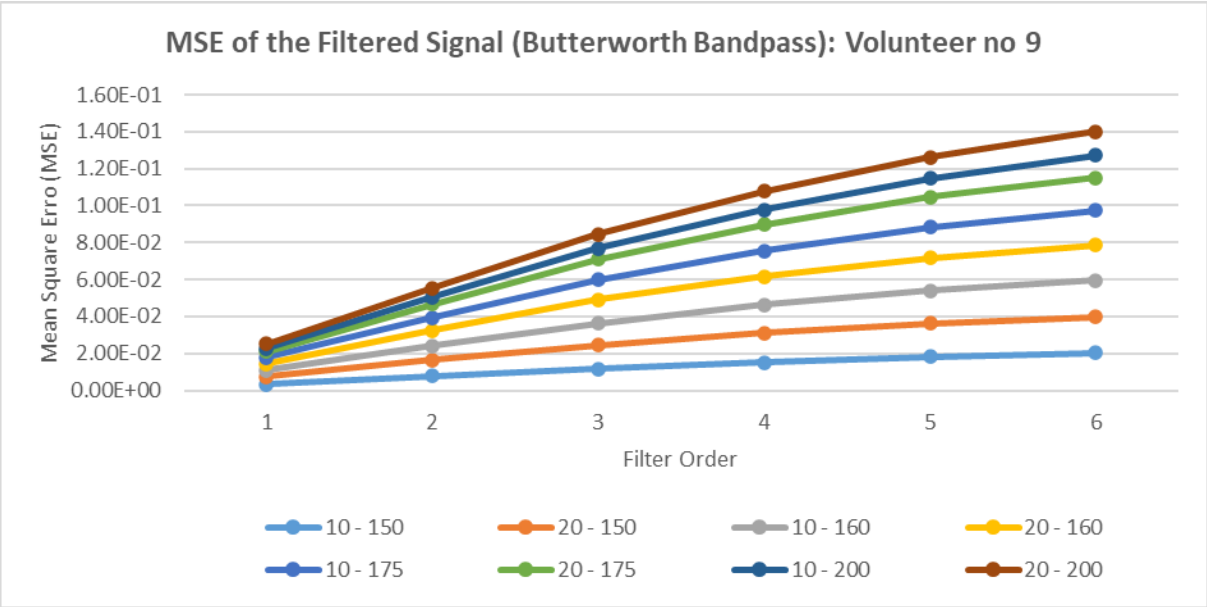

Figure E.10: MSE values of the filtered signal when six order different Bandpass Butterworth filters were applied – Volunteer number 9.

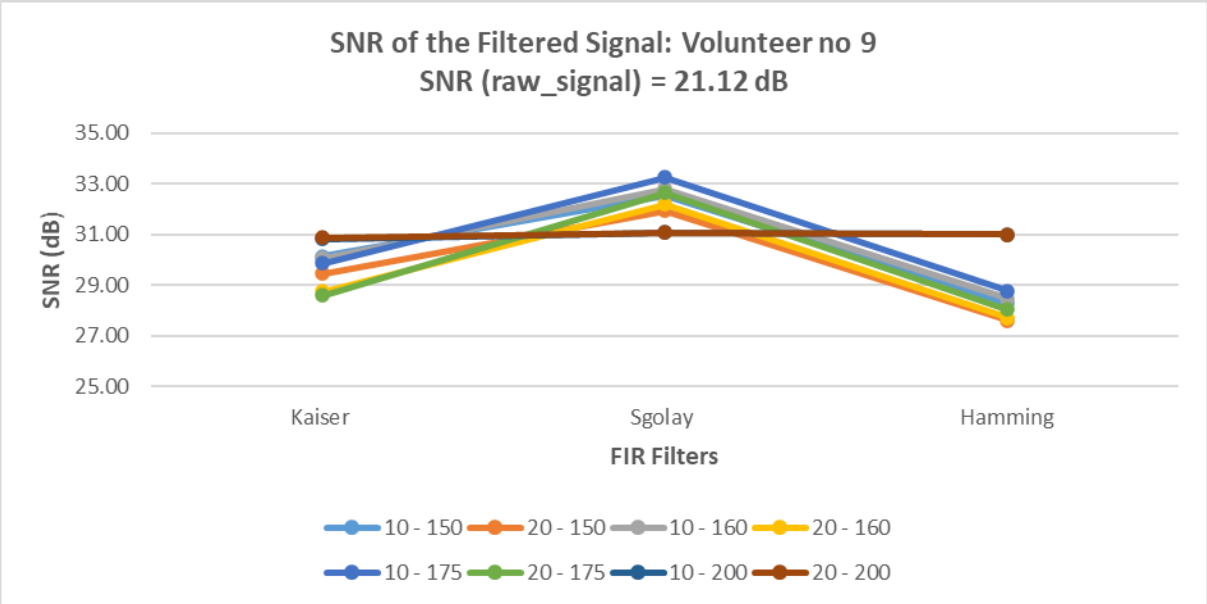

Figure E.11: SNR values of the filtered signal when the FIR filters were applied – Volunteer number 9.

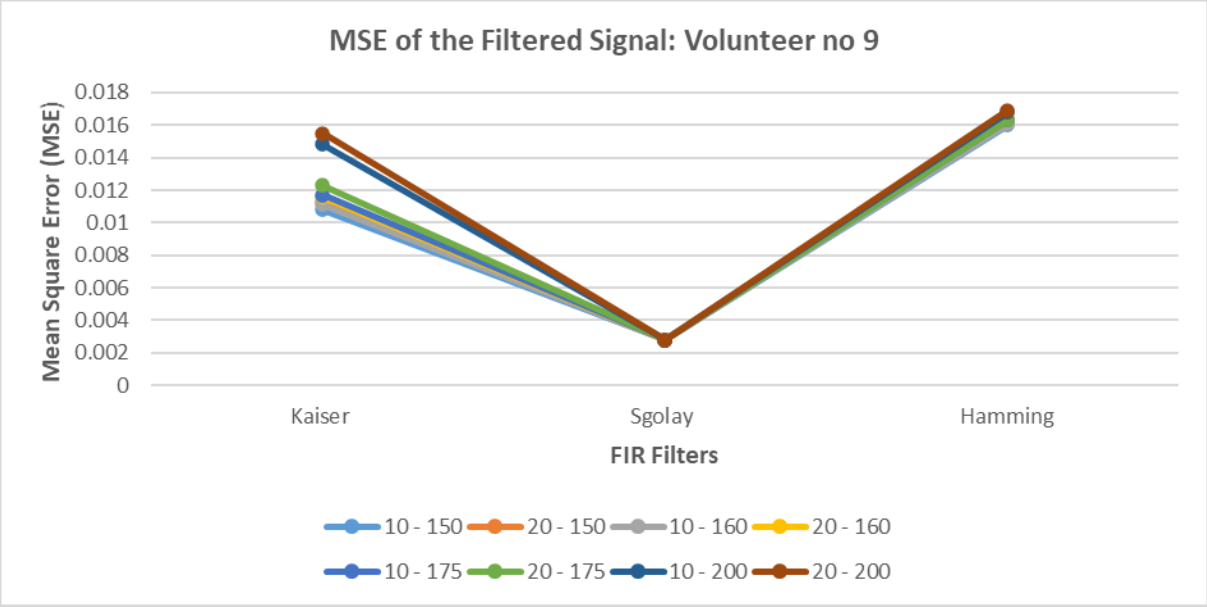

Figure E.12: MSE values of the filtered signal when the FIR filters were applied – Volunteer number 9.

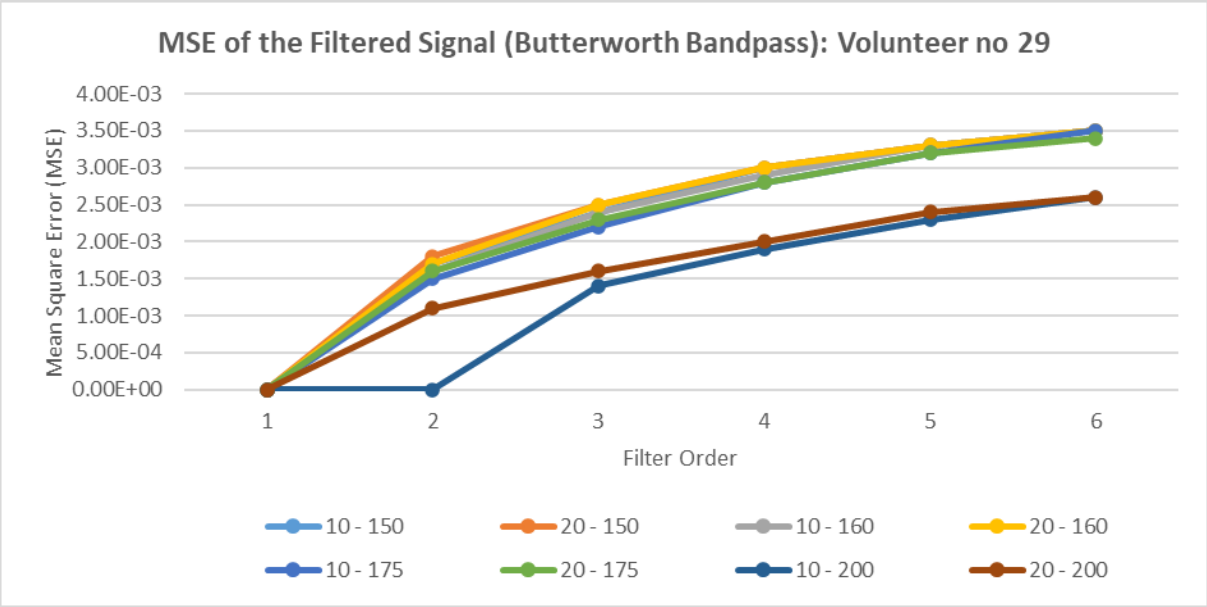

Figure E.13: MSE values of the filtered signal when six order different Bandpass Butterworth filters were applied – Volunteer number 29.

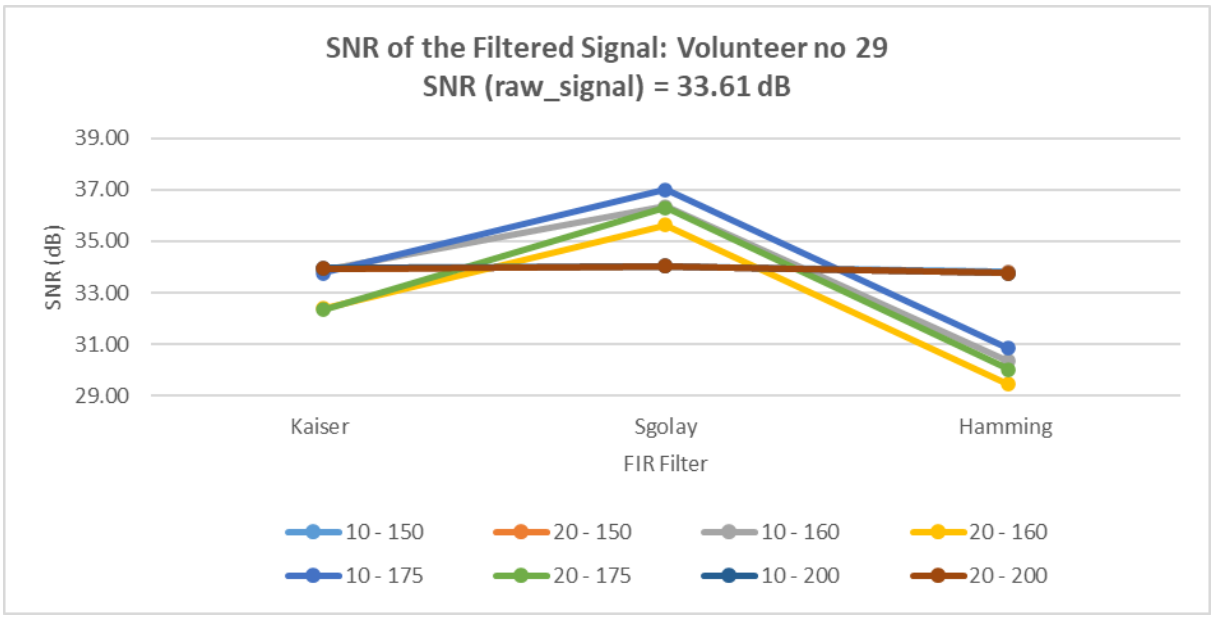

Figure E.14: MSE values of the filtered signal when the FIR filters were applied – Volunteer number 29.

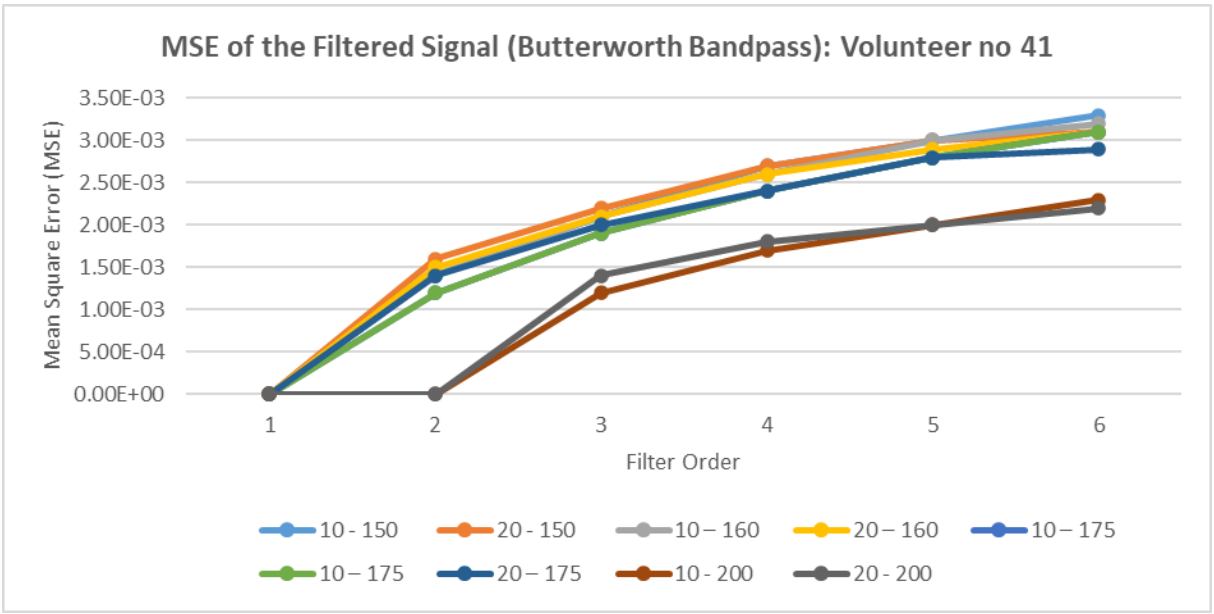

Figure E.15: MSE values of the filtered signal when six order different Bandpass Butterworth filters were applied – Volunteer number 41

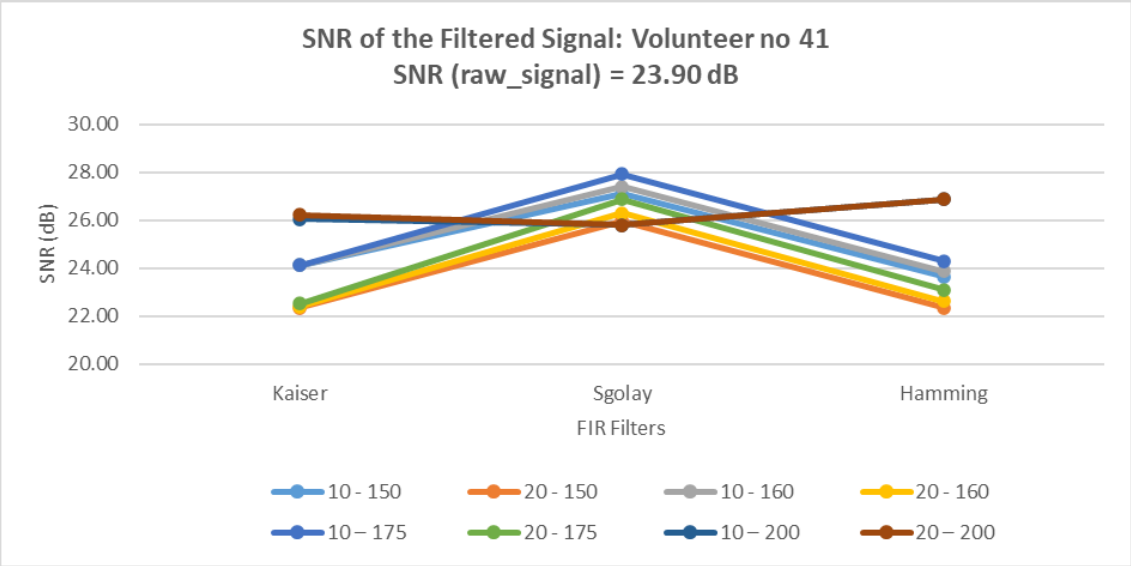

Figure E.16: SNR values of the filtered signal when the FIR filters were applied – Volunteer number 41.

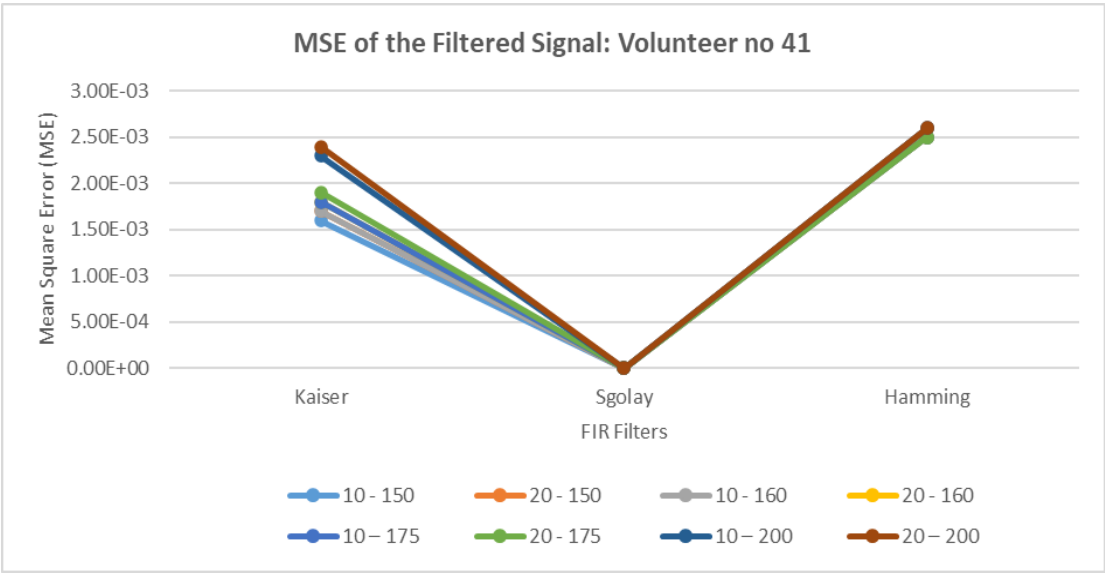

Figure E.17: MSE values of the filtered signal when the FIR filters were applied – Volunteer number 41.

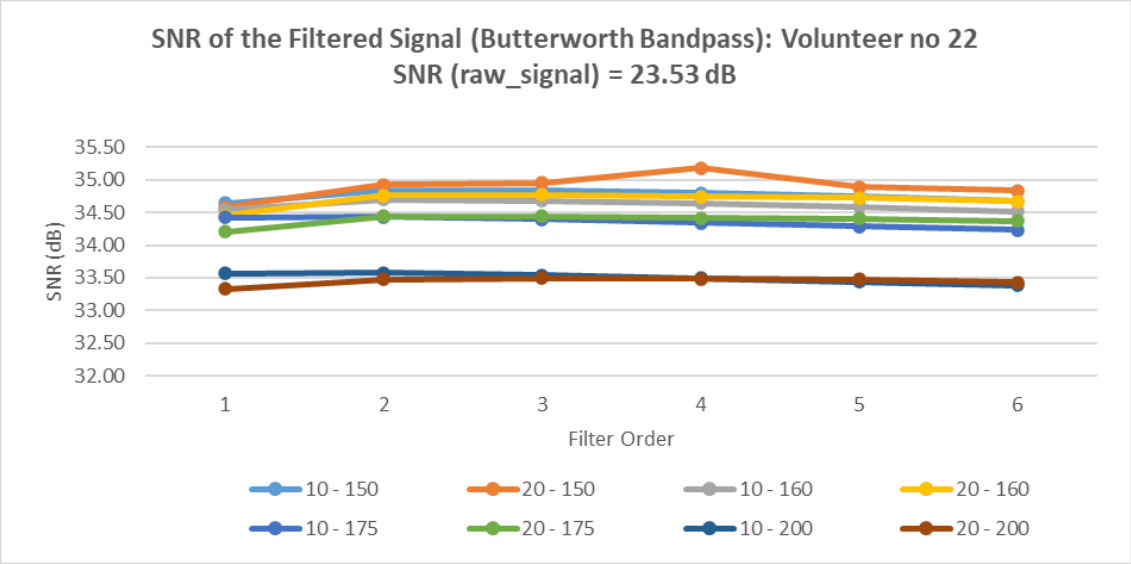

Figure E.18: SNR values of the filtered signal when six order different Bandpass Butterworth filters were applied – Volunteer number 22.

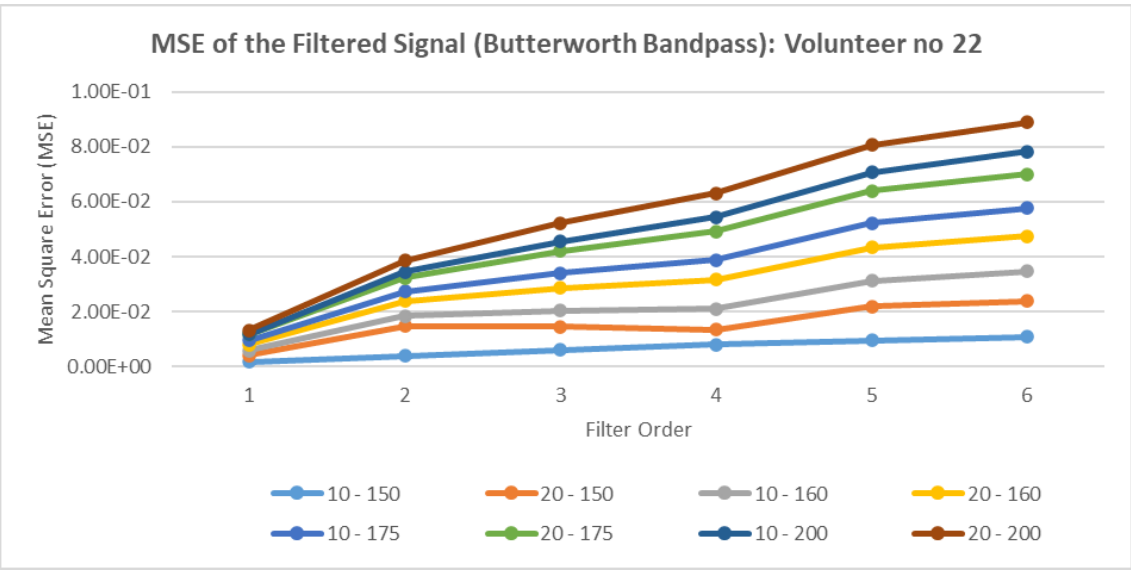

Figure E.19: MSE values of the filtered signal when six order different Bandpass Butterworth filters were applied – Volunteer number 22.

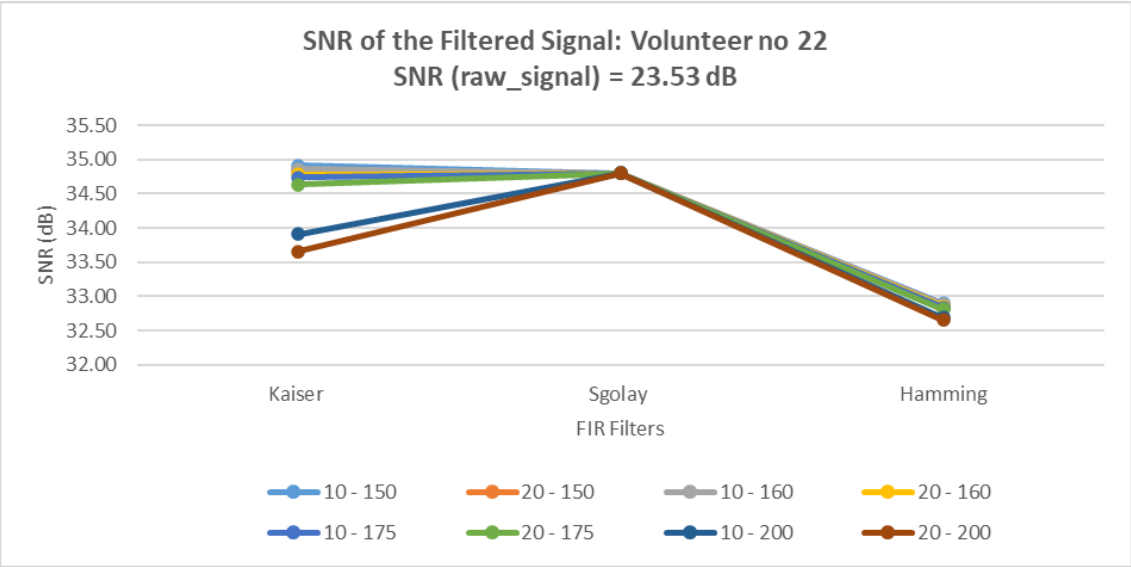

Figure E.20: SNR values of the filtered signal when the FIR filters were applied – Volunteer number 22.

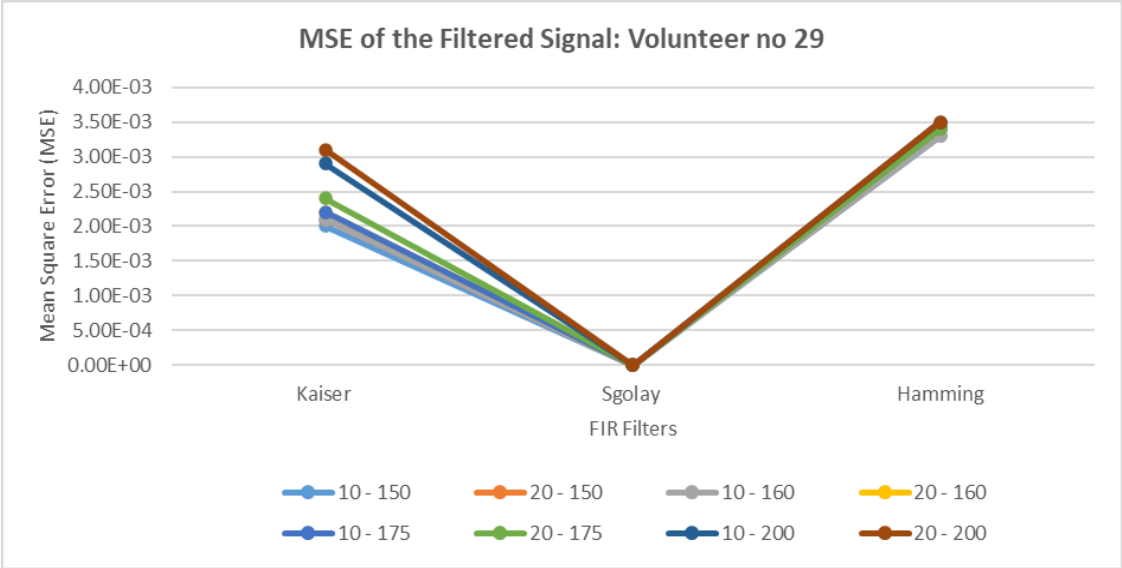

Figure E.21: SNR values of the filtered signal when the FIR filters were applied – Volunteer number 29.

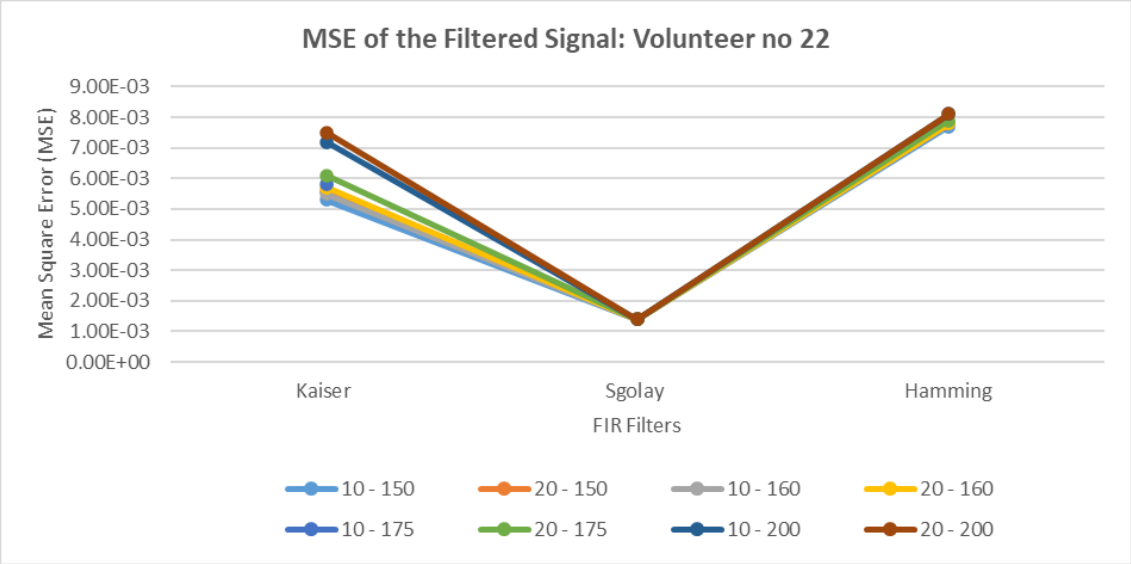

Figure E.22: MSE values of the filtered signal when the FIR filters were applied – Volunteer number 22.

F. Wavelet transform noise reduction method results

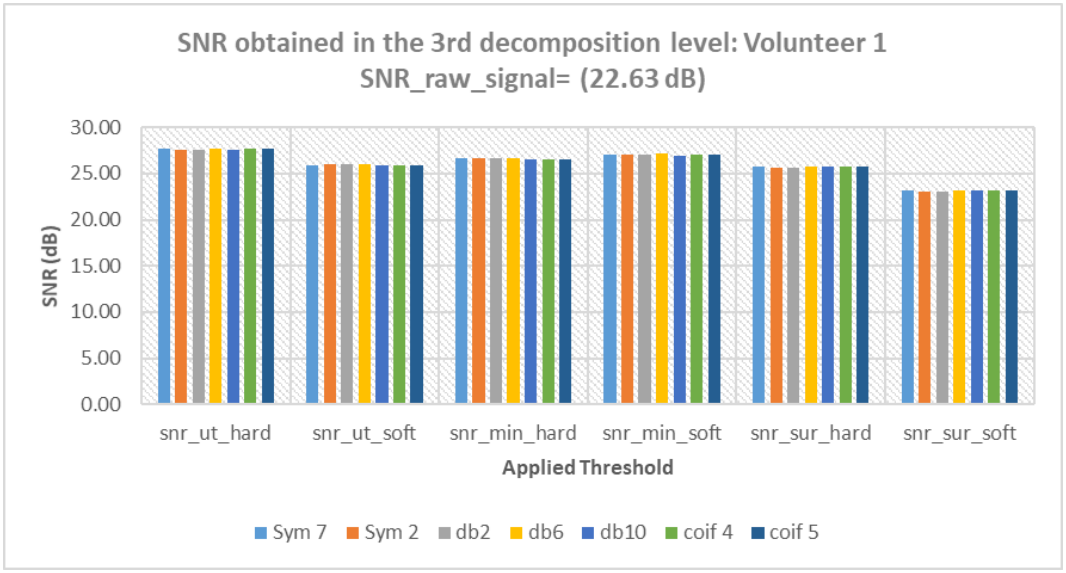

Figure F.1: SNR obtained for the third decomposition level when several wavelet families and thresholds were tested – volunteer number 1.

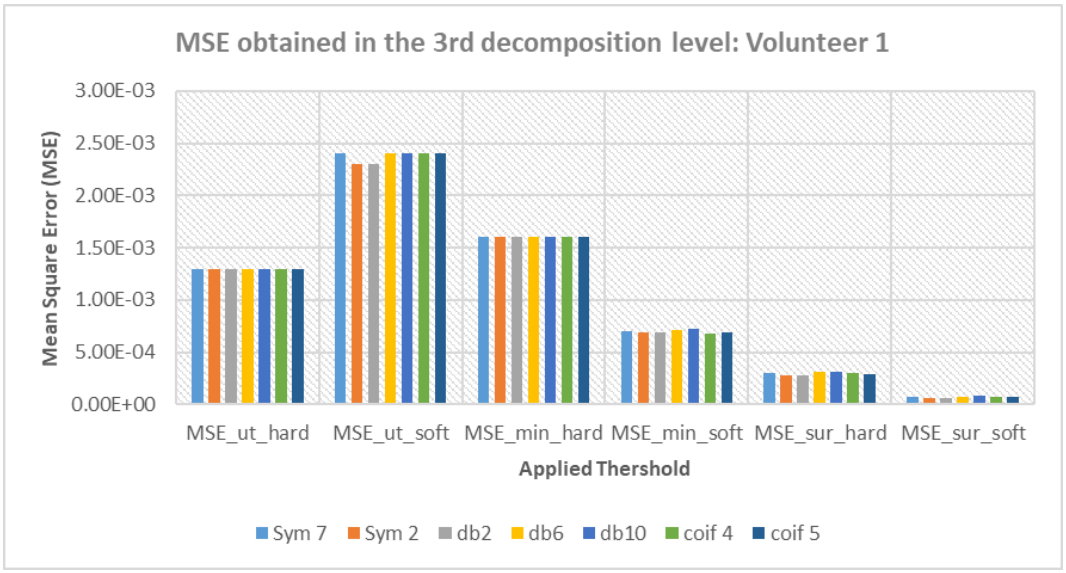

Figure F.2: MSE obtained for the third decomposition level when several wavelet families and thresholds were tested – volunteer number 1.

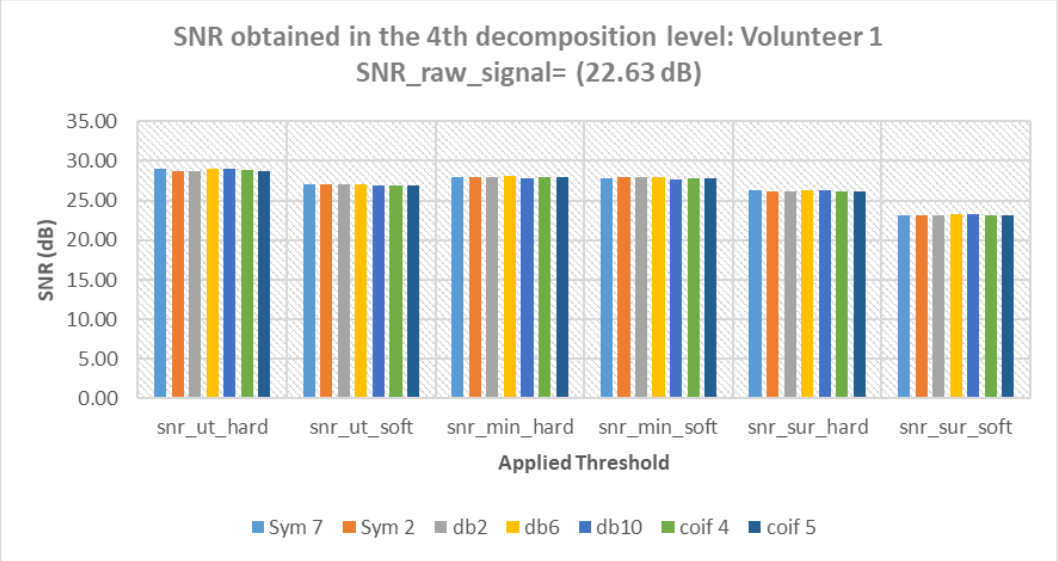

Figure F.3: SNR obtained for the fourth decomposition level when several wavelet families and thresholds were tested – volunteer number 1.

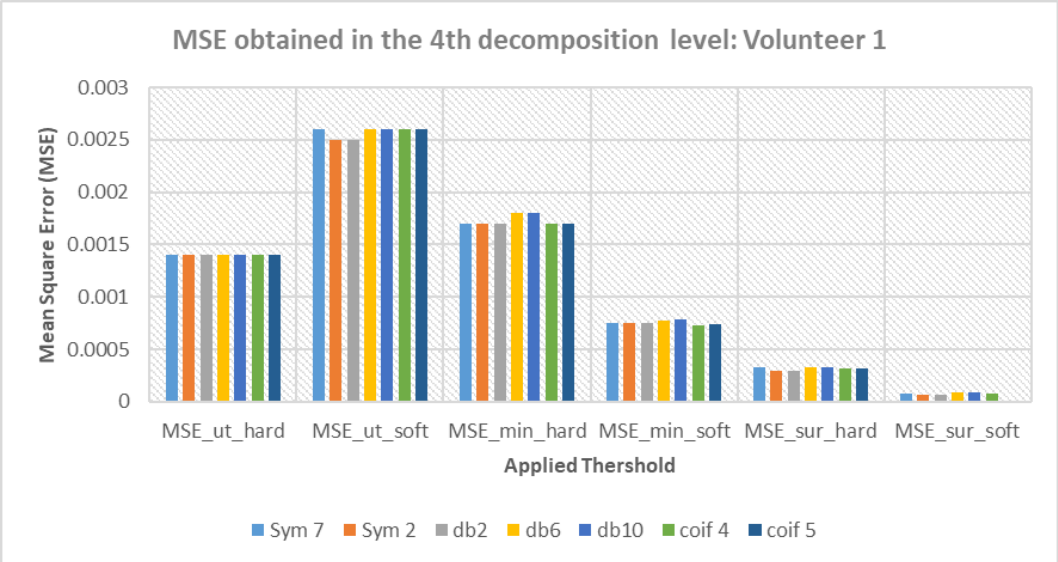

Figure F.4: MSE obtained for the fourth decomposition level when several wavelet families and thresholds were tested – volunteer number 1.

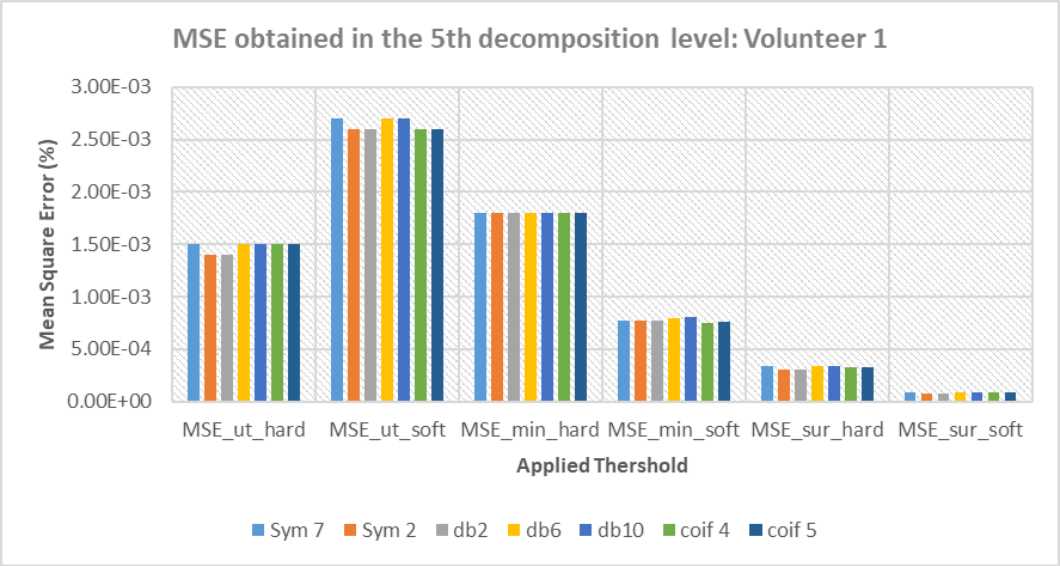

Figure F.5: MSE obtained for the fifth decomposition level when several wavelet families and thresholds were tested – volunteer number 1.

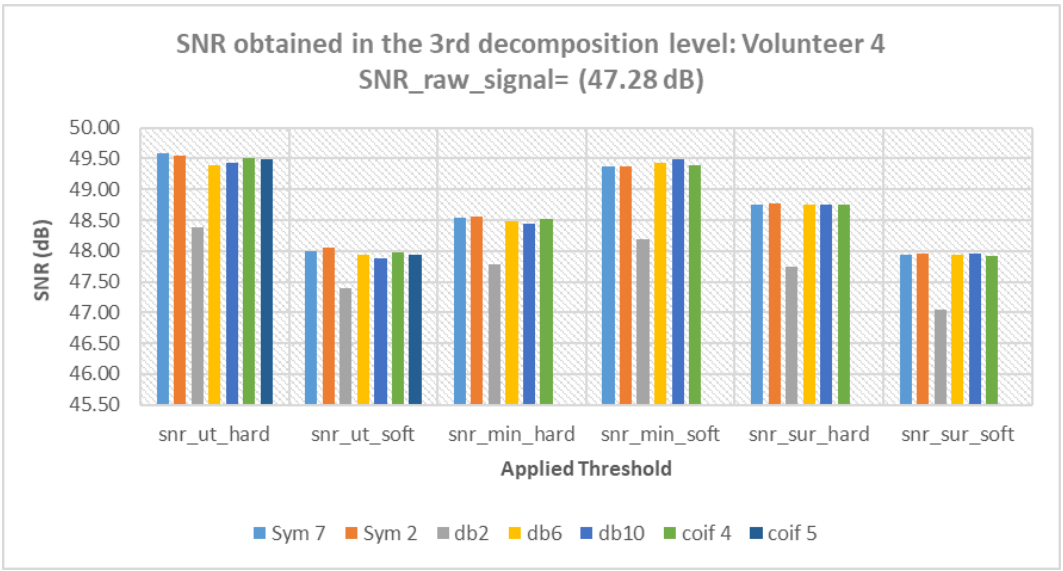

Figure F.6: SNR obtained for the third decomposition level when several wavelet families and thresholds were tested – volunteer number 4.

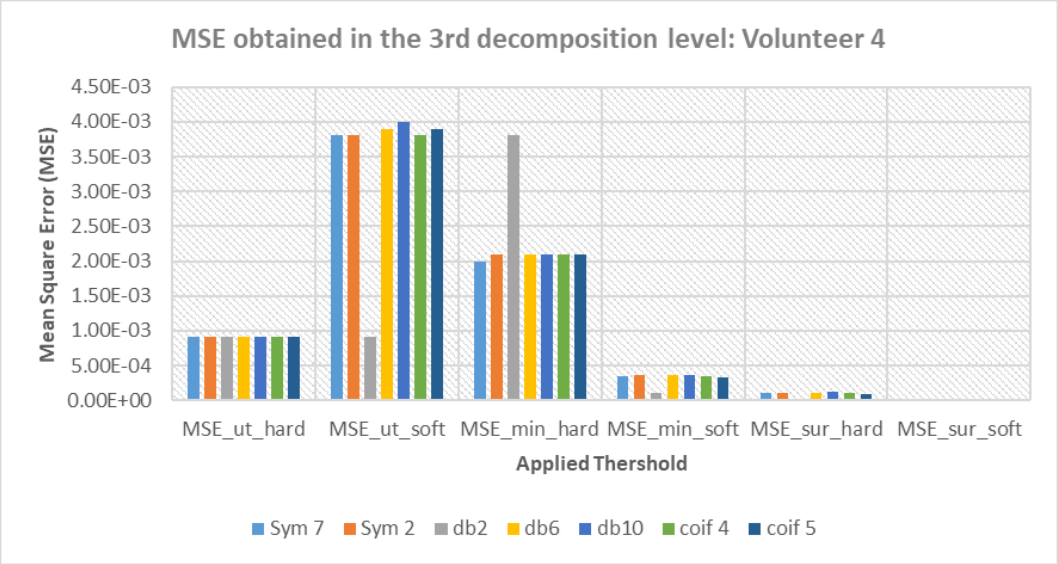

Figure F.7: MSE obtained for the third decomposition level when several wavelet families and thresholds were tested – volunteer number 4.

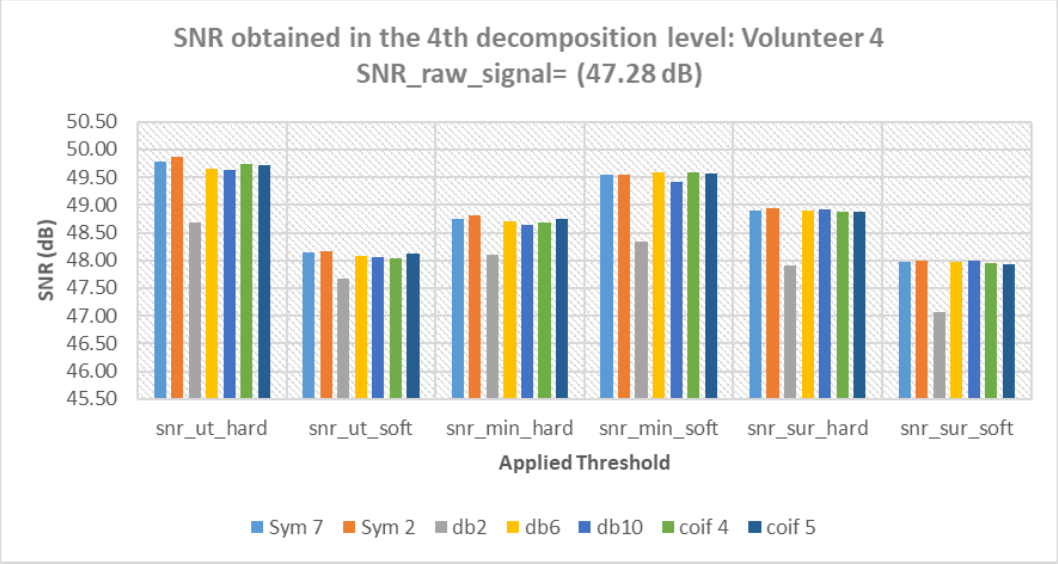

Figure F.8: SNR obtained for the fourth decomposition level when several wavelet families and thresholds were tested – volunteer number 4.

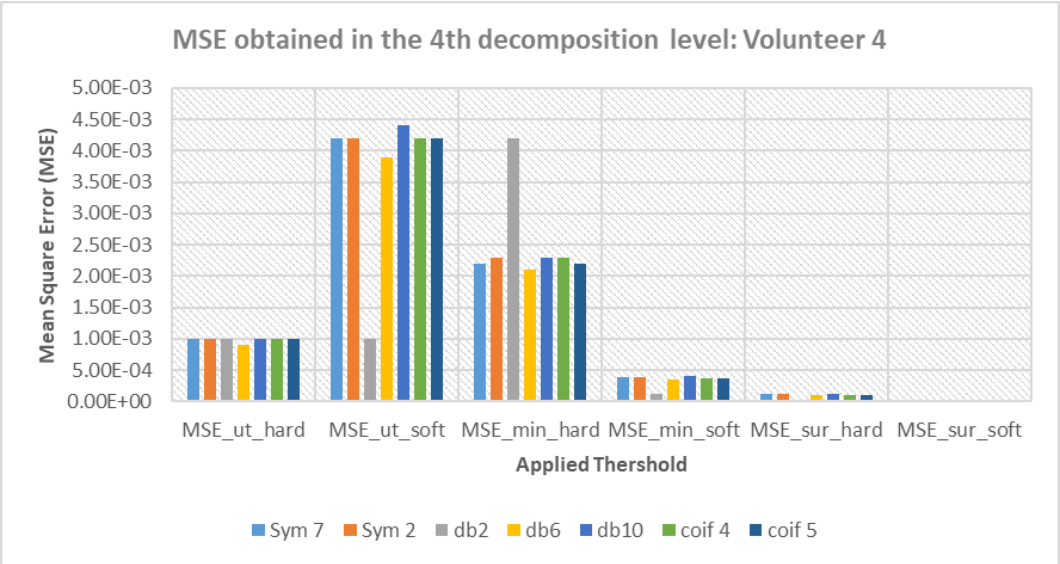

Figure F.9: MSE obtained for the fourth decomposition level when several wavelet families and thresholds were tested – volunteer number 4.

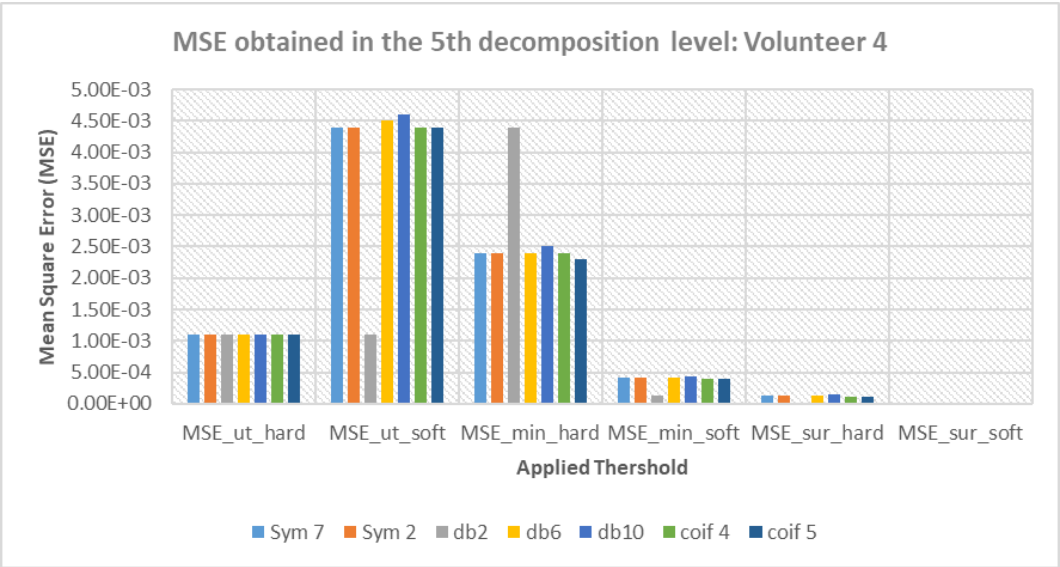

Figure F.10: MSE obtained for the fifth decomposition level when several wavelet families and thresholds were tested – volunteer number 4.

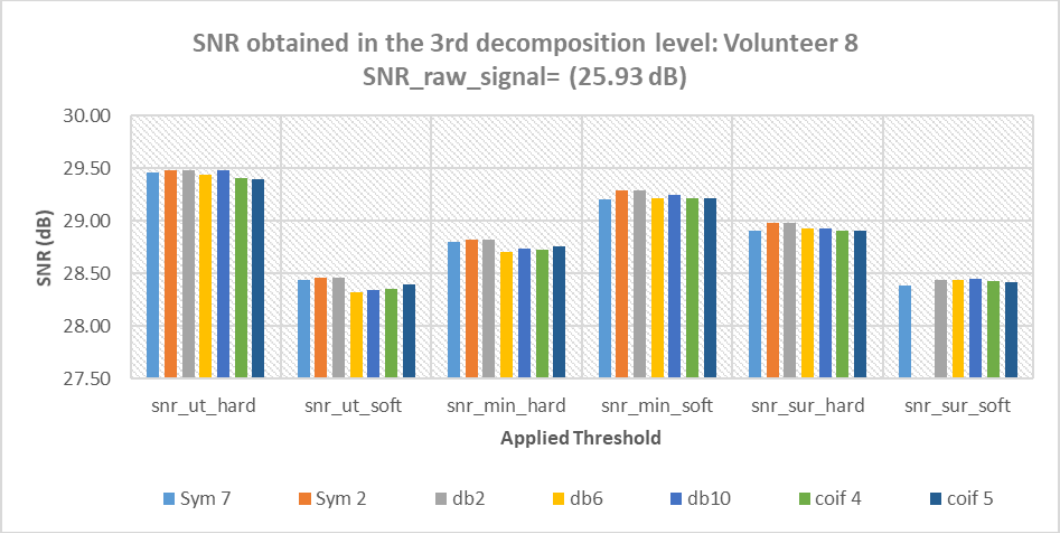

Figure F.11: SNR obtained for the third decomposition level when several wavelet families and thresholds were tested – volunteer number 8.

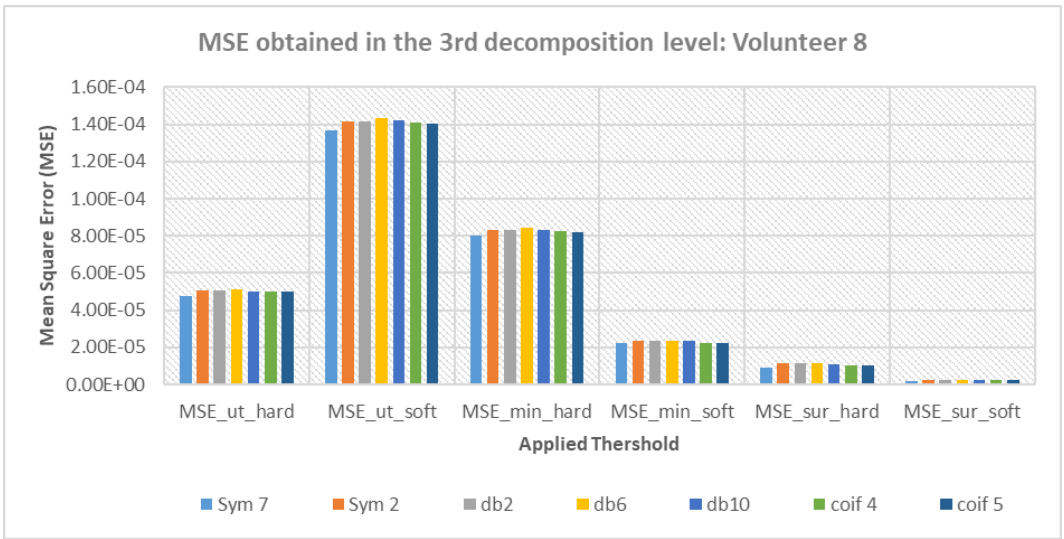

Figure F.12: MSE obtained for the third decomposition level when several wavelet families and thresholds were tested – volunteer number 8.

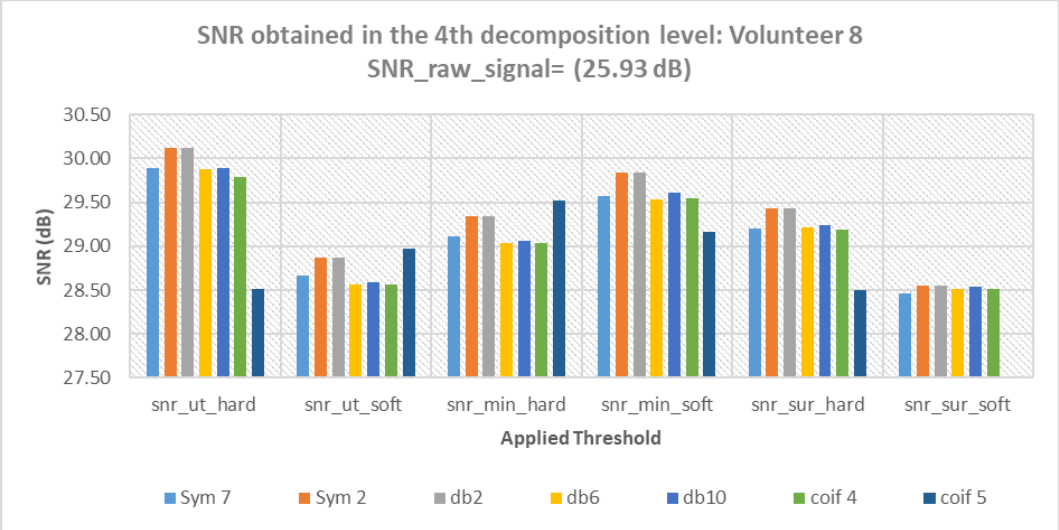

Figure F.13: SNR obtained for the fourth decomposition level when several wavelet families and thresholds were tested – volunteer number 8.

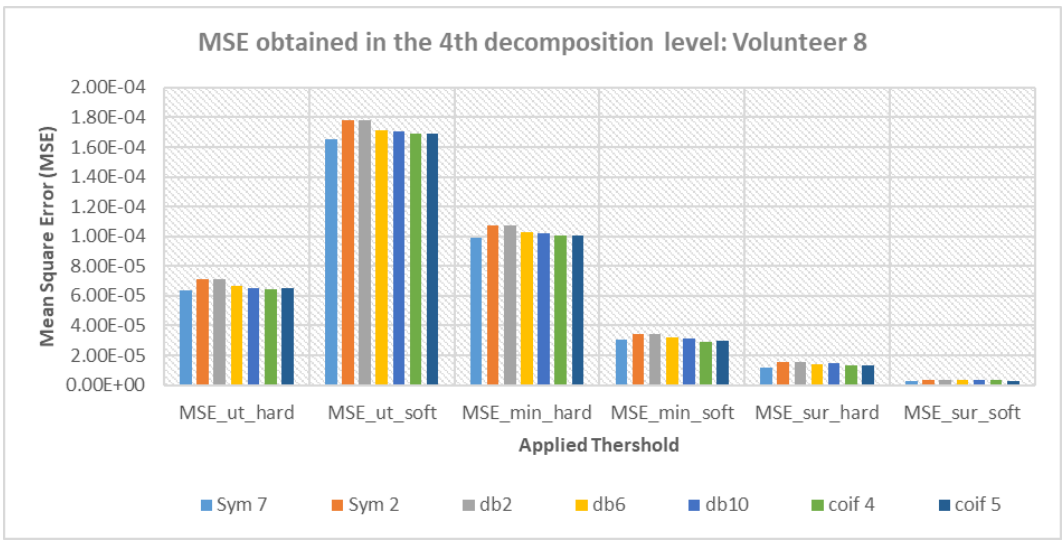

Figure F.14: MSE obtained for the fourth decomposition level when several wavelet families and thresholds were tested – volunteer number 8.

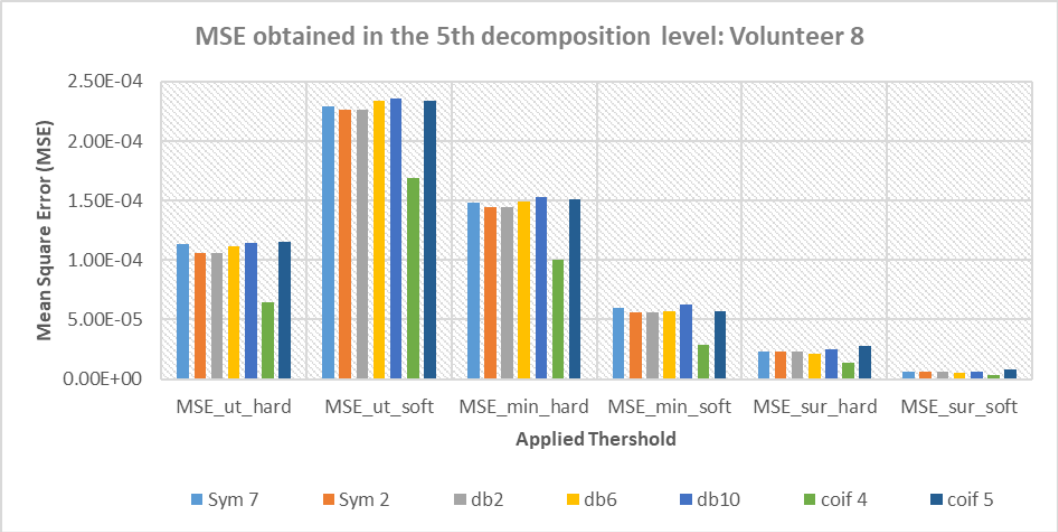

Figure F.15: MSE obtained for the fifth decomposition level when several wavelet families and thresholds were tested – volunteer number 8.

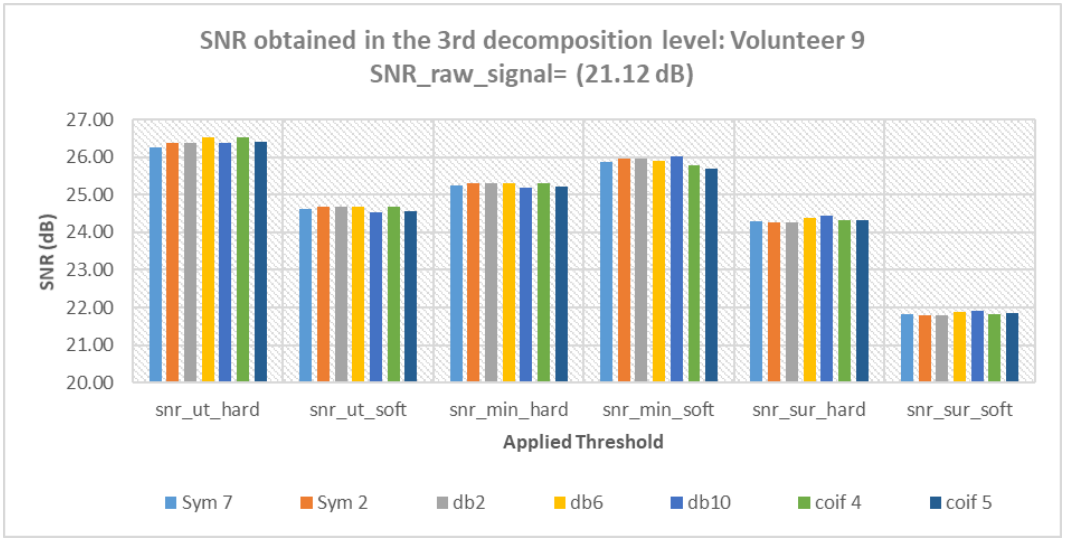

Figure F.16: SNR obtained for the third decomposition level when several wavelet families and thresholds were tested – volunteer number 9.

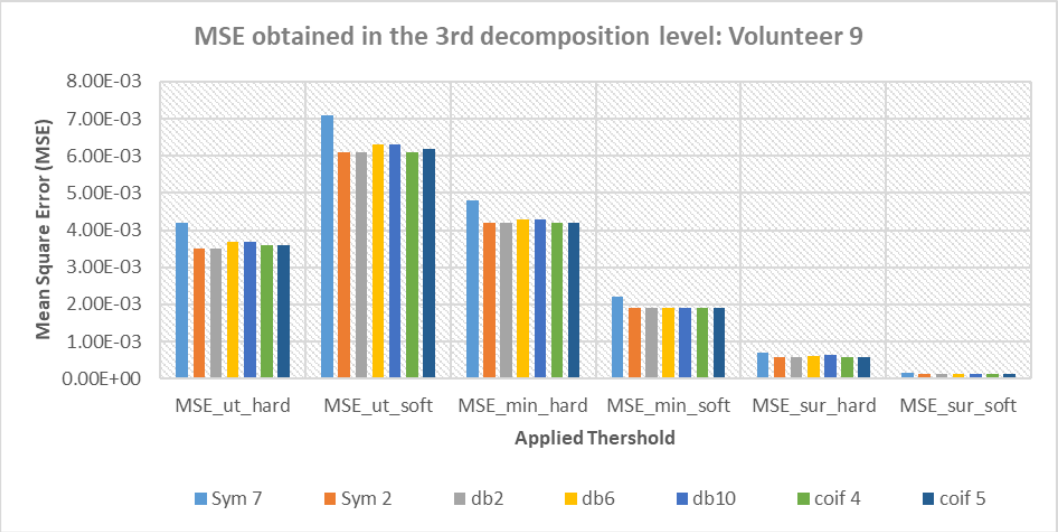

Figure F.17: MSE obtained for the third decomposition level when several wavelet families and thresholds were tested – volunteer number 9.

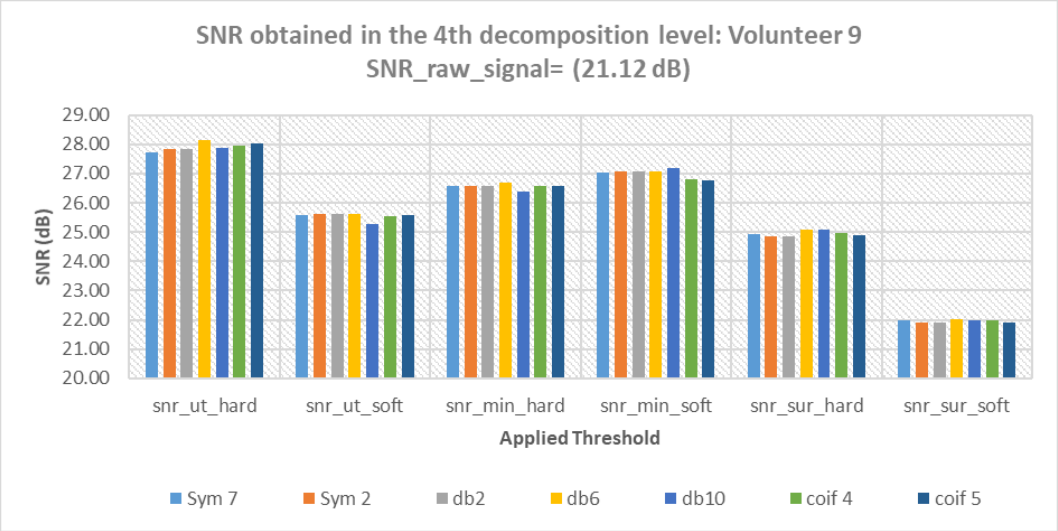

Figure F.18: SNR obtained for the fourth decomposition level when several wavelet families and thresholds were tested – volunteer number 9.

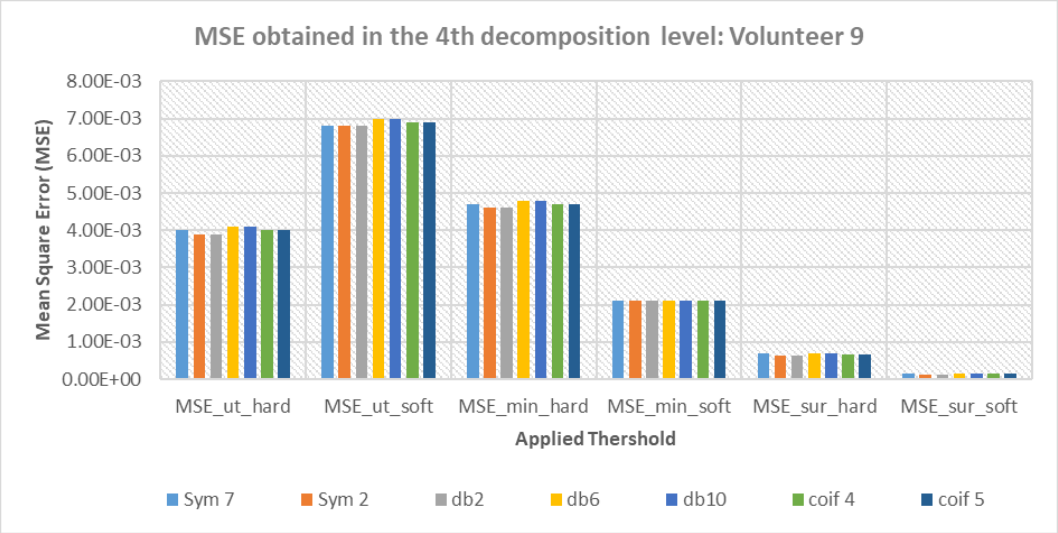

Figure F.19: MSE obtained for the fourth decomposition level when several wavelet families and thresholds were tested – volunteer number 9.

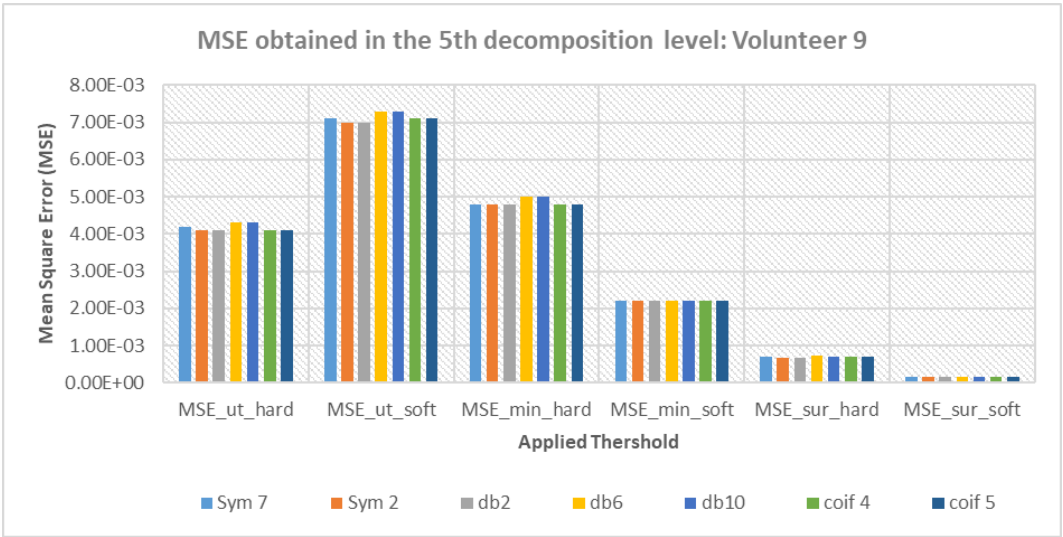

Figure F.20: MSE obtained for the fifth decomposition level when several wavelet families and thresholds were tested – volunteer number 9.

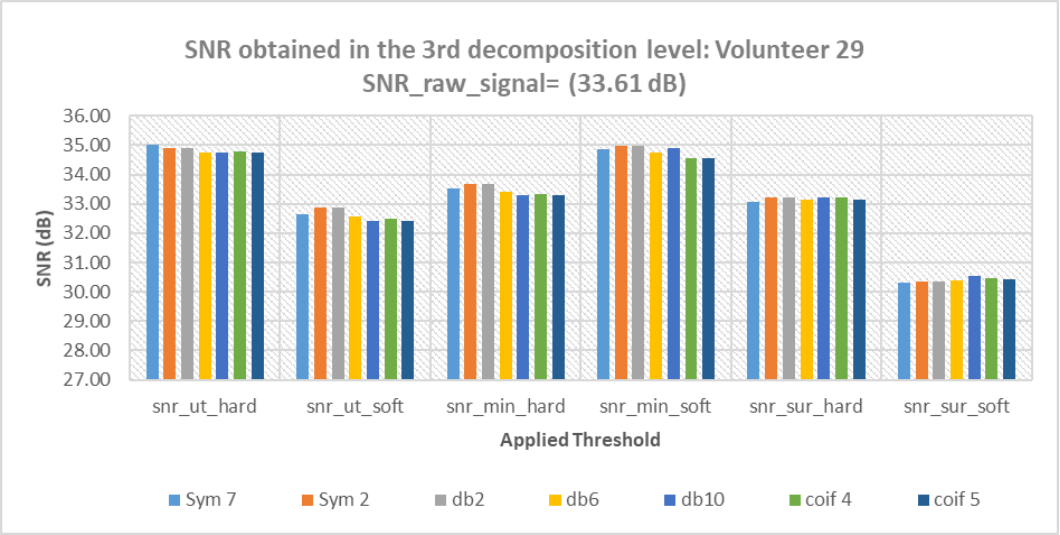

Figure F.21: SNR obtained for the third decomposition level when several wavelet families and thresholds were tested – volunteer number 29.

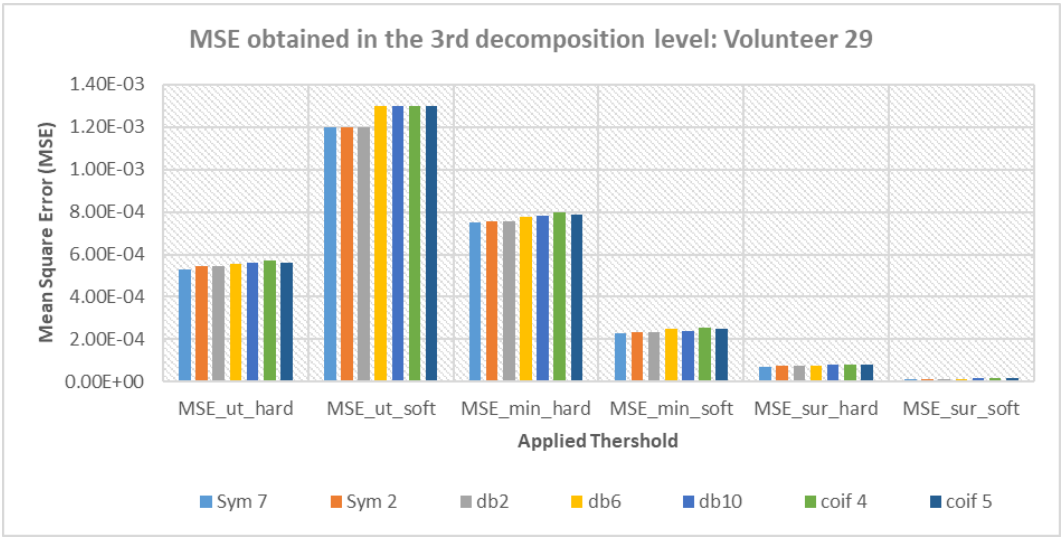

Figure F.22: MSE obtained for the third decomposition level when several wavelet families and thresholds were tested – volunteer number 29.

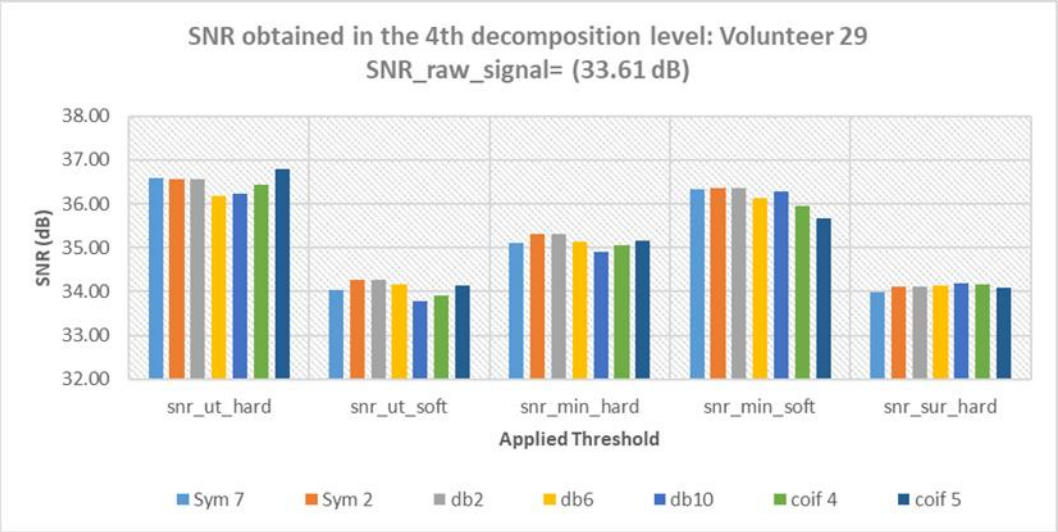

Figure F. 23: SNR obtained for the fourth decomposition level when several wavelet families and thresholds were tested – volunteer number 29.

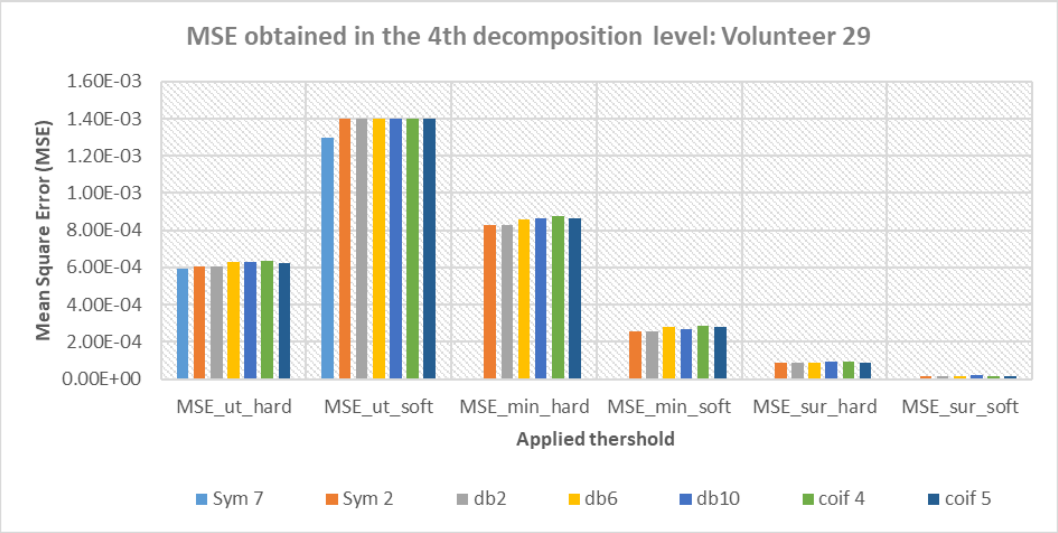

Figure F.24: MSE obtained for the fourth decomposition level when several wavelet families and thresholds were tested – volunteer number 29.

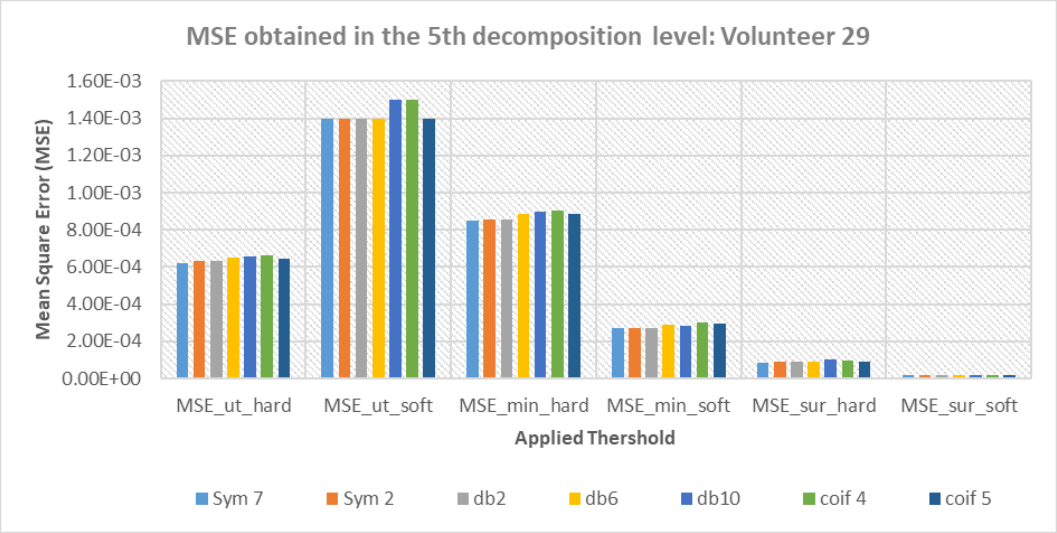

Figure F.25: MSE obtained for the fifth decomposition level when several wavelet families and thresholds were tested – volunteer number 29.

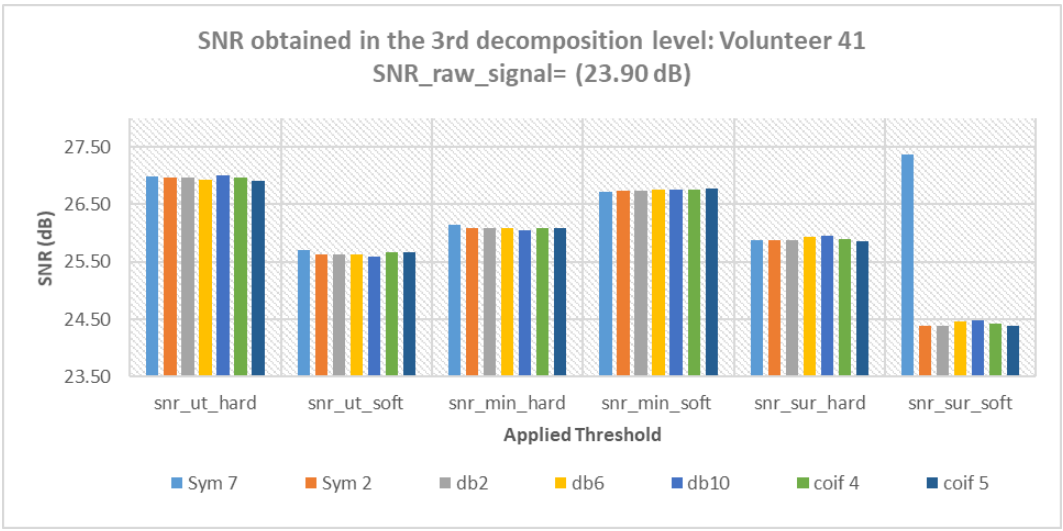

Figure F.26: SNR obtained for the third decomposition level when several wavelet families and thresholds were tested – volunteer number 41.

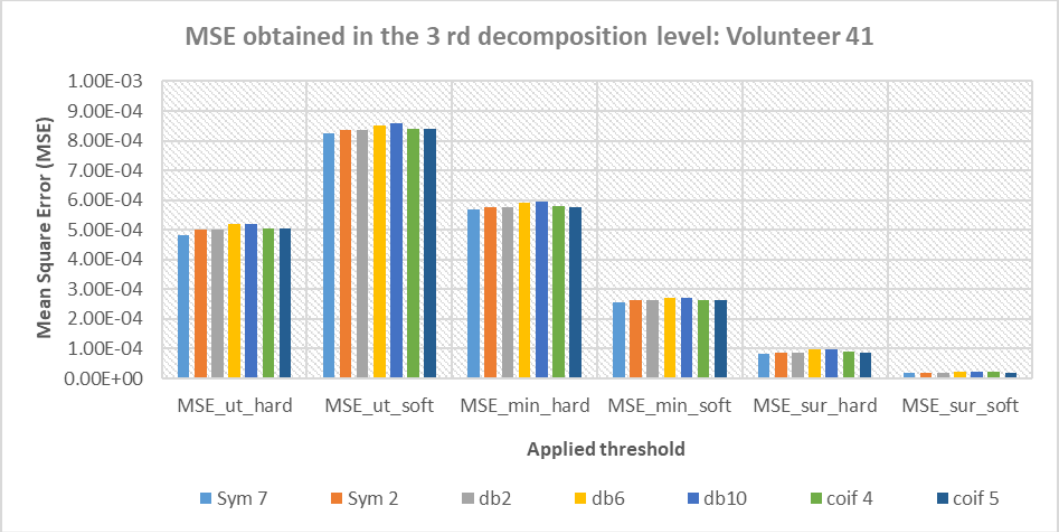

Figure F.27: MSE obtained for the third decomposition level when several wavelet families and thresholds were tested – volunteer number 41.

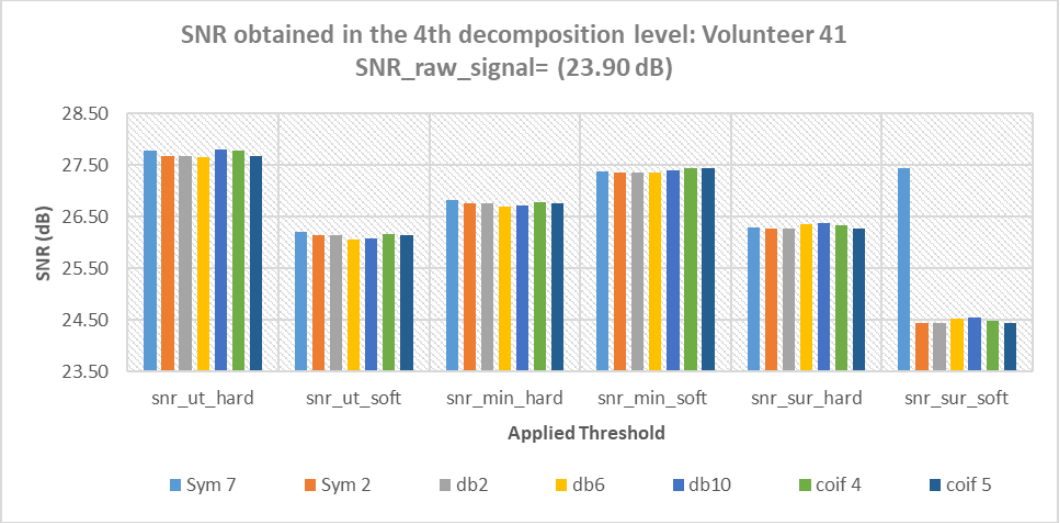

Figure F.28: SNR obtained for the fourth decomposition level when several wavelet families and thresholds were tested – volunteer number 41.

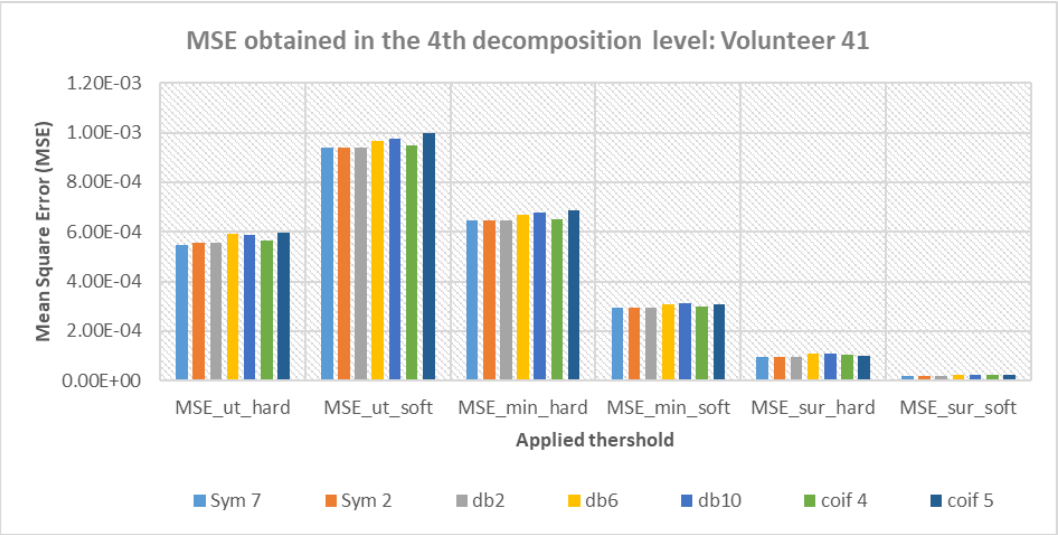

Figure F.29: MSE obtained for the fourth decomposition level when several wavelet families and thresholds were tested – volunteer number 41.

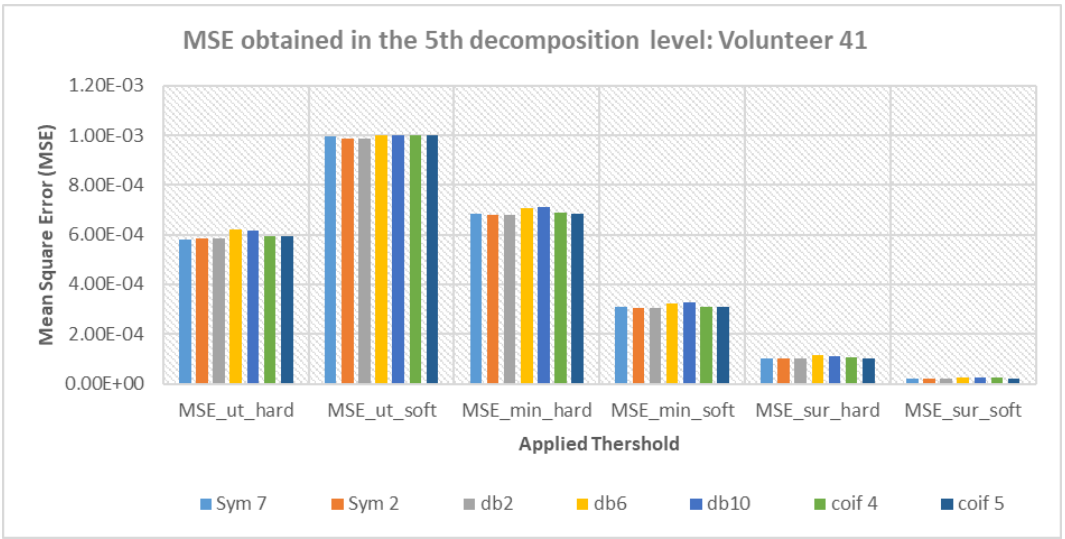

Figure F.30: MSE obtained for the fifth decomposition level when several wavelet families and thresholds were tested – volunteer number 41.

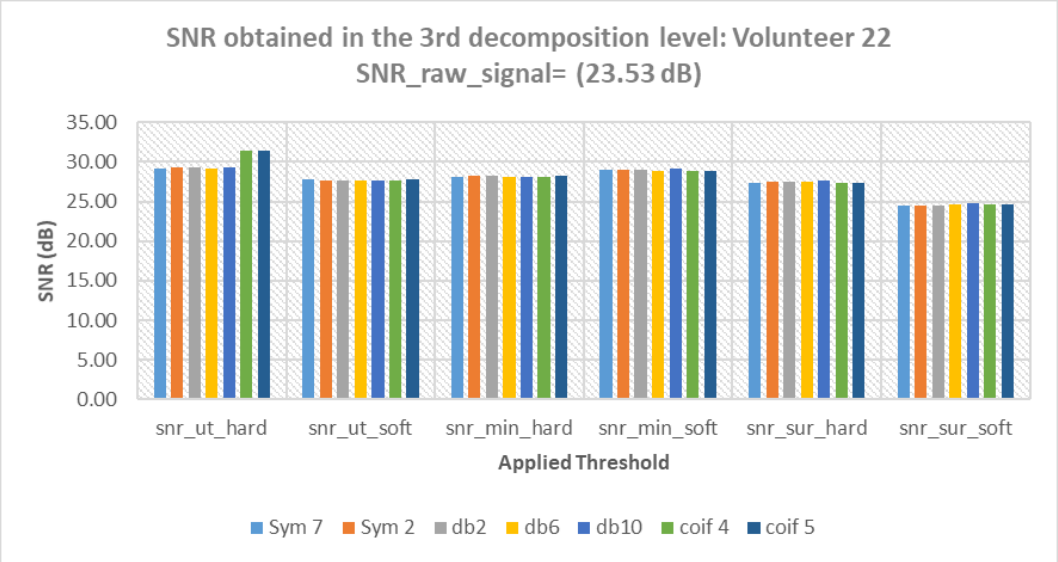

Figure F.31: SNR obtained for the fourth decomposition level when several wavelet families and thresholds were tested – volunteer number 22.

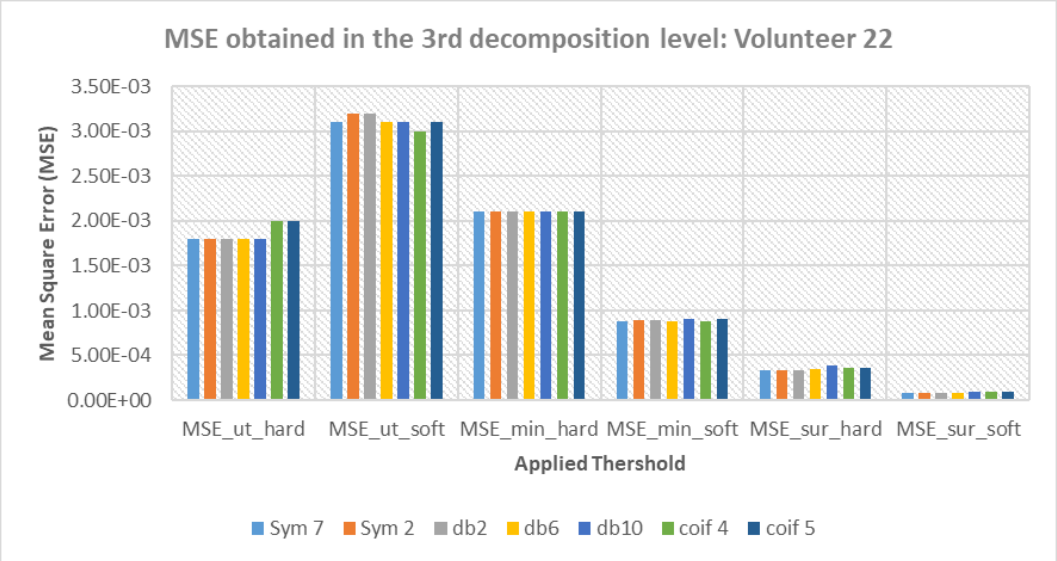

Figure F.32: MSE obtained for the fifth decomposition level when several wavelet families and thresholds were tested – volunteer number 22.

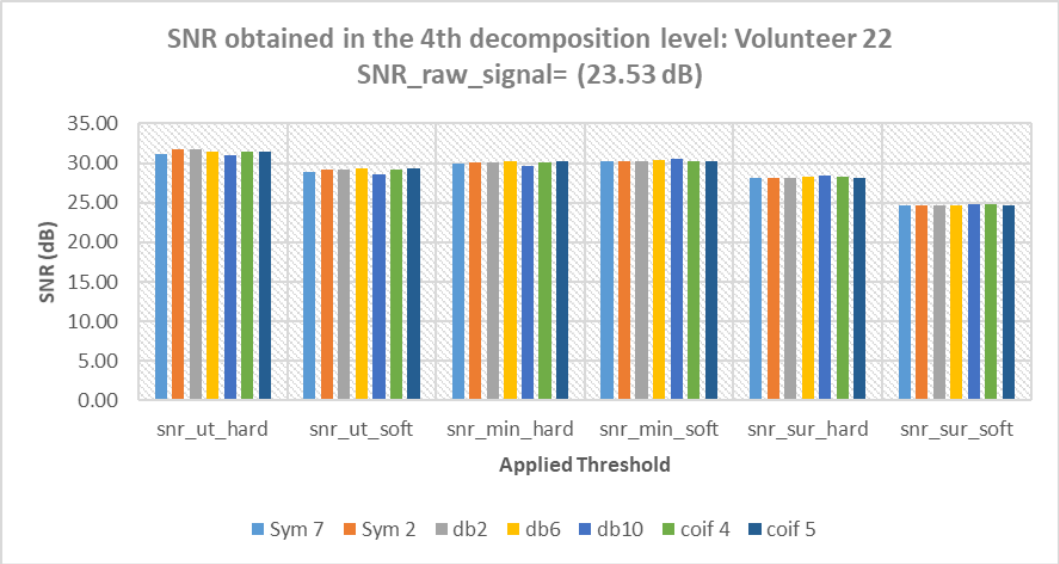

Figure F.33: SNR obtained for the fourth decomposition level when several wavelet families and thresholds were tested – volunteer number 22.

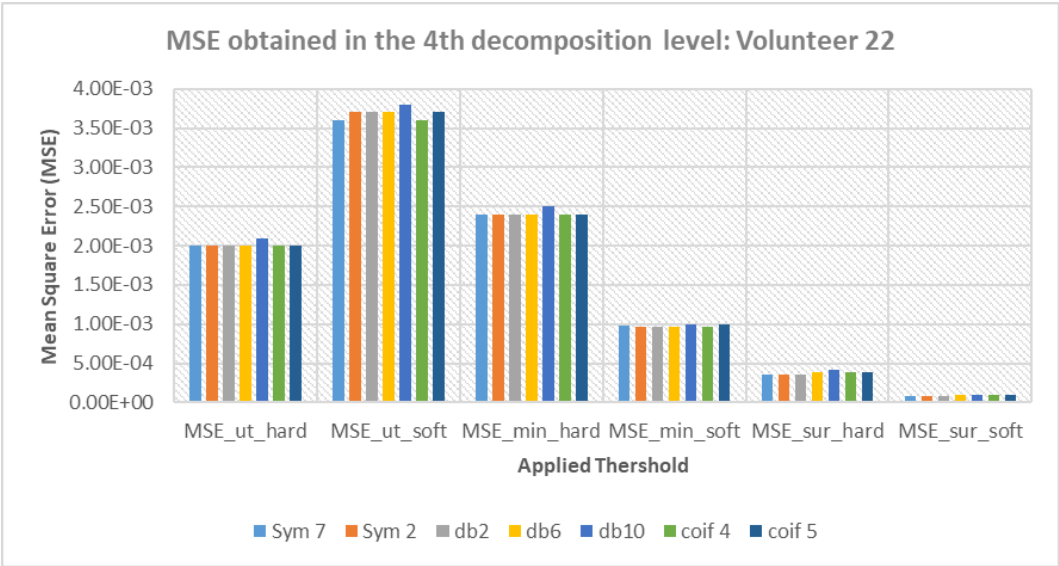

Figure F.34: MSE obtained for the fourth decomposition level when several wavelet families and thresholds were tested – volunteer number 22.

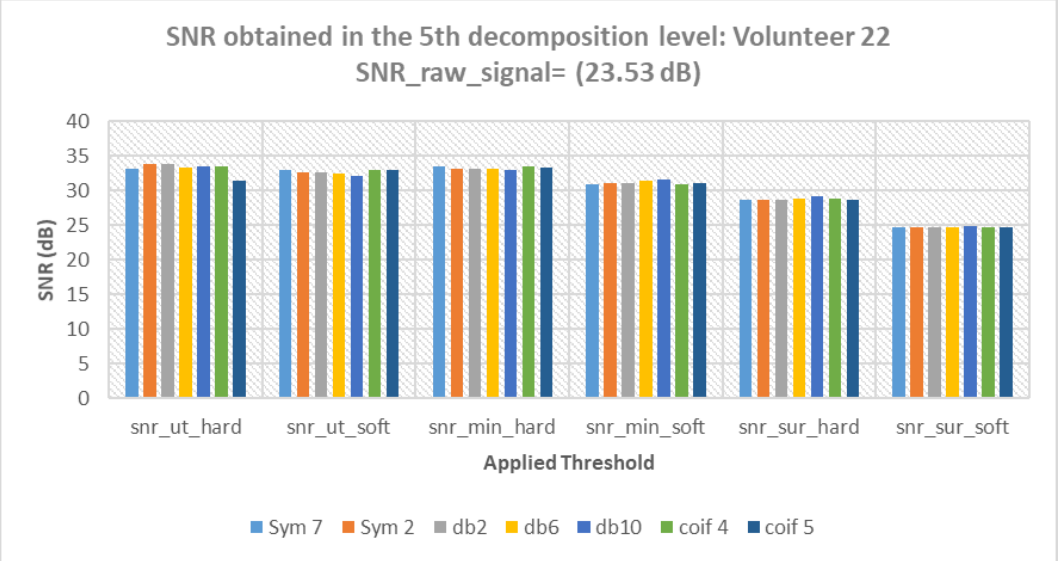

Figure F.35: MSE obtained for the fourth decomposition level when several wavelet families and thresholds were tested – volunteer number 22.

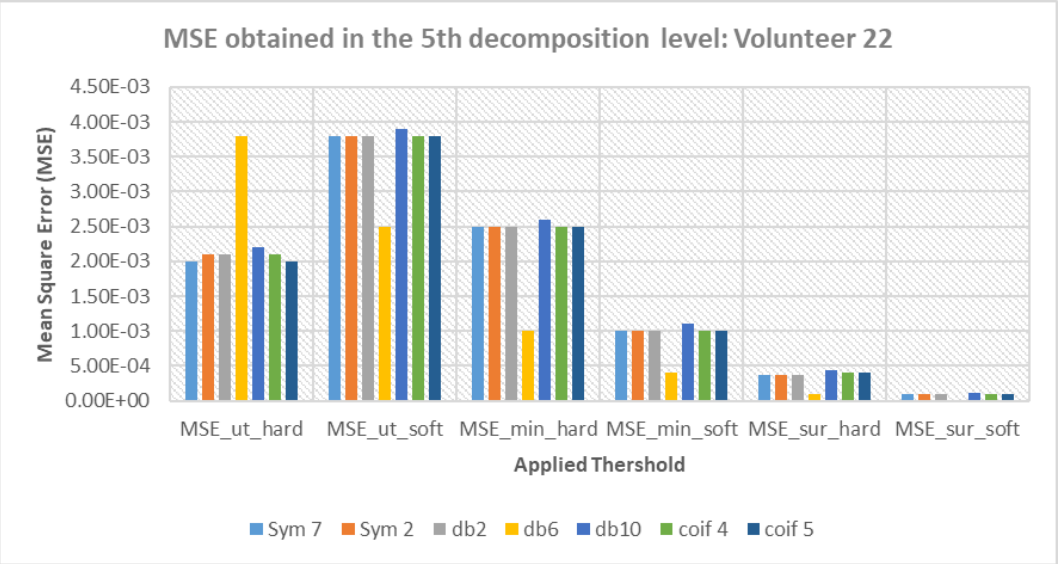

Figure F.36: MSE obtained for the fifth decomposition level when several wavelet families and thresholds were tested – volunteer number 22.

G. 10 - fold cross validation results

Table G.1: Classification results for a window length of 250 *ms* when the 10-fold cross validation method was applied. The results are distributed by classification levels.

Evaluation Metrics (%)	KNN (k=2)	KNN (k=5)	KNN (k=7)	KNN (k=9)	KNN (k=11)	KNN (k=15)	LDA
First Classification Level – Movements vs Rest							
Accuracy	92.54	93.61	93.77	93.91	93.98	94.10	94.19
Recall	92.54	93.61	93.77	93.91	93.98	94.10	94.19
Precision	92.47	93.59	93.74	93.89	93.96	94.08	94.15
Second Classification Level – Spherical Grip vs Tripod Grip vs Finger Flexion							
Accuracy	52.26	46.34	45.76	43.59	44.64	43.78	45.19
Recall	52.26	46.34	45.76	43.59	44.64	43.78	45.19
Precision	51.52	46.35	45.82	38.72	44.69	43.86	44.76
Second Classification Level – Grasp Movements vs Finger Flexion							
Accuracy	64.06	63.33	62.25	64.06	62.55	62.32	64.06
Recall	59.23	56.27	58.16	58.02	50.21	59.29	49.09
Precision	64.06	63.33	62.25	64.06	62.55	62.32	64.06
Third Classification Level – Tripod Grip vs Spherical Grip							
Accuracy	67.13	65.10	64.15	64.16	63.77	63.57	64.77
Recall	56.14	58.64	58.86	59.43	59.18	59.14	62.28
Precision	67.13	65.10	64.15	64.16	63.77	63.57	64.77

Table G.2: Classification results for a window length of 100 *ms* when the 10-fold cross validation method was applied. The results are distributed by classification levels.

Evaluation metrics (%)	KNN (K=2)	KNN (k=5)	KNN (k=7)	KNN (k=9)	KNN (k=11)	KNN (k=15)	LDA
First Classification Level (Movements Vs Rest Position)							
Accuracy	89.26	91.13	91.29	91.49	91.58	91.67	91.81
Recall	89.22	91.12	91.28	91.48	91.57	91.66	91.80
Precision	89.26	91.13	91.29	91.49	91.58	91.67	91.82
Second Classification Level (Tripod Grip Vs Spherical Grip vs Finger Flexion)							
Accuracy	43.35	42.58	43.03	47.80	44.02	45.09	47.56
Recall	43.36	42.58	43.04	47.80	44.52	45.09	47.56
Precision	37.34	38.27	38.88	37.45	38.89	39.52	40.60

Second Classification Level (Grasp Movements vs Finger Flexion)							
Accuracy	67.76	64.50	65.87	66.73	67.51	62.32	69.87
Recall	67.76	64.50	69.55	66.73	67.51	62.32	69.87
Precision	49.38	50.64	51.39	49.24	50.73	49.87	42.90
Third Classification Level (Spherical Grip and Tripod Grip)							
Accuracy	61.70	61.38	62.09	62.97	63.49	64.18	66.64
Recall	61.70	61.38	62.09	62.97	63.49	64.18	66.64
Precision	54.53	58.46	58.81	56.31	59.69	56.58	58.93

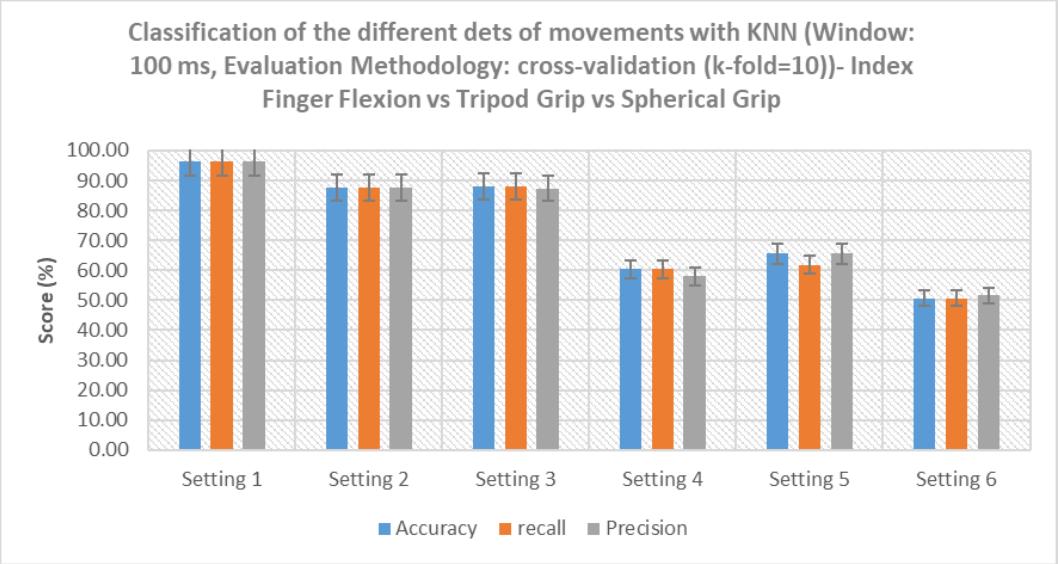

Figure G.1: Accuracy, precision and recall average obtained values for a window of 100 *ms* when the objective was to study the different sets – Setting 1: 96.27 %, Setting 2: 87.69 %; Setting 3: 87.85 %; Setting 4: 60.40 %; Setting 5: 65.56% and Setting 6: 50.71 %.

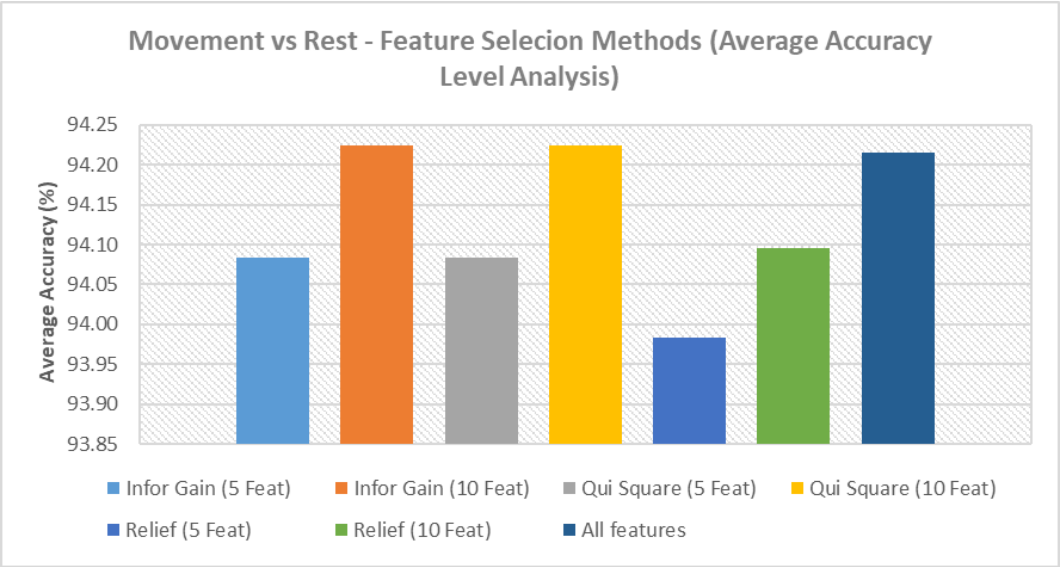

Figure G.2: Average accuracy obtained results for the three different filter methods for feature selection – Movement vs Rest (KNN – k=5).

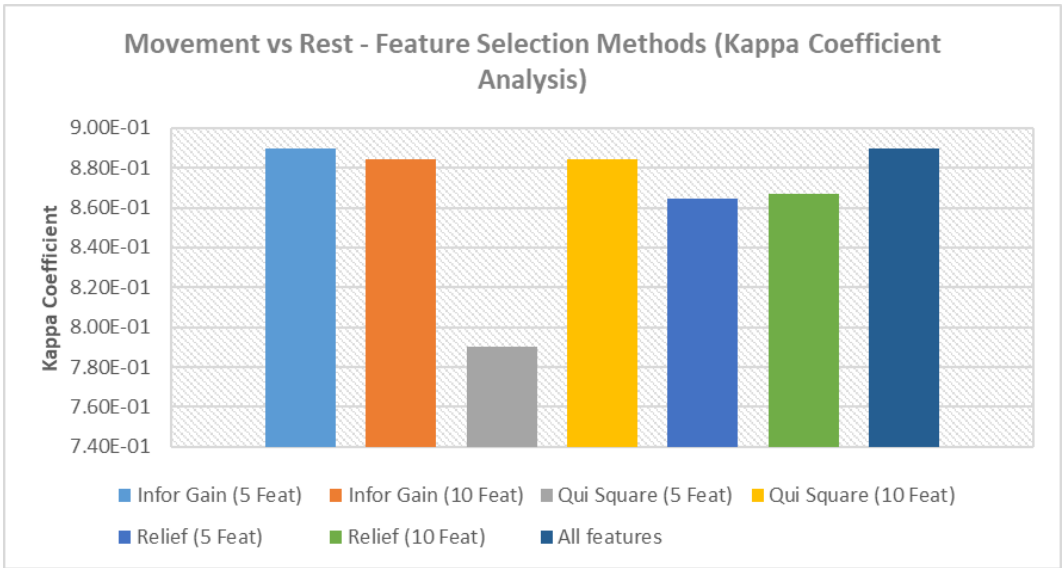

Figure G.3: Kappa coefficient obtained results for the three different filter methods for feature selection – All movements (KNN – k=5).

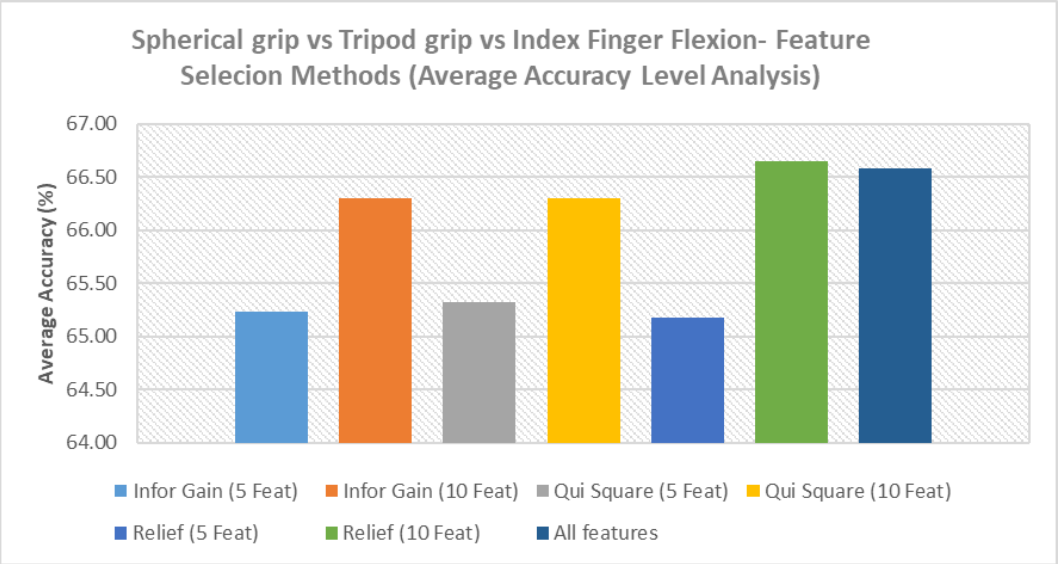

Figure G.4: Average accuracy obtained results for the three different filter methods for feature selection – All movements (KNN – k=5).

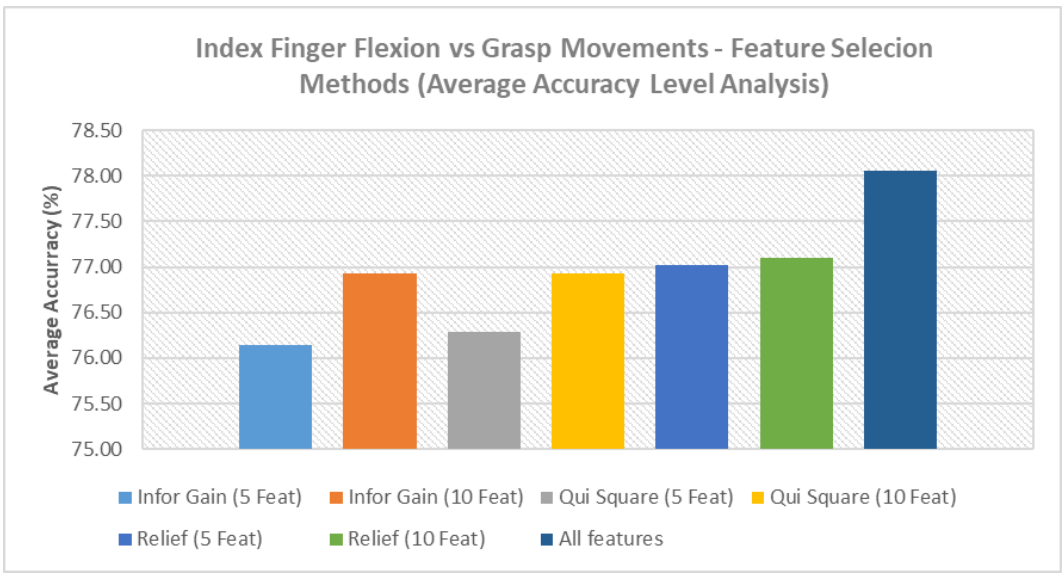

Figure G.5: Average accuracy obtained results for the three different filter methods for feature selection – Grasp Movements vs Index Finger Flexion (KNN – k=5).

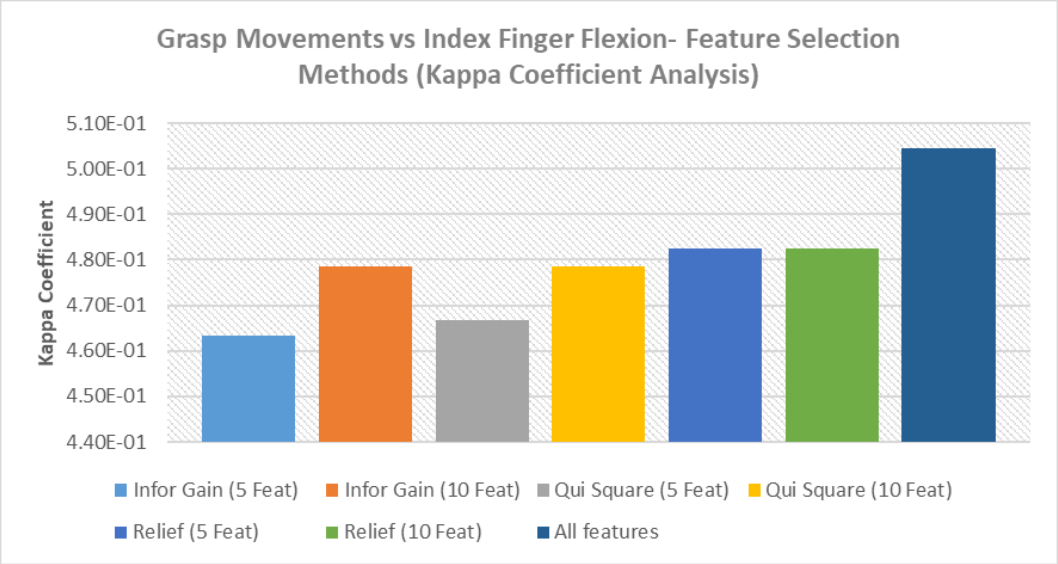

Figure G.6: Kappa coefficient obtained results for the three different filter methods for feature selection – Grasp Movements vs Index Finger Flexion (KNN – k=5).

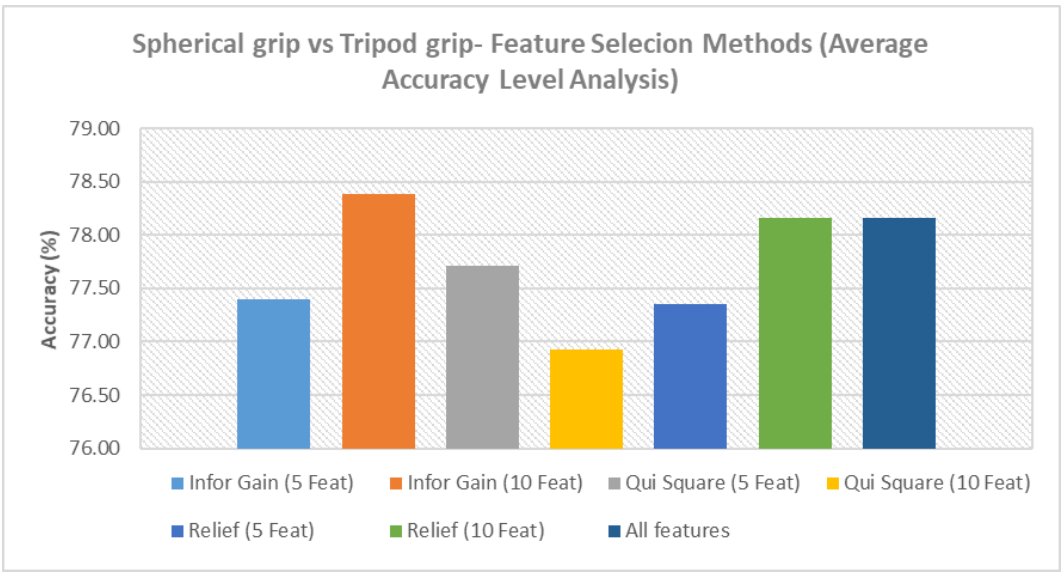

Figure G.7: Average accuracy obtained results for the three different filter methods for feature selection – Spherical Grip vs Tripod Grip (KNN – k=5).

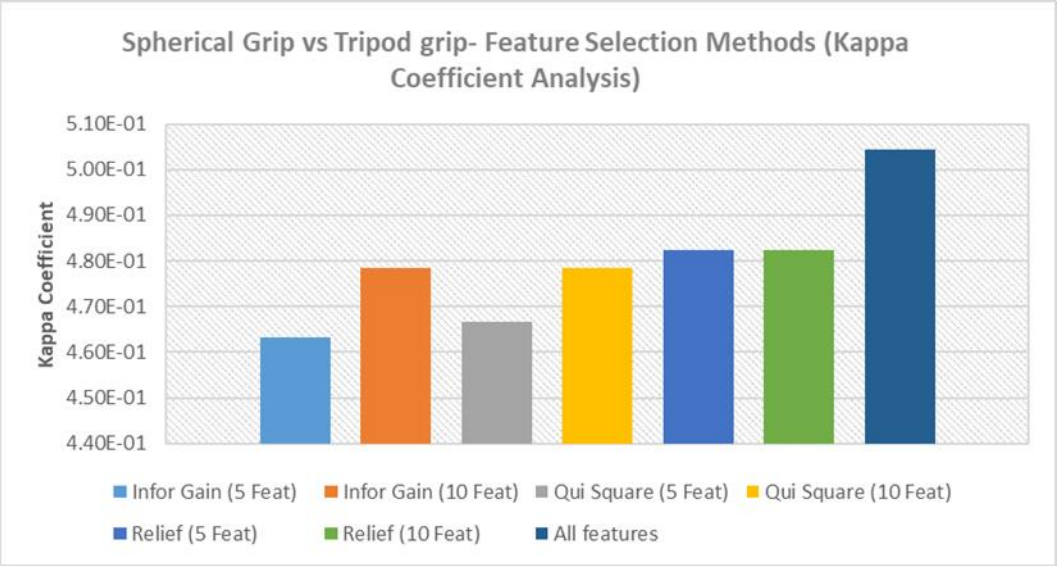

Figure G.8: Kappa coefficient obtained results for the three different filter methods for feature selection – Movement Vs Rest (KNN – k=5).

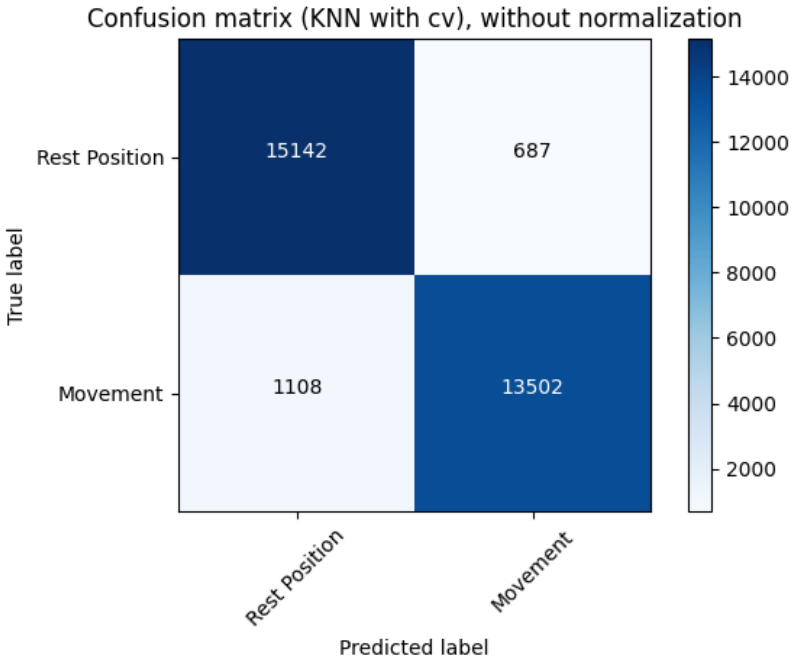

Figure G.9: Confusion Matrix for the first classification level when the 10-fold cross-validation method was applied for a window of 250 *ms*. Represents the number of instances that were classified correctly for both classes (15142 for rest position and 13502 for movement class) and the misclassified ones (687 for rest position and 1108 for movement class) - KNN (k=15).

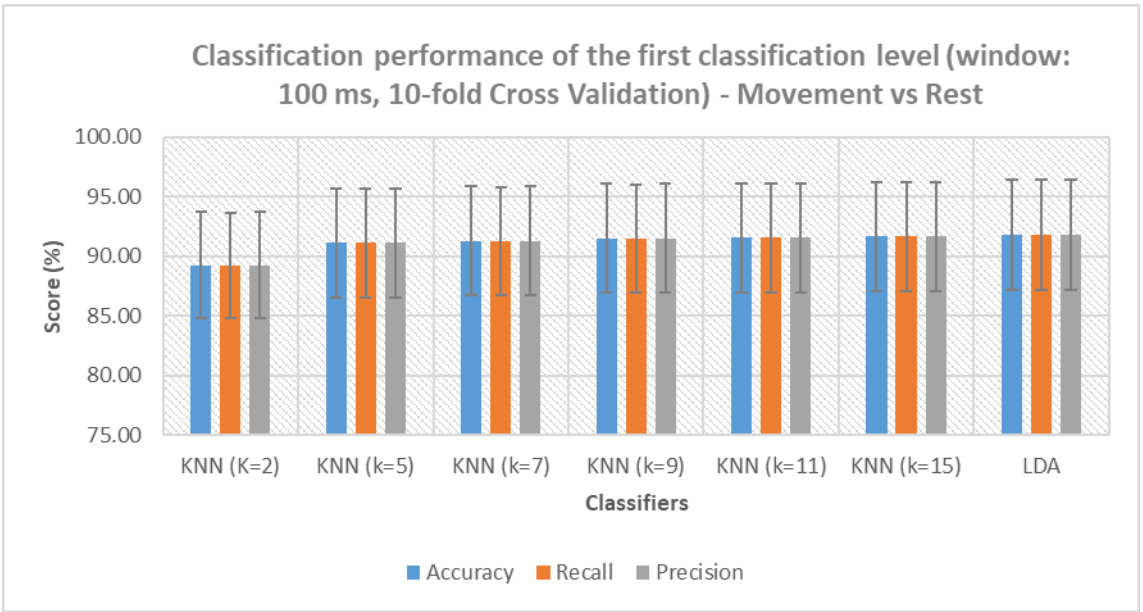

Figure G.10: Results obtained in the first level of the tree classifier for a window of 100 *ms*: Movements vs Rest Position. The minimum accuracy was reached for KNN=2 (89.26 %) and the maximum for LDA (91.81 %).

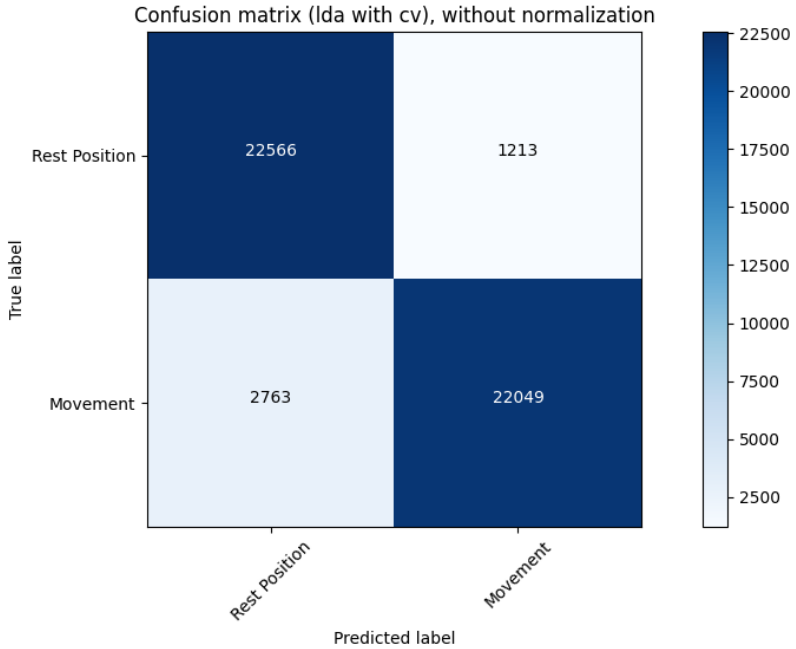

Figure G.11: Confusion Matrix for the first level of the tree classifier when the 10-fold cross validation method was applied for a window of 100 *ms*. Represents the number of instances that were classified correctly for both classes (22566 for rest position and 22049 for movement class) and the misclassified ones (1213 for rest position and 2763 for movement class) – LDA.

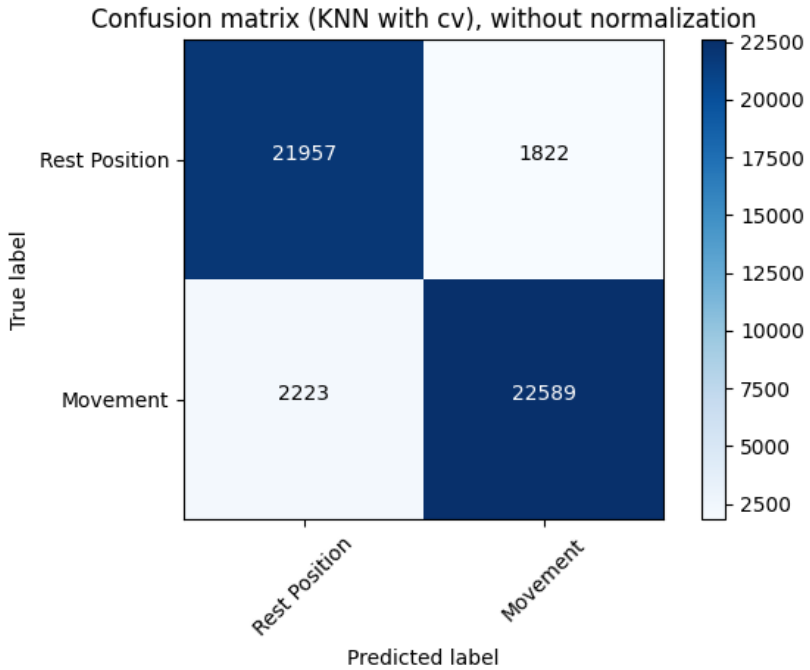

Figure G.12: Confusion Matrix for the first level of the tree classifier when the 10-fold cross-validation method was applied for a window of 100 *ms*. Represents the number of instances that were classified correctly for both classes (21957 for rest position and 22589 for movement class) and the misclassified ones (1822 for rest position and 2223 for movement class) - KNN (k=15).

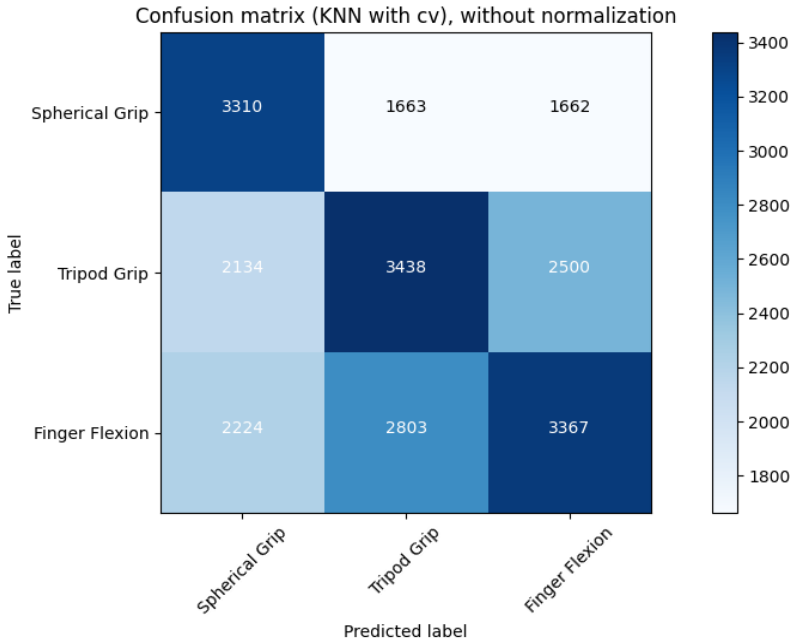

Figure G.13: Confusion Matrix for the all the movements of the second level when the 10-fold cross-validation method was applied for a window of 250 *ms*. Represents the number of instances that were classified correctly for both classes (3310 for spherical grip, 3438 for tripod grip and 3367 for Index Finger Flexion) and the misclassified ones (3325 for spherical grip, 4634 for tripod grip and 5027 for Index Finger Flexion) - KNN (k=15).

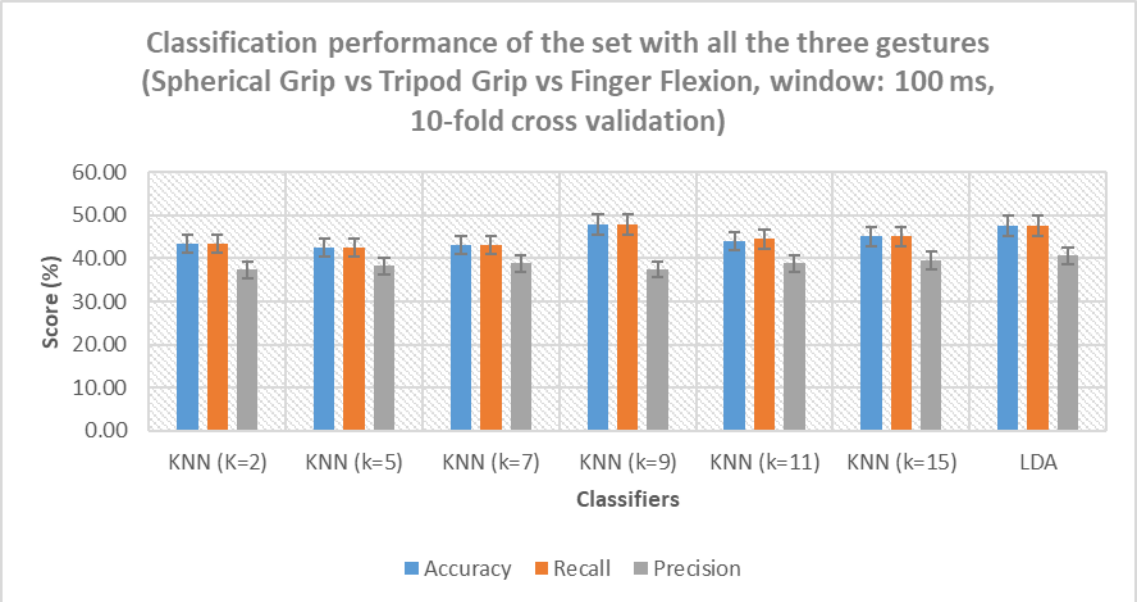

Figure G.15: Results obtained when all the movements were classified for a window of 100 ms: Spherical Grip vs Tripod Grip vs Finger Flexion. The minimum accuracy was reached for KNN=2 (43.03 %) and the maximum for LDA (47.56 %).

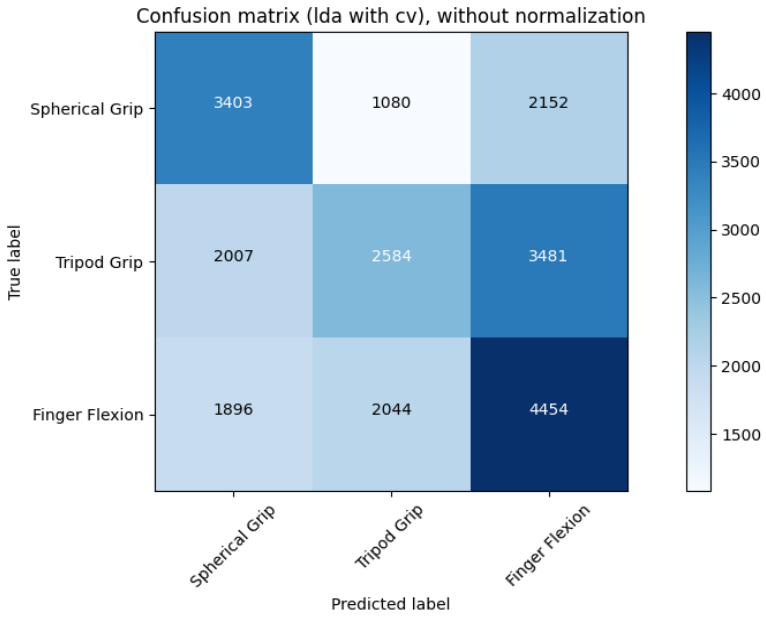

Figure G.14: Confusion Matrix for the all the movements of the second level when the 10-fold cross-validation method was applied for a window of 250 *ms*. Represents the number of instances that were classified correctly for both classes (3403 for spherical grip, 2584 for tripod grip and 4454 for Index Finger Flexion) and the misclassified ones (3232 for spherical grip, 5488 for tripod grip and 3940 for Index Finger Flexion) – LDA.

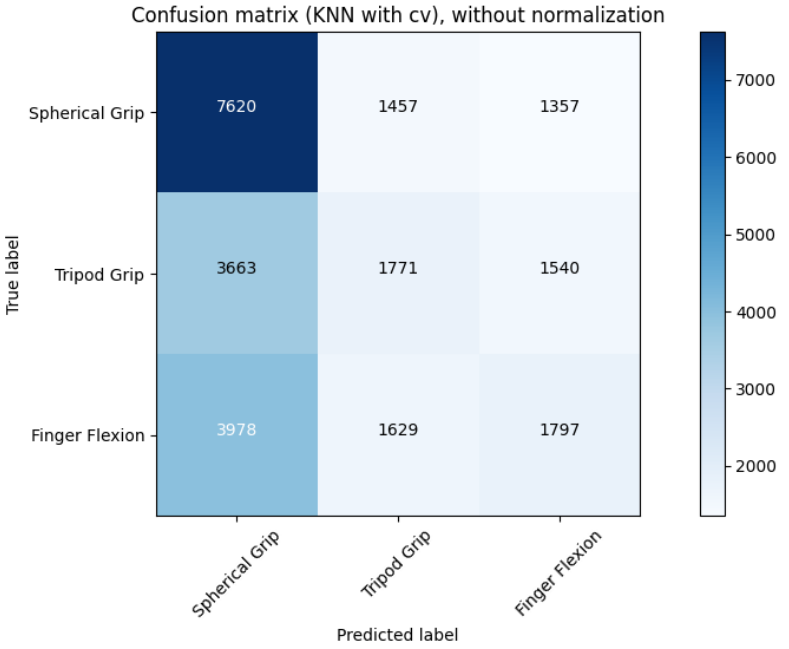

Figure G.16: Confusion Matrix for the second level of the tree classifier when the 10-fold cross-validation method was applied for a window of 100 *ms*. Represents the number of instances that were classified correctly for the three classes (7620 for spherical grip, 1771 for tripod grip and 1797 for finger flexion) and the misclassified ones (2814 for spherical grip, 5203 for tripod grip and 5607 for finger flexion) - KNN (k=15).

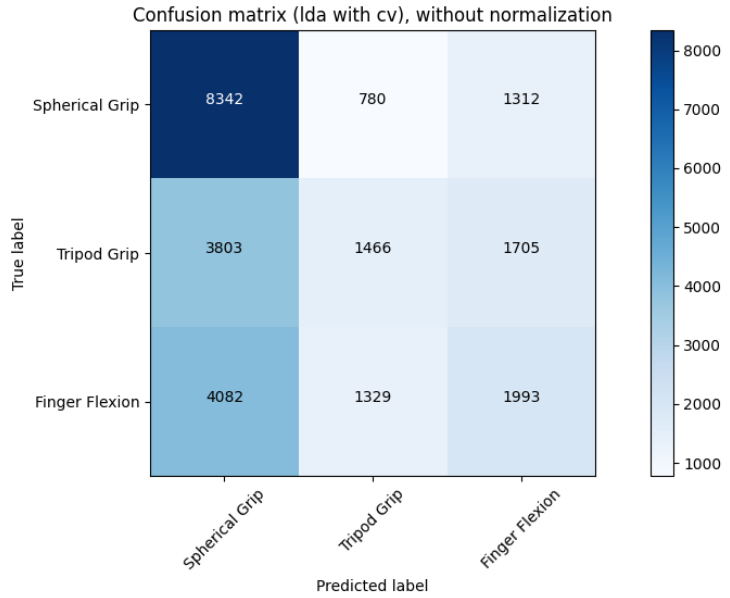

Figure G.17: Confusion Matrix for the second classification level when the 10-fold cross-validation method was applied for a window of 100 *ms*. Represents the number of instances that were classified correctly for the three classes (8342 for spherical grip, 1466 for tripod grip and 1993 for finger flexion) and the misclassified ones (2092 for spherical grip, 5508 for tripod grip and 3322 for finger flexion) – LDA.

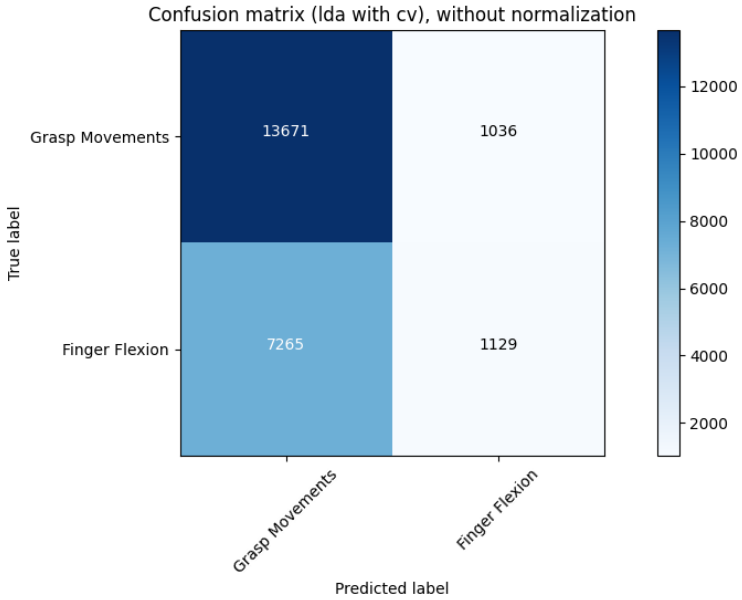

Figure G.18: Confusion Matrix for the second level when the 10-fold cross validation method was applied for a window of 250 *ms*. Represents the number of instances that were classified correctly for the two classes (13671 for grasp movements and 1129 for finger flexion) and the misclassified ones (1036 for grasp movements and 7265 for finger flexion).- LDA.

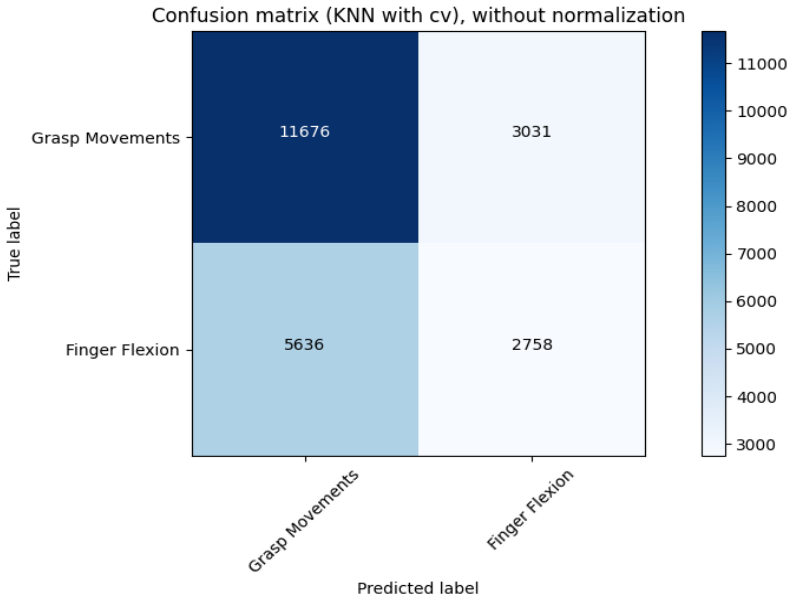

Figure G.19: Confusion Matrix for the second level when 10-fold cross validation method was applied for a window of 250 *ms*. Represents the number of instances that were classified correctly for the two classes (11676 for grasp movements and 2758 for finger flexion) and the misclassified ones (3031 for grasp movements and 5636 for finger flexion) - KNN (k=9).

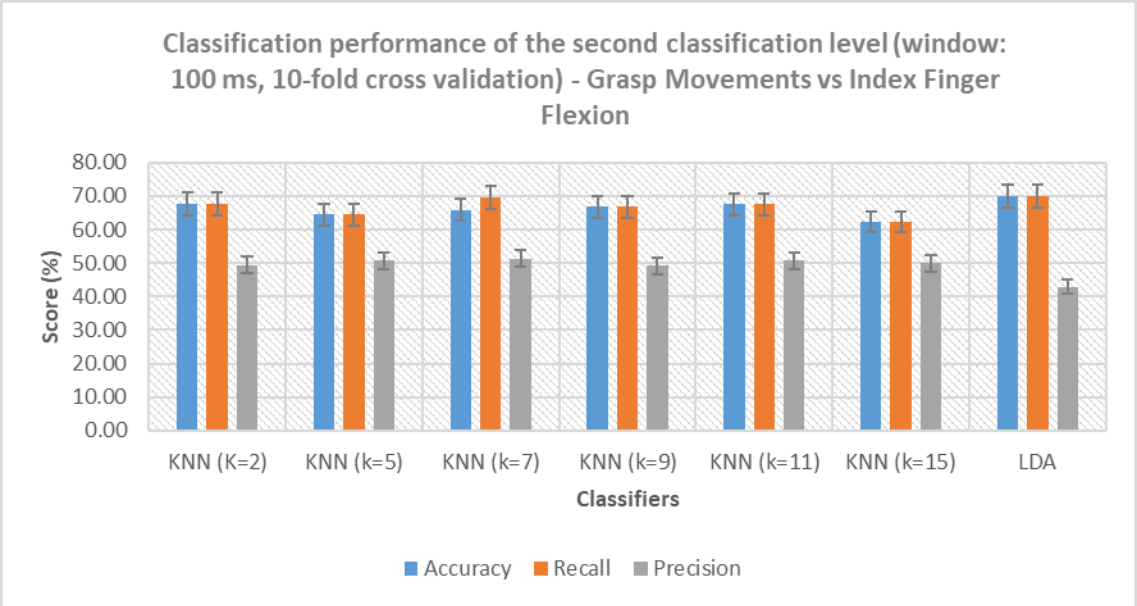

Figure G.20: Results obtained in the second level of the classifier for a window of 100 *ms*: Grasp Movements vs Finger Flexion. The minimum accuracy was reached for KNN=15 (62.32 %) and the maximum for LDA (69.87 %).

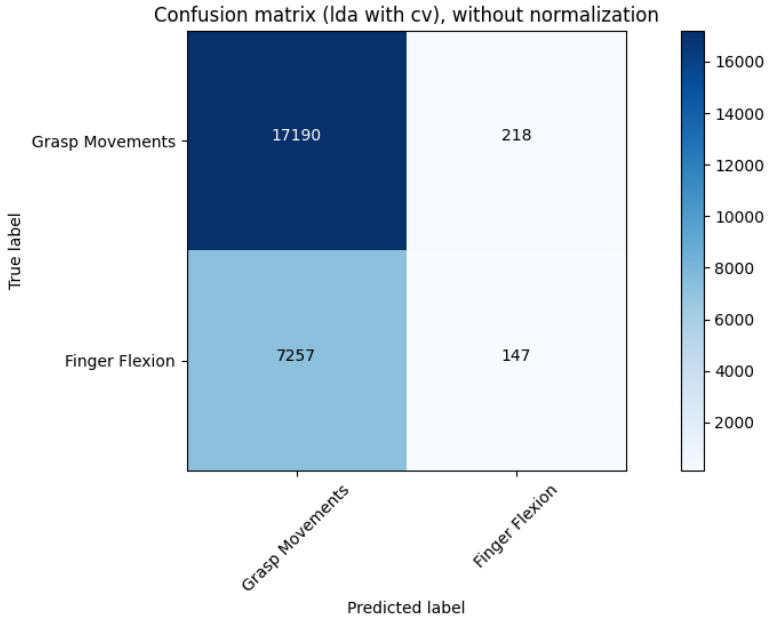

Figure G.21: Confusion Matrix for the second level when the 10-fold cross validation method was applied for a window of 100 *ms*. Represents the number of instances that were classified correctly for the two classes (17190 for grasp movements and 147 for finger flexion) and the misclassified ones (218 for grasp movements and 7257 for finger flexion) – LDA.

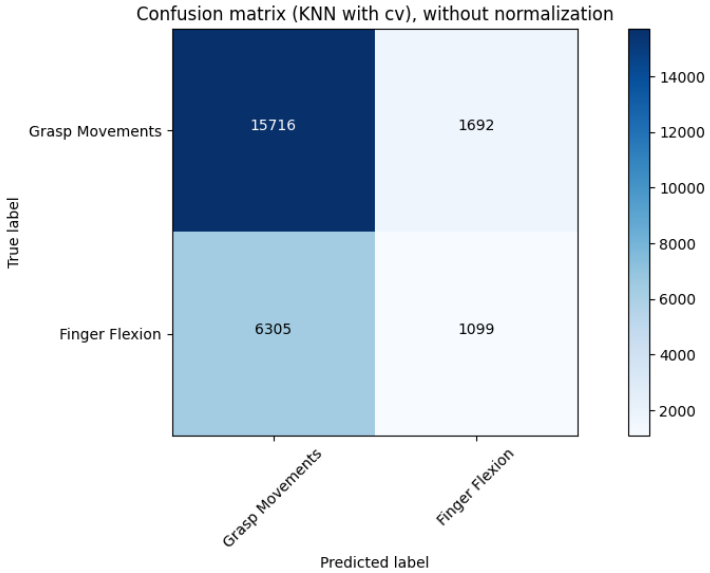

Figure G.22: Confusion Matrix for the second level when the 10-fold cross validation method for a window of 100 *ms*. Represents the number of instances that were classified correctly for the two classes (15716 for grasp movements and 1099 for finger flexion) and the misclassified ones (1692 for grasp movements and 6305 for finger flexion) - KNN (k=2).

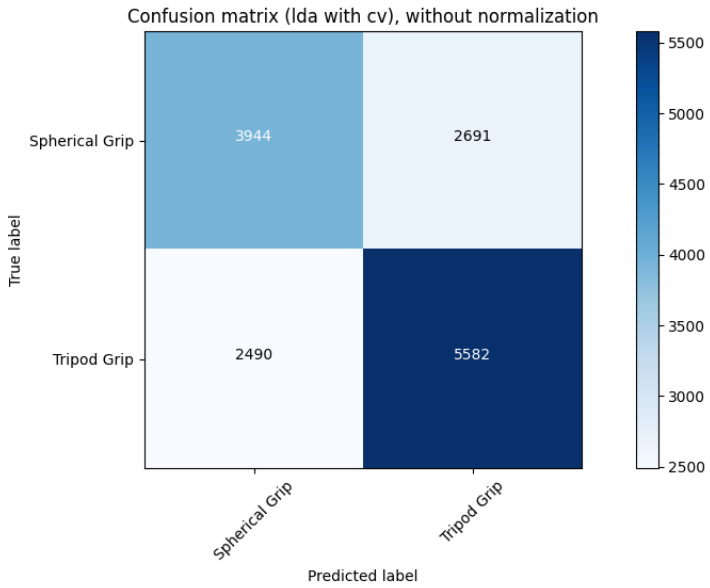

Figure G.23: Confusion Matrix for third level when the 10-fold cross validation method was applied for a window of 250 *ms*. Represents the number of instances that were classified correctly for the two classes (3944 for spherical grip and 5582 for tripod grip) and the misclassified ones (2691 for spherical grip and 2490 for tripod grip) – LDA.

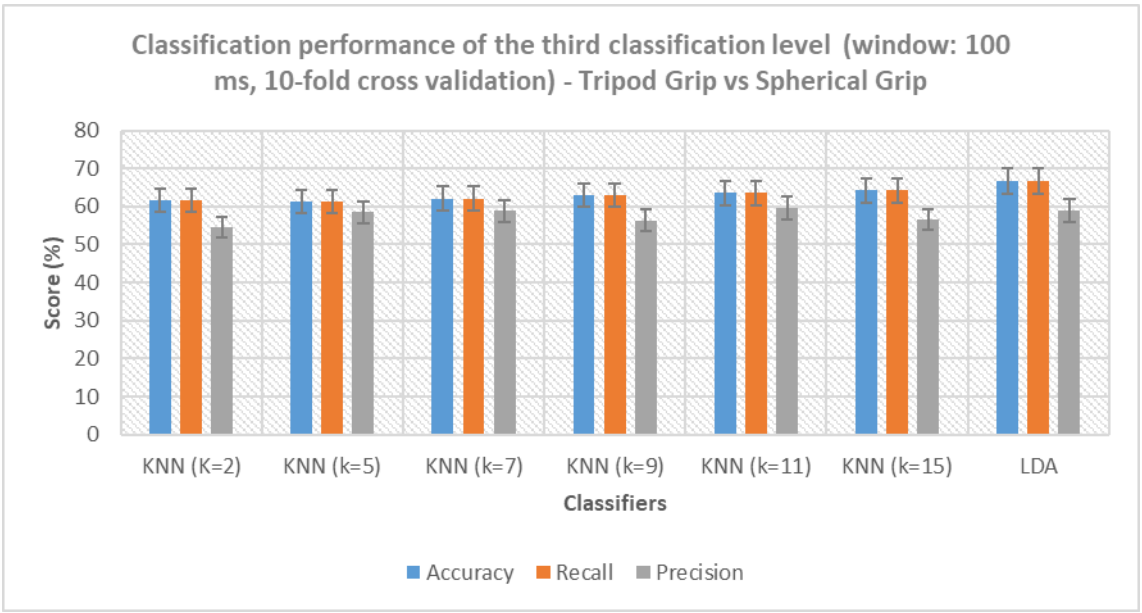

Figure G.24: Results obtained in the third level of the classifier for a window of 100 *ms*: Tripod grip vs spherical grip. The minimum accuracy was reached for KNN=5 (61.38 %) and the maximum for LDA (66.64 %).

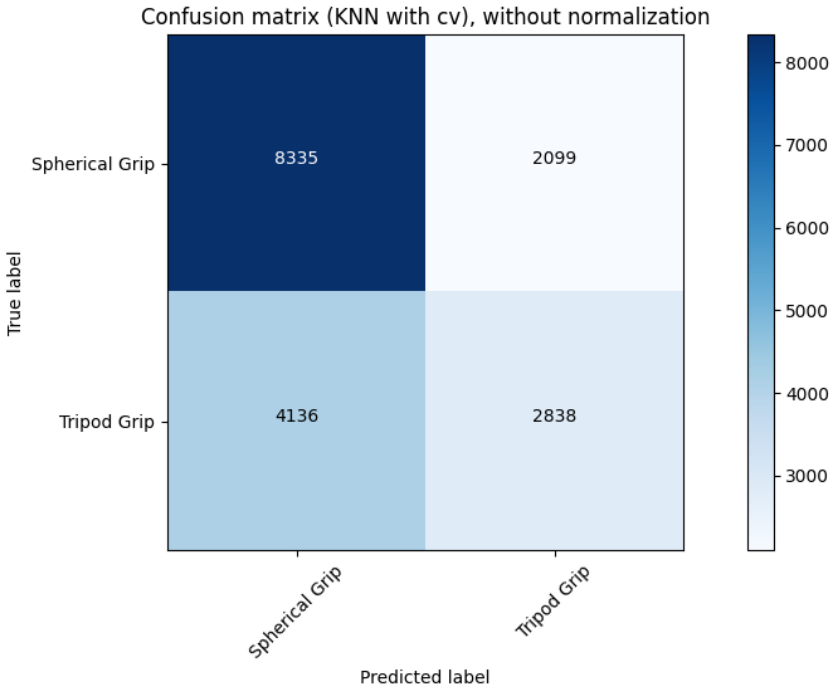

Figure G.25: Confusion Matrix for the third level when the 10-fold cross validation method was applied for a window of 100 *ms*. Represents the number of instances that were classified correctly for the two classes (8335 for spherical grip and 2838 for tripod grip) and the misclassified ones (2099 for spherical grip and 4136 for tripod grip) - KNN (k=15).

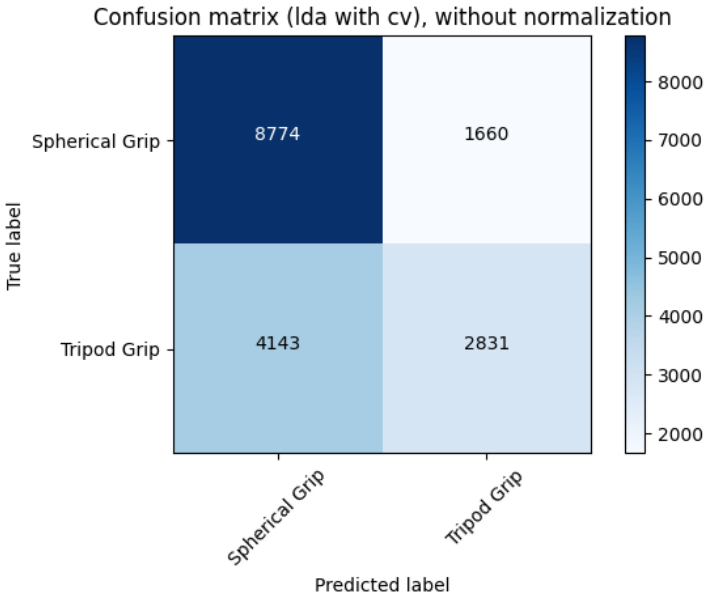

Figure G.26: Confusion Matrix for the third level when the 10-fold cross validation method for a window of 100 *ms*. Represents the number of instances that were classified correctly for the two classes (8774 for spherical grip and 2831 for tripod grip) and the misclassified ones (1660 for spherical grip and 4143 for tripod grip) - LDA.

H. Split validation method results

Table H.1: Classification results for a window length of 250 *ms* when the split validation method was applied. The results are distributed by classification levels.

Evaluation Metrics (%)	KNN (k=2)	KNN (k=5)	KNN (k=7)	KNN (k=9)	KNN (k=11)	KNN (k=15)	LDA
Window of 250 *ms*							
First Classification Level – Movement vs Rest							
Accuracy	91.53	92.63	92.78	93.19	93.03	93.07	93.47
Recall	91.53	92.63	92.78	93.19	93.03	93.07	93.47
Precision	91.48	92.56	92.70	93.13	92.97	93.00	93.35
Second Classification Level – Spherical Grip vs Tripod Grip vs Finger Flexion							
Accuracy	72.47	59.57	57.68	54.29	52.92	50.89	44.83
Recall	72.47	59.57	57.68	54.29	52.92	50.89	44.83
Precision	78.19	60.19	57.78	54.42	53.11	50.96	44.95
Second Classification Level – Grasp Movements vs Finger Flexion							
Accuracy	80.45	73.00	71.35	69.01	68.30	67.16	63.61
Recall	80.45	73.00	71.35	69.01	68.30	67.16	63.61
Precision	88.24	71.20	69.35	66.60	68.07	64.37	63.30
Third Classification Level – Spherical Grip vs Tripod Grip							
Accuracy	81.09	73.62	70.80	69.28	68.30	66.65	63.61
Recall	81.09	73.62	70.80	69.28	68.30	66.65	63.61
Precision	85.41	73.49	70.62	69.06	68.07	66.43	63.30

Table H.2: Classification results for a window length of 100 *ms* when the split validation method was applied. The results are distributed by classification levels.

Evaluation Metrics (%)	KNN (K=2)	KNN (k=5)	KNN (k=7)	KNN (k=9)	KNN (k=11)	KNN (k=15)	LDA
Window of 100 *ms*							
First Classification Level – Movement vs Rest							
Accuracy	88.34	91.08	91.33	91.52	91.46	91.34	91.23
Recall	88.34	91.08	91.33	91.52	91.46	91.341	91.23
Precision	88.8	91.05	91.29	91.49	91.43	91.32	91.36
Second Classification Level – Spherical Grip vs Tripod Grip vs Finger Flexion							
Accuracy	46.08	43.5	44.08	44.66	44.52	46.19	48.84

Recall	46.08	43.5	44.08	44.66	44.52	46.19	48.84
Precision	39.86	38.53	39.52	39.8	39.26	41.18	44.64
Second Classification Level – Grasp Movements vs Finger Flexion							
Accuracy	76.36	67.60	69.55	70.47	71.83	72.73	76.36
Recall	76.36	67.60	69.55	70.47	71.83	72.73	76.36
Precision	55.29	52.51	53.03	53.40	54.55	54.53	55.29
Third Classification Level – Spherical Grip vs Tripod Grip							
Accuracy	61.91	60.44	61.71	62.46	62.73	64.07	67.13
Recall	61.91	60.44	61.71	62.46	62.73	64.07	67.13
Precision	58.08	57.94	59.23	59.87	60.13	61.47	64.97

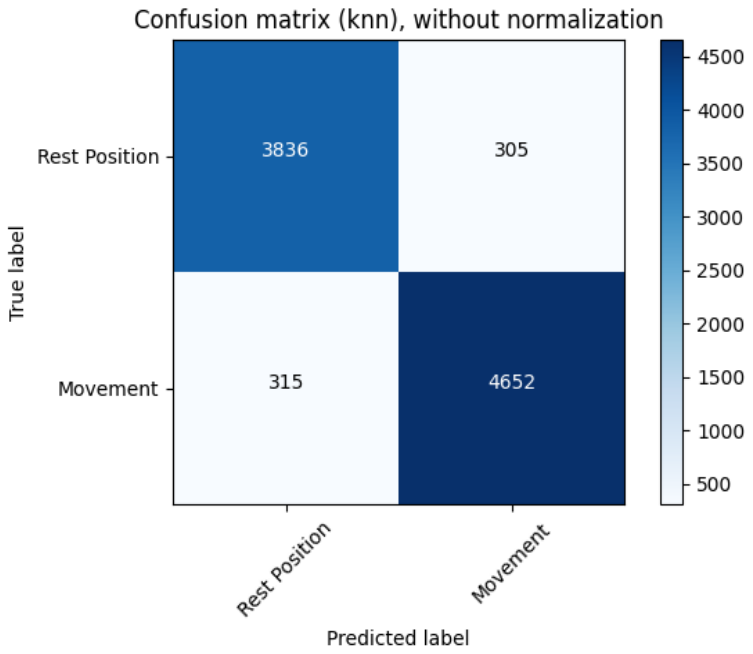

Figure H.1: Confusion Matrix for the first classification level when the split validation methdo was applied to data for a window of 250 *ms*. Represents the number of instances that were classified correctly for both classes (3836 for rest position and 4652 for movement class) and the misclassified ones (305 for rest position and 315 for movement class) - KNN (k=9).

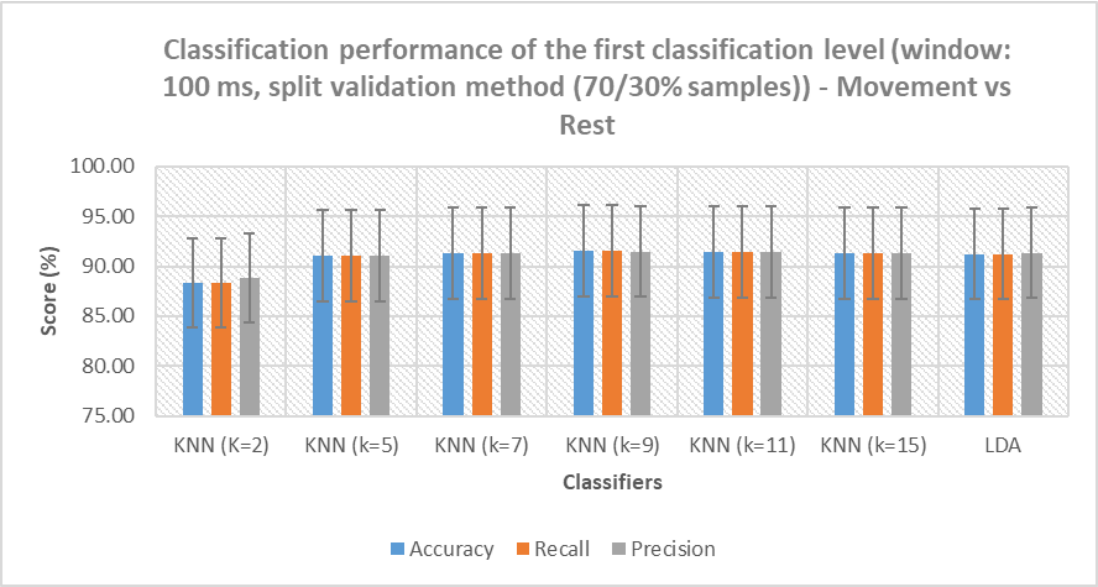

Figure H.2: Results obtained in the first classification level for a window of 100 *ms*: Movements vs Rest Position. The minimum accuracy was reached for KNN=2 (88.34 %) and the maximum for KNN with k=9 (91.52 %).

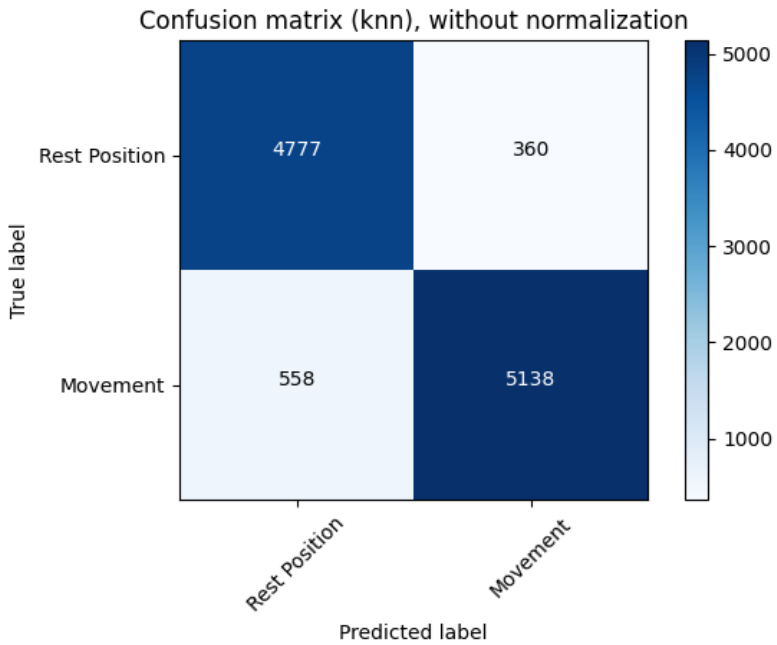

Figure H.3: Confusion Matrix for the first classification level when the split validation method was applied for a window of 100 *ms*. Represents the number of instances that were classified correctly for both classes (4777 for rest position and 5138 for movement class) and the misclassified ones (360 for rest position and 558 for movement class) - KNN (k=9).

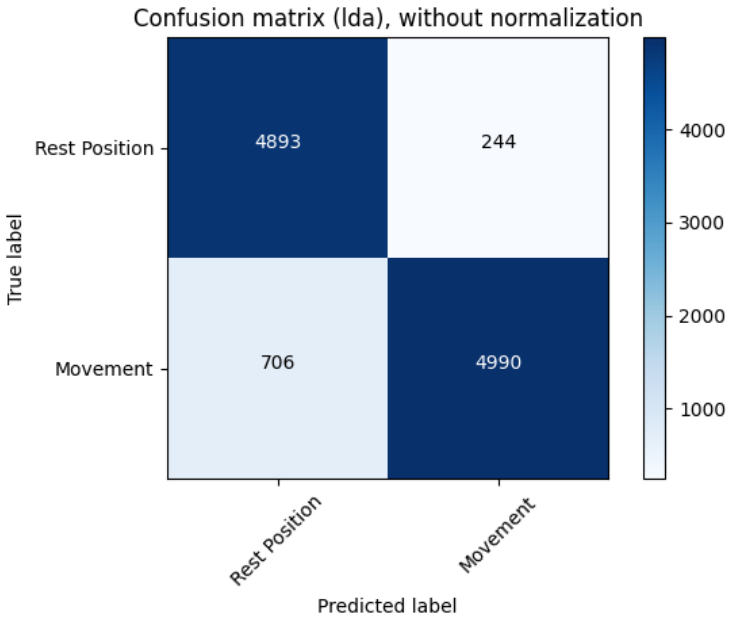

Figure H.4: Confusion Matrix for the first classification level when the split validation method was applied for a window of 100 *ms*. Represents the number of instances that were classified correctly for both classes (4893 for rest position and 4990 for movement class) and the misclassified ones (244 for rest position and 706 for movement class) – LDA.

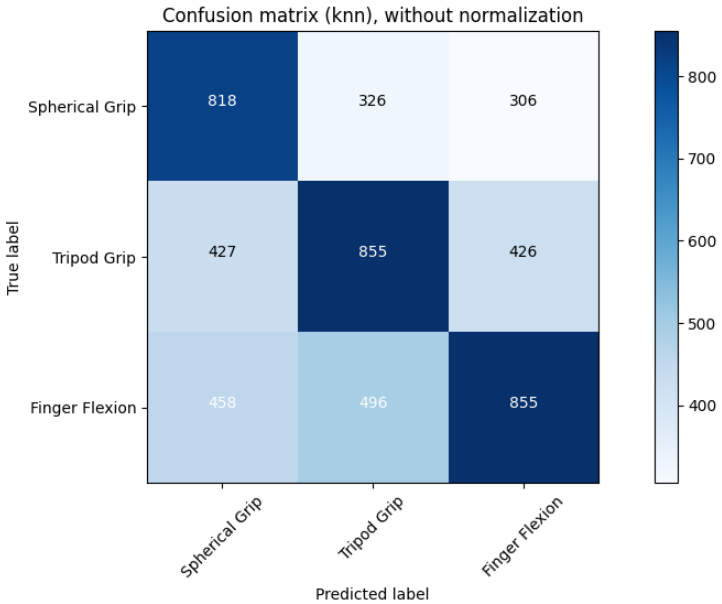

Figure H.5: Confusion Matrix for the second classification level (Tripod Grip vs Spherical Grip vs Finger Flexion) when the split validation method was applied for a window of 250 *ms*. Represents the number of instances that were classified correctly for both classes (818 for spherical grip, 855 for tripod grip and 855 for Index Finger Flexion) and the misclassified ones (632 for spherical grip, 853 for tripod grip and 954 for Index Finger Flexion) - KNN (k=15).

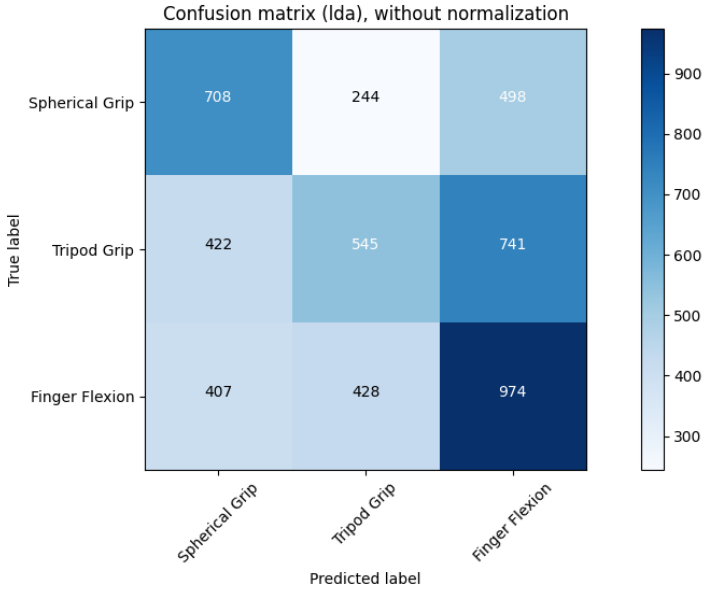

Figure H.6: Confusion Matrix for the all the movements of the second classification level when the split validation was applied for a window of 250 *ms*. Represents the number of instances that were classified correctly for both classes (742 for spherical grip, 545 for tripod grip and 974 for Index Finger Flexion) and the misclassified ones (632 for spherical grip, 1163 for tripod grip and 835 for Index Finger Flexion) – LDA.

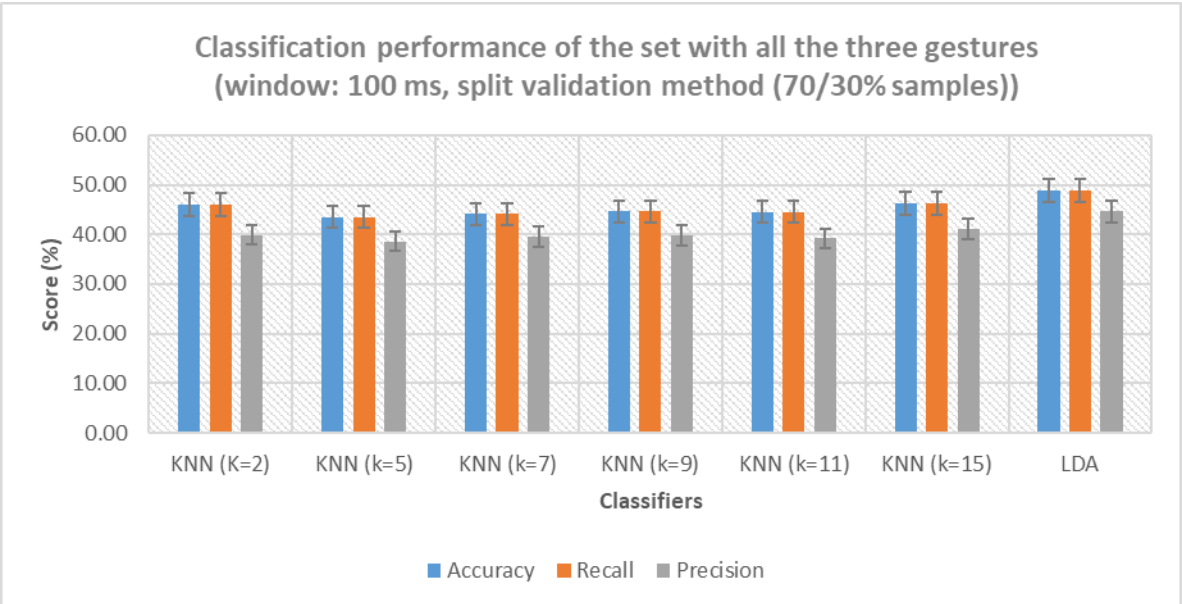

Figure H.7: Results obtained when all the movements were classified for a window of 100 *ms*: Spherical Grip vs Tripod Grip vs Finger Flexion. The minimum accuracy was reached for KNN=5 (43.50 %) and the maximum for LDA (48.84 %).

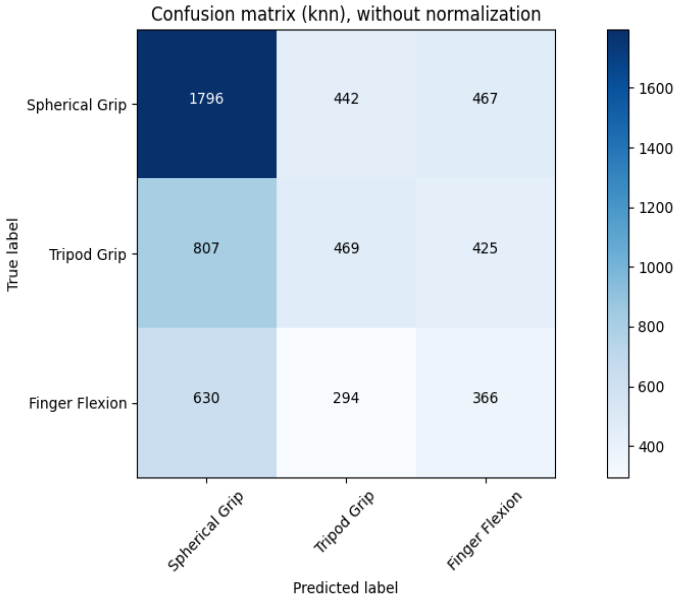

Figure H.8: Confusion Matrix for the second classification level when the split validation method was applied for a window of 100 *ms*. Represents the number of instances that were classified correctly for the three classes (1796 for spherical grip, 469 for tripod grip and 366 for finger flexion) and the misclassified ones (909 for spherical grip, 1232 for tripod grip and 996 for finger flexion) - KNN (k=15).

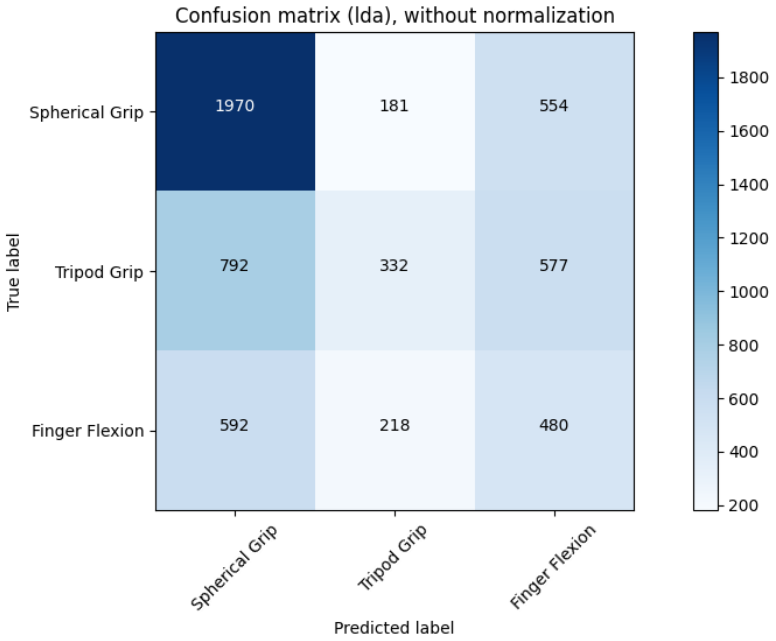

Figure H.9: Confusion Matrix for the second classification level when the split validation was applied for a window of 100 *ms*. Represents the number of instances that were classified correctly for the three classes (1970 for spherical grip, 332 for tripod grip and 480 for finger flexion) and the misclassified ones (735 for spherical grip, 1369 for tripod grip and 810 for finger flexion) - LDA.

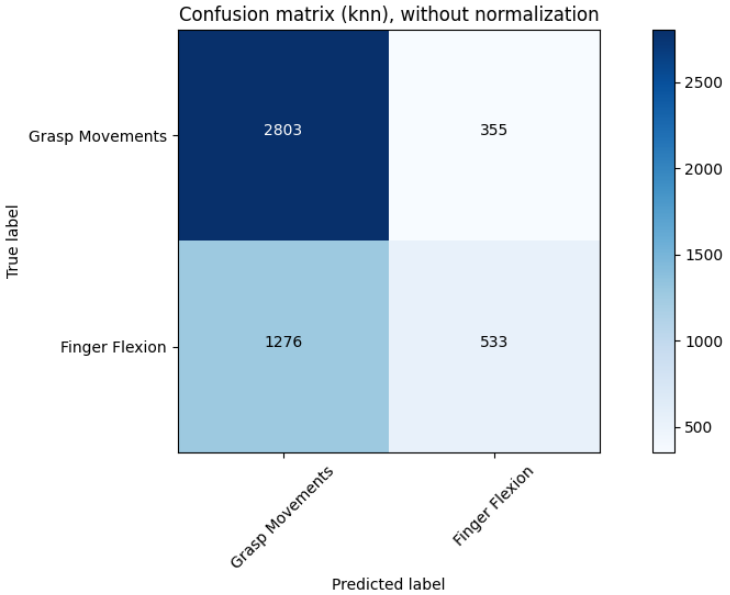

Figure H.10: Confusion Matrix for the second level when the split validation method was applied for a window of 250 *ms*. Represents the number of instances that were classified correctly for the two classes (2803 for grasp movements and 533 for finger flexion) and the misclassified ones (355 for grasp movements and 1276 for finger flexion) - KNN (k=15).

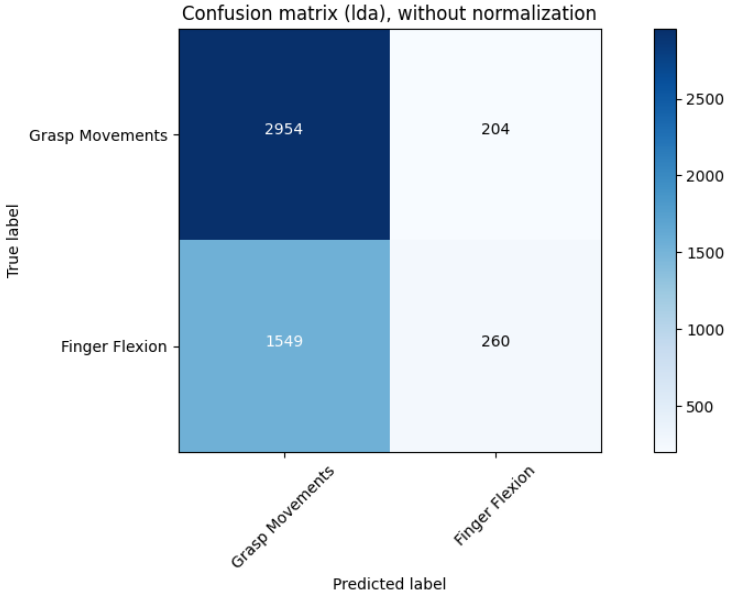

Figure H.11: Confusion Matrix for the second level when the split validation method was applied for a window of 250 *ms*. Represents the number of instances that were classified correctly for the two classes (2954 for grasp movements and 260 for finger flexion) and the misclassified ones (204 for grasp movements and 1549 for finger flexion) -LDA.

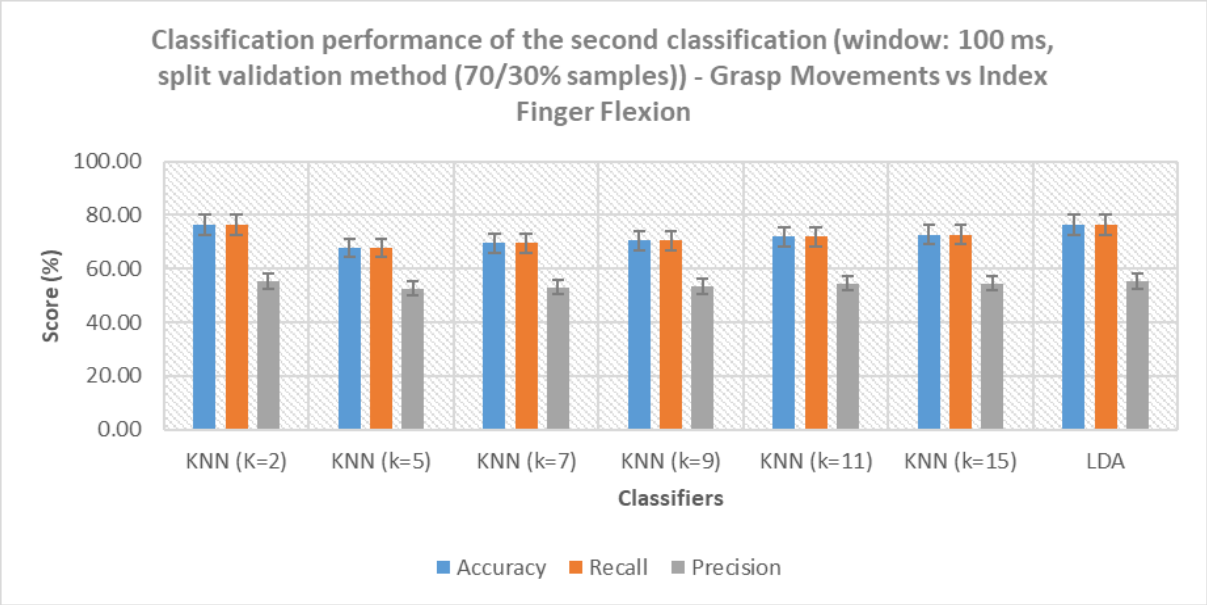

Figure H.12: Results obtained in the second level of the classifier for a window of 100 *ms*: Grasp Movements vs Finger Flexion. The minimum accuracy was reached for KNN=5 (67.60 %) and the maximum for LDA and KNN (k=2) (76.36 %)..

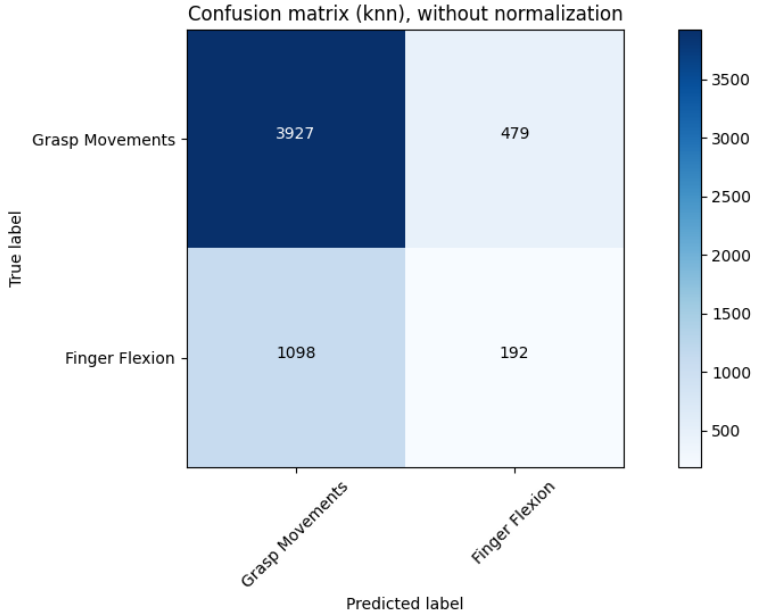

Figure H.13: Confusion Matrix for the second level when the split validation method for a window of 100 *ms*. Represents the number of instances that were classified correctly for the two classes (3927 for grasp movements and 192 for finger flexion) and the misclassified ones (479 for grasp movements and 1098 for finger flexion) - KNN (k=2).

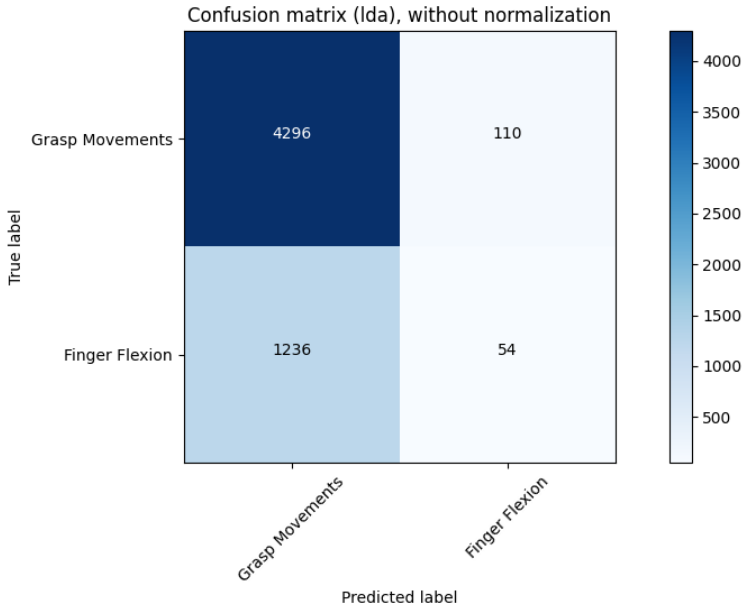

Figure H.14: Confusion Matrix for the second level when the split validation method was applied to data for a window of 100 *ms*. Represents the number of instances that were classified correctly for the two classes (4296 for grasp movements and 54 for finger flexion) and the misclassified ones (110 for grasp movements and 1236 for finger flexion) – LDA.

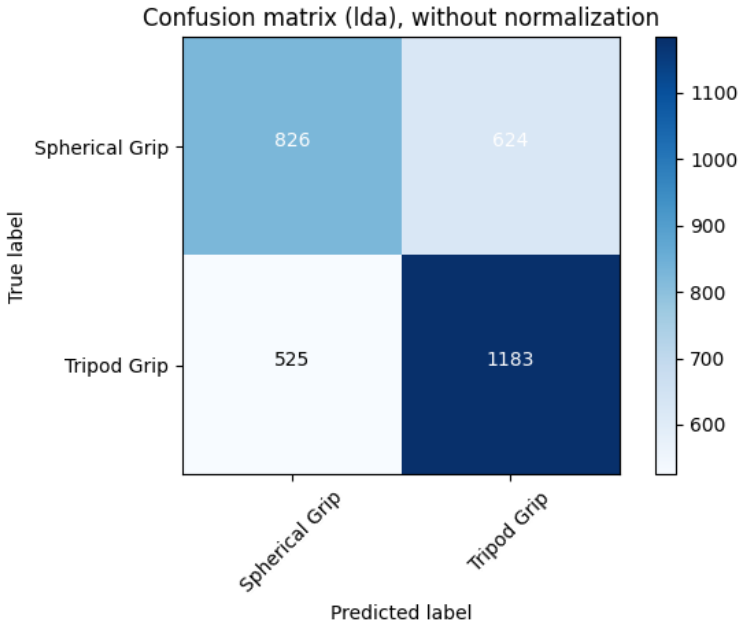

Figure H.15: Confusion Matrix for the third level when the split validation method was applied for a window of 250 *ms*. Represents the number of instances that were classified correctly for the two classes (826 for spherical grip and 1183 for tripod grip) and the misclassified ones (6241 for grasp movements and 525 for finger flexion) – LDA.

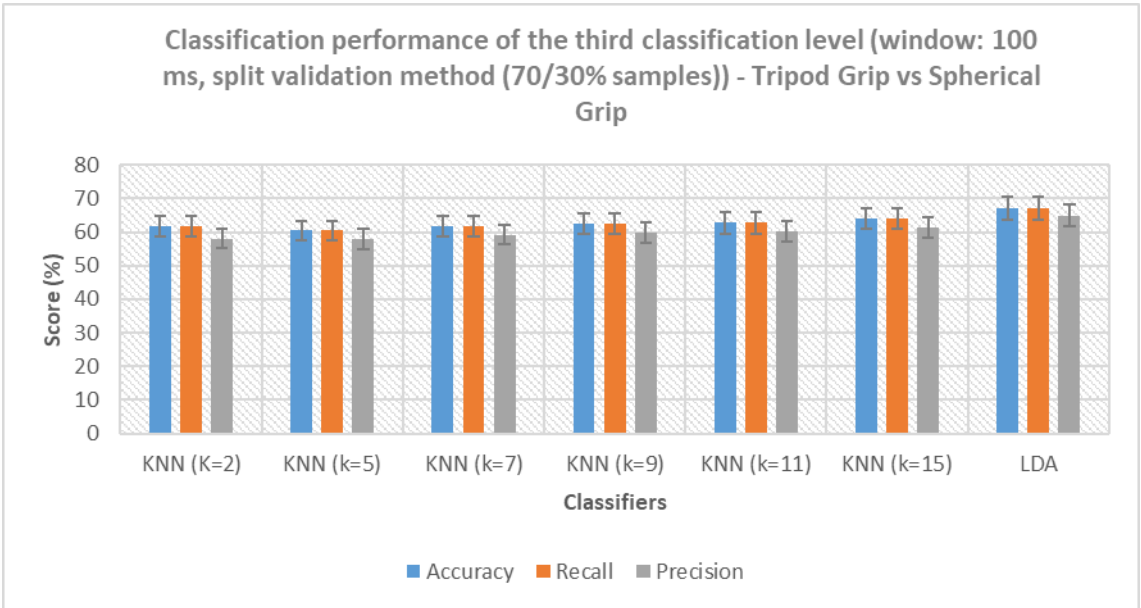

Figure H.16: Results obtained in the third level of the classifier for a window of 100 *ms*: Tripod grip vs spherical grip. The minimum accuracy was reached for KNN=5 (60.44 %) and the maximum for LDA (67.13 %).

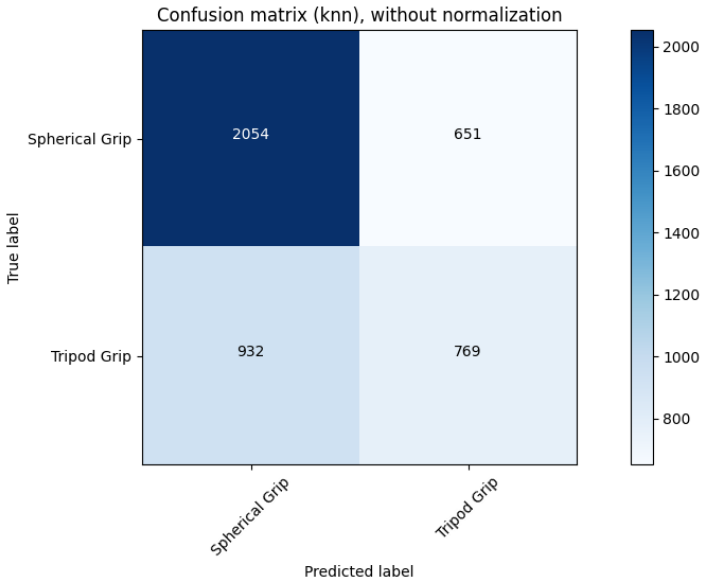

Figure H.17: Confusion Matrix for the third level when the split validation method was applied for a window of 100 *ms*. Represents the number of instances that were classified correctly for the two classes (2054 for spherical grip and 769 for tripod grip) and the misclassified ones (651 for spherical grip and 932 for tripod grip) - KNN (k=15).

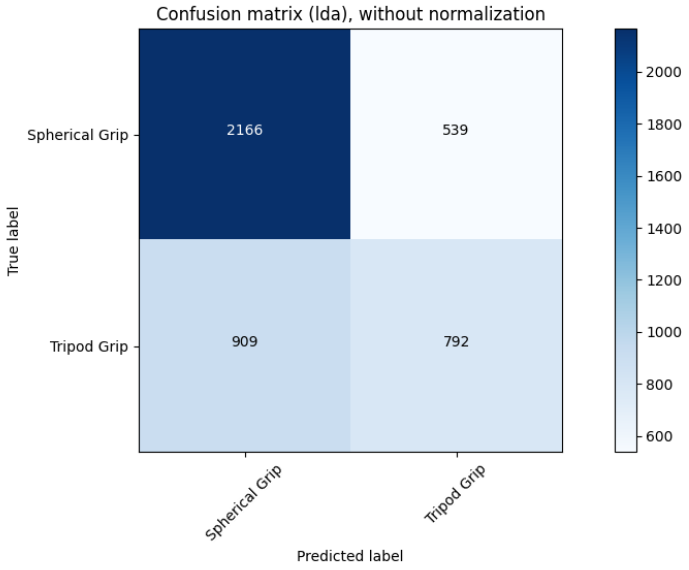

Figure H.18: Confusion Matrix for the third level when the split validation method was applied for a window of 100 *ms*. Represents the number of instances that were classified correctly for the two classes (2166 for spherical grip and 792 for tripod grip) and the misclassified ones (539 for spherical grip and 909 for tripod grip) – LDA.